

**EFFECT OF MICRO ALLOYING ON MECHANICAL  
PROPERTIES AND WEAR CHARACTERISTICS  
OF  
HADFIELD MANGANESE STEEL**

**A THESIS**

submitted in fulfilment of the  
requirements for the award of the degree

of

**DOCTOR OF PHILOSOPHY**

**IN**

**METALLURGICAL ENGINEERING**

By

**SUBODH KUMAR**



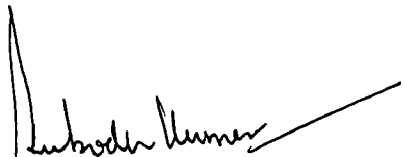
**DEPARTMENT OF METALLURGICAL ENGINEERING  
UNIVERSITY OF ROORKEE  
ROORKEE - 247 667 (INDIA)**

**APRIL, 1988**

## CANDIDATE'S DECLARATION


I hereby certify that the work which is being presented in the thesis entitled, 'EFFECT OF MICRO ALLOYING ON MECHANICAL PROPERTIES AND WEAR CHARACTERISTICS OF HADFIELD MANGANESE STEEL' in fulfilment of the requirement for the award of the Degree of Doctor of Philosophy submitted in the Department of METALLURGICAL ENGINEERING of the University is an authentic record of my own work carried out during a period from March 1984 to March 1988 under the supervision of Dr. D.B. Goel.

The matter embodied in this thesis has not been submitted by me for the award of any other Degree.

  
Candidate's Signature

This is to certify that the above statement made by the candidate is correct to the best of my knowledge.

Dated: April 11, 1988

  
(D.B. GOEL)  
Professor  
Metallurgical Engg. Department  
University of Roorkee  
ROORKEE, U.P. INDIA

The candidate has passed the Viva-Voce Examination held on \_\_\_\_\_ at \_\_\_\_\_. The thesis is recommended for award of the Ph.D. Degree.

Signature of Guide/s

Signature of External Examiners

## ABSTRACT

Austenitic Mn steel, known as Hadfield steel, has a nominal composition: 1.0-1.4 C (wt. pct.), 11.0-14.0 Mn, 1.0 Si (Max) and 0.07 P (Max). This steel with its extremely high strength and toughness possesses high work hardening capacity and resistance to wear. Although this steel has been used for nearly a century since its development in 1882, the mechanisms of rapid work hardening and of wear remain unclear. No systematic study has been made to correlate the wear characteristics with work hardening tendency. It is also observed that no systematic attempts have been made to study the role of various micro alloying elements in Hadfield Mn steel to improve casting characteristics, grain refinement, mechanical properties, and wear characteristics. In the present investigation the effect of micro alloying of Hadfield steel by B, V and cb has been studied on the grain refinement, mechanical properties, work hardening and wear characteristics.

The micro alloyed Hadfield steels using four concentrations of B in the range of 0.001 to 0.004 pct. and three concentrations of V and Cb each in the range of 0.05 to 0.50 pct. were prepared by induction melting. The pouring temperature of liquid was kept within  $1500 \pm 10^\circ\text{C}$  in all the compositions. Test samples of appropriate dimensions were poured for carrying out tensile, impact, hardness and wear tests. All tests

were conducted after a standard heat treatment, which included austenitising at 1050°C for 90 minutes followed by water quenching. Light microscopy and scanning electron microscopy were extensively employed to study the work hardening and wear mechanisms under different test conditions.

Micro alloying additions have been observed to significantly affect the tensile properties. For example, addition of 0.003 pct. B (0.003 B alloy) enhances the yield strength (YS) of base steel (13 Mn alloy) from 392.4 to 439.0 MPa, ultimate tensile strength (UTS) from 650.4 to 740.4 MPa and pct. elongation (El) from 20.0 to 35.7 pct. Micro additions of V at lower concentrations (0.05 V and 0.10 V alloys) also enhance YS, UTS and El but there is marginal drop in El in higher concentration (0.50 V alloy). With additions of Cb, the YS and UTS show an improvement, but the El is reduced. Higher concentration of Cb (0.50 Cb alloy) also shows reduction in UTS in comparison to lower concentrations.

The strain hardening exponents ( $\eta$ ) have been determined from the true stress-true strain diagrams in the plastic range derived from tensile curves. It is observed that all the micro alloying additions increase the strain hardening exponents of the base steel, the effect of V addition being maximum. The load-elongation curves under slow strain rate ( $3 \times 10^{-4} \text{ Sec}^{-1}$ ) show serrated flow which are also maximum in amplitude

and in frequency in 0.10 V steel. The serrations are directly related with the value of strain hardening exponents. The present investigations have shown that work hardening characteristics during tensile loading differ significantly from those observed during impact loading.

The micro alloying of Hadfield Mn steel by B, V and Cb has been observed to affect significantly the impact strength. Maximum improvement in impact value is observed in case of 0.003 B alloy. Additions of 0.05 and 0.10 pct. V marginally improve the toughness value, whereas 0.5 pct. V addition causes deterioration in the impact value. Toughness is significantly reduced by Cb additions.

From the results obtained, it is observed that 0.003 B alloy gives the optimum mechanical properties out of four different concentrations of B selected for experiments. Similarly 0.10 V alloy gives higher YS and UTS without affecting ductility and toughness of base alloy (13 Mn). However, 0.50 Cb alloy shows maximum improvement in YS though elongation and toughness are adversely affected with all other concentrations. Hence these three compositions (0.003 B, 0.10 V and 0.50 Cb alloys) were selected for further investigation on work hardening and wear characteristics.

All the Hadfield steels investigated exhibit significant work hardening capacity under impact loading. The maximum improvement in hardness is observed in 0.003 B steel. The 0.10 V alloy shows almost the same hardness level as of base steel; whereas there is decrease in hardness level with Cb addition. The saturation in hardness (486 VHN) is attained very rapidly (50 blows) in 0.003 B alloy in comparison to all other compositions studied in the present investigation.

The depth of hardening was studied for all samples subjected to impact loading. A sharp drop occurs in the hardness below the impacted surface upto a depth of 0.3-0.8 mm, beyond which the hardness attains a constant level which is about 60 to 140 VHN higher than the as quenched hardness. Most predominant effect is observed in the 0.003 B alloy. In this alloy the thickness of variable hardness below the impacted layer is only 0.30 mm beyond which a constant hardness level (350 VHN) is attained which is about 140 VHN higher than as quenched hardness.

The wear resistance, as measured by weight loss, for various Hadfield compositions was studied under conditions of impact-slide and slide ( by grinding on emery wheel). The 0.003 B alloy shows remarkable improvement in wear resistance under both conditions. additions of V and Cb have been observed

to deteriorate marginally the wear resistance of Hadfield steel. The present investigations have revealed that the wear resistance of Hadfield steel is directly linked to its saturation hardness under impact-slide wear conditions and has higher wear resistance in comparison to only slide wear conditions. The wear resistance, as determined after grinding off the variable hardness layer, closely corresponds to the wear resistance of as quenched, unimpacted samples. It, therefore, appears that the nature of the variable hardness surface layer formed on impact loading plays a vital role in enhancing the wear properties of Hadfield steels. It is also established that in addition to its relationship with saturation hardness, the wear resistance also is governed by metallographic structure and other mechanical properties like toughness, UTS and El etc. The 0.003 B alloy, which shows maximum improvement in wear resistance in all conditions, is also observed to possess maximum toughness and higher UTS and El among all the compositions investigated.

Metallographic studies reveal that all micro alloying additions cause refinement in the as cast grain structure. The refinement is almost of the same order with all micro alloying compositions. It has been observed that there is no alteration in the grain structure by heat treatment except that there are certain structural changes. The addition of B results in an austenitic structure almost free of carbides relative to base composition (13 Mn alloy). The 0.10 V alloy shows some

fine precipitates of  $V_4C_3$  at grain boundaries and within the grains. The Cb addition results in the formation of carbides mainly on the austenite grain boundaries. The presence of these carbides is observed to significantly affect the mechanical properties, work hardening and wear characteristics. Light microscopy and Scanning Electron Microscopic (SEM) studies on impacted samples reveal the formation of cracks around these particles indicating decohesion at the carbide-matrix interfaces. Formation of twins has been observed in all the samples which is the principal cause of work hardening under impact loading. Maximum density of twins has been observed in 0.003 B alloy, whereas 0.50 Cb alloy shows minimum concentration of twins. SEM studies on fracture surfaces of impact tested samples reveal extensive elongation of grains before separation in the case of 0.003 B alloy indicating a high toughness of this steel. Tensile fracture of 0.003 B steel indicate a fine network of small size dimples which are formed around closely spaced striations. This indicates the higher ductility and deformation characteristics of 0.003 B alloy. Formation of fine cracks at carbide matrix interfaces have been observed in Cb and V bearing compositions which lead to the ultimate failure. Extensive SEM studies on wear surfaces at various stages of impact-slide wear reveal that abrasion is accompanied by simultaneous plastic deformation (micro-ploughing and micro-cutting) and brittle fracture (micro-cracking). The deformation is maximum



in 0.003 B alloy due to its higher elongation and toughness, whereas it is relatively less in 0.10 V and 0.50 Cb alloys. In V and Cb bearing alloys, micro cracks are observed to form at the interfaces of carbide particles and matrix which further propagate resulting in material removal in the form of relatively bigger flakes showing poor wear resistance. This observation was also confirmed by the size of debris formed in various micro alloyed compositions. Very fine sized debris is formed in 0.003B alloy in comparison to other compositions. Thus the SEM studies have confirmed the significant improvement in wear resistance by B additions and a deterioration by V and Cb additions.

The entire work reported in this thesis has been spread over six Chapters.

Chapter 1 deals with the critical review of the available literature on Hadfield Mn steel. This includes the structural characteristics of the alloy, heat treatment, various mechanisms to explain work hardening and wear characteristics. The effect of various alloying elements in the nominal range and some of micro alloying elements on mechanical properties is critically reviewed.

In Chapter-2 the problem of the present investigation has been formulated and posed on the basis of the perspective of present investigation.

Chapter 3 describes details of experimental set-up; alloy and sample preparation; method and machines used for measuring the various properties and corresponding micro-structural changes.

The details of various microstructural characteristics, mechanical properties viz. tensile properties, impact strength, hardness, effect of impact loading on hardness and wear properties under various test conditions of base alloy and micro alloyed compositions have been presented in different sections of Chapter 4.

The effect of micro alloying additions on mechanical properties, work hardening tendency and wear characteristics observed in the present investigation is critically discussed in Chapter 5.

Conclusions and suggestions for further work in this field of study are given in Chapter 6.

## ACKNOWLEDGEMENTS

The author is highly indebted to Dr. D.B.Goel, Professor, Department of Metallurgical Engineering, University of Roorkee, for his expert guidance and unfailing inspiration throughout the course of this investigation and preparation of the thesis. His valuable suggestions at various stages and thought provoking discussions have immensely contributed to this thesis for which the author wishes to record his deep sense of gratitude to him.

Thanks are due to Dr. A.K. Patwardhan, Professor and Head, Department of Metallurgical Engineering for his constant encouragement and help in providing various departmental facilities for this work.

The author is grateful to Mr. Ranjit Puri, Joint Managing Director and Mr. D.D. Sharma, General Manager, Uttar Pradesh Steel, Muzaffarnagar(India) in providing all kind of help to pursue this work. Constant encouragement from Mr. D.D. Sharma is sincerely acknowledged.

Thanks are also due to Dr. Kailash Chandra, Director, USIC, University of Roorkee, for providing the facilities of Scanning Electron Microscopic studies.

The author is thankful to Dr. Surendra Singh, Reader and Mr. Sharvan Kumar, Lecturer, Department of Metallurgical Engineering for their timely help in pursuing this work.

The author wishes to record his appreciation for the untiring help rendered by Mr. Asutosh Sharma, Metallurgist and other colleagues at Uttar Pradesh Steel who have helped at various stages during this work.

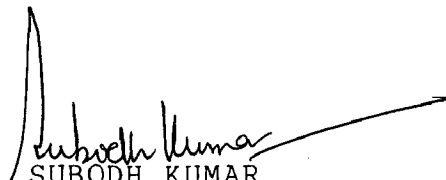
The author is thankful for the assistance and active cooperation rendered by the technical staff at Department of Metallurgical Engineering, University of Roorkee, particularly M/S S.K. Seth, S.P. Kush, S.C. Kaushik and Jai Prakash Sharma during experimentation. Excellent draftsmanship of Mr. M.C. Vaish and flawless typing of Mr. S.C. Sharma is also acknowledged.

It remains to express the sincere thanks for the assistance rendered by Mrs. Rekha Sharma, Technician, USIC in Scanning Electron Microscopic studies. The author is very much thankful to Mr. Mukesh Sharma, Research Scholar, Metallurgical Engineering Department for his untiring help in completing this work.

The author is also thankful to his parents, wife and daughter Neha who have shown extreme perseverance and made him free from various family obligations during the course of this research work.

ROORKEE

APRIL 11, 1988

  
SUBODH KUMAR

CONTENTS

Chapter		Page
	ABSTRACT	i
	ACKNOWLEDGEMENTS	ix
	LIST OF FIGURES	xiv
	LIST OF TABLES	xix
1	LITERATURE REVIEW	1
1.1	Introduction	1
1.2	Structural Characteristics of Hadfield Steel	7
1.3	Heat Treatment	19
1.4	Characteristic Properties of Hadfield Steel	21
1.4.1	Work hardening characteristics	25
1.4.2	Wear resistance	28
1.5	Effect of Alloying Elements on Characteristics of Hadfield Steel	38
1.5.1	Effect of variations in composition within the nominal range	38
1.5.2	Effect of additional alloying elements	42
2	FORMULATION OF PROBLEM	48
3	EXPERIMENTAL PROCEDURE AND TECHNIQUES	55
3.1	Alloy Preparation	55
3.1.1	Melting	55
3.1.2	Micro alloying	57
3.1.3	Chemical analysis	58
3.2	Preparation of Test Samples	58

contd.

## Contents(contd.)

Chapter	Page
3.2.1 Foundry procedure for preparation of test samples	60
3.3 Heat Treatment	66
4 Mechanical Testing	67
3.4.1 Hardness measurement	67
3.4.2 Tensile properties	67
3.4.3 Impact testing	68
3.5 Study of Wear Characteristics	68
3.6 Study of Material Behaviour Under Impact Loading	70
3.7 Metallographic Studies	71
4 RESULTS AND ANALYSIS	72
4.1 Effect of Micro Alloying on Mechanical Properties	72
4.1.1 Tensile properties	72
4.1.2 Hardness	85
4.1.3 Impact properties	86
4.1.4 Strain hardening coefficient	102
4.2 Effect of Micro Alloying on Hardening Under Impact Loading	106
4.3 Effect of Micro Alloying on wear characteristics	112
4.3.1 Impact-slide wear	113
4.3.2 Slide wear	120
4.4 Microstructural Observations	122
4.4.1 As cast microstructures	123
4.4.2 As heat treated microstructures	125
4.4.3 Microstructures of impact hardened alloys	127

Contd.

	Contents(contd.)	Page
Chapter		
4.5	Fractographic Studies	134
	4.5.1 Fracture under tensile loading	134
	4.5.2 Fracture under impact loading	143
4.6	SEM Studies on Wear Surfaces	145
5	DISCUSSION	158
5.1	Effect of Micro Alloying on Structural Characteristics and Mechanical Properties	158
5.2	Effect of Micro Alloying on Mechanism of Work Hardening	166
5.3	Effect of Micro Alloying on wear Mechanism	176
	5.3.1 Impact-slide wear	176
	5.3.2 Slide wear	182
5.4	Correlation of Mechanical Properties with Wear	183
6	CONCLUSIONS AND SUGGESTIONS FOR FUTURE WORK	186
6.1	Conclusions	186
6.2	Suggestions for Future Work	189
	REFERENCES	192
	APPENDIX: Tables of experimental data	210

## LIST OF FIGURES

Fig.No.	Caption	Page
1.1	Effect, of Mn contents on the C limitations for pure austenite at elevated temperatures	10
1.2	Section through the Fe-Mn-C system at 13 pct. Mn	11
1.3	Section through the Fe-Mn-C system at 1.0 pct. C	12
1.4	Effect of various alloying elements including Mn on eutectoid temperature	13
1.5	Effect of various alloying elements including Mn on eutectoid composition	14
1.6	Solubility of C in 13 pct. Mn steel	15
1.7	Variation of Ms temperature with C and Mn contents	17
1.8	Time-temperature relationship for embrittlement of 13 Mn-1.2 C-0.5 Si steel	22
1.9	Effect of reheating temperatures on elongation and hardness of toughened Hadfield steel	24
1.10	Course of flow under impact loading and associated increase in hardness	26
1.11	Relative wear ratios of various ferrous alloys in jaw crusher test	31
1.12	Schematic illustration of the deformed surface layer of an abraded or eroded material. The curve on the right hand side indicates the change in micro hardness, dis-location density or strain with depth below the worn surface	34
1.13	The hypothetical stress-strain curves for the wear of three classes of materials superimposed upon the frequency distribution of abrasive or erosive strikes of a given stress magnitude	35
1.14	Variation of properties with C content for austenitic Mn steel containing 12.6 to 13.0 pct. Mn	39



## List of Figures(contd.)

1.15	Variation of properties with Mn content for austenitic Mn steel containing 1.15 pct. C	41
1.16	Effect of Ni, Mo and Cr contents on tensile properties of austenitic Mn steel	43
1.17	Solubility range of vanadium carbide in austenite	46
3.1	Specimen for tensile test	61
3.2	Charpy V-notch specimen for impact test	62
3.3	Specimen for wear test	63
3.4	Schematic arrangement for pouring tensile and impact test samples	64
3.5	Schematic arrangement for pouring wear test samples	65
3.6	Disc Pin Rig for gouging wear test	69
4.1	Effect of Boron additions on tensile properties	73
4.2	Effect of Vanadium additions on tensile properties	74
4.3	Effect of Columbium additions on tensile properties	75
4.4	Effect of Boron additions on yield strength	76
4.5	Effect of Vanadium additions on yield strength	77
4.6	Effect of Columbium additions on yield strength	78
4.7	Effect of Boron additions on tensile strength	79
4.8	Effect of Vanadium additions on tensile strength	80
4.9	Effect of Columbium additions on tensile strength	81
4.10	Effect of Boron additions on elongation	82
4.11	Effect of Vanadium additions on elongation	83
4.12	Effect of Columbium additions on elongation	84
4.13	Effect of Boron additions on as quenched hardness	87
4.14	Effect of Vanadium additions on as quenched hardness	88
4.15	Effect of Columbium additions on as quenched hardness	89
4.16	Effect of Boron additions on impact value	90
4.17	Effect of Vanadium additions on impact value	91
4.18	Effect of Columbium additions on impact value	92

## List of Figures(contd.)

4.19	Effect of Boron additions on impact value	93
4.20	Effect of Vanadium additions on impact value	94
4.21	Effect of Columbium additions on impact value	95
4.22	Effect of Boron additions on improvement/deterioration in mechanical properties of 13 Mn alloy	97
4.23	Effect of Vanadium additions on improvement/deterioration in mechanical properties of 13 Mn alloy	98
4.24	Effect of Columbium additions on improvement/deterioration in mechanical properties of 13 Mn alloy	99
4.25	Effect of micro alloying on strain hardening exponent	103
4.26	Portions of load-elongation curves showing the effect of micro alloying on serrated flow (strain rate $3 \times 10^{-4}$ sec <sup>-1</sup> )	105
4.27	Effect of micro alloying on hardening under impact loading	107
4.28	Histogram showing effect of micro alloying on hardening under impact loading at intervals of 25 blows	108
4.29	Depth of hardening in impact hardened alloys	109
4.30	Histogram showing depth of hardening in impact hardened alloys	110
4.31	Hardness and abrasion loss in impact-slide wear after successive stages of 30 second intervals.	114
4.32	General relationship between abrasion loss and hardness in impact-slide wear	115
4.33	Hardness and abrasion loss in slide wear after successive stages of 30 second intervals	116
4.34	Histogram showing abrasion loss in impact-slide wear and slide wear at successive intervals of 30 seconds	117
4.35	Cumulative abrasion loss in impact-slide wear and slide wear	118
4.36	As cast microstructure (a) 13 Mn (b) 0.003 B (c) 0.10V (d) 0.50 Cb	124

## List of Figures(contd.)

4.37	Microstructure of heat treated alloys (a) 13 Mn (b) 0.003 B (c) 0.10 V (d) 0.50 Cb	126
4.38	Twins in impact hardened alloys (low magnification ) (a) 13 Mn (b) 0.003 B(c) 0.10 V (d) 0.50 Cb	128
4.39	Twins in impact hardened alloys (high magnification) (a) 13 Mn (b) 0.003 B (c) 0.10 V (d) 0.50 Cb	129
4.40	Decohesion at carbide-matrix interfaces in 0.50 Cb alloy (a) formation of voids (b) formation of white etching layer	131
4.41	Decohesion at carbide-matrix interfaces in 0.10 V alloy (a) formation of voids (b) formation of white etching layer	132
4.42	Scanning electron micrographs showing decohesion around carbide particles (a) 0.10 V (b) 0.50 Cb	133
4.43	SEM micrographs showing characteristics of tensile fracture in 13 Mn alloy (a,b and c different locations)	135
4.44	SEM micrographs showing characteristics of tensile fracture in 0.003 B alloy (a and b different locations)	136
4.45	SEM micrographs showing characteristics of tensile fracture in 0.10 V alloy ( a and b different locations)	137
4.46	SEM micrographs showing characteristics of tensile fracture in 0.50 Cb alloy (a and b different locations)	138
4.47	SEM micrographs showing characteristics of impact fracture in 13 Mn alloy (a and b different locations)	139
4.48	SEM micrographs showing characteristics of impact fracture in 0.003 B alloy (a and b different locations)	140
4.49	SEM micrographs showing characteristics of impact fracture in (a) 0.10 V alloy and (b) 0.50 Cb alloy	141
4.50	Micro-ploughing in 13 Mn alloy at different intervals of impact slide wear (a) 15 seconds (b) 2 minutes	146

**List of Figures(contd.)**

4.51	Microploughing in 0.003 B alloy at different intervals of impact-slide wear (a) 15 seconds (b) 2 minutes	147
4.52	Microploughing in 0.10 V alloy at different intervals of impact slide wear (a) 5 seconds (b) 2 minutes	148
4.53	Microploughing in 0.50 Cb alloy at different intervals of impact-slide wear (a) 5 seconds (b) 2 minutes	149
4.54	Extensive plastic deformation during impact-slide wear in 0.003 B alloy (a) 5 seconds (b) 2 minutes	150
4.55	Fragmentation of deformed regions during impact-slide wear in 0.003 B alloy (a) 5 seconds (b) 2 minutes	151
4.56	(a) Formation of deformed layer and (b) subsequent fragmentation during impact-slide wear in 13 Mn alloy	152
4.57	Particle-matrix decohesion and void formation during impact-slide wear in 0.10 V alloy (a) 15 seconds (b) 2 minutes	153
4.58	Particle-matrix decohesion and void formation during impact-slide wear in 0.50 Cb alloy (a) 5 seconds (b) 2 minutes	154
5.1	Relationship between wear resistance and various mechanical properties of micro alloyed Hadfield steels	184

## LIST OF TABLES

Table No.	Title	Page
1.1	Standard composition ranges for austenitic Mn steel	3
1.2	Physical properties of Hadfield steel	4
1.3	Mechanical properties of conventional Hadfield Mn steel	5
1.4	Effect of section thickness on mechanical properties of 12.7 Mn-1.10C-05 Si-0.043P castings water quenched from 1040°C	8
1.5	Effect of composition on Ms temperature of Mn steels	18
1.6a)	Effect of soaking temperature on mechanical properties of 1.1 C-12.6 Mn-0.38 Si-3.13 Ni cast steel	20
1.6b)	Effect of soaking temperature and time on mechanical properties of austenitic Mo-Mn steels	20
1.7	Mechanical properties of Hadfield Mn steel at various elevated temperatures and times	23
1.8	Relative gouging abrasion resistance in the jaw crusher test	32
1.9	Relative resistance of various materials to high stress grinding abrasion by wet quartz sand	33
3.1a)	Chemical composition of mild steel scrap used to prepare base alloy	56
3.1b)	Chemical composition of Ferro-Manganese and Ferro-silicon	56
3.2	Chemical analysis of master alloys of B, V and Cb	57
3.3	Chemical compositions of various micro alloyed Hadfield steels	59

APPENDIX : Tables of Experimental Data		Page
1.	Mechanical properties of 13 Mn steel	210
2.	Effect of B additions on mechanical properties	211
3.	Effect of V additions on mechanical properties	212
4.	Effect of Cb additions on mechanical properties	213
5.	Effect of micro alloying on strain hardening exponent ( $\eta$ )	214
6.	Effect of impact loading on surface hardening	215
7.	Work hardening and slide wear characteristics of 13 Mn steel	216
8.	Work hardening and slide wear characteristics of 0.003 B steel	217
9.	Work hardening and slide wear characteristics of 0.10 V steel	218
10.	Work hardening and slide wear characteristics of 0.50 Cb steel	219
11.	Work hardening and impact-slide wear characteristics of 13 Mn steel	220
12.	Work hardening and impact-slide wear characteristics of 0.003 B steel	221
13.	Work hardening and impact-slide wear characteristics of 0.10 V steel	222
14.	Work hardening and impact-slide wear characteristics of 0.50 Cb steel	223

---

\*\*\*\*\*

CHAPTER-1

LITERATURE REVIEW

\*\*\*\*\*

## CHAPTER-1

### LITERATURE REVIEW

#### 1.1 INTRODUCTION

The austenitic Mn steel, also known as Hadfield steel, was invented by Sir Robert Hadfield[1-6] in 1882. Hadfield steel is unique in that it combines high toughness and ductility with high work hardening capacity and good resistance to abrasion. Hence Hadfield steel has rapidly gained acceptance as a very useful engineering material.

Austenitic Mn steel is used extensively in the fields of earthmoving, mining, quarrying and oil well drilling. It is also used for grinding and crushing equipments for cement manufacturing, coal crushing, rail roading, dredging and lumbering. Another important use is in railway track work at frog switches and crossings, where multiple impacts at intersections are especially severe. Since Hadfield steel resists metal to metal wear, it is used in sprockets, pinions, gears, wheels, conveyor chains, wear plates and shoes. Non-magnetic characteristics of this material expands its field of application in lifting magnets, induction furnaces and special electrical application equipments.

Austenitic Mn steel has certain properties that tend to restrict its applications. It is difficult to machine and



usually has a low yield strength. Consequently it is not well suited for parts that require close tolerance machining or that must resist plastic deformation when highly stressed in service. Though by advancement in machining technology, it has been possible to machine Hadfield steel to certain extent.

Standard composition ranges for austenitic Mn steel, as listed in ASTM A-128-64 [7], are given in Table 1.1. These cover C from 1.0 to 1.4 pct. and Mn from 10 to 14 pct. with or without addition of other alloying elements such as Cr, Mo, Ni, V, Ti and Bi. However, commercial alloys with Mn contents greater than 12 to 13 pct. are seldom used because of cost consideration. Work hardening tendency, which is an important property of such steels, also appears to be optimum at 13 pct. Mn [8].

Hadfield steel attains its characteristic properties only after correct heat treatment. It is usually austenitized to dissolve carbides and to produce homogeneous austenite which is preserved by water quenching from above 1050°C. The physical and mechanical properties of this steel have been studied by many workers [9-14] and these are given in Tables 1.2 and 1.3. It is seen that there is significant difference in the mechanical properties of wrought and cast steels, which is primarily because of difference in grain size. Wrought Mn steels are of finer grain size.

TABLE 1.1

## STANDARD COMPOSITION RANGES FOR AUSTENITIC Mn STEEL[Ref.7]

ASTM A128 grade	C	Composition, (wt. pct)					
		Mn	Cr	Mo	Ni	Si (max)	P (max)
A	1.05-1.35	11.0min	...	...	...	1.00	0.07
B-1	0.9-1.05	11.5-14.0	...	...	...	1.00	0.07
B-2	1.05-1.2	11.5-14.0	...	...	...	1.00	0.07
B-3	1.12-1.28	11.5-14.0	...	...	...	1.00	0.07
B-4	1.2-1.35	11.5-14.0	...	...	...	1.00	0.07
C	1.05-1.35	11.5-14.0	1.5-2.5	...	...	1.00	0.07
D	0.7-1.3	11.5-14.0	...	...	3.0-4.0	1.00	0.07
E-1	0.7-1.3	11.5-14.0	...	0.9-1.2	...	1.00	0.07
E-2	1.05-1.45	11.5-14.0	...	1.8-2.1	...	1.00	0.07
F	1.05-1.35	6.0-8.0	...	0.9-1.2	...	1.00	0.07

TABLE 1.2

## PHYSICAL PROPERTIES OF HADFIELD STEEL [Ref.14]

1)	Melting point	:	Liquidus	:	1400°C				
			Solidus	:	1350°C				
2)	Specific gravity	:	7.9	at	15°C				
3)	Density	:	7.8	Kg-m <sup>-3</sup>					
4)	Specific heat	:	J/Kg/°C						
	Temperature range °C	:	50-100		150-200		350-	440	
	Mean specific heat								
	(x10 <sup>-3</sup> )	:	0.518		0.565		0.607		
			550-600		750-800		950-1000		
			0.703		0.648		0.674		
5)	Thermal conductivity	:	J/m/sec/°C						
	Temperature °C	:	0		200		400		600 800 1000
	Thermal conductivity								
	(x10 <sup>-3</sup> )	:	1.30		1.63		1.92		2.17 2.34 2.55
6)	Magnetic permeability:		1.003 - 1.03		( H = 24)				
7)	Electrical Resistivity:		micro-ohms - m <sup>3</sup>						
	Temperature °C	:	-183		0		100		200 400 800
	Resistivity(x10 <sup>-6</sup> )	:	53		66		76		84 99 121

TABLE 1.3

## MECHANICAL PROPERTIES OF CONVENTIONAL HADFIELD Mn STEEL

[Ref. 13, 14]

## 1. TENSILE :

Condition	YS	UTS	El	Reduction in area	VHN
	MPa	MPa	pct.	pct.	
Cast	330-410	610-990	15-40	15-40	200-235
Wrought	330-425	840-990	40-60	35-50	200-235

## 2. BEND TEST:

Cast steel 120° unbroken

Wrought steel 180° unbroken

## 3. IMPACT STRENGTH: (Charpy V notch impact strength)

110-130 Joules

4. COMPRESSION : Manganese steel is capable of withstanding a compressive stress of 5320 MPa without rupture, with a corresponding deformation of 50 to 55 pct.

5. WORK HARDENING CAPACITY: From an initial hardness of 200-235 VHN to 650-700 VHN

contd.

Table 1.3 (contd.)

## 6. FATIGUE:

C	Compositions (Wt.pct)			Stress MPa	Cycles to failure
	Mn	Si	P		
1.17	12.8	0.34	0.046	270	4,071,500
1.17	12.8	0.34	0.046	270	806,000
1.13	12.8	0.55	0.056	320	294,800
1.13	12.8	0.55	0.056	270	853,900
1.13	12.8	0.55	0.056	260	12,663,600
1.13	12.8	0.55	0.056	245	30,600,000

## 7. RUPTURE STRESS : (MPa, to give rupture in 1000 hours)

Temperature °C	200	300	400	550
Rupture stress MPa	870	680	450	110

Mechanical properties also vary largely with section thickness. For example, tensile strength, elongation, reduction in area and impact strength are substantially lower in thicker sections (Table 1.4) [13]. This occurs because heavy sections do not solidify fast enough in the mould to prevent coarse grain structure, a condition that is not altered by heat treatment. Fine grained specimen exhibits strength and elongation as much as 30 pct. greater than those of coarse grained specimens. Austenitic Mn steel remains tough at sub zero temperature. It is apparently immune to hydrogen embrittlement. Hardness of most grades is about 220 VHN after toughening. This value increases rapidly under applied stress with deformation. Hadfield steels generally show high wear resistance in service. Resistance to crack propagation in Hadfield steel is high and is associated with very sluggish progressive failures. Because of this, any fatigue cracks that develop can be monitored closely, and affected parts can be removed from service before complete failure occurs. The fatigue properties of austenitic Mn steel are given in Table 1.3[13].

## 1.2 STRUCTURAL CHARACTERISTICS OF HADFIELD STEEL

Austenitic Mn steel is toughened by a high temperature quenching treatment and embrittled by subsequent tempering, a tendency which is directly opposite to that of the usual hardenable engineering steels. The Fe-C-Mn system is able to yield a reasonable comprehensive knowledge of the structural characteristics of Hadfield steel [15-32].

TABLE 1.4

EFFECT OF SECTION THICKNESS ON MECHANICAL PROPERTIES OF 12.7Mn-1.10C-0.5Si-0.043P CASTINGS WATER QUENCHED FROM 1040°C [Ref.13]

Plate thickness mm	Type of grain	UTS		El (in 25mm gauge length) pct.	Reduction in area, pct.	Impact strength (Izod V-notch)	
		MPa	ksi			J	Ft-lb
50	Coarse	635	92	37.0	35.7	137	101
	Fine	820	119	45.5	37.4	134	99
83	Coarse	620	90	25.0	34.5	133	98
	Fine	765	111	36.0	33.0	115	85
140	Coarse	545	79	22.5	25.6	115	85
	Fine	705	102	32.0	28.3	100	74
190	Coarse	455	66	18.0	25.1	77	67
	Fine	725	105	33.5	29.2	66	49

Fig. 1.1 represents the effect of Mn content on stability of the austenite phase at elevated temperature [15]. The areas above the solid lines for each Mn content represent regions of austenite. Increase in Mn percentage increases the stability of austenite phase even at lower temperature. It also affects the eutectoid temperature and eutectoid C percentage. Linden [19] summarised information on the constitution of Fe-C-Mn alloys in a series of sections through the Fe-C-Mn equilibrium diagrams along planes of constant C and constant Mn. Two of these diagrams for 1.0 pct. C and for 13.0 pct. Mn are reproduced in Figs.1.2 and 1.3 respectively. The phases present for various C and Mn concentrations at various temperatures under equilibrium conditions are austenite( $\gamma$ ), carbide  $(\text{Fe Mn})_3\text{C}$  and  $\alpha$  and  $\epsilon$  irons. The eutectoid C concentration at 13.0 pct Mn is approximately 0.3 pct. and the eutectoid temperature ( $A_1$ ) is 600°C.

It is seen that Mn content displaces the various critical temperatures, composition of the eutectoid and alters the position of the austenite field (Figs.1.4 and 1.5) which add to the stability of austenite[15]. In the 13.0 pct. Mn steel, the  $AC_3$  temperature rises with the C content from 600°C at 0.37 pct. C to 1100°C at 1.4 pct. C(Fig.1.6). At 1.0 pct. C the  $A_1$  temperature falls from approximately 725°C to 450°C as concentration of Mn increases from zero to 20 pct., while



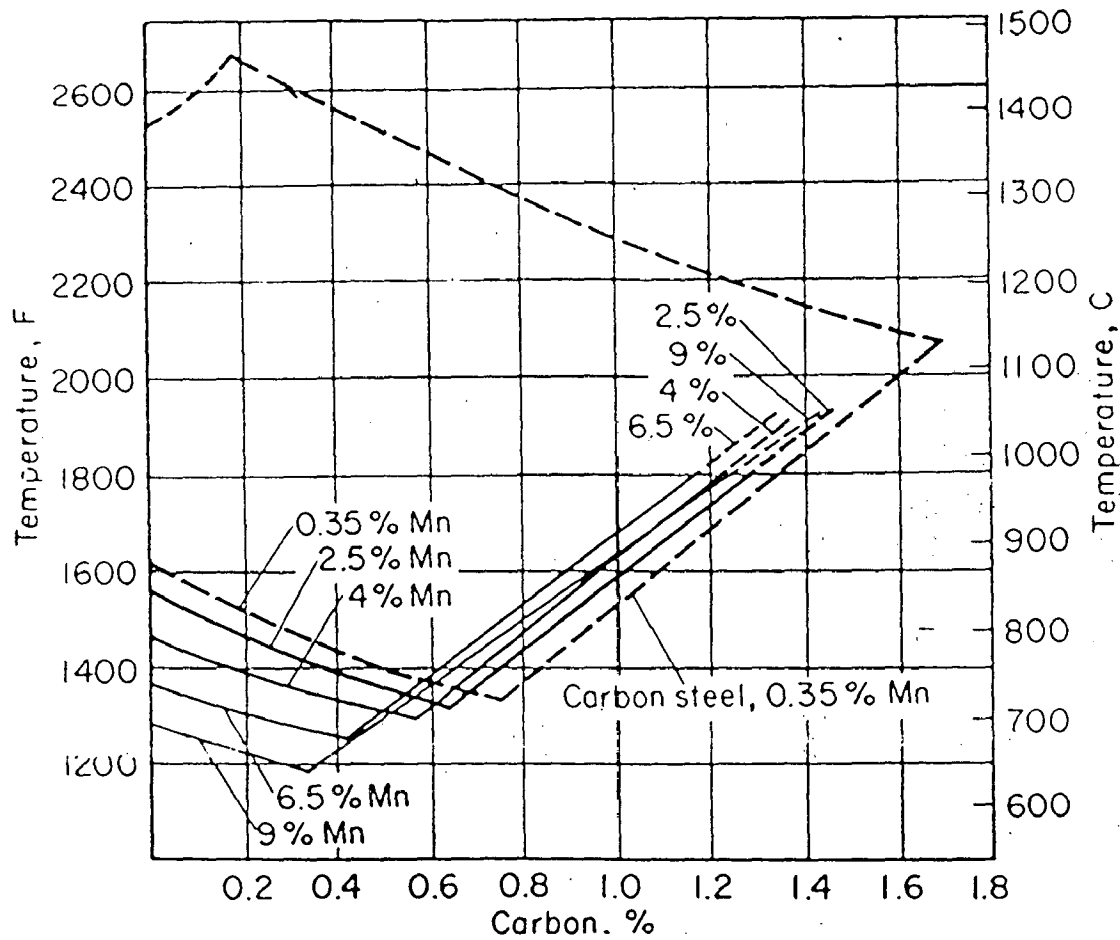


FIG.1.1 EFFECT OF Mn CONTENTS ON THE C LIMITATIONS FOR PURE AUSTENITE AT ELEVATED TEMPERATURES[Ref.15]

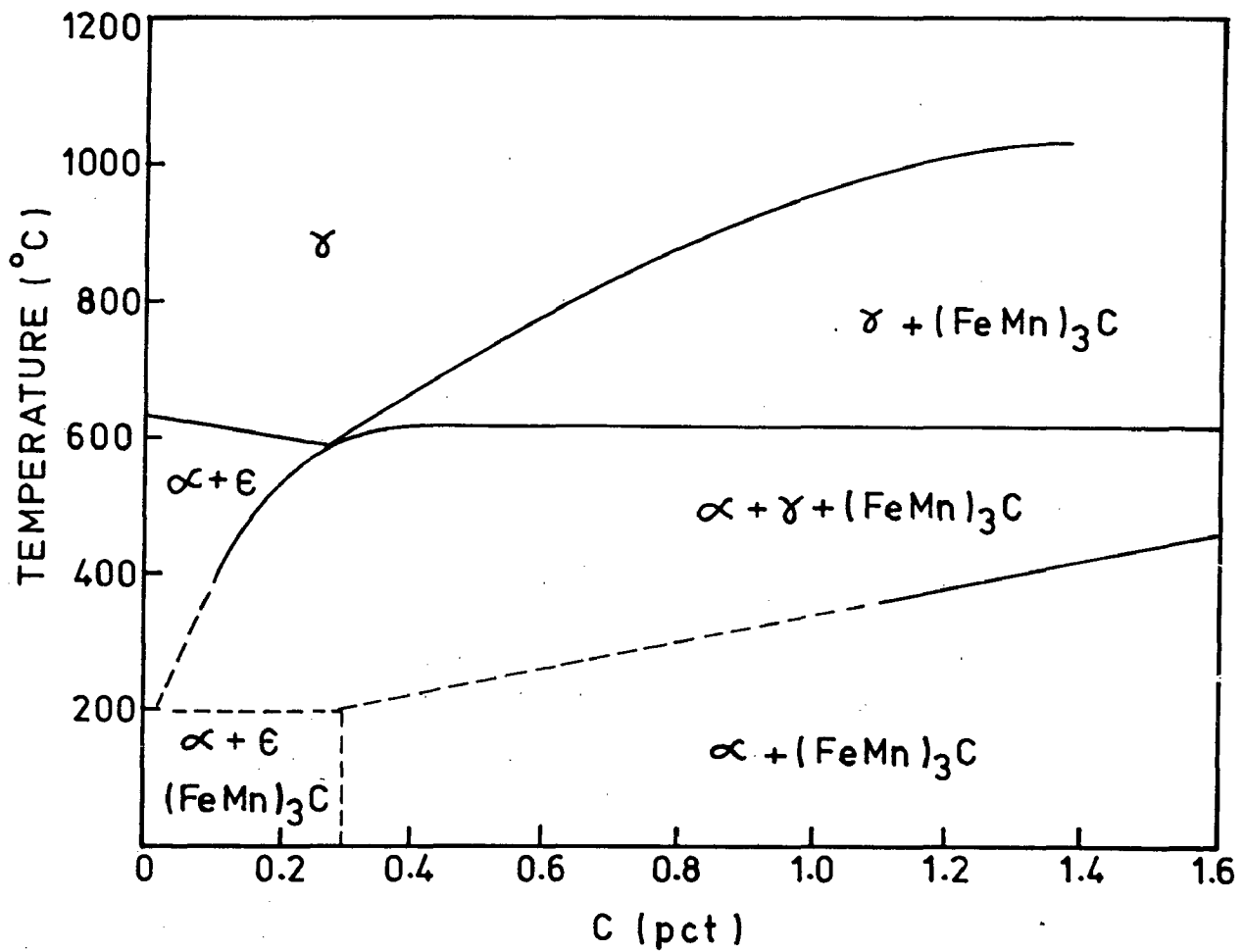


FIG.1.2 SECTION THROUGH THE Fe-Mn-C SYSTEM  
AT 13 pct Mn [ Ref.19 ]

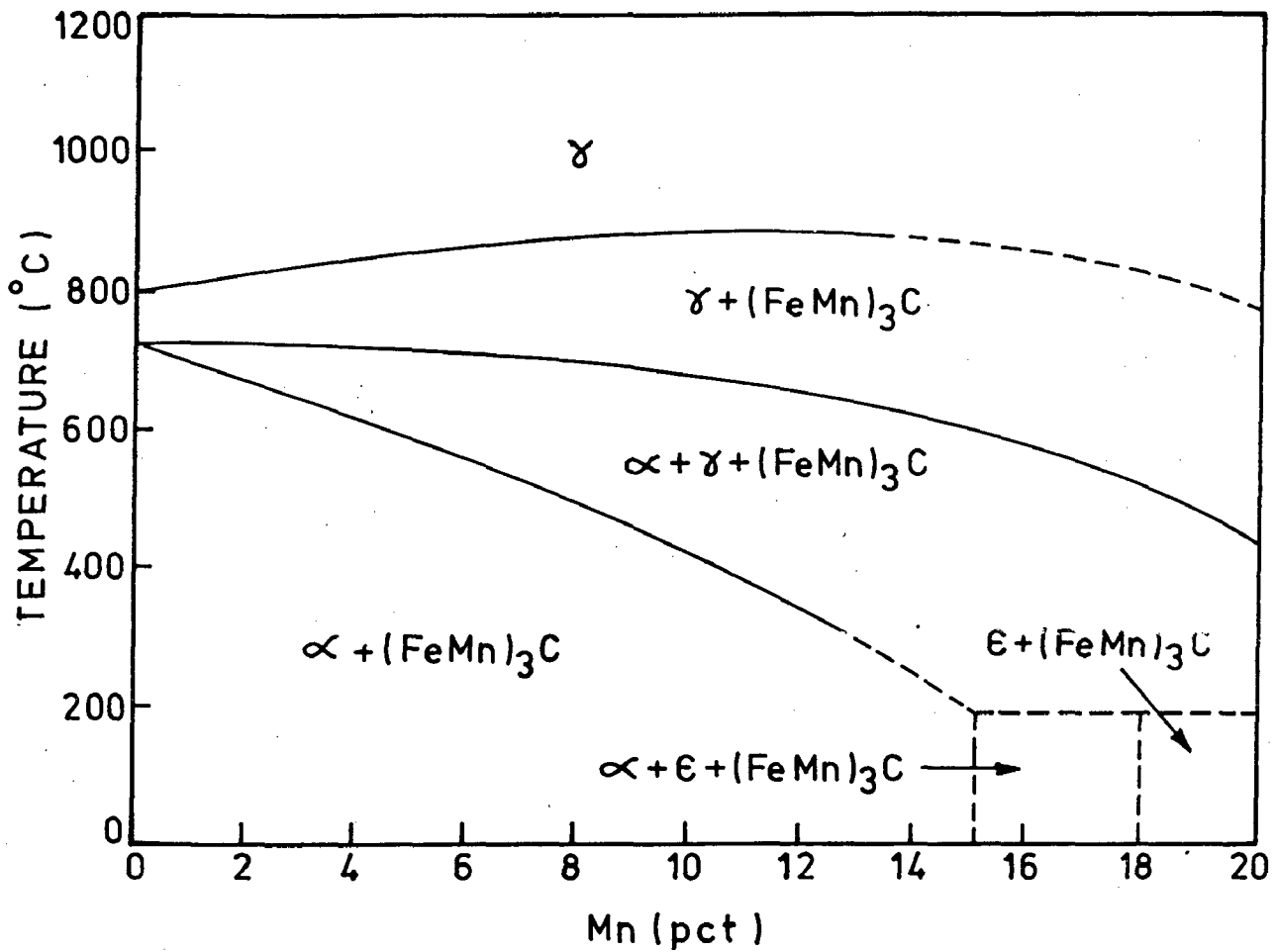


FIG.1.3 SECTION THROUGH THE Fe-Mn-C SYSTEM AT 1.0 pct C [Ref. 19]

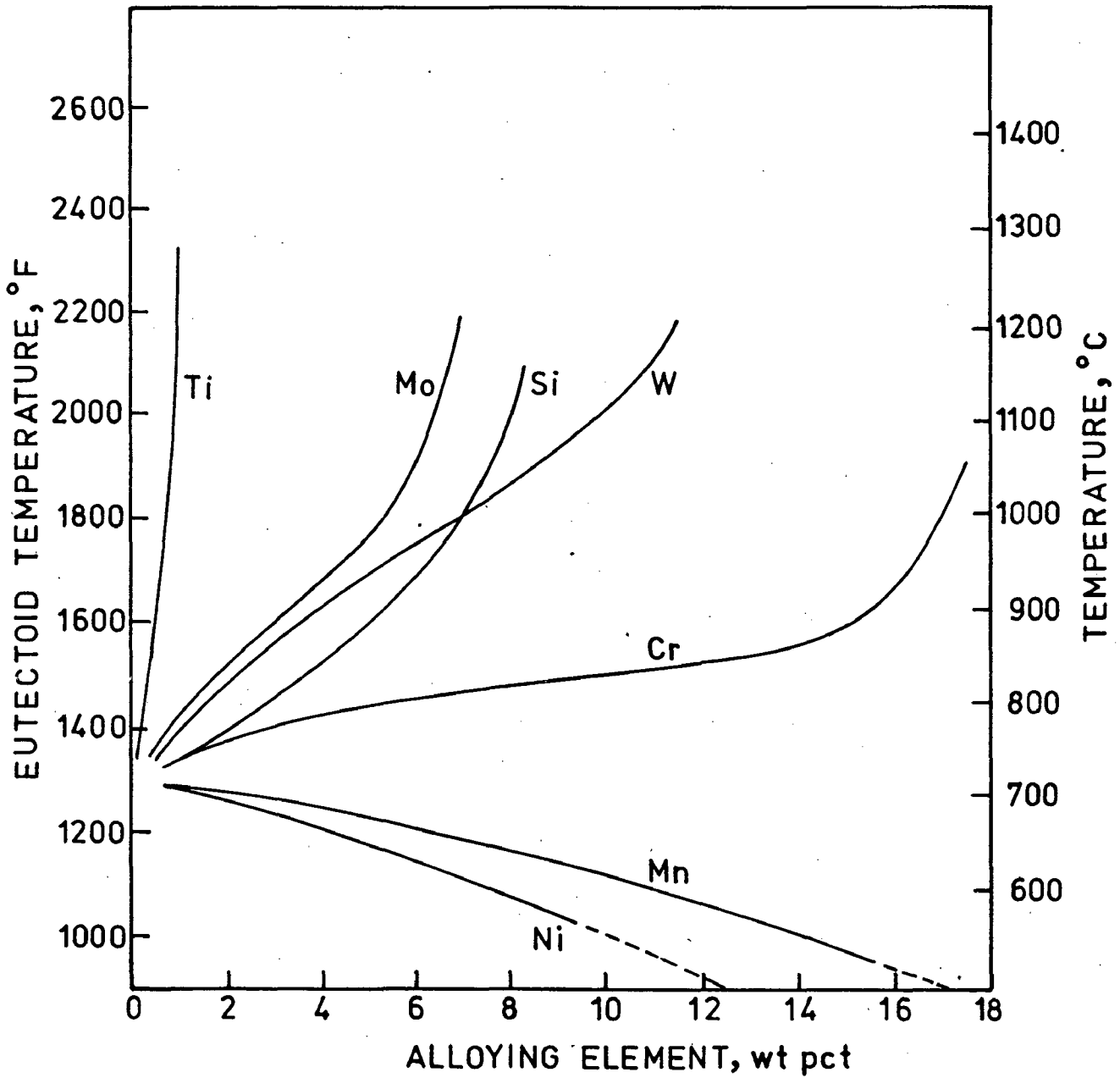


FIG.1.4 EFFECT OF VARIOUS ALLOYING ELEMENTS INCLUDING Mn ON EUTECTOID TEMPERATURE. [Ref.15]

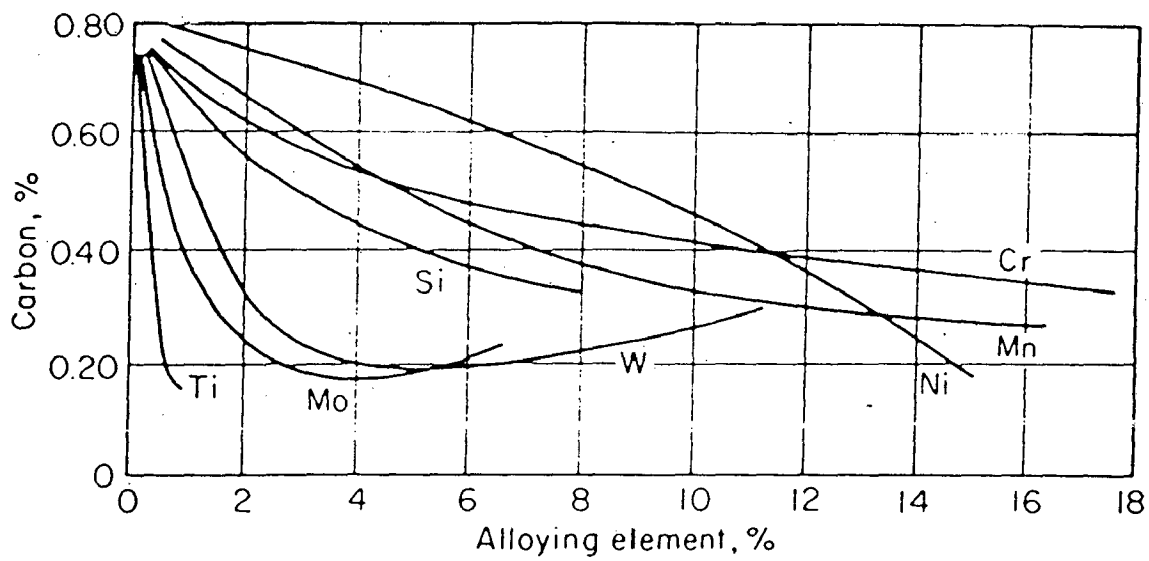


FIG.1.5 EFFECT OF VARIOUS ALLOYING ELEMENTS INCLUDING Mn ON EUTECTOID COMPOSITION (Ref.15)

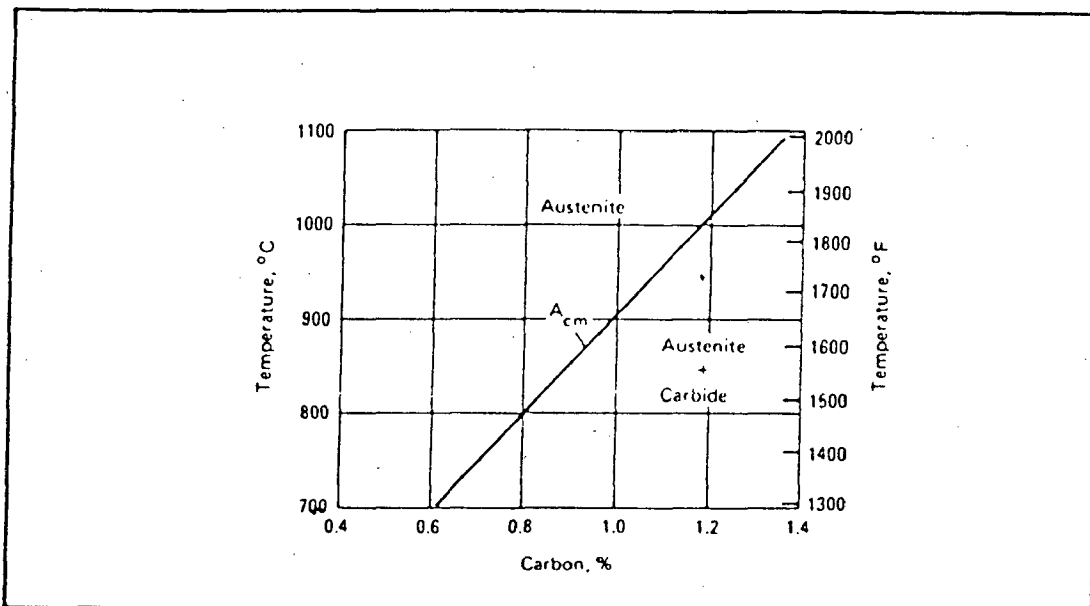


FIG.1.6 SOLUBILITY OF C IN 13 pct. Mn STEEL[Ref.13]

the  $AC_3$  temperature remains between  $800^\circ\text{C}$  to  $880^\circ\text{C}$  over the Mn range 0-20 pct. In conventional commercial composition of Mn steel the  $A_e$  temperature is of the order of  $650-670^\circ\text{C}$ .

Transformations on continuous cooling will largely depend on rate of cooling. Rapid cooling from the austenitising temperature is necessary to retain the C in solution and to maintain the austenitic condition. On cooling from temperatures over  $Ar_3$ , the critical cooling rate to ensure retention of the whole of the C in solution is higher than that necessary to retain the austenitic condition. At a rate of cooling slower than that critical cooling rate, but still fast enough to prevent  $Ar_1$  transformation, carbide is precipitated at the austenite grain boundary. At still slower cooling rates, some of austenite transforms to pearlite, the concentration of which increases as the cooling rate is further lowered.

Isothermal transformation of austenitised Mn steel occurs at temperatures between  $300^\circ\text{C}$  and  $A_1$  with slow production of acicular or granular pearlitic structures associated with free carbide [28].

The effect of C and Mn contents on the variation of martensitic transformation is shown in Fig.1.7 and Table 1.5[33]. It is seen that with increase in Mn content the  $M_s$  temperature is reduced and the stability of austenite is increased.

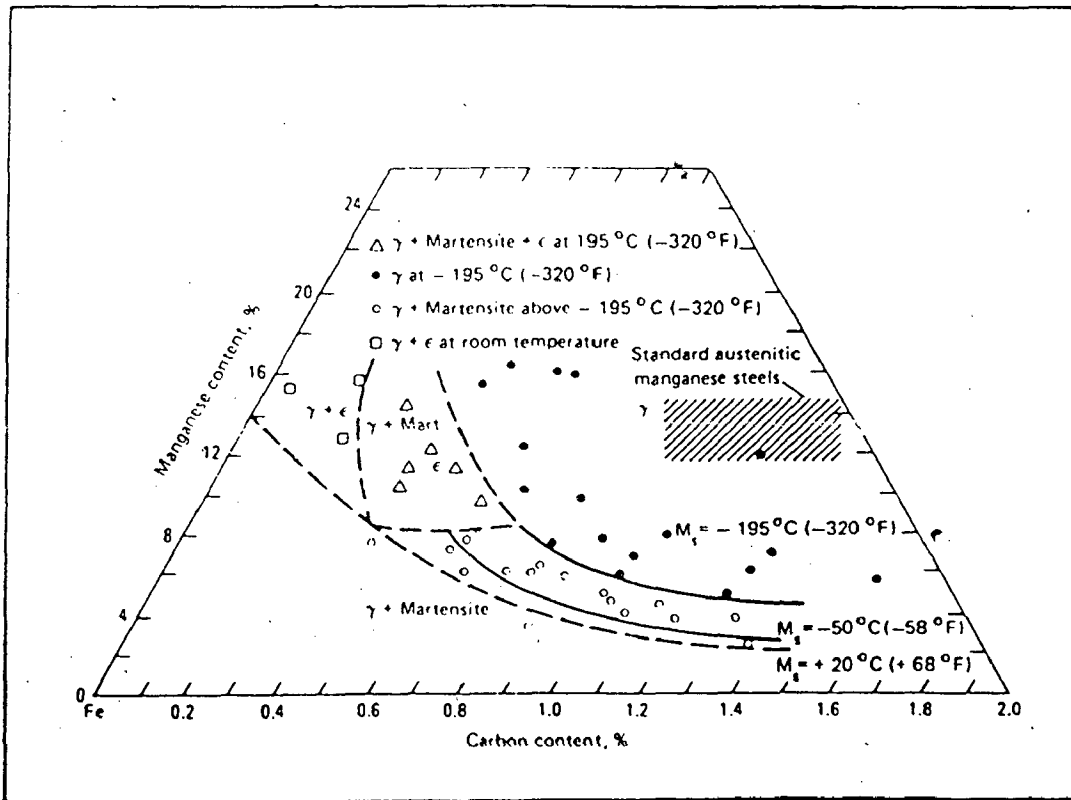


FIG.1.7 VARIATION OF  $M_s$  TEMPERATURE WITH C AND Mn CONTENTS (Ref.27)



Conventional Mn steel possess stable austenite at room temperature. The Ms temperature for 12.0 pct. Mn alloy is  $-196^{\circ}\text{C}$  [33]. The alloys with less than 12 pct. Mn have metastable austenites and martensitic transformation begins spontaneously at temperatures below Ms.

TABLE 1.5

EFFECT OF COMPOSITION ON Ms TEMPERATURE OF Mn STEELS[Ref.33]

Alloy	Chemical composition (wt.pct)			Ms $^{\circ}\text{C}$
	C	Mn	Si	
12 Mn	1.14	13.4	0.43	-196
8 Mn	1.16	7.75	0.33	-196
6 Mn	1.16	6.03	0.29	-196
5 Mn	1.16	4.98	0.31	- 57
4 Mn	1.15	3.97	0.29	- 31
8 Mn-0.7C	0.69	8.30	0.22	- 2

Stress-induced transformation of metastable austenites is observed to occur at temperatures greater than Ms when a shear stress  $T_{\text{M}}$  acts in the direction of martensite shear [34].  $T_{\text{M}}$  is zero at Ms and increases with decreasing under cooling  $\Delta T < T_0 - M_s$ , i.e. with decreasing chemical driving

force for the martensitic transformation. Surface martensite has also been observed in metastable austenitic Mn steels [35, 36].

### 1.3 HEAT TREATMENT

Heat treatment strengthens austenitic Mn steel so that it can be used safely and reliably in a wide variety of engineering applications. Commercial heat treatment of Mn steel involves heating slowly to 1010-1090°C, soaking for 1 to 2 hours at temperature and then quenching in agitated water. Variation of this treatment can be used to enhance specific desired properties.

The change in soaking temperature, soaking time and rate of cooling causes variations in the mechanical properties of austenitic Mn steel. The effect of soaking temperature on mechanical properties of austenitic Ni-Mn steel is given in Table 1.6(a) [32] and effect of soaking time on mechanical properties of austenitic Mo-Mn steel is given in Table 1.6(b) [32]. The effect of cooling rate (in terms of section thickness) on the mechanical properties of standard Mn steel is presented in Table 1.4 [13]. It is seen that speed of quenching is an important factor to avoid any carbide precipitation. But it is difficult to increase it beyond the rate of heat transfer from a hot surface to agitated water or the rate fixed by the thermal conductivity of the metal. This is the

TABLE 1.6

(a) EFFECT OF SOAKING TEMPERATURE ON MECHANICAL PROPERTIES OF 1.1C - 12.6 Mn-0.38Si-3.13 Ni CAST STEEL [Ref.32]

Soaking temperature °C	Soaking time hr	UTS MPa	El pct.	Reduction in area pct	VHN
1040	1	915	63.0	43	187
960	1	885	53.0	38	200
930	1	855	51.0	38	196

(b) EFFECT OF SOAKING TEMPERATURE AND TIME ON MECHANICAL PROPERTIES OF AUSTENITIC Mo-Mn STEELS [Ref.32]

Chemical composition (wt. pct)				Soaking Temp. °C	Soaking time hr.	UTS MPa	El pct.	Reduction in area pct.	VHN
C	Mn	Si	Mo						
0.52	14.3	0.47	2.4	1040	2	725	25.0	18	228
0.91	14.1	0.60	2.0	1040	2	860	48.5	31	230
1.03	13.9	0.54	1.0	1090	2	785	45.0	37	220
1.23	12.9	0.56	2.0	1090	4	805	40.0	33	228

reason for lower mechanical properties in heavier sections relative to thinner sections.

Reheating of the austenitized and toughened Mn steel to intermediate temperature has pronounced effects upon the properties. The structural transformation when reheated induces acicular carbide precipitates and some transformation of the austenite to pearlite causing embrittlement in the structure of toughened Mn steel. Time-temperature relationship for embrittlement of 13 Mn-1.2C-0.5 Si steel is shown in Fig.1.8. Reheating upto 260°C does not cause any embrittlement in Mn steel.

The effect of reheating of the toughened Mn steel on the physical and mechanical properties has been studied by many workers[30,31]. Reheating between 400°C to 700°C causes significant decrease in ductility and increase in hardness. Physical properties like magnetic properties, thermal and electrical conductivity are also significantly altered by reheating. The effect of various reheating temperatures on mechanical properties are given in Table 1.7 [13] and Fig.1.9.

#### 1.4 CHARACTERISTIC PROPERTIES OF HADFIELD STEEL

Hadfield steel with high strength and toughness has a unique property of high work hardening capacity under impact loading and usually good resistance to abrasion. These combinations of properties make this steel of vast importance in

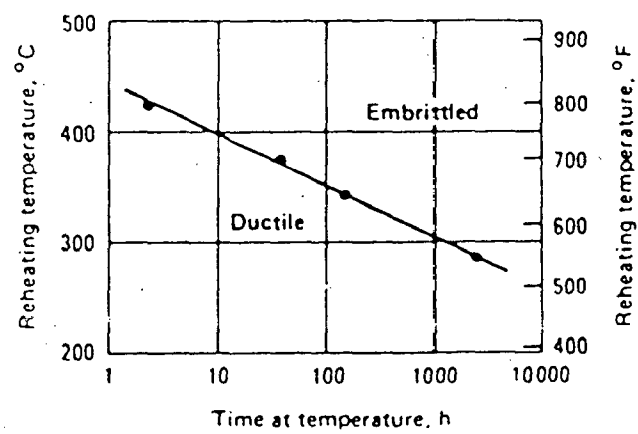


FIG.1.8 TIME-TEMPERATURE RELATIONSHIP FOR EMBRITTLEMENT OF 13 Mn-1.2 C-0.5 Si STEEL [Ref.13]

TABLE 1.7

MECHANICAL PROPERTIES OF HADFIELD Mn STEEL AT VARIOUS REHEATED TEMPERATURES AND TIME [Ref.13]

Condition	Time of reheat- ing hr.	UTS MPa	YS MPa	El pct.	Reduc- tion in area pct.	VHN		Charpy V- notch im- pact st- rength	
						J	Ft-lb	J	Ft-lb
12% Mn steel solution treat- ed, reheated at 370°C	0.0	615	340	28	31	164	129	95.5	
	0.5	560	325	26	25	175	117	86.2	
	2.0	600	315	27	30	168	137	100.7	
	10.0	670	330	31	30	177	112	82.5	
Reheated at 480°C	0.5	620	330	29	31	177	138	101.7	
	2.0	565	325	24	20	171	115	84.5	
	10.0	460	345	6	6	177	12	8.5	
Reheated at 590°C	0.5	395	325	4	7	173	12	8.8	
	2.0	475	350	1	1	182	5	3.8	
	10.0	540	340	1	1	180	3	2.3	

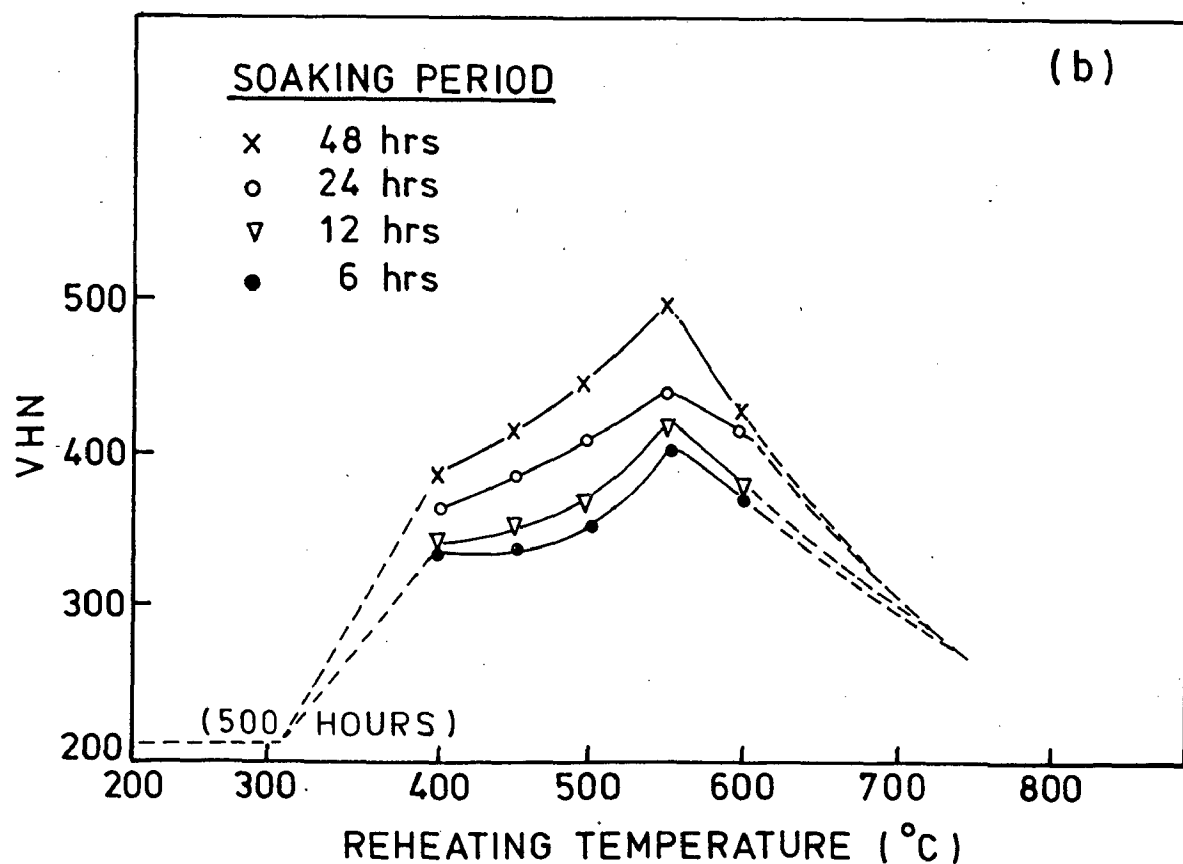
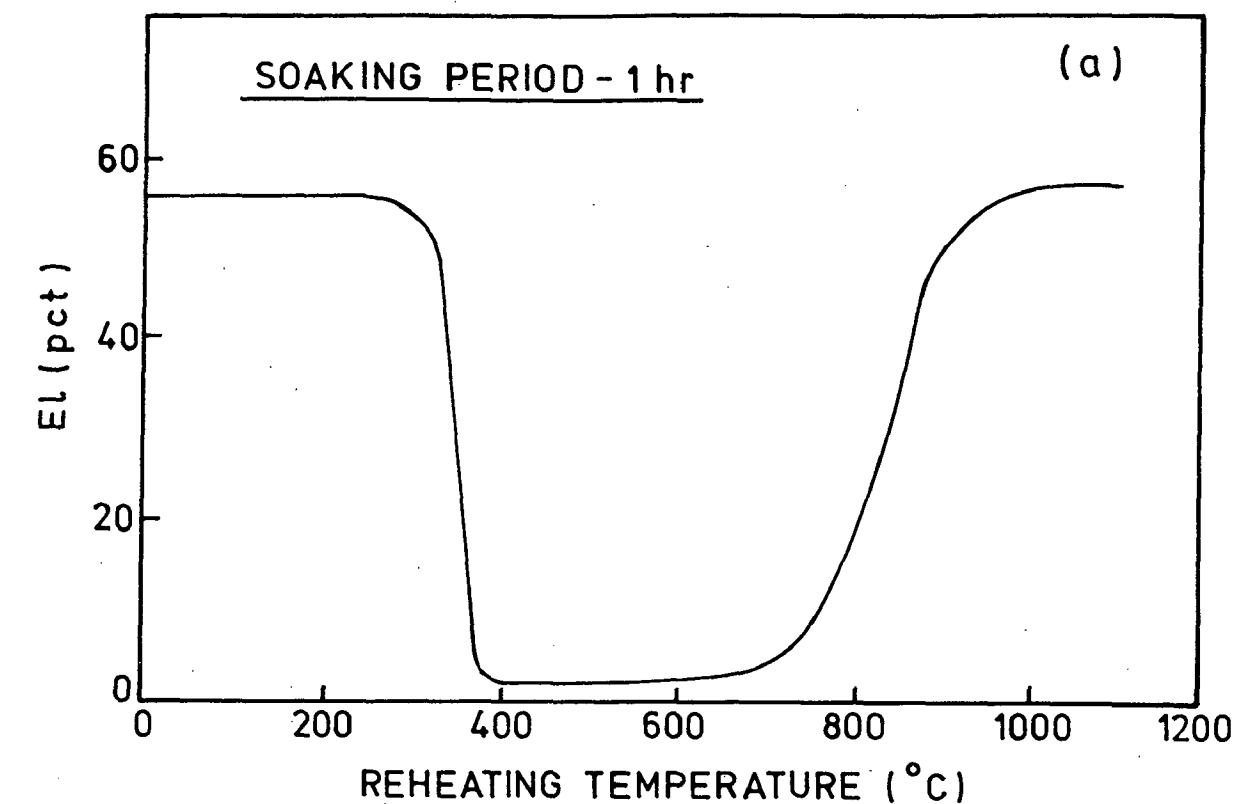


FIG.1.9 EFFECT OF REHEATING TEMPERATURES ON ELONGATION AND HARDNESS OF TOUGHENED HADFIELD STEEL. [ Ref. 14 ]

diverse applications such as crawler treads, grinding mill liners, crusher jaws and cones, impact hammers and dipper teeth etc. In these steels, the pronounced abrasion resistance results largely from the rapid work hardening produced by service conditions.

#### 1.4.1 Work Hardening Characteristics

Hadfield steel is unequalled in its ability to work harden, exceeding even the metastable austenitic stainless steel in this feature [13,37]. A standard Mn steel can be work hardened from an initial level of 220 VHN to more than 900 VHN. Maximum attainable hardness depends upon many factors including specified composition, service limitations and method of work hardening. Work hardening in Mn steels is usually induced by impact from hammer blows. Light blows with high velocity cause shallow deformation with only superficial hardening even though the resulting surface hardness is high. Heavy impact produces deeper hardening with lower values of surface hardness. The course of flow under impact and the associated increase in hardness is given in Fig.1.10, which compares a standard 12 pct. Mn steel with an air-hardening Cr-Ni-Mo alloy steel.

Mechanisms of work hardening in Hadfield steels have been studied very extensively [38-72]. The various mechanisms to explain the cause of rapid work hardening of Hadfield steel are listed as below :



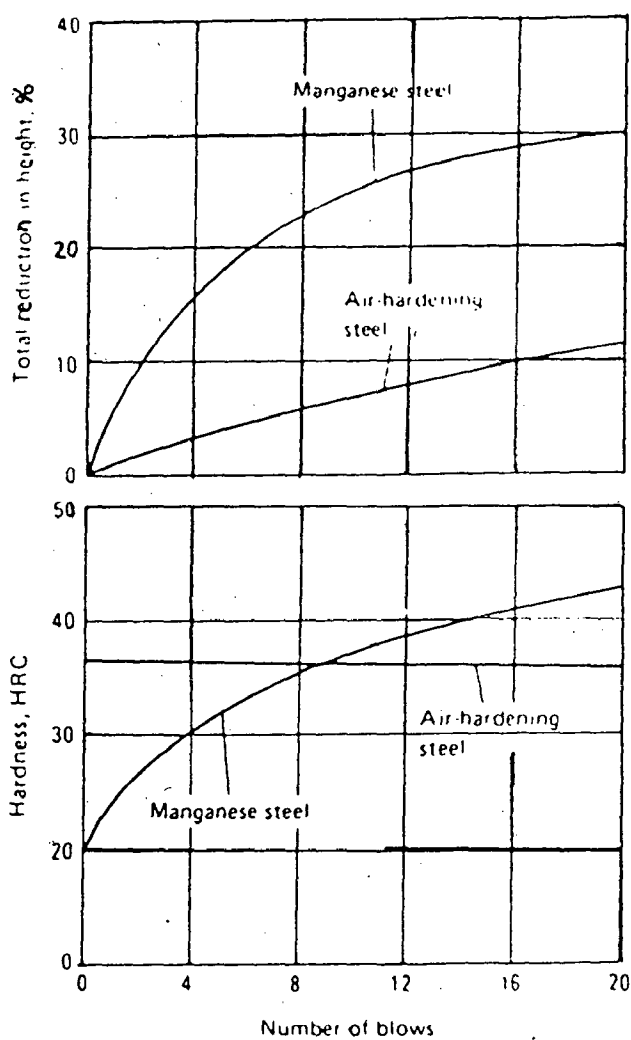


FIG.1.10 COURSE OF FLOW UNDER IMPACT LOADING AND ASSOCIATED INCREASE IN HARDNESS [Ref.13]

- i) Strain induced transformation of austenite to martensite [39-45]
- ii) Fine mechanical twinning [46-48]
- iii) Stacking fault-dislocation interaction[45,49-53]
- iv) Dynamic strain aging, brought about by the re-orientation of C member of C-Mn couples in the cores of dislocations. [38, 54-72]

It has been argued that the rapid work hardening in Hadfield steel arises from strain-induced transformation of the austenite to martensite [39]. In metastable austenites the martensitic transformation begins spontaneously at  $M_s$ . The austenite phase in conventional Hadfield Mn steel is however stable during plastic strain and hence does not transform to martensite under normal conditions [40-43]. Nakagowa [46] and Sastri [47] attributed the rapid work hardening to fine mechanical twinning. Dastur and Leslie[38] observed that at  $-50^\circ\text{C}$  numerous twins were formed but the work hardening was low and no twins were observed above  $225^\circ\text{C}$  even though work hardening was high. Drobnyak and Parr[49] suggested that ~~stacking fault dislocation interaction is responsible~~ for increasing the strain hardening rate. The large number of substitutional atoms of Mn considerably lowers the stacking fault energy in Hadfield steel and also during deformation, interstitial C atoms are able to diffuse to defects, such as dislocations and stacking faults, and to lock them resulting

into exceptional work hardening of Hadfield steel. The stacking fault energy of conventional Mn steel is determined to be  $50 \text{ mJ/m}^2$  at room temperature [50]. But it was observed that stacking fault energy of Hadfield steel is higher than those of other fcc metals such as Ag ( $16 \text{ mJ/m}^2$ ) [52], austenitic stainless steel ( $2.0 \text{ mJ/m}^2$ ) [51] and Au ( $32 \text{ mJ/m}^2$ ) [53] whose work hardening rates are much lower than that of Hadfield steel so stacking fault dislocation interaction could not be the principal cause of rapid work-hardening of austenitic Mn steel. According to some observations [38, 54-72], dynamic strain aging is the principal cause of rapid work hardening. When Hadfield steel in the single phase austenitic condition is strained in tension, in the temperature range  $-25^\circ\text{C}$  to  $300^\circ\text{C}$ , it exhibits a jerky (serrated) flow, a negative strain-rate dependence of flow stress and high work hardening.

#### 1.4.2 Wear Resistance

The unique characteristics of high toughness, strength coupled with rapid work hardening property make Hadfield steel useful for severe service conditions combining abrasion and impact. The wear characteristics are largely influenced by the type of abrasion it is exposed to [73].

Hadfield steel has excellent resistance to 'metal to metal' wear. Work hardening of Mn steel is a distinct advantage because it decreases the coefficient of friction and confers

resistance to galling if temperatures are not excessive. In metal to metal contact compressive loads, rather than impact, provide the deformation required, producing a smooth, hard surface that has good resistance to wear but that does not abrade the contacting part. Crane wheels, rails and castings for railway track work are common examples of applications of this type.

This steel has moderately good resistance to gouging abrasion, as in equipment for handling and crushing rocks. In applications that involve heavy blows or high compressive and structural stresses, the very hard and abrasion-resistant martensitic cast irons may wear more slowly than Hadfield steel. However, these irons usually fail by early fracture with a considerable portion of the original cross-section unworn, whereas Mn steel will wear almost to paper thinness before fracturing due to its high toughness. In clay crusher rolls, Mn steel lasted two to three times as long as white or chilled iron and in grinding-barrel liners, cast irons lasted only two to three years compared with ten years for Hadfield steel [32].

Austenitic Mn steel has intermediate wear resistance to high stress abrasion in ball mill and rod-mill liners, and relatively low wear resistance to low stress abrasion [74] as in equipment for handling loose sand or sand slurries.

It is not corrosion resistant and where corrosion and abrasion are combined, the metal will wear or will be dissolved at a rate only slightly lower than that of carbon steel.

Borik and Scholz [75] studied the relative wear ratios of various ferrous alloys in Jaw-crusher test. The superiority of Mn steel over other grades of steel is seen from Fig.1.11. Tables 1.8 and 1.9 give the ranking of various metals in abrasion test.

Ball [76] studied the importance of work hardening in the design of wear resistant material. According to him material is lost from a metal surface by abrasive or erosive wear when a critical fracture strain condition is experienced. A worn surface can be considered to have reached this critical strain. As material is lost at the attainment of the critical strain, material well below the surface is at the point of plastically yielding. Fig.1.12 shows the change in strain (dislocation density) with depth below worn surface. It is seen that a material which ideally never accumulates the critical fracture strain ( $\epsilon_f$ ) under the imposed abrasive stress conditions or take long time to reach the critical strain will have better wear resistance. Any component under abrasive wear will experience a spectrum or distribution of abrasive stresses but for simplicity purpose, a mean level  $\sigma_m$  may be considered (Fig.1.13). Material with type I stress-strain curve should

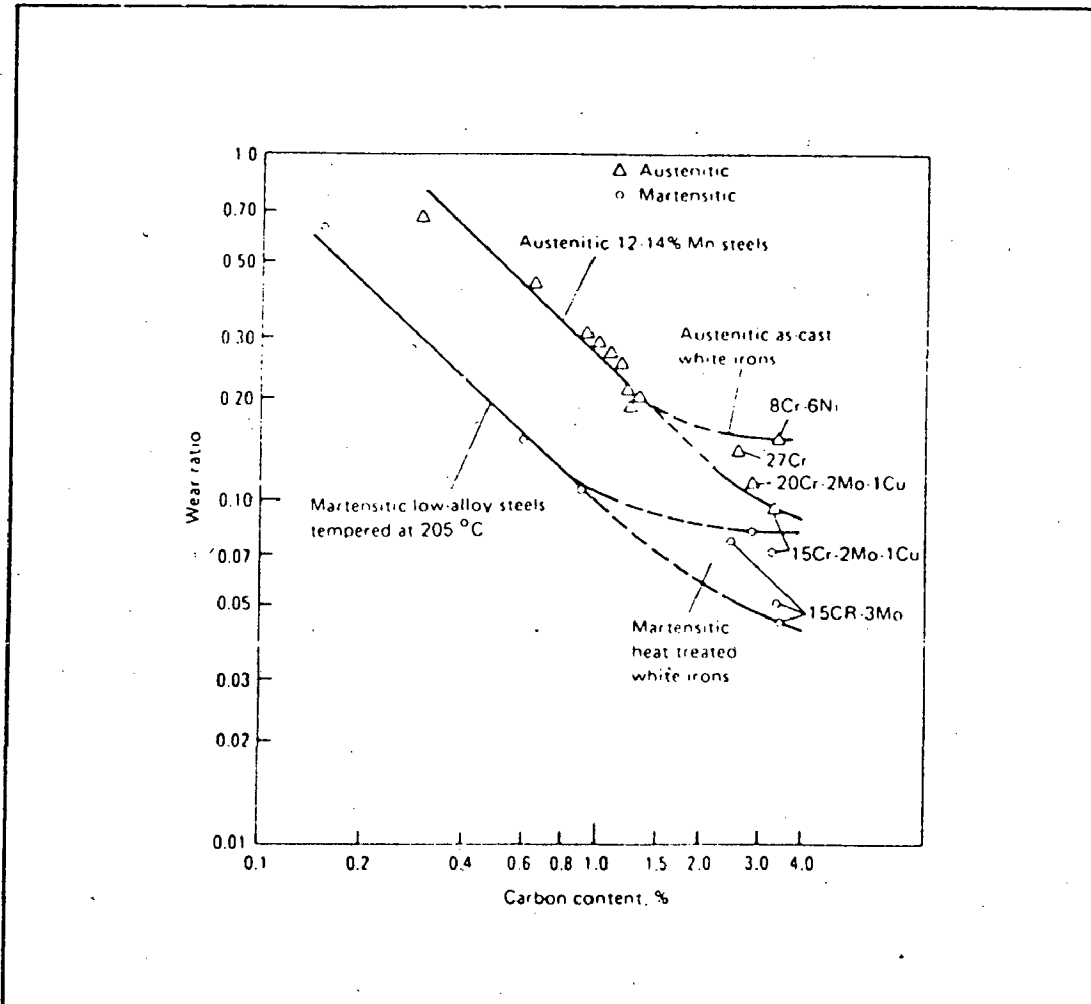


FIG.1.11 RELATIVE WEAR RATIOS OF VARIOUS FERROUS ALLOYS IN JAW CRUSHER TEST [ Ref.75 ]

TABLE 1.8

RELATIVE GOUGING ABRASION RESISTANCE IN THE JAW CRUSHER TEST  
 [Ref.75]

Material	Hardness prior to test HB	Abrasion factor (a)*
Martensitic Cr.Mo		
white iron	750	0.088
A <sub>2</sub> tool steel	653	0.127
0.50C-3Cr tool steel	653	0.164
4340 steel	555	0.262
Austenitic 12 Mn-1.16C steel	217	0.279
Martensitic 0.18C-Cr Ni steel (b)	461	0.386
4340 steel	321	0.788
Martensitic T-1 steel plate (tempered)	269	1.000
Pearlitic mild steel plate	197	1.198

Note: (a)\* Ratio of weight loss of sample to weight loss of the  
 standard material martensitic T-1 plate

TABLE 1.9

RELATIVE RESISTANCE OF VARIOUS MATERIALS TO HIGH STRESS  
GRINDING ABRASION BY WET QUARTZ SAND [Ref. 13]

Material	Brinell Hardness	Abrasion Factor(a)*
Cemented tungsten carbide	...	0.17
Martensitic cast iron(Ni- Hard)	550-750	0.25-0.60
Martensitic 4150 steel	715	0.60
Bainitic 4150 steel	512	0.75
Austenitic 12% Mn steel	500	0.75-0.85
Pearlitic 0.85% C Steel	220-300	0.75-0.85
Alloy white cast iron	400-600	0.70-1.00
Unalloyed white cast iron	400	0.90-1.00
1020 steel(standard)	107	1.00
Gray cast irons	200	1.00-1.50
Ferritic ingot iron	90	1.40

Note (a)\* Ratio of weight loss of the sample to weight loss of  
the standard material, 1020 steel



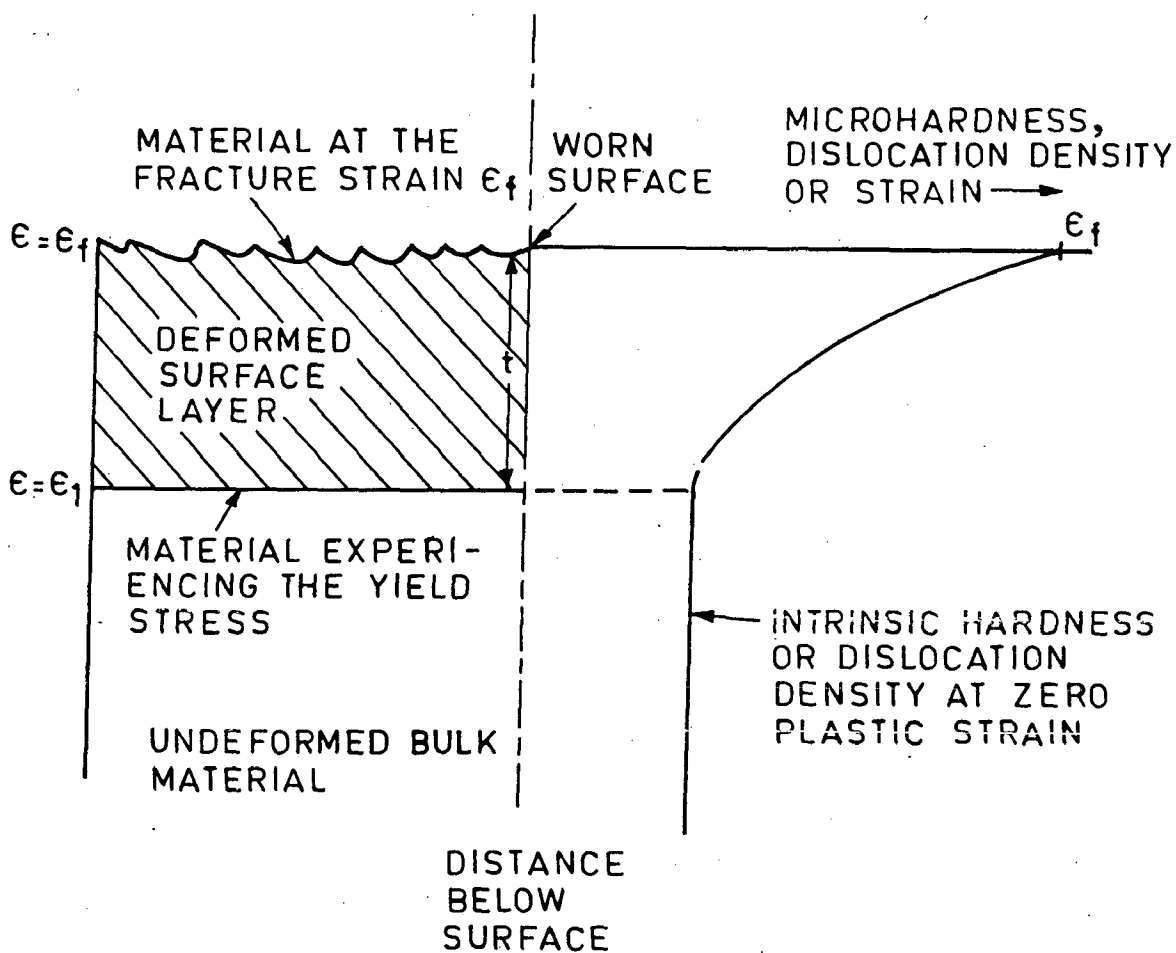


FIG.1.12 SCHEMATIC ILLUSTRATION OF THE DEFORMED SURFACE LAYER OF AN ABRADED OR ERODED MATERIAL. THE CURVE ON THE RIGHT-HAND SIDE INDICATES THE CHANGE IN MICROHARDNESS, DISLOCATION DENSITY OR STRAIN WITH DEPTH BELOW THE WORN SURFACE. [Ref. 76 ]

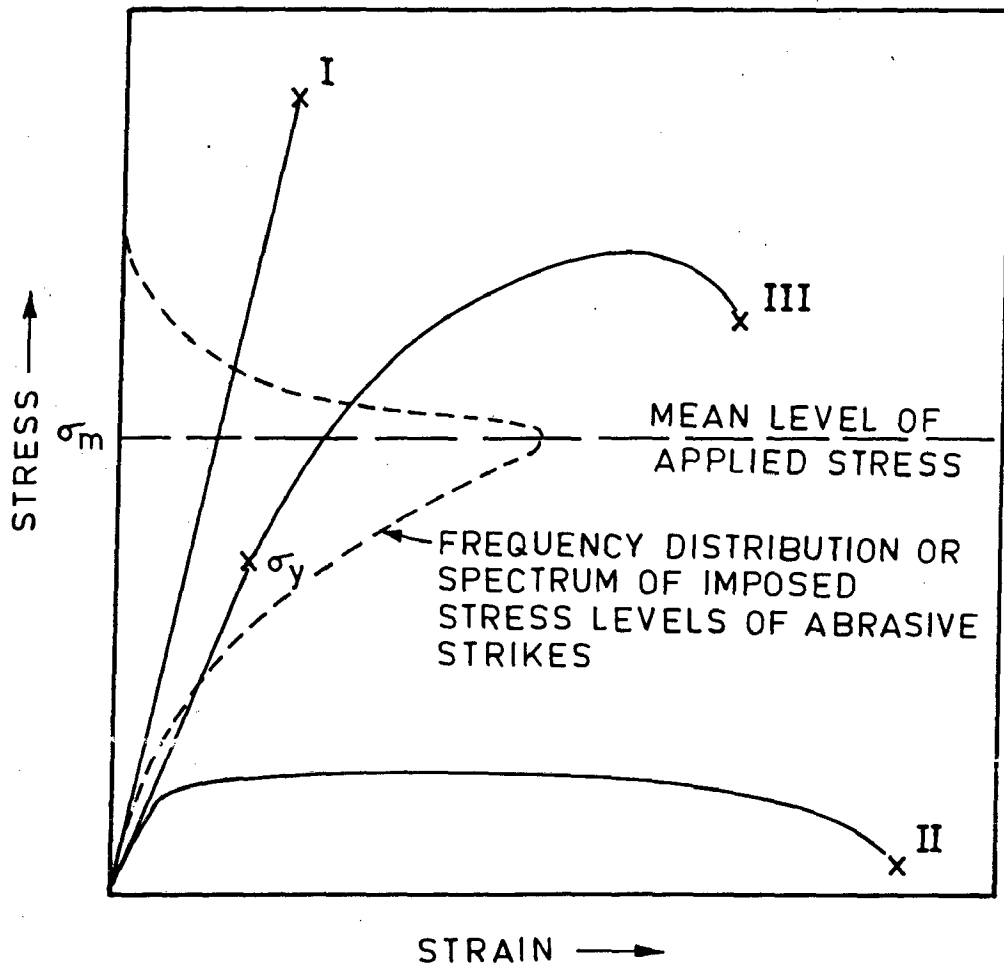


FIG.1.13 THE HYPOTHETICAL STRESS-STRAIN CURVES FOR THE WEAR OF THREE CLASSES OF MATERIALS SUPERIMPOSED UPON THE FREQUENCY DISTRIBUTION OF ABRASIVE OR EROSION STRIKES OF A GIVEN STRESS MAGNITUDE. [ Ref.76 ]

provide ideal resistance to abrasion since the applied stress never causes plastic yielding no matter how many times it is applied. However, such materials are very susceptible to sudden fracture due to very poor ductility. Hence they have no potential as good abrasion resistant materials. Materials with stress-strain curves of type II are soft and have high ductility. Although these materials show high strains prior to fracture, but these strains are produced at low stress levels. The majority of abrasive strikes will create stresses which will immediately cause shear of the surface beyond the critical strain for fracture and material will be lost quickly by abrasion after one or more strikes. The materials with a stress-strain curve of type III have an advantage over above two types. The area covered under curve is larger and the toughness or work to fracture with respect to abrasion is high as compare to other two cases. In such materials the critical strain to fracture will eventually be attained, but the life time of the material is extended because of the rising stress-strain curve.

It has recently been pointed out by De-Gee[77] that the superior wear resistance of f.c.c. metals compared with bcc metals at equivalent hardness is due to their higher work hardening coefficient ( $n$ ). This coefficient appears in the relationship  $\sigma_t = C \epsilon^n$  between true stress and true strain. Confidence in this analysis is provided by the excellent wear

resistance of alloys which are known to have high work hardening capacity such as metastable austenitic stainless steel [78], Hadfield Mn steel, dual-phase steels[79] and 'memory alloys' as Ni Ti [80].

It is often difficult to compare published wear data obtained by different investigators, either because some of the experimental conditions are not reported or because significantly different wear tests have been used. Wear testing has not yet been adequately standardized. Hundreds of different wear test devices and procedures have been described in the technical literature. Different methods that can be employed would depend upon whether they utilize physical, mechanical or optical principles as their basis. Another important aspect related with wear testing is that it would be difficult to simulate actual service conditions in laboratory test. Therefore, it is difficult to prescribe any particular test as a standard wear test. As such any test that is employed can at best help in evaluating i) the relative performance of different materials, and ii) a newly developed material with reference to a standard material (i.e. one which has been in extensive use). The simplest method of characterizing wear is by abrading a specimen surface against a hard surface followed by assessing the wt. loss in pct.wt. loss over a predetermined period at fixed intervals, keeping the speed, pressure and positioning of the specimen constant.

## 1.5 EFFECT OF ALLOYING ELEMENTS ON CHARACTERISTICS OF HADFIELD STEEL

Effect of various alloying elements on characteristics of Hadfield steels may be described in two parts: (i) variations within nomination composition and (ii) additional alloying elements.

### 1.5.1 Effect of Variations in Composition within the Nominal Range

Many variations in the composition of the original Hadfield steel have been proposed but only a few have been accepted as significant improvements. These usually involve variations of C and Mn with or without variations in other ingredients like Si, S and P.

#### Effect of C and Mn

The mechanical properties of austenitic Mn steel vary with both C and Mn contents. Fig.1.14 shows the variations in properties for cast 13 pct. Mn steel in the C range from .08 to 1.7 pct. It is seen that there is gradual increase in the yield strength with increase in C concentration, whereas tensile strength and ductility reach a maximum at about 1.2 pct. C and then decrease steadily. This is because embrittlement is caused above 1.2 pct. C by carbide precipitation.

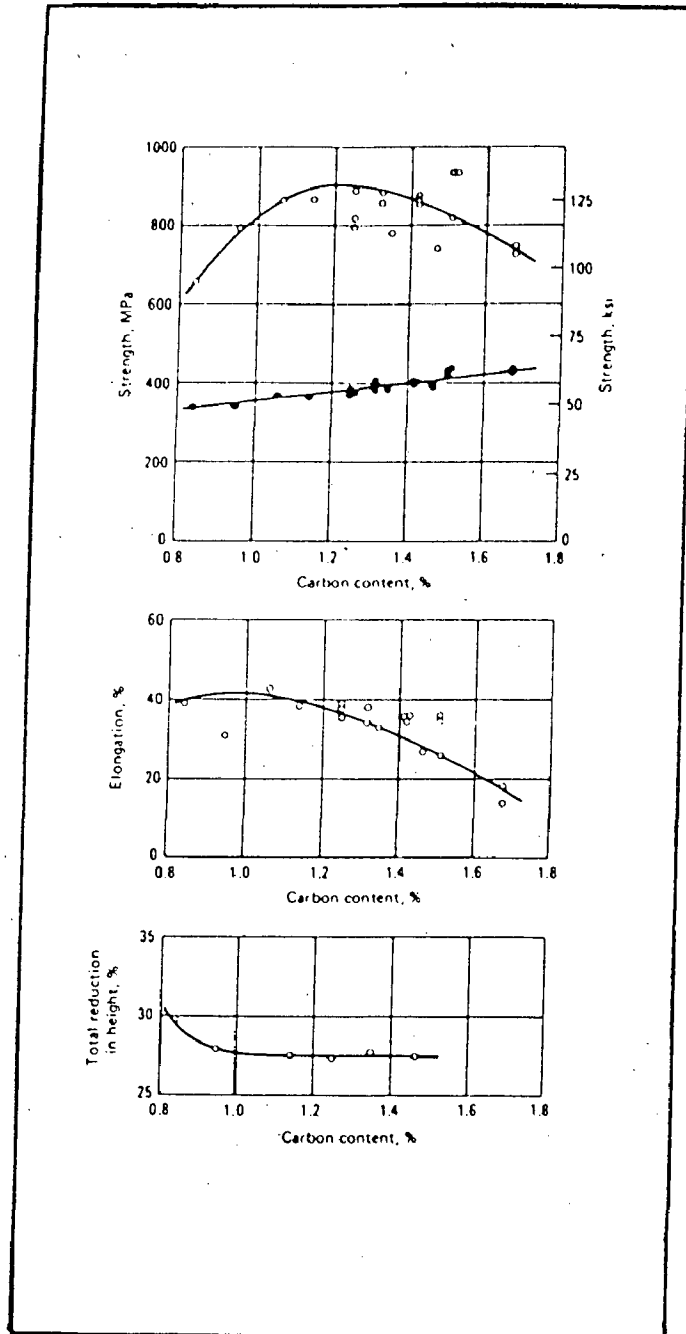


FIG.1.14: VARIATION OF PROPERTIES WITH C CONTENT FOR AUSTENITIC Mn STEEL CONTAINING 12.6 TO 13.0 Pct.Mn[Ref.13]

Dastur and Leslie [38] reports that wear characteristics of Hadfield steel may be improved by increasing the C content in solution of austenite. Normally C is limited to 1.4 pct. to get good abrasion resistance coupled with strength and ductility.

The influence of Mn content on mechanical properties of cast Hadfield steel, duly heat treated, is shown in Fig.1.15. Manganese content has little effect on YS but UTS and ductility increases rapidly with increasing Mn content upto about 14 pct. and then tends to level off. Higher Mn contents help to keep higher percentage of C into austenite solution since Mn contributes the vital austenite stabilising effect by delaying transformation. The presence of Mn decreases the activity of C in austenite [38]. The large number of substitutional atoms of Mn also contributes to rapid work hardening of Hadfield steel leading to improvement in abrasion resistance. Generally Mn is limited to 12 to 14 pct.

#### **Effect of Si**

Silicon in Hadfield steel results due to its additions during steel making process. Silicon contents exceeding 1.0 pct. are not usual and upto this concentration no noticeable influence is exerted on the mechanical properties. To improve the yield strength, 1.0 to 2.0 pct. Si may be added, but other elements like Cr, Mo, V have been preferred over Si to improve

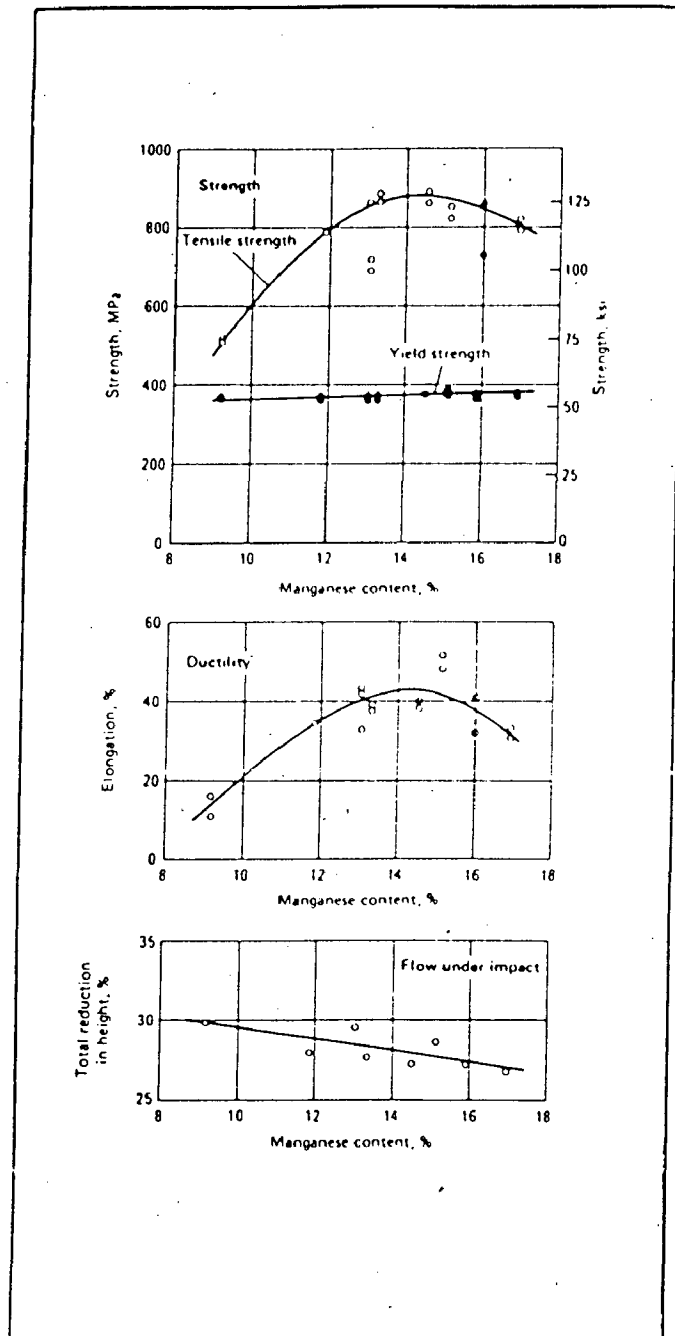


FIG.1.15: VARIATION OF PROPERTIES WITH Mn CONTENT FOR AUSTENITIC Mn STEEL CONTAINING 1.15 Pct. C [Ref.13]



the yield strength. Abrupt loss of strength and ductility is observed above 2.2 pct. Si [14].

### **Effect of P and S**

The preferred concentration of P in Hadfield composition is 0.06 pct. Phosphorus levels above this contribute to hot shortness and poor ductility at high temperatures, and frequently are the cause of hot tears in castings and underbead cracking in weldments. In general, P in Mn steel tends to lower the ductility and this effect is more critical at or below ambient temperatures[14].

The S content of Hadfield steel is invariably low by reason of its ready combination with Mn to form sulphide which goes mostly to the slag. Any slight residual MnS in the steel present in form of inclusions rarely has any influence on the properties of Hadfield steel [13].

### **1.5.2 Effect of Additional Alloying Elements**

Other alloying elements like Cr, Ni and Mo are added to Hadfield steel to achieve desired properties. The effect of these elements on mechanical properties of austenitic Mn steel is shown in Fig.1.16.

Chromium levels from 1.8 to 2.2 pct. (occasionally as high as 5.0 pct) are employed to moderately raise YS from 370 MPa to 450 MPa. But UTS and ductility are adversely

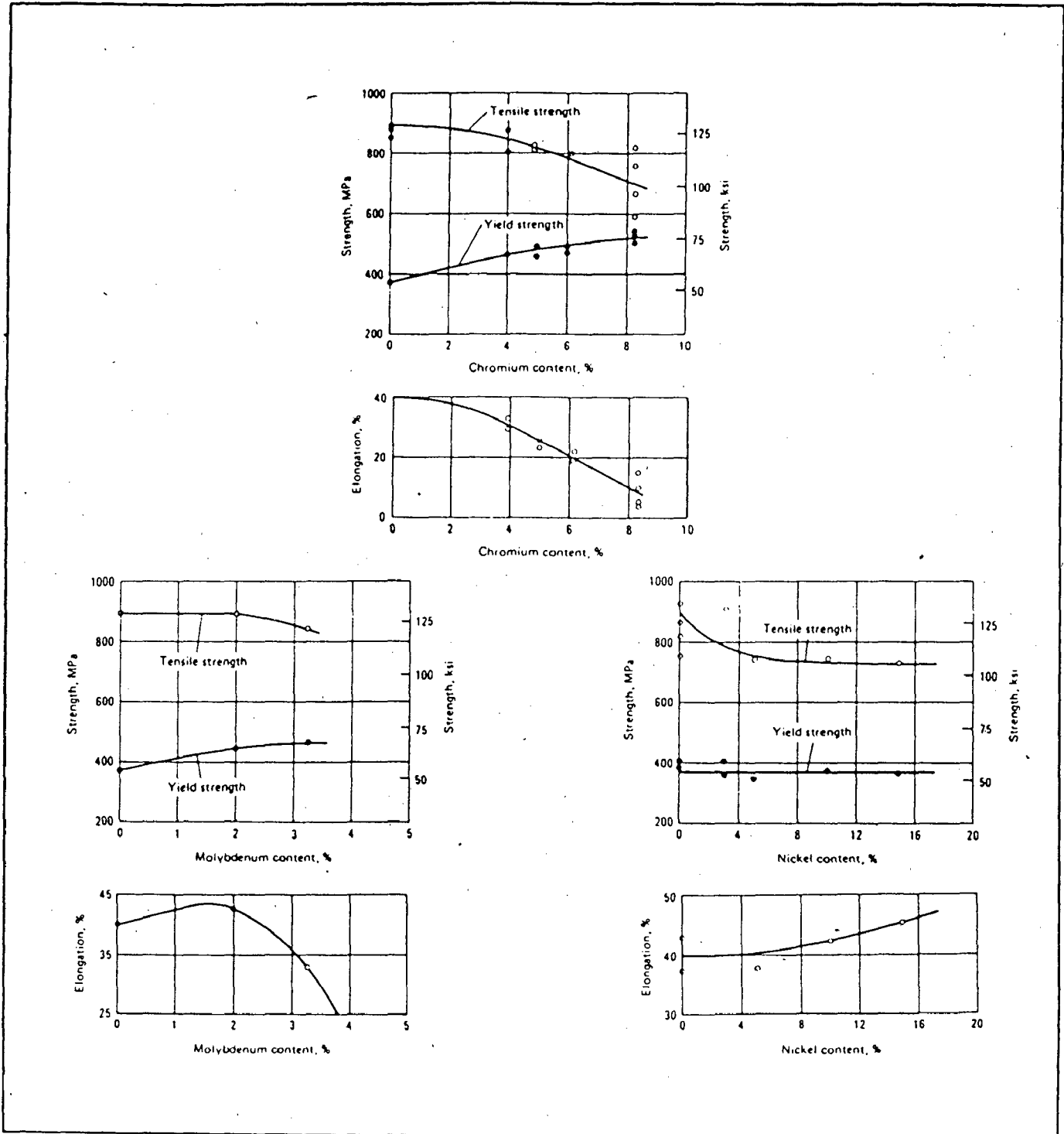


FIG.1.16 : EFFECT OF Ni, Mo AND Cr CONTENTS ON TENSILE PROPERTIES OF AUSTENITIC Mn STEEL [Ref.13]

affected [13]. Chromium reduces ductility by increasing the number of embrittling carbides in the austenite and that is why Cr bearing Mn steel crumbles under a much lower load than does the plain Mn steel. The effect of Cr addition on resistance to abrasion is unproven and appears to be inconsistent [14].

Molybdenum additions, usually 0.5 to 2.0 pct. are made to improve the toughness and resistance to cracking of castings and to raise the yield point of heavy section castings in heat treated condition [13]. These effects occur because Mo in Mn steel is distributed partly in solution in the austenite and partly in primary carbides formed during solidification of the steel. The Mo in solution effectively suppresses formation of both embrittling carbide precipitates and pearlite even when the austenite is exposed to temperatures above 275°C and the Mo in primary carbides tends to change distribution of the carbides from continuous envelopes around the austenite grains to less harmful nodular carbides. With addition of Mo, under same conditions, an improvement in abrasion resistance is observed [13].

Nickel addition upto 4.0 pct. to standard Mn steel composition stabilizes the austenite because it remains in solid solution. It is effective in suppressing precipitates of carbide. The presence of Ni increases the ductility. YS

is not altered while there is slight drop in UTS[13]. It slows down the rate of work hardening, hence abrasion resistance is also lowered.

Other elements like Cu, Bi and Ti are also added to standard Mn steel. Copper in amount of 1.0 to 5.0 pct. is sometimes used to stabilize the austenite as with Ni. The effect of Cu on mechanical properties has not been clearly established, but scattered reports [13] indicate that it may have an embrittling effect due to its limited solubility in austenite. Addition of Bi improves machinability of Hadfield steel while addition of Ti forms very stable carbides and thus reduces C in the austenite. The resulting properties simulate to these of a lower C grades. Titanium somewhat neutralizes the effect of too much P.

Vanadium additions to standard Mn steel composition have been studied by many workers [81-86]. Grigorkin [82] observed that small addition of V(0.48 pct.) gives roughly two times improvement in wear resistance of Mn steel. Richardson and Smith [84] claimed that an addition of 2 pct. V to the standard Mn steel improves wear resistance by five fold. Since V is a strong carbide former it increases the YS. However a comparable decrease in ductility occurs. The solubility range of V-carbide in austenite is shown in Fig.1.17. Tests in a jaw crusher demonstrated that the abrasion resistance of V bearing steel is not as great as that of conventional Hadfield steel [75].

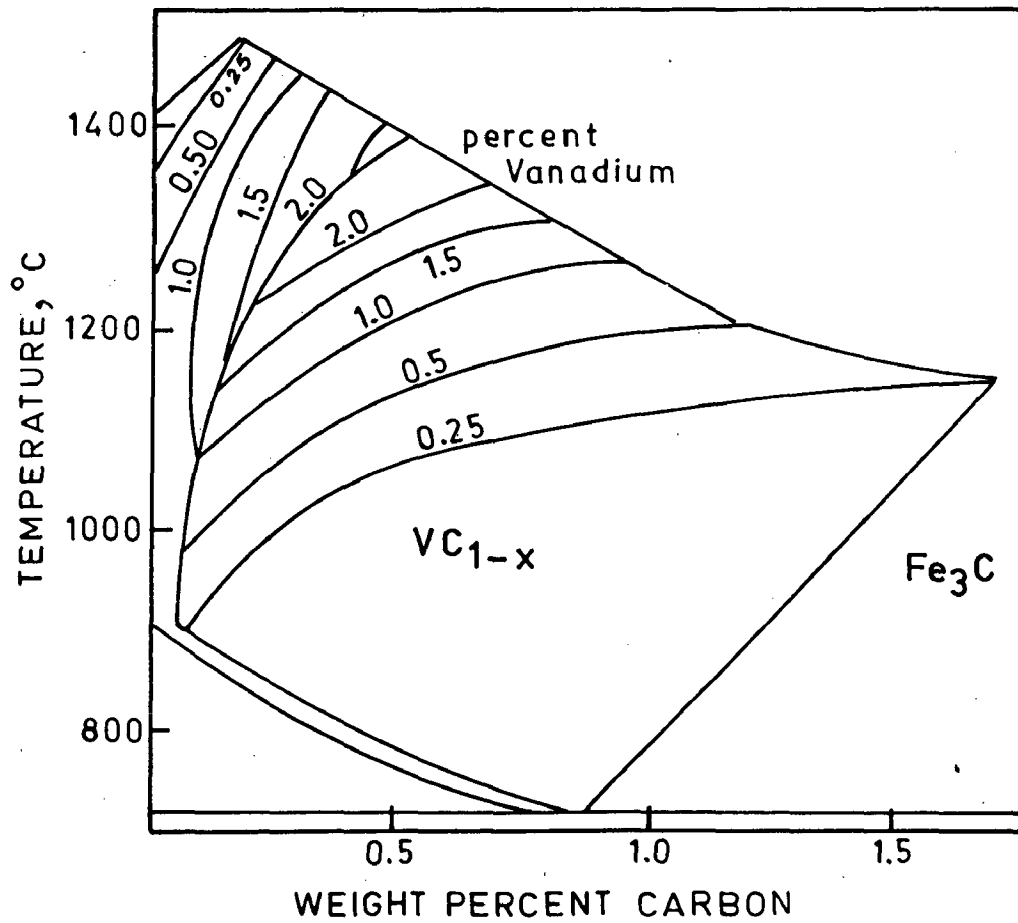


FIG.1.17 SOLUBILITY RANGE OF VANADIUM CARBIDE IN AUSTENITE. [Ref. 81]

Boron in lower concentrations and Cb additions have not been experimented in Hadfield composition. The addition of small percentages of B to structural steel results in remarkable increase in the hardenability of heat treatable steels [87-105]. Columbium additions in steels have been proved to be very useful towards enhancing the properties of steels by forming an intermetallic compound in austenite and combining with C to form Cb carbide [106-112]. Columbium produces useful properties in steel by i) imparting an extremely fine grain size, ii) preventing grain coarsening at elevated temperatures, iii) retarding softening during tempering, iv) preventing air hardening, and v) enabling steel to resist creep and rupture at elevated temperatures.

\*\*\*\*\*

CHAPTER-2

FORMULATION OF PROBLEM

\*\*\*\*\*

## CHAPTER-2

### FORMULATION OF PROBLEM

Austenitic Mn steel exhibits a marked wear resistance during severe service conditions, combining gouging abrasion and heavy impact. This is attributed to the exceptional work hardening behaviour of this material. Though this steel has been used for nearly a century since its development in 1882, the mechanism of rapid work hardening remains unclear. A review of literature reveals that the work hardening has been attributed to different mechanisms, viz. (i) strain induced transformation of  $\gamma$  austenite to  $\alpha$  or  $\epsilon$  martensites [39-45], (ii) lowering of stacking fault energy and formation of mechanical twins [46-48] and (iii) locking of dislocations due to segregation of C atoms [54-72]. The results obtained by different workers [38-72] are highly conflicting from each other. It has been shown, for example, that austenite in normal Hadfield steel is stable and if there is any evidence of martensite formation, it may be only due to decarburisation [40-43]. Correlation between the work hardening tendency and formation of mechanical twins has also been challenged [38]. There is no systematic study on the formation of twins and the resultant microstructure which may affect the rate of work hardening. In some cases it has been concluded that the hardness of Hadfield steel is more likely a function of general dislocation structure than of the specific microstructure. As a result, the observed work hardening



has also been attributed to stacking fault-dislocation interaction [45,49-53]. However, stacking faults in some studies have not been observed in all types of deformation. For example, Roberts [41] observed stacking faults only in hammered specimens, whereas work hardening in this steel is observed under all types of deformation. Several authors [54-72] have proposed that the rapid work hardening is due to the interaction of dislocations with C atoms in solid solution in austenite. Leslie[72] has concluded that the most likely cause of rapid work hardening in Hadfield steel is interaction between dislocations and Mn-C couples in solution in austenite. Dastur and Leslie[38] in a recent study have attributed rapid work hardening to dynamic strain ageing. But their studies are related with tensile loading under very slow strain rates on a single phase austenitic structure which is generally not the case in actual applications. Although work hardening is considered as the principal cause of high wear resistance of Hadfield steel, its actual mechanism has not yet been fully understood. There is no systematic study available to critically analyse the mechanisms of work hardening under different kinds of loading. Moreover, it is expected that second phase particles, if present in austenite, should also influence the work hardening characteristics. The present investigation has been undertaken to study the mechanisms of work hardening under normal tensile tests as well as under impact loading. It is also intended to study the influence of second phase carbide particles on the work hardening behaviour of Hadfield steel.

Different types of wear have been observed in austenitic Mn steel by different workers [73-77]. Abrasive wear has been observed to take place by the movement of abrasive particles across the steel surface leading to the removal of material by deformation and cutting mechanisms. Repeated impact wear has been generally attributed to a process of micro-spall formation on the surface undergoing impact. In some cases [113] presence of thin flakes or tongues of material have been observed on the wear surface, which suggests that metal loss may occur by a delamination mechanism. The mechanism proposes that subsurface deformation leads to the nucleation of cracks, which propagate below the wear surface and emerge at points of weakness causing thin films of material to separate. In a recent study, Ball [76] has attempted to correlate the wear characteristic with the tensile properties. However, whether such correlations are valid under actual load conditions, to which this steel is subjected, is highly questionable. No systematic study is yet carried out to simulate the actual service conditions in laboratory wear tests. The present study has been undertaken to study wear in conditions of combined impact and slide and attempts have been made to correlate wear characteristics with work hardening. The role of second phase particles on wear properties has not yet been studied so far. In this investigation the role of carbide particles in the austenite matrix on the wear has been undertaken.

The review of literature on Hadfield steel also shows that almost no systematic attempts have been made to study the role of various micro alloying elements to improve the general casting characteristics, grain refinement and to modify the various mechanical properties. It is generally expected that second phase carbide particles should have favourable effect on grain refinement and the general mechanical properties. Some attempts have been made to refine the grain structure by use of Ti, B, Cb, V, Ce and Al[114] in small quantities, but no correlation has been reported with respect to observed mechanical properties, work hardening and wear resistance. Results on grain refinement are also contradictory [114].

Boron, in low alloy steel is a very attractive element for increasing the stability of austenite [87-105] even under slow rate of cooling. The literature on mechanism of work hardening of Hadfield steel [38] reflects that gouging abrasion resistance of this steel can be improved by keeping the higher C contents in solid solution of austenite. Since B reduces the activity of C in Hadfield steel, its presence is expected to improve wear life as it will allow higher C retention in austenite phase. It is also expected to improve work hardening since like C, B forms an interstitial solid solution with  $\gamma$  iron, although its solubility is much less than that of C and amounts to only 0.001-0.003 wt.pct.[87-88]. It is also observed from literature that B improves the

notch toughness and impact properties of austenite by grain refinement [115]. In austenitic stainless steels B exhibits marked beneficial effects on the creep rupture life and hot workability [116]. Boron additions to cast iron in 0.001-0.48 wt.pct. range increases undercooling effects and decreases the temperature range between liquidus and solidus resulting in fine grain structure and also reduction in the amount and size of graphite flakes [117]. Boron is also added to malleable iron in the range of .001 to 0.003 pct. to improve response to annealing by increasing the rate of graphitization and by decreasing the size of graphite particles [118,119]. Many beneficial effects of B additions in high speed steels and precipitation-hardening alloys are also seen from a review of literature [120-122]. Boron also acts a powerful de-oxidising element and it also forms nitrides resulting refinement in grain structure. In view of these beneficial effects of small B additions to various steels and cast irons, it is expected that its additions to Hadfield steel may also result in development of a fine grain structure and an overall improvement in various mechanical properties.

The effect of V additions on mechanical properties are reported in literature [81-86]. Improvement in YS has been observed but there is deterioration in ductility and impact properties [84]. Some modified heat treatments are recommended to improve these properties. Conflicting results have however

been reported in literature on wear characteristics with V addition. Grigorkin [82] reported that 0.48 pct. V addition improves abrasion resistance by two times. Richardson and Smith [84] claimed that 2 pct. V improves wear resistance by five fold. However, it is also reported [123] that V alone does not improve wear resistance; it should be used alongwith higher concentrations of B to resist only mild abrasion effects.

Columbium additions in low alloy steels have proved to be very useful towards enhancing the properties by forming intermetallic compounds and carbides [106-112]. Columbium has been observed to impart fine grain structure, prevent grain coarsening at elevated temperature and retard softening during tempering [110,111]. Its addition to austenitic Cr-Ni steels has been recommended for grain refinement, prevention of intergranular attack and improving toughness and creep properties at high temperatures. It is therefore expected that Cb addition may also cause grain refinement, improve casting characteristics and mechanical properties of Hadfield steel.

In view of the above observations, efforts have been made in the present investigation to study the effect of micro alloying additions of B, V and Cb on the grain refinement, mechanical properties and resultant work hardening characteristics and wear resistance of conventional Hadfield steel. Boron additions in the range of 0.001-0.004 pct. have been selected looking into its solubility in  $\gamma$  iron and also

due to the observation that most of the beneficial effects of this element in other steels have been observed in this range only. Microalloying of conventional Hadfield composition by V and Cb has been done in the range 0.05-0.50 pct. in view of the observation that their beneficial effects in other alloy steels have also been reported in this range only [106-112].

Various alloys containing microalloying additions of B, V and Cb in the specified ranges have been prepared. After standard heat treatment mechanical properties, viz. hardness,  $\sigma_s$ , UTS,  $E_l$  and impact strength are measured. An analysis of these properties is made to identify the most optimum concentrations of microalloying elements. Further studies on work hardening and wear are conducted only on alloys having these optimum concentrations. Efforts have also been made to simulate the laboratory wear tests with actual service conditions by combining impact with slide wear. Extensive light and scanning electron metallographic studies are undertaken for an analysis of the results obtained and for understanding the mechanism of work hardening and wear under test conditions.

\*\*\*\*\*

CHAPTER-3

EXPERIMENTAL PROCEDURE AND TECHNIQUES

\*\*\*\*\*

## CHAPTER-3

### EXPERIMENTAL PROCEDURE AND TECHNIQUES

#### 3.1 ALLOY PREPARATION

The alloy used in this investigation was prepared by using mild steel scrap of known quality having minimum percentages of residual elements, and using ferro alloys of Mn and Si in appropriate proportions to attain the required chemical composition of Hadfield steel. Melting was carried out in a medium frequency inductoin furnace under controlled conditions. Micro alloying with B, V and Cb was done in a 50 kg. crucible.

##### 3.1.1 Melting

A charge mix of known composition of mild steel scrap and ferro-alloys (Table 3.1) was prepared. This mix was charged into a basic lined medium frequency 600 kw induction furnace for melting. After melt down, one representative sample was analysed on spectrometer to get the chemical analysis report of the liquid metal. The addition of Fe-Mn and Fe-Si of known composition (Table 3.1.b) was done to adjust the bath composition and to attain the required chemical composition of the base alloy. Final check sample was analysed on the spectrometer.



TABLE 3.1(a)

CHEMICAL COMPOSITION OF MILD STEEL SCRAP USED TO PREPARE BASE ALLOY  
(Spectro analysis of 7 samples)

Sample No.	1	2	3	4	5	6	7	Average
Element (pct)								
C	0.27	0.25	0.42	0.15	0.45	0.25	0.11	0.2714
Mn	0.57	0.83	0.72	0.78	0.80	0.73	0.32	0.6785
Si	0.31	0.29	0.19	0.20	0.25	0.26	0.14	0.2342
P	0.009	0.010	0.02	0.01	0.02	0.01	0.07	0.0212
S	0.007	0.038	0.01	0.02	0.028	0.022	0.052	0.0252
Ni	0.148	0.322	0.26	0.22	0.128	0.147	0.121	0.1922
Cr	0.135	.156	.250	.288	0.139	0.150	-	.1597
Cu	0.112	.244	.193	.149	.111	0.107	0.031	0.1352
Ti	0.000	.000	.000	.000	.000	0.000	0.000	0.000
Sn	0.003	.004	.006	.014	.012	0.006	0.009	0.0077
Al	0.003	.003	.022	.024	.016	0.025	0.044	0.0195
Nb	0.002	.001	.004	.002	.001	0.002	0.003	0.00214
B	.0001	.0002	.0003	.0003	.0001	.0002	.0002	0.0002
Pb	.0001	.0000	.0034	.0018	.0008	.0010	.0027	0.0016

TABLE 3.1(b)

CHEMICAL COMPOSITION OF FERRO-MANGANESE AND FERRO-SILICON

Element	Composition of Ferro-manganese (pct)	Composition of Ferro-silicon (pct)
C	7.00	0.15
Si	1.5	72.0
Mn	70.0	0.3
S	0.03	0.05
P	0.35	0.04
Al	-	0.90

The temperature of the liquid bath was measured by using an immersion type pyrometer with Pt/Pt -10 pct. Rh temp.-tips. The temperature of liquid bath was maintained at  $1500^{\circ} \pm 10^{\circ}\text{C}$ .

### 3.1.2 Micro Alloying

Elements chosen for micro alloying were B, V and Cb. Master alloys of these elements in form of Fe-B, Fe-V and Fe-Cb were used for addition. The percentages of the respective elements in master alloys were analysed. The chemical analysis of each master alloy is given in Table 3.2. Master alloys were used in form of small size granuals for proper mixing into melt and these were wrapped in Al foil and kept in the bottom of 50 kg refractory coated crucible duly pre-heated.

TABLE 3.2.

CHEMICAL ANALYSIS OF MASTER ALLOYS OF B,V and Cb(wt.pct)

Master alloys	C	S	B	Cb	V	Balance
Fe-B	0.10	0.015	16.0	-	-	Fe
Fe-V	0.70	0.10	-	-	50.8	Fe
Fe-Cb	0.08	0.04	-	52.0	-	Fe

Liquid metal was transferred from the induction furnace to refractory coated crucible in the measured quantity at

a temperature which was about 60-80°C higher than that finally required to ensure complete dissolution of the master alloy in the base composition. Stirring from a steel wire rod was done for uniform mixing of the alloy. It was ensured that metal temperature of micro alloyed composition was maintained within  $1500 \pm 10^\circ\text{C}$  before pouring it into various test moulds. Since pouring temperature has a vital effect on the casting characteristics and on the mechanical properties, this variable was kept within control. The alloyed metal was distributed into various test moulds. The same procedure was adopted for micro alloying of all elements and test samples for tensile, impact and wear tests were poured for each composition.

### 3.1.3 Chemical Analysis

The chemical composition was analysed on 22-channel Jarrel-ash make direct reading spectrometer duly calibrated by standard samples. The C content was also determined using a combustion method on a Carbon-Sulphur apparatus and Mn content was verified by wet analysis method. The percentages of micro-alloyed elements i.e. B, V and Cb were checked up on spectrometer. The finally achieved chemical compositions of various micro alloyed Hadfield steel are given in Table 3.3.

## 3.2 PREPARATION OF TEST SAMPLES

Manganese steel with its characteristics of high toughness and work hardening at the point of cutting tool causes

TABLE 3.3

## CHEMICAL COMPOSITIONS OF VARIOUS MICRO-ALLOYED HADFIELD STEELS

Alloy designation	Composition (wt.pct)						
	C	Mn	Si	P	B	Cb	V
13 Mn	1.16	13.6	0.48	0.061	-	-	-
0.001 B	1.16	13.5	0.49	0.061	0.0008	-	-
0.002 B	1.16	13.5	0.49	0.060	0.0022	-	-
0.003 B	1.16	13.5	0.48	0.061	0.0030	-	-
0.004 B	1.15	13.5	0.49	0.061	0.0042	-	-
0.05 V	1.17	13.5	0.50	0.061	-	0.05	-
0.10 V	1.17	13.4	0.50	0.061	-	0.10	-
0.50 V	1.18	13.5	0.50	0.061	-	0.50	-
0.05 Cb	1.17	13.5	0.50	0.061	-	-	0.06
0.10 Cb	1.18	13.5	0.50	0.061	-	-	0.10
0.50 Cb	1.18	13.5	0.50	0.061	-	-	0.50

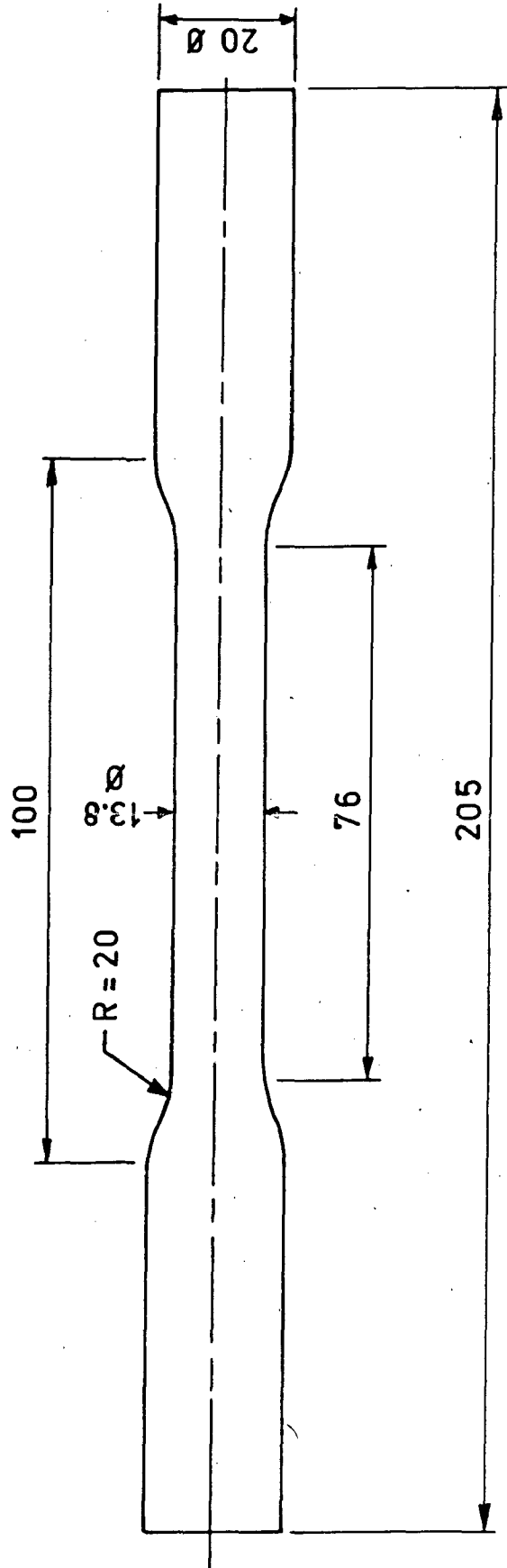
the machining operation of this steel to be extremely difficult. It is recommended to keep the machining requirements to a minimum to attain the original properties of the material. Since in this investigation it was important to study the original properties of this steel, it became important to cast the test samples nearly of the same size and shape as of final test pieces.

### 3.2.1 Foundry Procedure for Preparation of Test Samples

Samples of tensile, impact and wear tests were developed in the foundry unit of Uttar Pradesh Steels Ltd., Muza-farnagar. Sizes of test samples for tensile and impact tests were selected as per IS 1608-1978 and ASTM E-23. The dimensions of various test samples are shown in Figs.3.1-3.3

It was very important to produce sound castings of shaped test bars. Since Mn steel has a wide freezing range and is very sensitive to pouring temperature, due care was taken in designing the risering and running systems to get sound test pieces. The schematic arrangement of risers and running system for pouring test samples is shown in Figs.3.4 and 3.5. Teak wood patterns of shaped test bars were prepared and were mounted on a match plate splitting into two halves from the centre.

Moulds were prepared by using Sodium-Silicate-CO<sub>2</sub> standard moulding process. The moulding sand used was washed



DIMENSIONS IN mm

FIG.3.1 SPECIMEN FOR TENSILE TEST ( IS 1608 - 1978 )

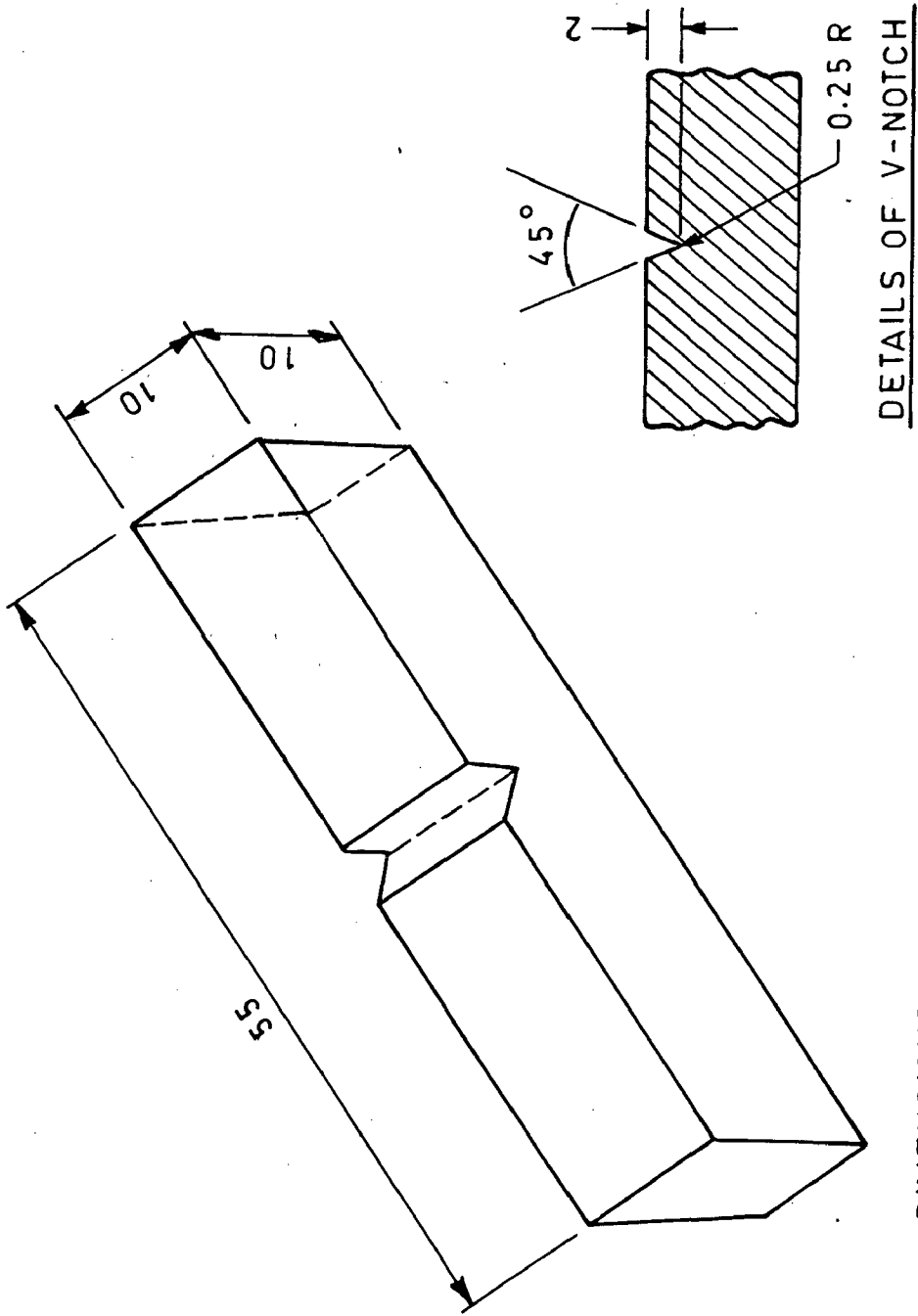
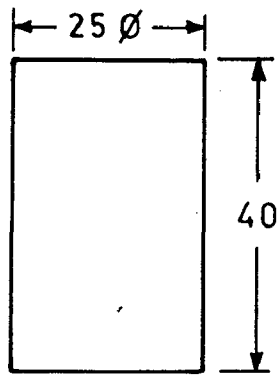


FIG. 3.2 CHARPY V-NOTCH SPECIMEN FOR IMPACT TEST.  
(ASTM E - 23)



DIMENSIONS IN mm

FIG. 3.3 SPECIMEN FOR WEAR TEST



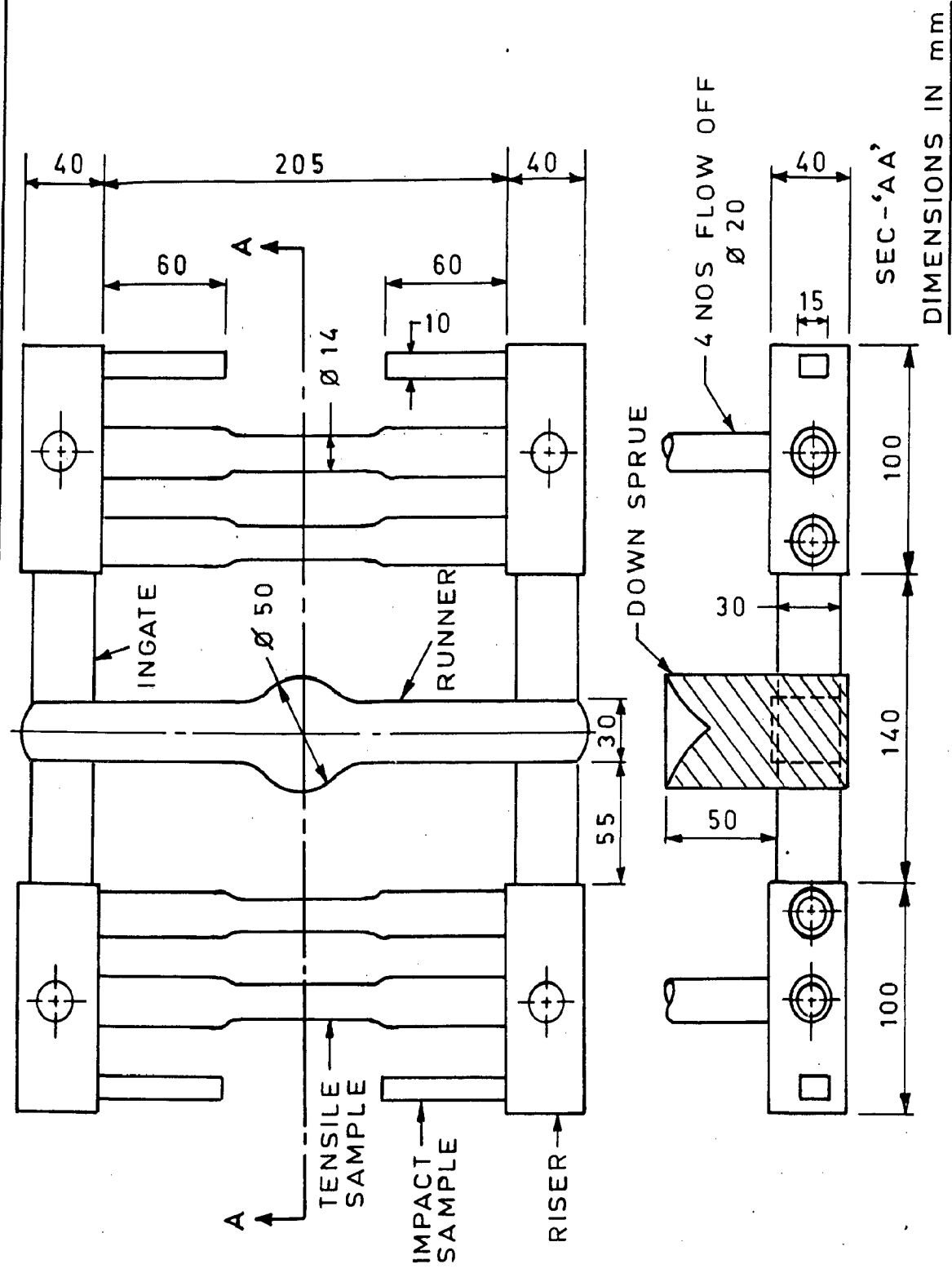
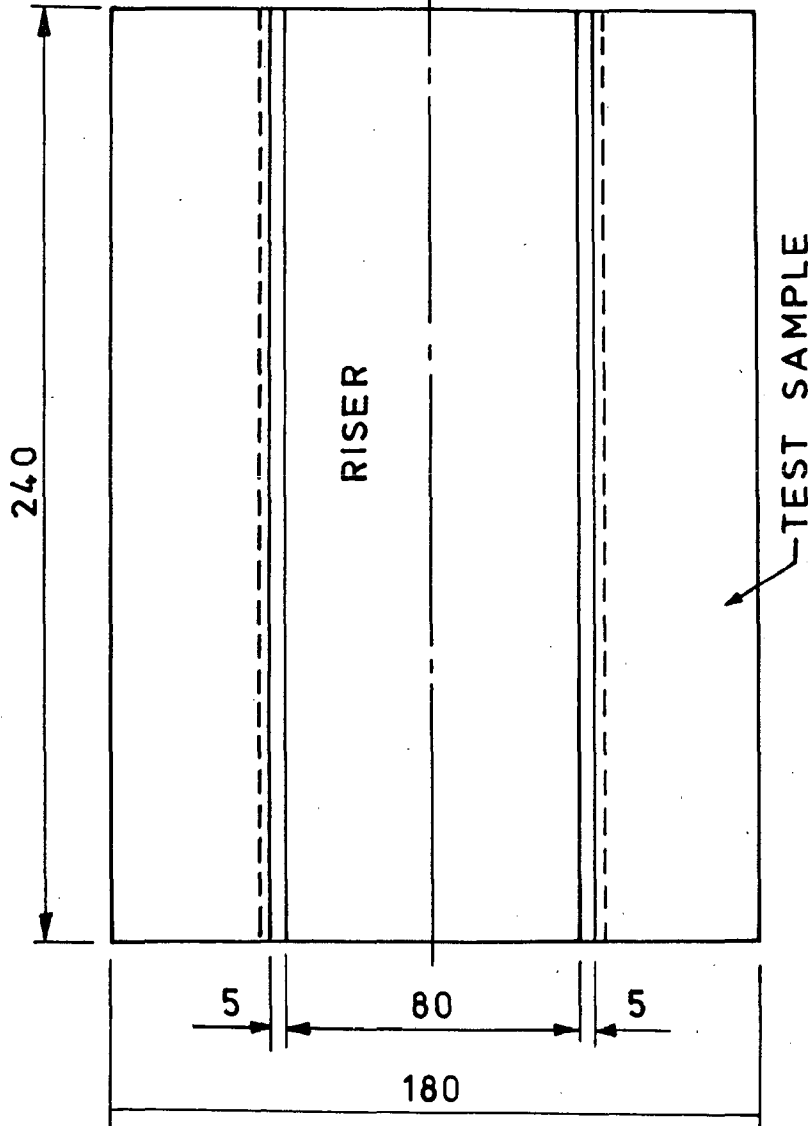
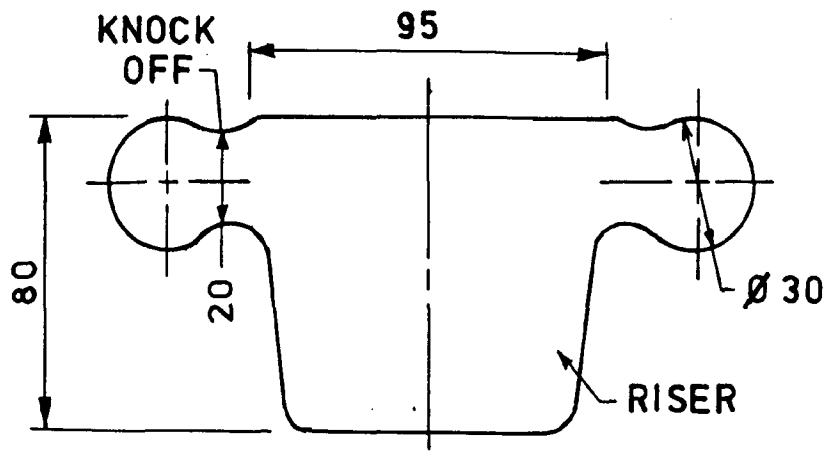


FIG. 3.4 SCHEMATIC ARRANGEMENT FOR POURING TENSILE AND IMPACT TEST SAMPLES.

DIMENSIONS IN mm



Dimensions in mm

FIG. 3.5 SCHEMATIC ARRANGEMENT FOR POURING WEAR TEST SAMPLES.

silica sand having 0.30 pct. maximum clay and 98.0 pct. silica. The size of the sand grains was corresponding to 55-60 AFS NO. The moulds were spray painted by a thinner base magnesite wash to avoid any metal-mould reaction during pouring of liquid metal.

Three sets of test bars were poured for each composition. Moulds were knocked out after 24 hours of pouring. Recommended heat treatment was given and test bars were finished by light grinding on a bench grinder and were made ready for testing.

### 3.3 HEAT TREATMENT

Manganese steel acquires its characteristic properties only by suitable composition coupled with a correct heat treatment. The standard heat treatment involves austenitizing followed by water quenching. In this investigation austenitizing was done at 1050°C for 90 minutes.

The heat treatment was carried out in a laboratory type electrically heated muffle furnace with a proper attachment of temperature recorder and indicator duly calibrated. The sample surfaces were properly protected to avoid any oxidation in heating.

### 3.4. MECHANICAL TESTING

Mechanical testing involved hardness, tensile and impact properties.

#### 3.4.1 Hardness Measurement

Hardness measurement was done on Vickers hardness testing machine using a load of 10 kg. A minimum of three impressions were taken on each specimen at various locations and average of these values was recorded as final reading.

#### 3.4.2 Tensile Properties

Tensile tests were conducted on shaped test bars on Universal Testing Machine model UTM-301. Load-elongation graph was plotted in each test. average value of three test results for YS, UTS and El were calculated and recorded. True stress-true strain curves were computed from load-elongation curves and the value of strain hardening exponent was calculated for each composition. The strain hardening exponent ( $n$ ) appears in relationship  $\sigma_t = K \epsilon_t^n$ .

Load-elongation curves were also recorded on INSTRON-100 KN universal testing machine at fixed strain rate of  $3 \times 10^{-4}$   $\text{sec}^{-1}$  to study work hardening mechanism in Hadfield steel.

### 3.4.3 Impact Testing

Impact test was conducted on standard charpy V-notch specimens as per ASTM E-23 standard. Pendulum type impact testing machine (PS-30) was used to carry out the impact test.

## 3.5 STUDY OF WEAR CHARACTERISTICS

Disc and pin type rig (Fig.3.6) was used to study the wear characteristics of the alloy. This equipment was used under dry condition. In this rig a bonded alumina fine emery wheel (Grade A80) was mounted horizontally on to a polishing machine. Cylindrical specimen of 25 mm dia and 40 mm height was held against its surface at a pre-decided distance from the axis of rotation through a specimen holder. This holder held the sample vertically in position by passing it through a heavy horizontal beam supported at both ends. The load on the specimen under testing was maintained constant at 2.5 kgs in all the cases. The speed of rotation of abrasive wheel, mounted with a tachometer, was adjusted at 1100 rpm. During testing, specimen rotated in its own axis in addition to being ground. This way it was ensured that specimen surface abraded evenly. The surface area of all the specimens undergoing abrasion was kept constant. Wear tests were conducted on as quenched samples (slide wear) and on samples subjected to saturation hardening by impact loading (impact-slide wear).

Wear data has been reported in terms of weight loss at equal intervals of 30 sec. of abrasion for a total of 5 minutes in each specimen. The advantage of this method is

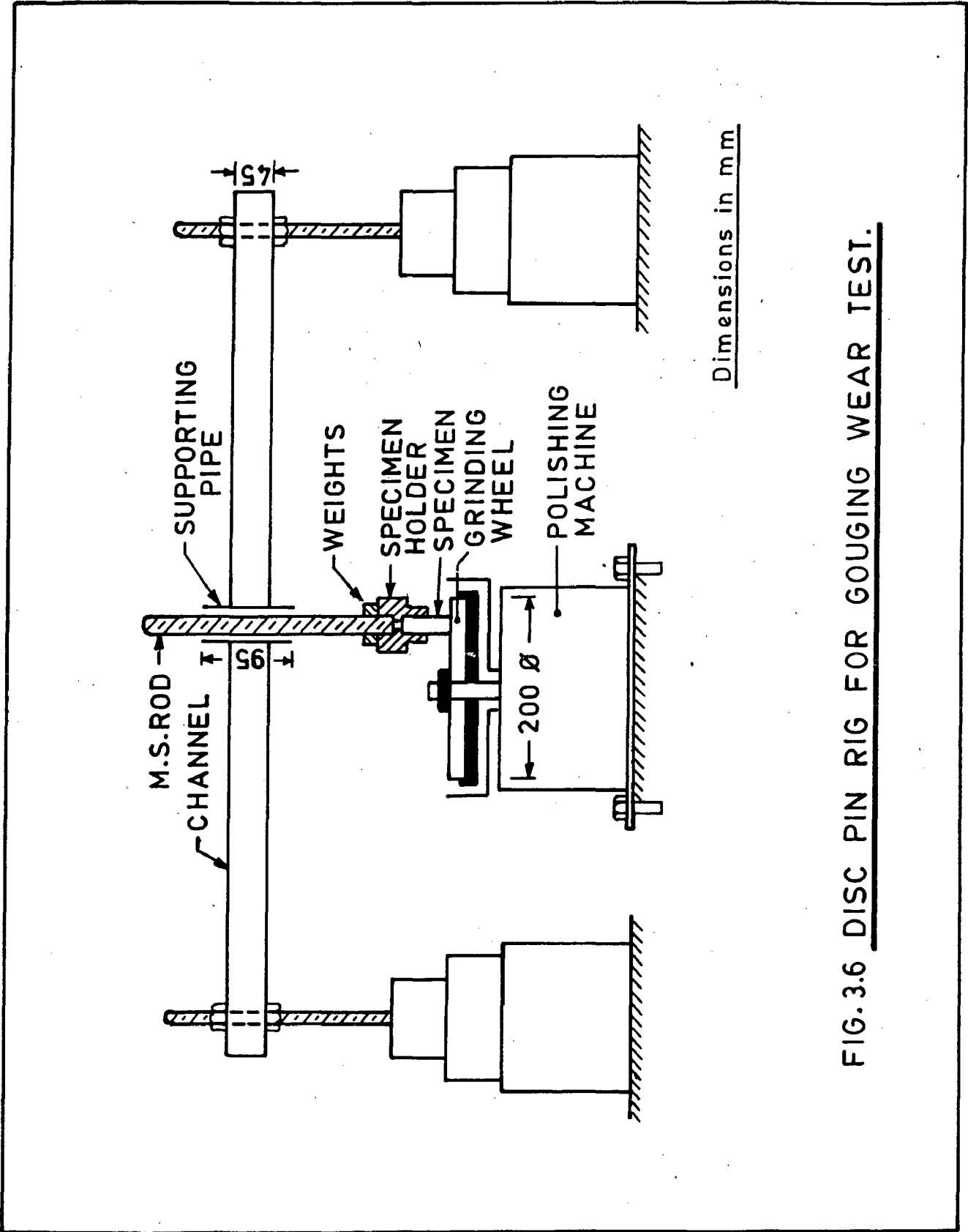


**FIG. 3.6 DISC PIN RIG FOR GOUGING WEAR TEST.**

in its simplicity and possibility of using bulk samples.

### 3.6 STUDY OF MATERIAL BEHAVIOUR UNDER IMPACT LOADING

Manganese steel has a pronounced tendency for work hardening under impact loading and this property has a significant importance for wear characteristics.

To study the work hardening characteristics of Mn steel, standard samples of 25 mm dia. and 40 mm height were used. Samples were ground and polished on emery paper upto 4/0 grade. Subsequently these samples were blown with a constant weight hammer (35 kg) dropping from a height of 0.3 meter on a 'variable type impact machine'. The hardness was measured at fixed interval of 25 number of blows of constant impact force. Maximum of 125 blows were given to each sample to reach a saturation in the surface hardness. The values of hardness for given number of blows were plotted to study the tendency of work hardening of micro alloyed Mn steels.

The samples used for study of the work hardening characteristics were subjected to wear test after attaining the saturation hardness. Wear data has been reported in terms of weight loss at intervals of 30 seconds for a total test duration of 5 minutes. At every successive stage, the values of hardness and reduction in the size of specimen were recorded to study the variation of hardness below the work hardened

layer and to establish correlation of wear properties with work hardening characteristics.

### 3.7 METALLOGRAPHIC STUDIES

Light microscopy was extensively used to comprehend the effect of micro alloying on the cast and heat treated structures of Mn steel and to correlate them with changes in mechanical properties. The specimens were polished by standard technique and etched with freshly prepared 2 pct. nital solution. Microscopic examination was also carried out on the test pieces which were hardened by repeated impact force to study the mechanism of work hardening under impact loading. Light microscopic examination was carried out on 'REICHERT MATAVER - 368' microscope and Neophote-21.

Scanning electron microscopy (SEM) was extensively used to study the fracture surfaces of broken tensile and impact test specimens. SEM was also employed to study work hardening and wear mechanisms under different test conditions. Philips SEM 501 scanning electron microscope was used.



\*\*\*\*\*

CHAPTER-4

RESULTS AND ANALYSIS

\*\*\*\*\*

## CHAPTER-4

### RESULTS AND ANALYSIS

The results of the present investigation have been presented in Figs.4.1 to 4.58 and Tables 1 to 14 and are described in the following sections.

#### 4.1 EFFECT OF MICRO ALLOYING ON MECHANICAL PROPERTIES

Micro alloying of Hadfield Mn steel with B, V and Cb has been observed to affect significantly the mechanical properties. All the mechanical properties have been determined in heat treated samples.

##### 4.1.1 Tensile properties

Various parameters of tensile properties viz. yield strength(YS), ultimate tensile strength(UTS) and percent elongation (El) have been determined for base composition (13 Mn steel) and the micro alloyed compositions. The results of tensile properties have been plotted for various concentrations of micro alloying additions (Figs.4.1-4.3) and have also been shown in Histograms (Figs.4.4-4.12). It is observed that addition of 0.001 pct. B (0.001 B alloy) to 13 Mn alloy enhances the YS from 392.4 to 457.0 MPa, UTS from 650.4 to 762.7 MPa and El from 20.0 to 23.0 pct. (Figs.4.1, 4.4,4.7,4.10). Further increase

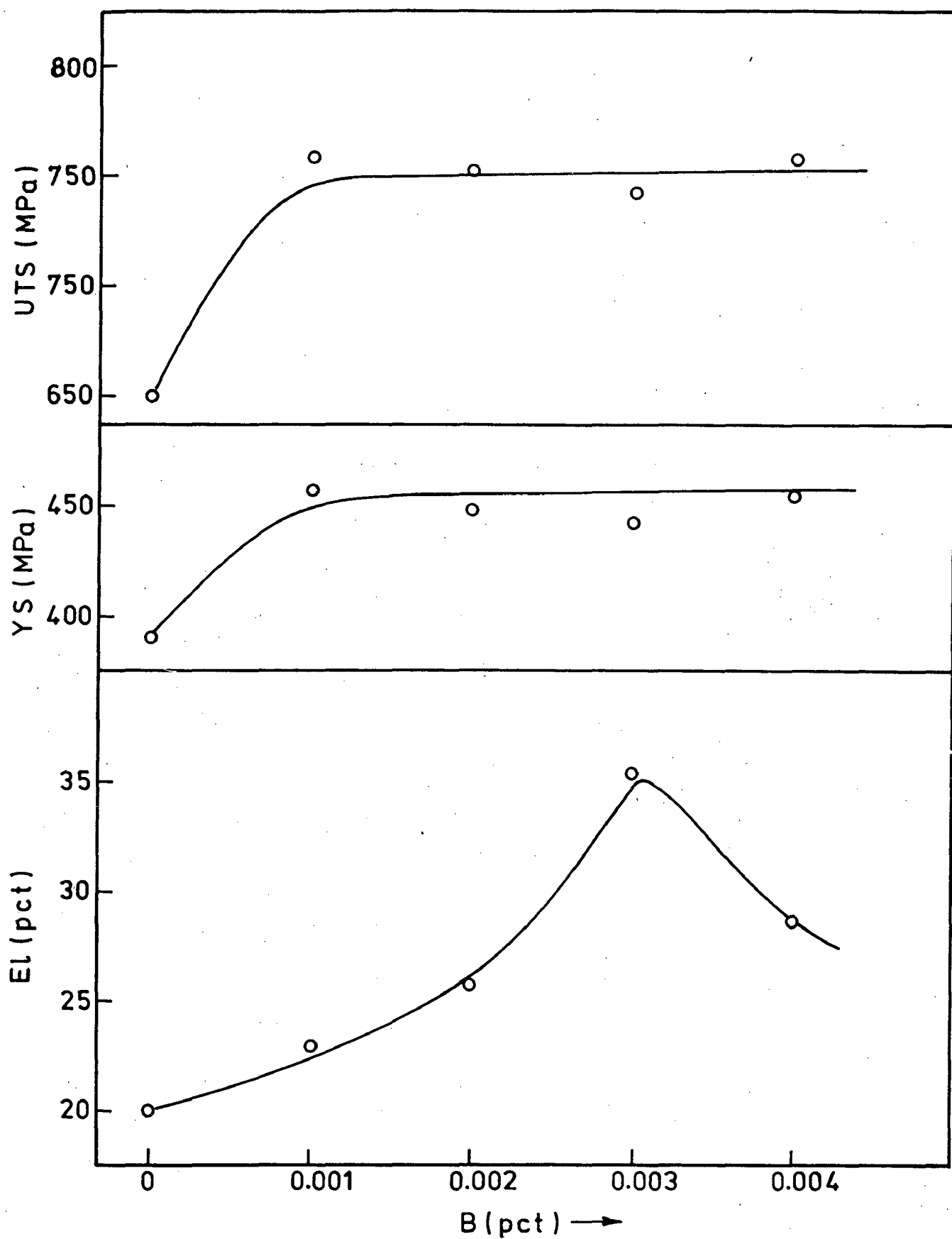


FIG. 4.1 EFFECT OF BORON ADDITIONS ON TENSILE PROPERTIES.

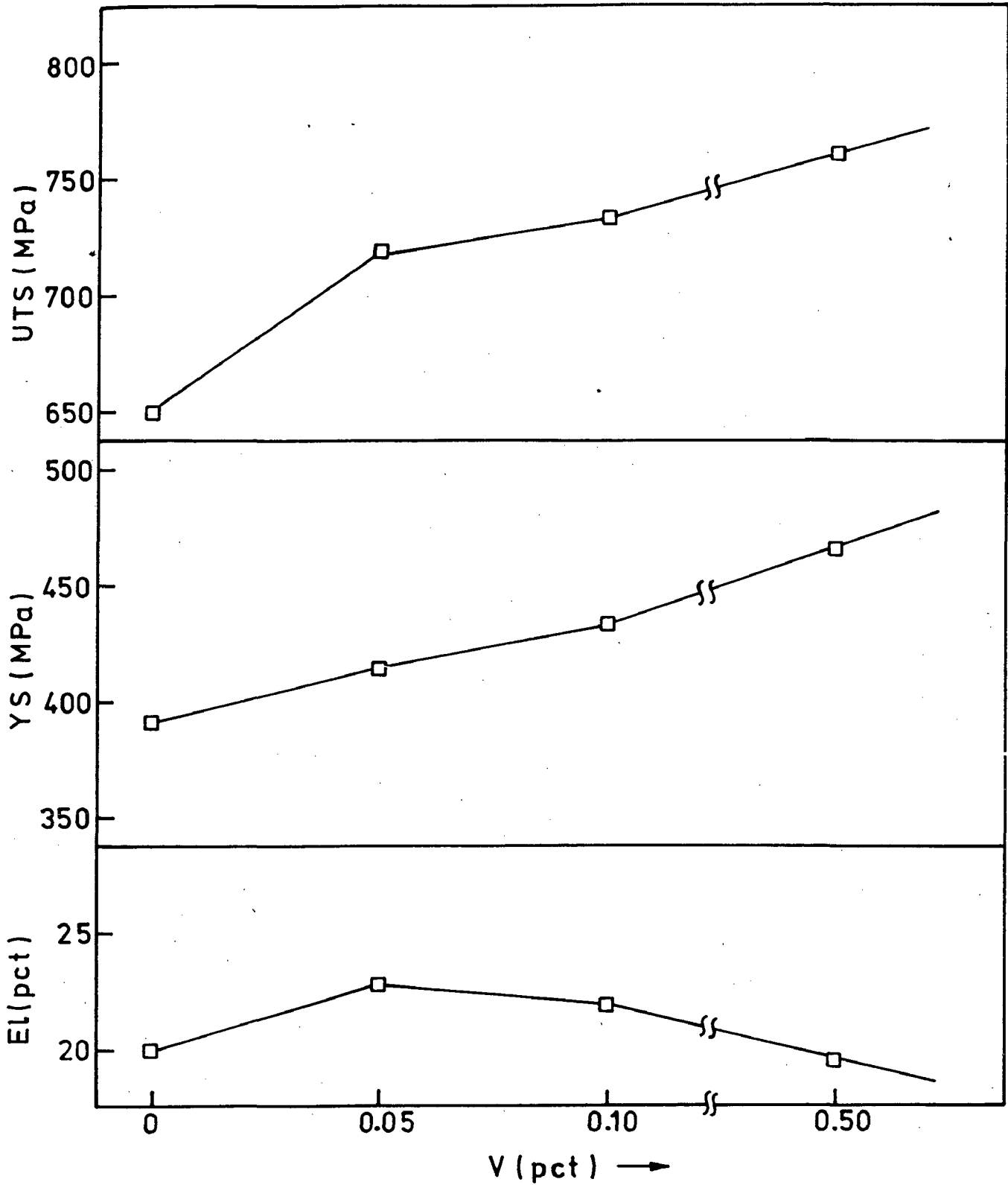


FIG. 4.2 EFFECT OF VANADIUM ADDITIONS ON TENSILE PROPERTIES.

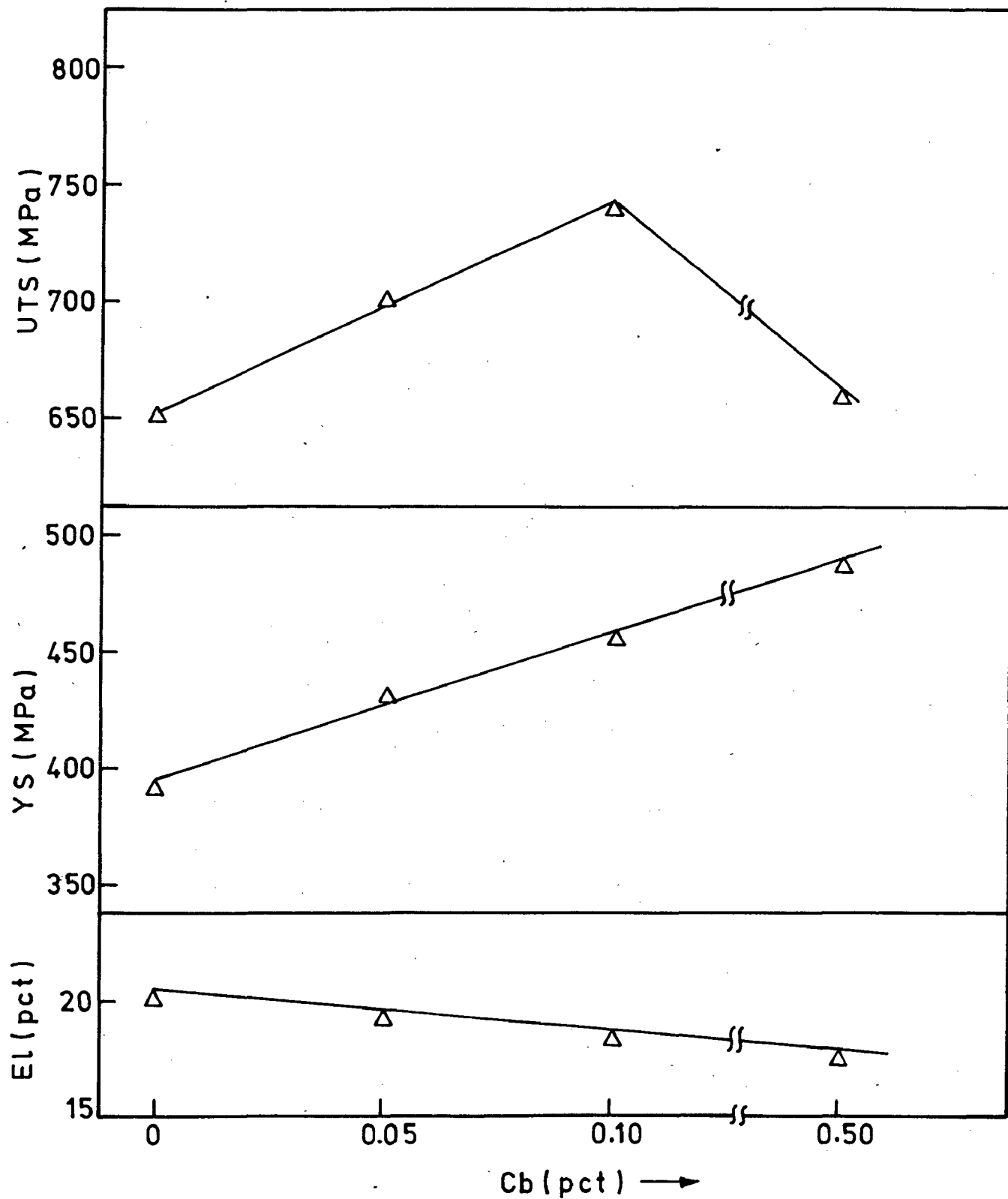


FIG. 4.3 EFFECT OF COLUMBIUM ADDITIONS ON TENSILE PROPERTIES.

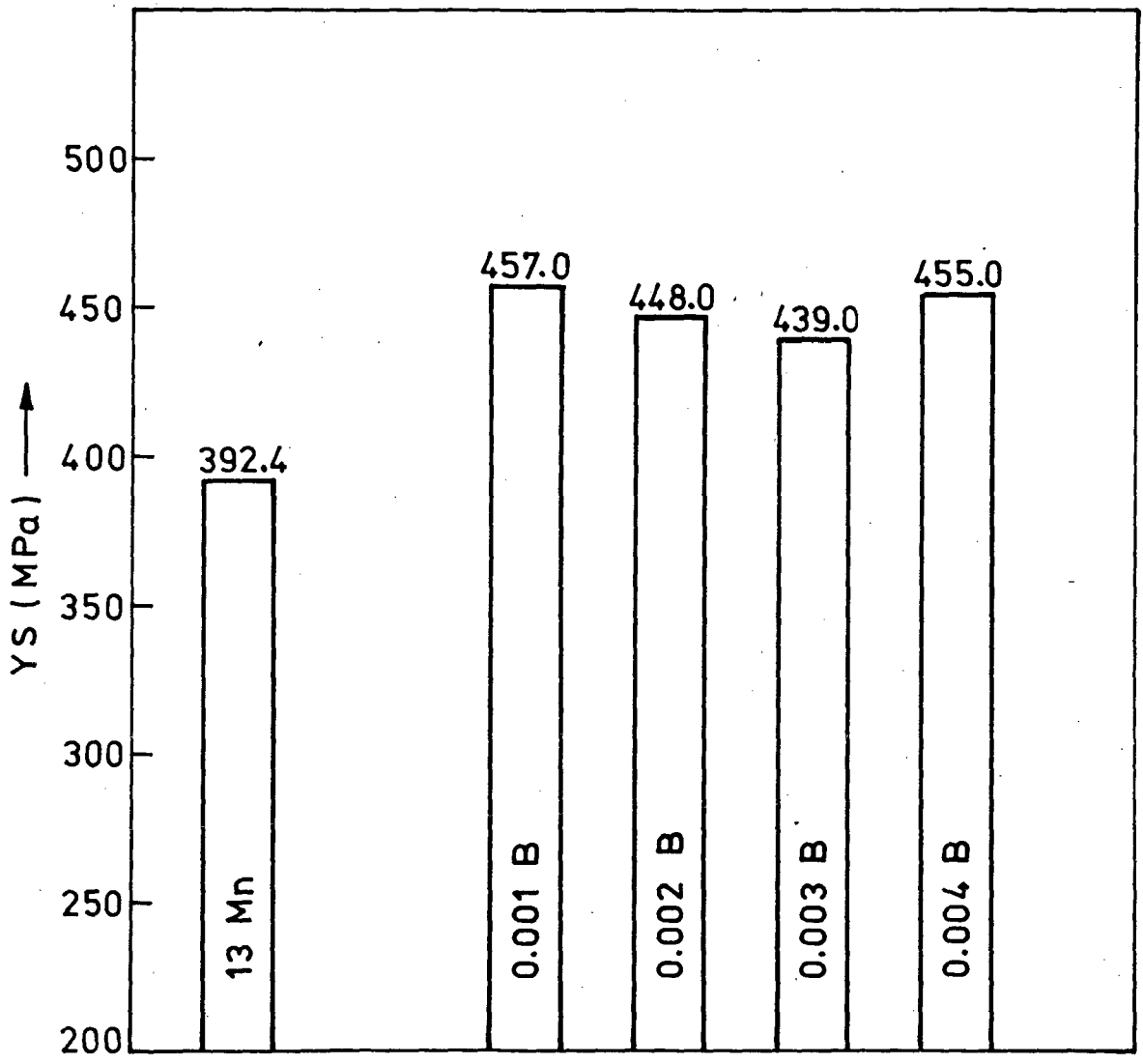


FIG. 4.4 EFFECT OF BORON ADDITIONS ON YIELD STRENGTH.

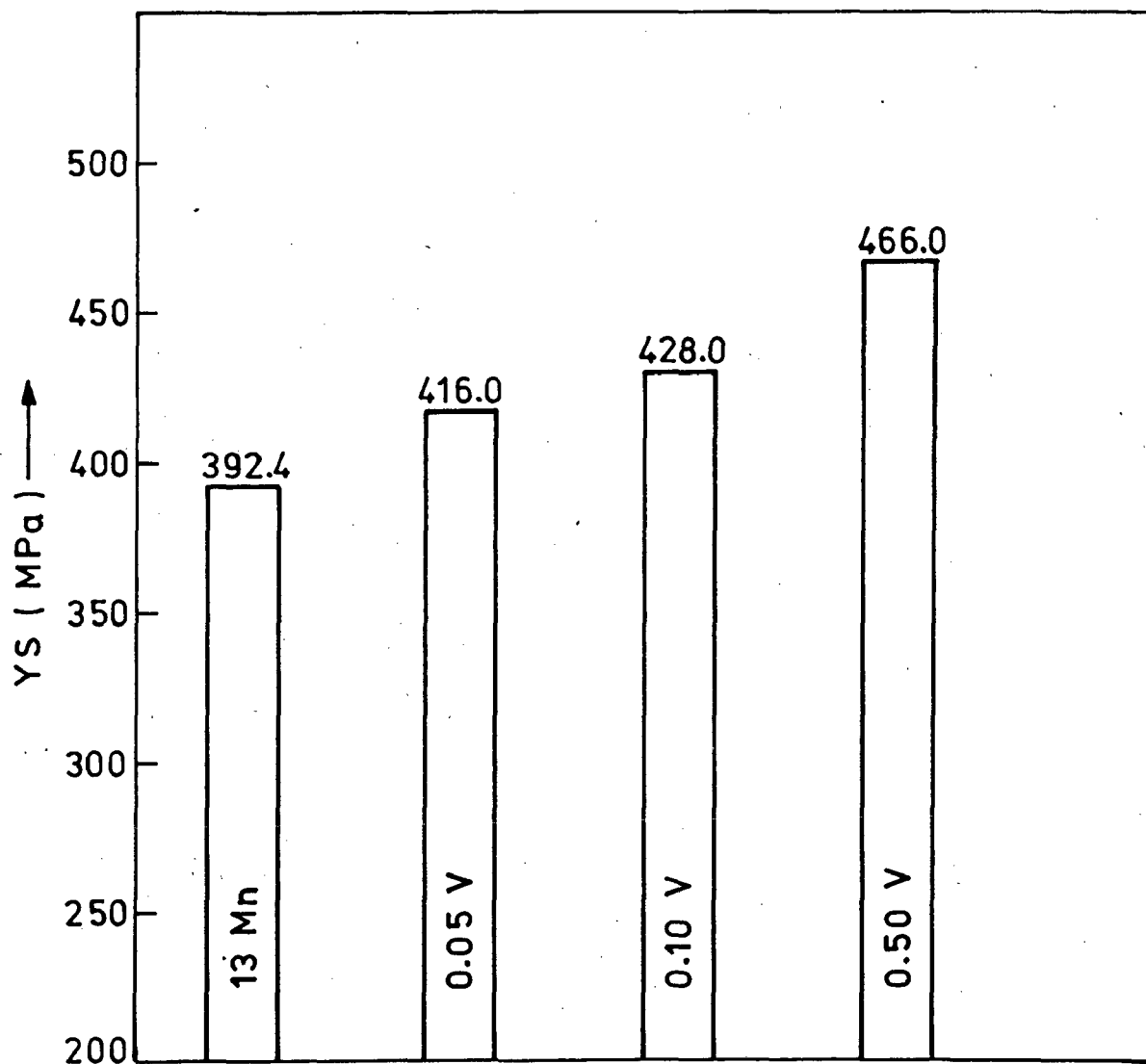


FIG. 4.5 EFFECT OF VANADIUM ADDITIONS ON YIELD STRENGTH.

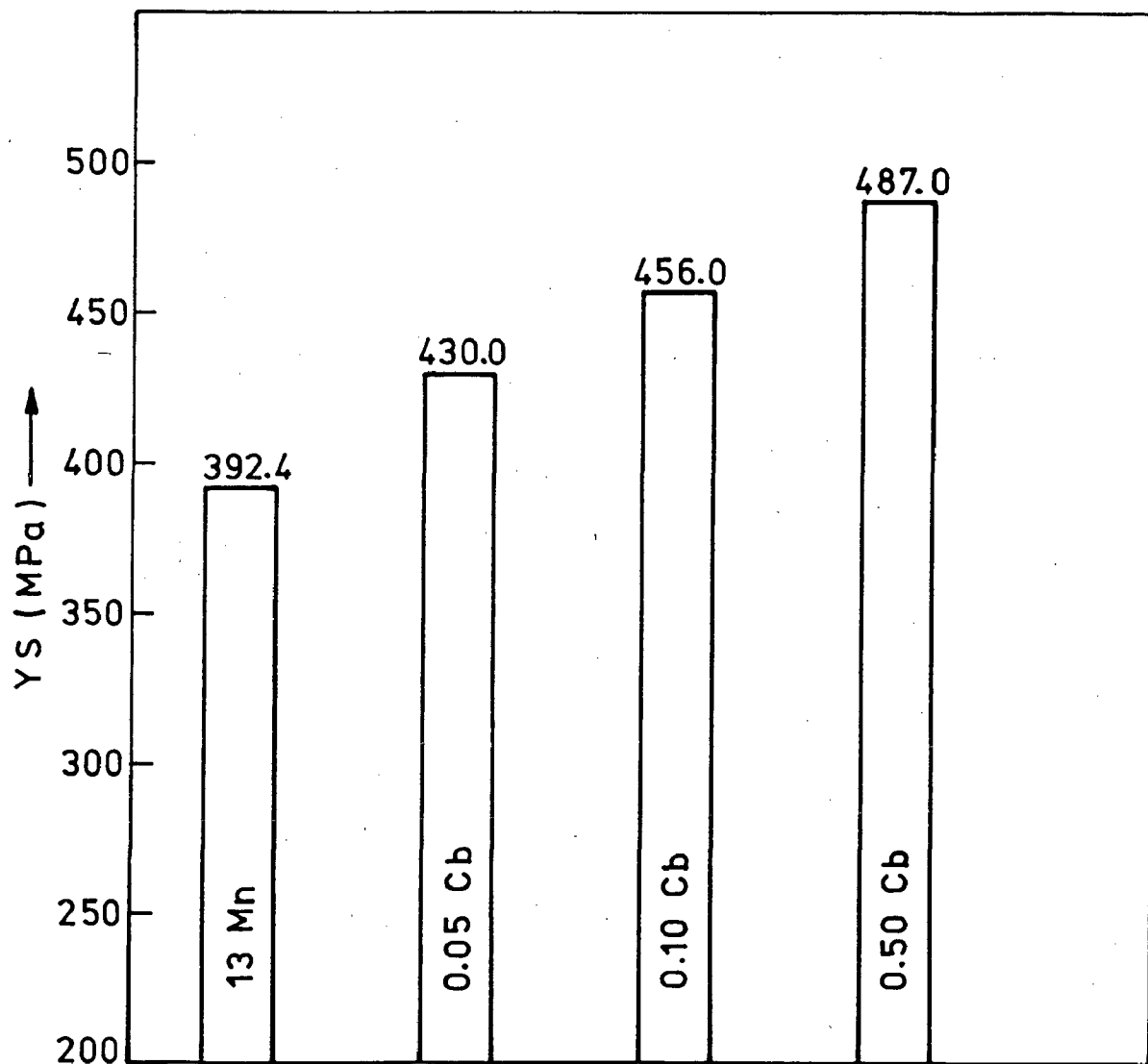


FIG. 4.6 EFFECT OF COLUMBIUM ADDITIONS ON YIELD STRENGTH.



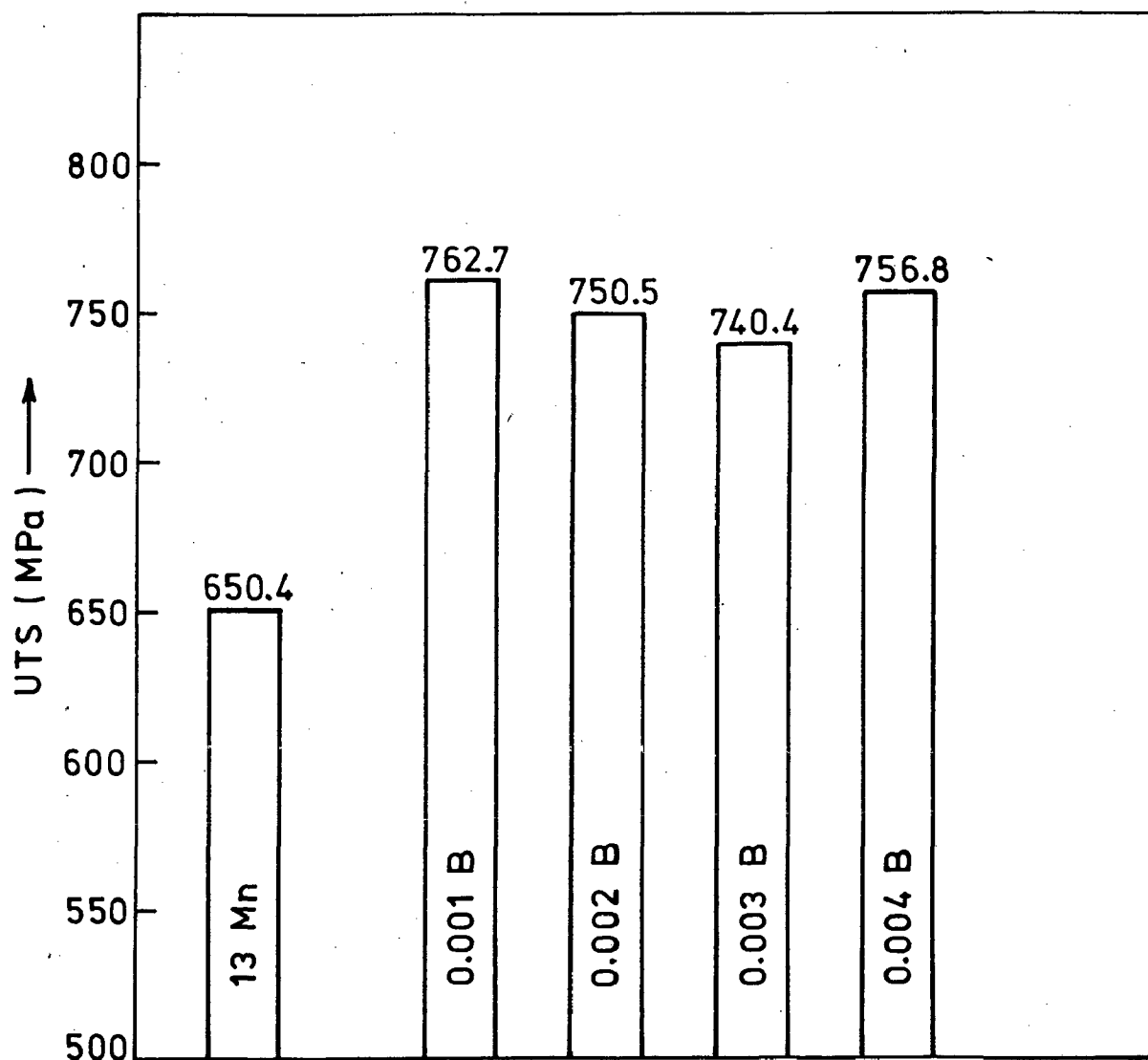


FIG. 4.7 EFFECT OF BORON ADDITIONS ON TENSILE STRENGTH.

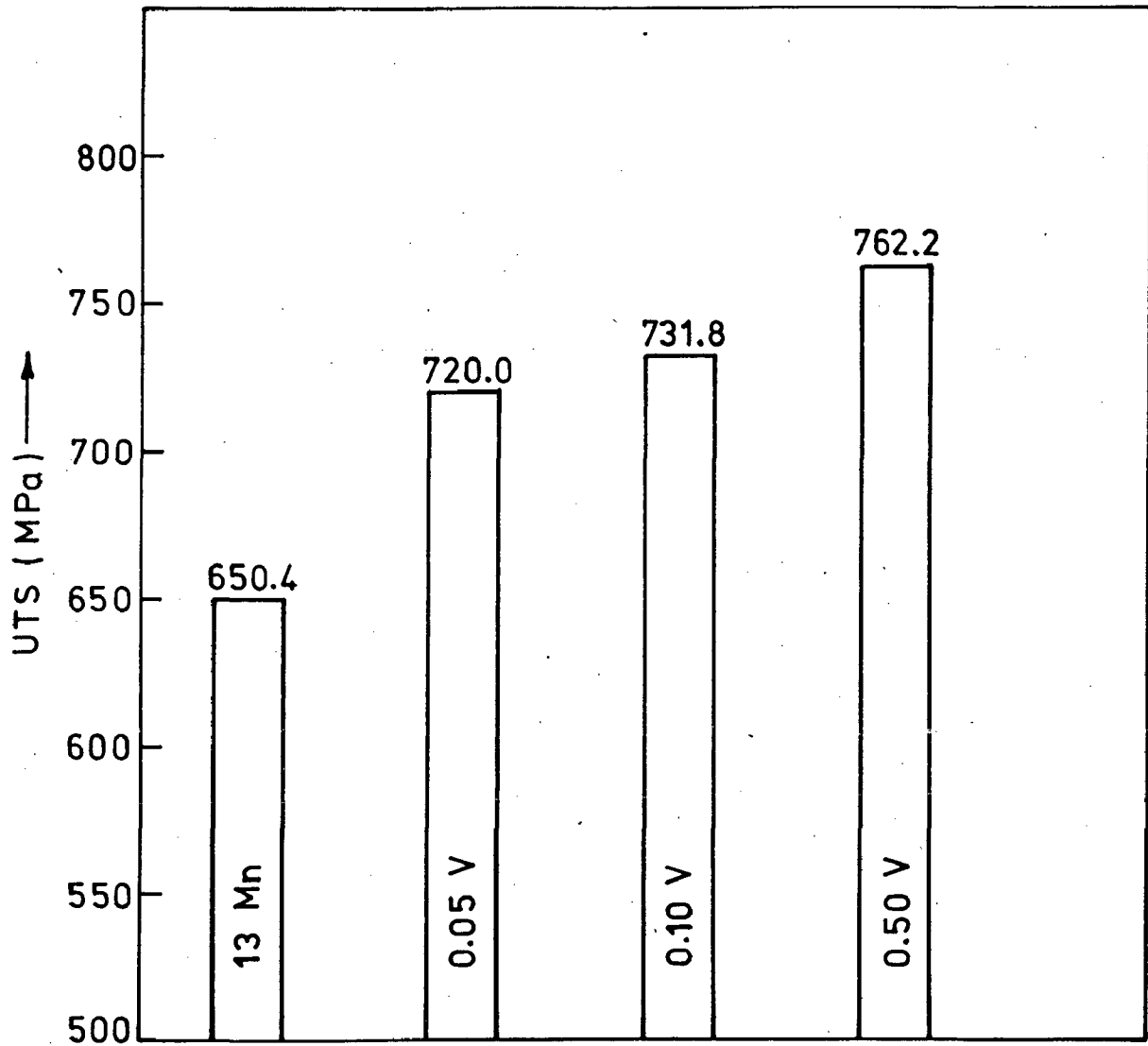


FIG. 4.8 EFFECT OF VANADIUM ADDITIONS ON TENSILE STRENGTH.

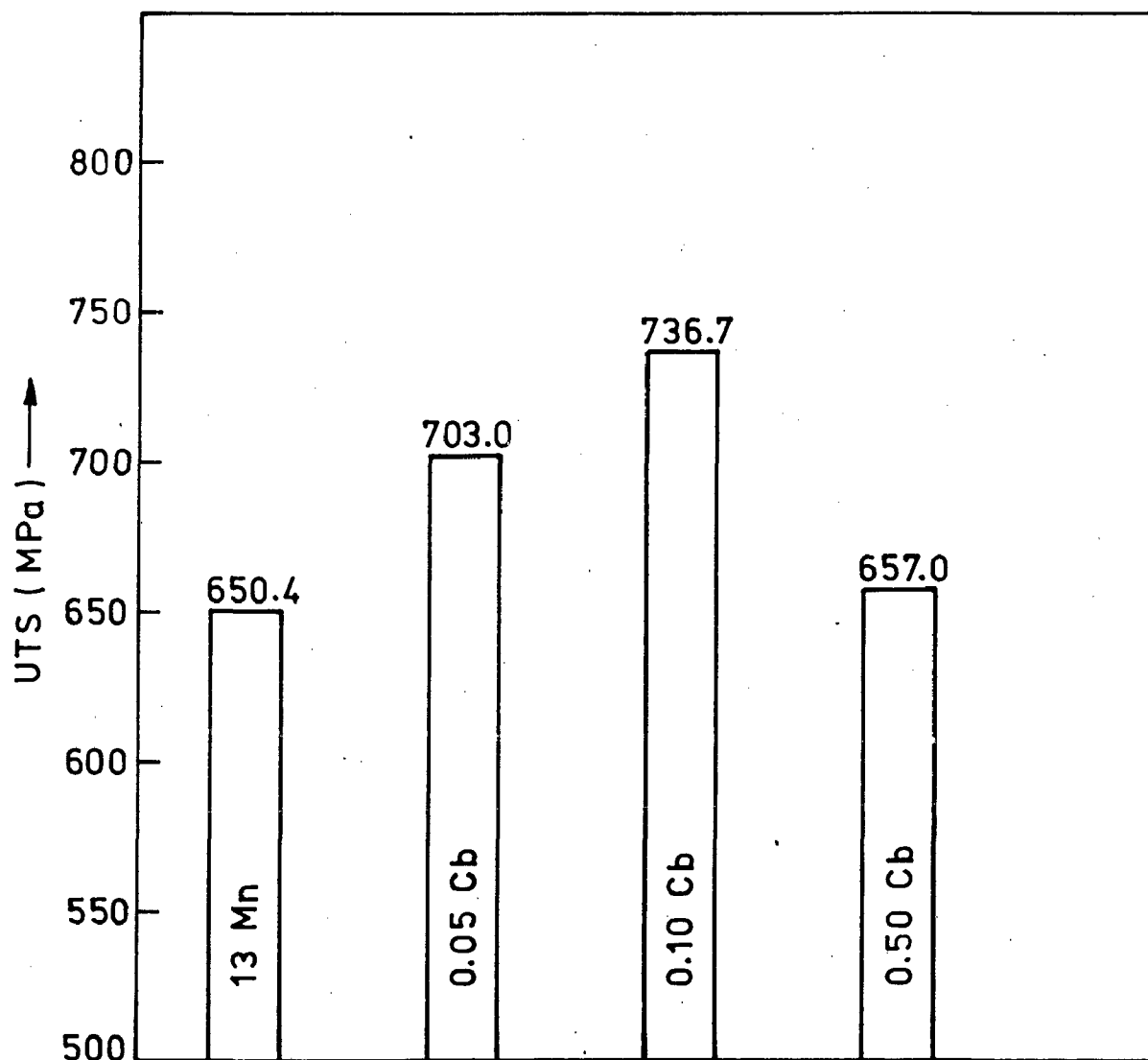


FIG. 4.9 EFFECT OF COLUMBIUM ADDITIONS ON TENSILE STRENGTH.

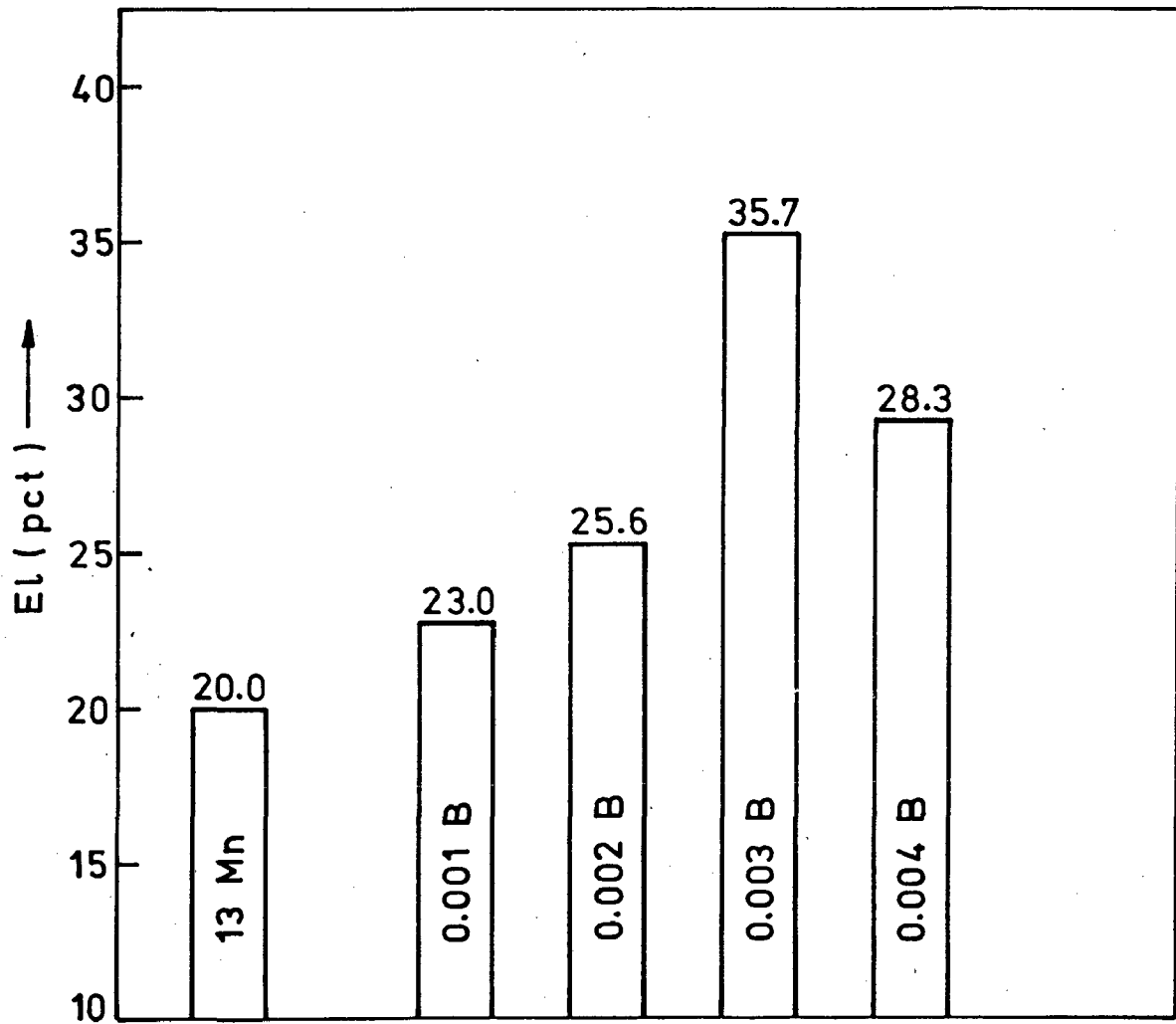


FIG. 4.10 EFFECT OF BORON ADDITIONS ON ELONGATION.

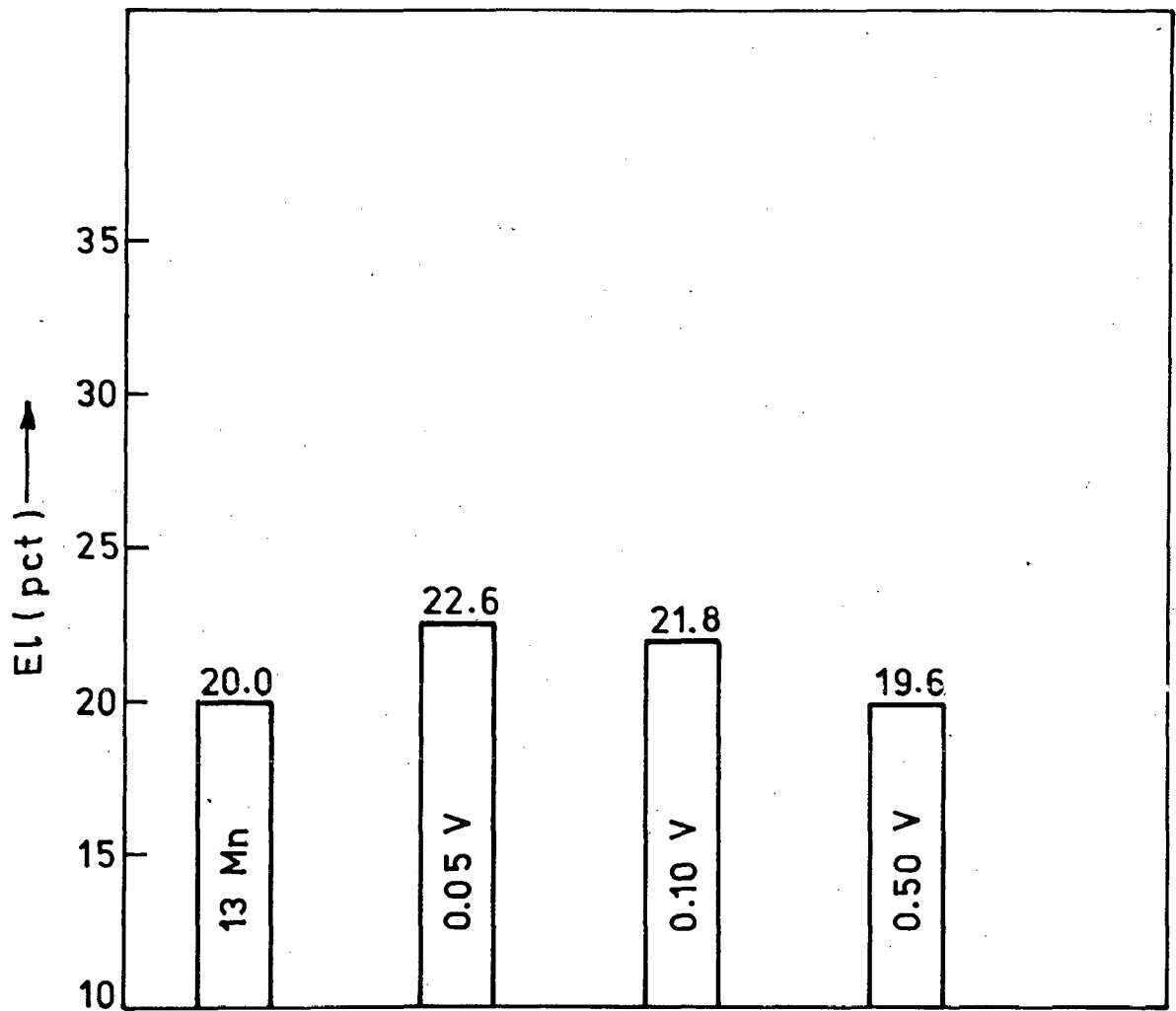


FIG. 4.11 EFFECT OF VANADIUM ADDITIONS ON ELONGATION.

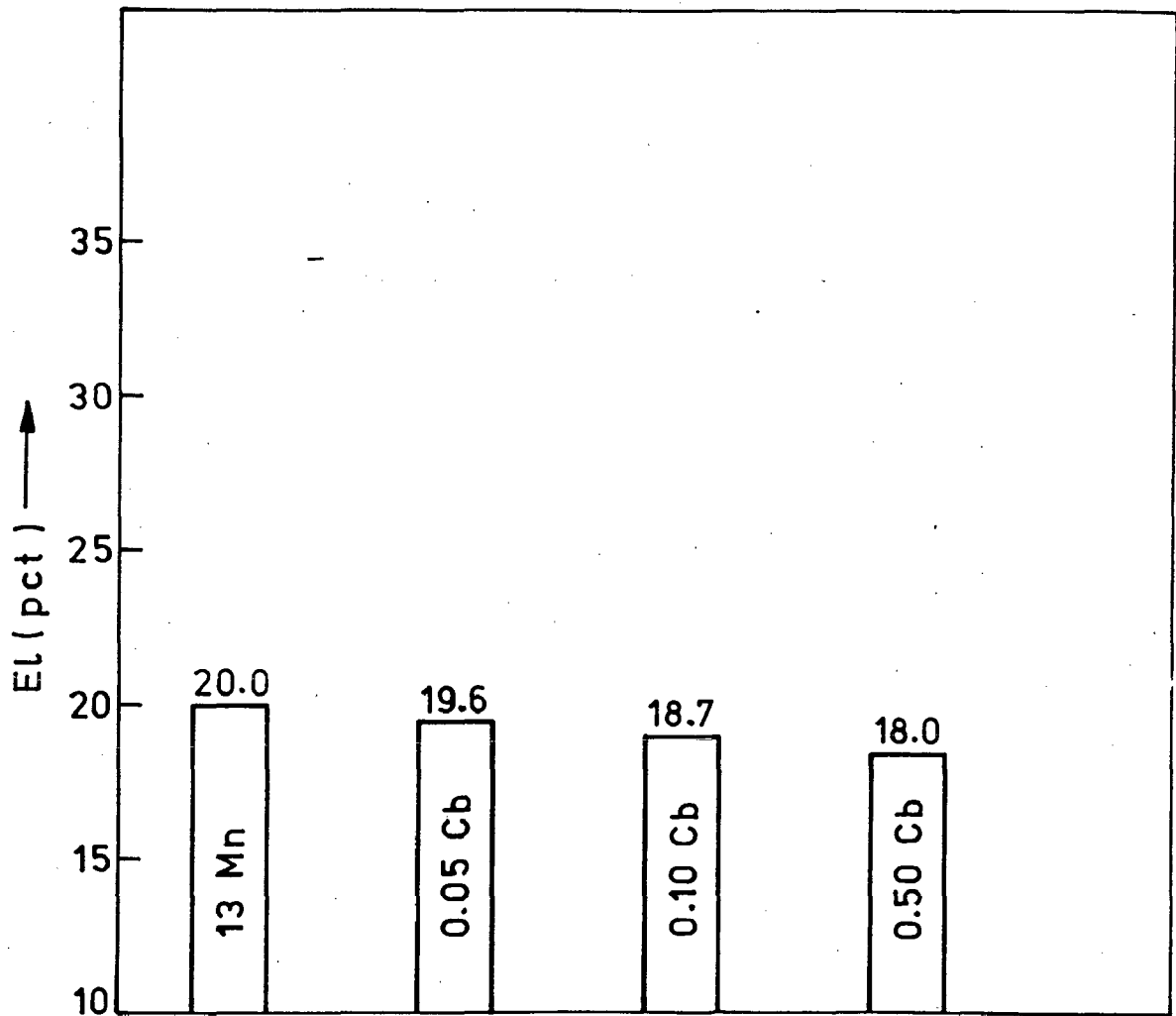


FIG. 4.12 EFFECT OF COLUMBIUM ADDITIONS ON ELONGATION.

in addition of B from 0.001 to 0.004 pct. does not alter significantly the YS and UTS values. However, there is increase in El and it rises to 35.7pct. in 0.003 B steel. Further increase in concentration of B causes El to drop. As seen from Fig.4.10 El in 0.004 B alloy is 28.3 pct. as against the maximum value (35.7 pct.) observed in the 0.003 B alloy. Hence it is observed that best tensile properties by B additions are obtained in 0.003 B steel. Micro alloying of 13 Mn steel by 0.05 pct. V (i.e. 0.05V alloy) raises the YS from 392.4 to 416.0 MPa, UTS from 650.4 to 720.0 MPa and El from 20.0 to 22.6 pct. The increase in concentration of V to 0.10 pct. (0.10 V alloy) further increases the YS to 428.0 MPa, UTS to 731.8 and there is drop in El to 21.8 pct. Further increase in V addition to 0.50 pct. (0.50 V alloy) increases YS to 466.0 MPa, UTS to 762.2 MPa and decreases El to 19.6 pct. (Figs.4.2, 4.5,4.8 and 4.11). Addition of 0.05 pct. Cb (0.05 Cb alloy) enhances YS of 13 Mn steel to 430.0 MPa, UTS to 703.0 MPa but decreases the El to 19.6 pct. Increase in concentration of Cb to 0.10 pct. (0.10 Cb alloy) further enhances the YS to 456.0 MPa, UTS to 736.7 MPa and there is further decrement in El to 18.7 pct. However, at 0.50 pct. Cb addition (0.5 Cb alloy) YS improves to 487.0 MPa but there is sharp decline in UTS from 736.7 to 657.0 MPa and El to 18.0 pct. (Figs.4.3,4.6,4.9 and 4.12).

#### 4.1.2 Hardness

The effect of micro alloying on as quenched hardness

of 13 Mn steel has been studied (Figs.4.13 to 4.15). It is seen from Fig.4.13 that there is very little change in the as quenched hardness of 13 Mn steel with B additions. There is decrease in hardness from 224 VHN to 220, 217 and 214 VHN in 0.001 B, 0.002 B and 0.003 B alloys respectively. Alloy 0.004 B shows an increase in hardness from 224 to 230 VHN. The addition of V increases the as quenched hardness from 224 to 252 (Fig.4.14). The effect of Cb addition on hardness is also similar as with addition of V. It raises the as quenched hardness from 224 to 245 with increase in concentration (Fig. 4.15). In the alloys 0.05 Cb, 0.10 Cb and 0.50 Cb the as quenched hardness is 238, 240 and 245 VHN respectively.

#### 4.1.3 Impact properties

Micro alloying of basic 13 Mn steel with B, V and Cb significantly alters the impact properties. The charpy impact values at room temperature for various alloying additions are shown in Figs.4.16 to 4.18 and in form of histograms in Figs. 4.19 to 4.21. The addition of 0.001 pct. B significantly improves the toughness of 13 Mn steel from 130 J to 158 J which is further enhanced to 202 J by increasing the B content to 0.003 pct. (0.003 B alloy). Further increase in B (0.004 B alloy) decreases the impact strength to 180 J, though it is still higher than 13 Mn steel (Figs.4.16, 4.19). The addition of V in low concentration (0.05 V alloy) shows marginal improvement in impact strength of 13 Mn steel from 130 J to 136 J.



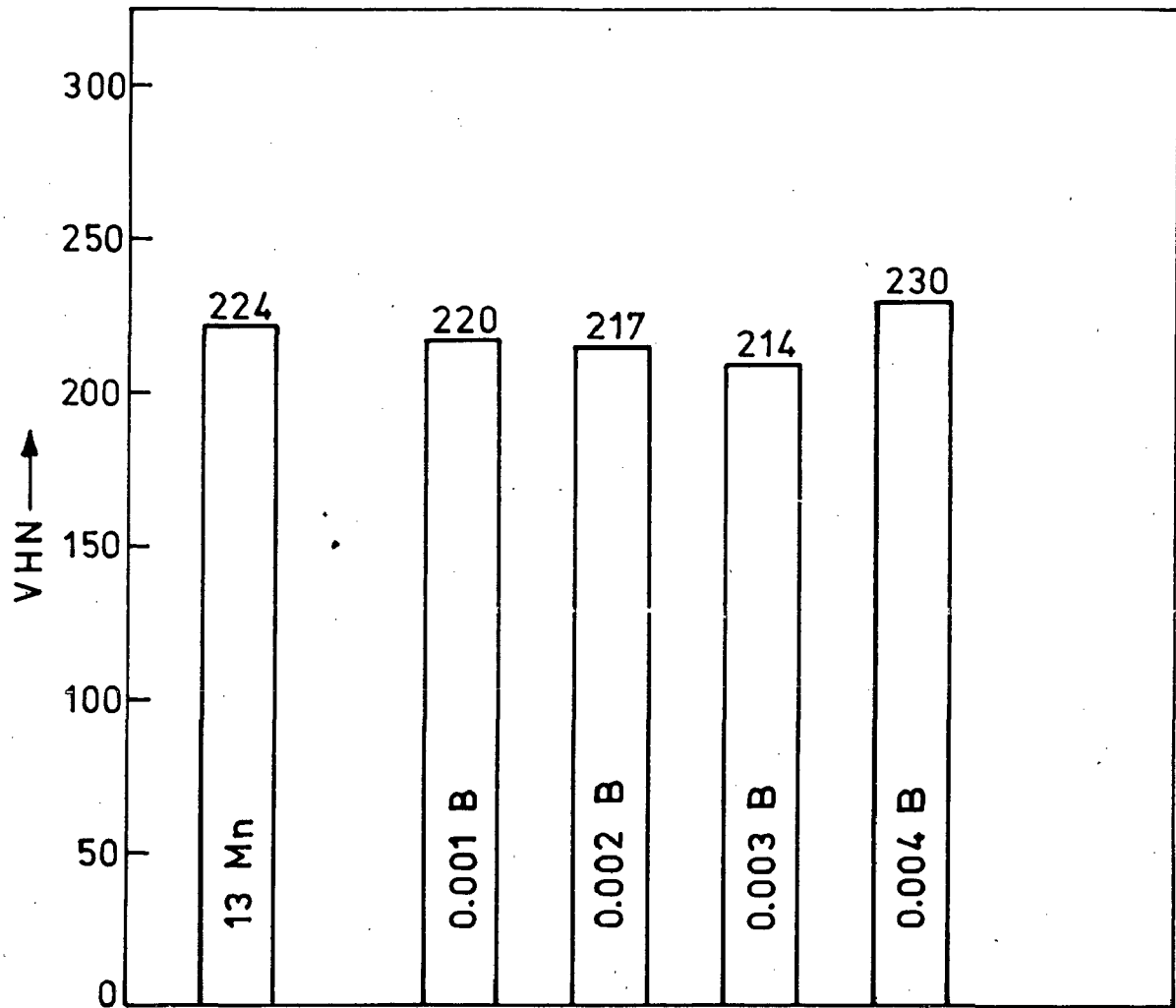


FIG. 4.13 EFFECT OF BORON ADDITIONS ON AS QUENCHED HARDNESS.

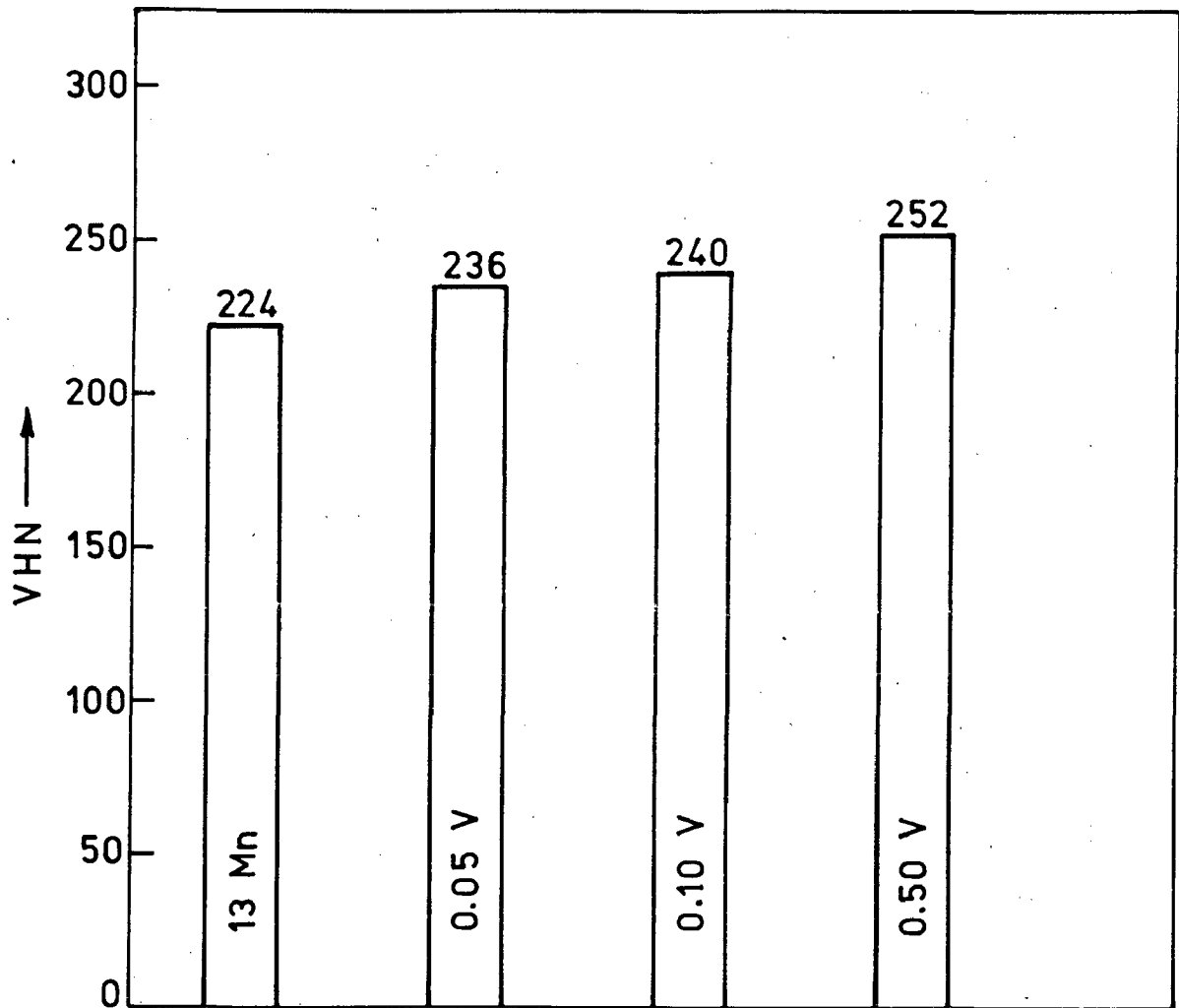


FIG.4.14 EFFECT OF VANADIUM ADDITIONS ON AS QUENCHED HARDNESS.

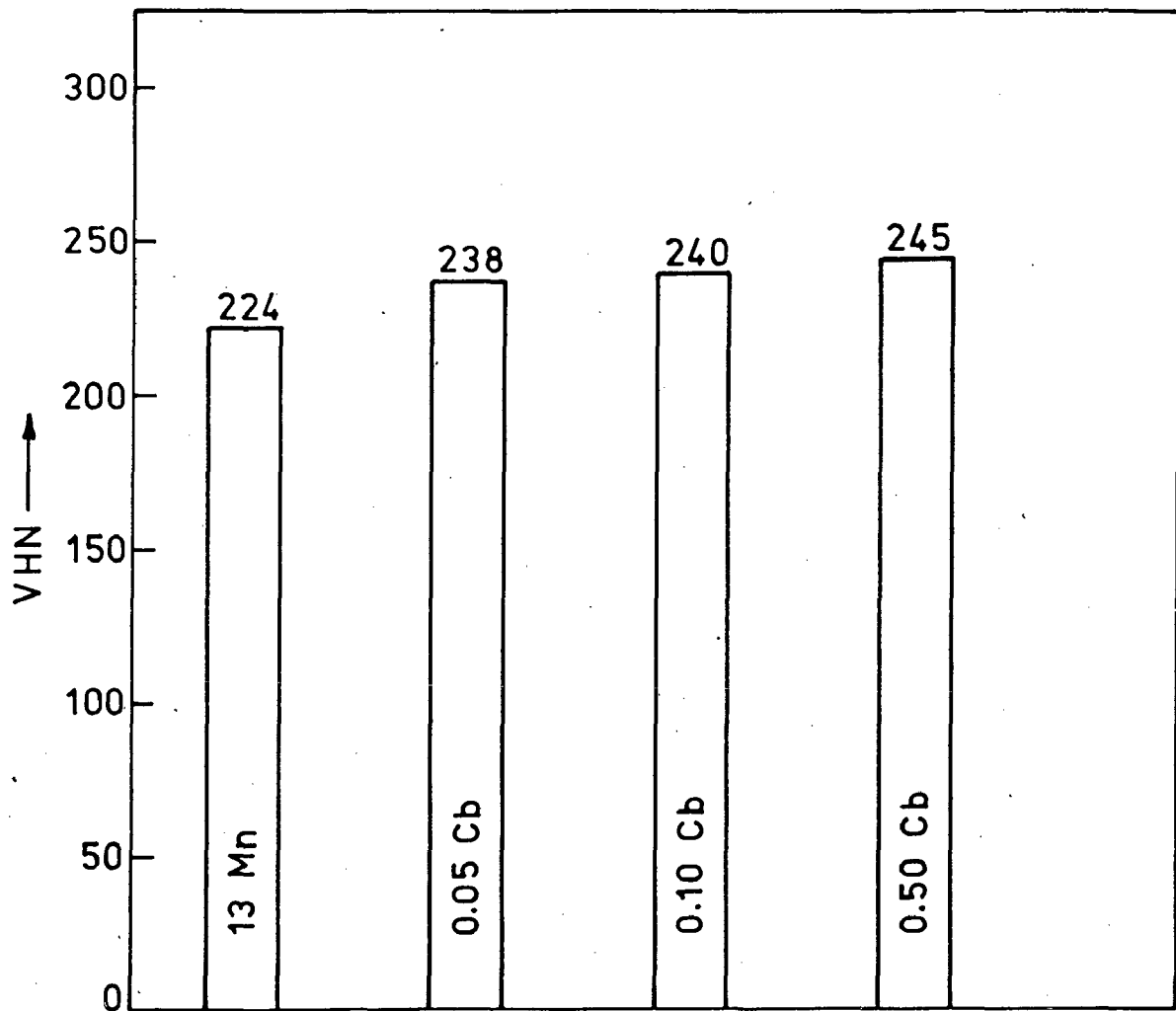


FIG. 4.15 EFFECT OF COLUMBIUM ADDITIONS ON AS QUENCHED HARDNESS.

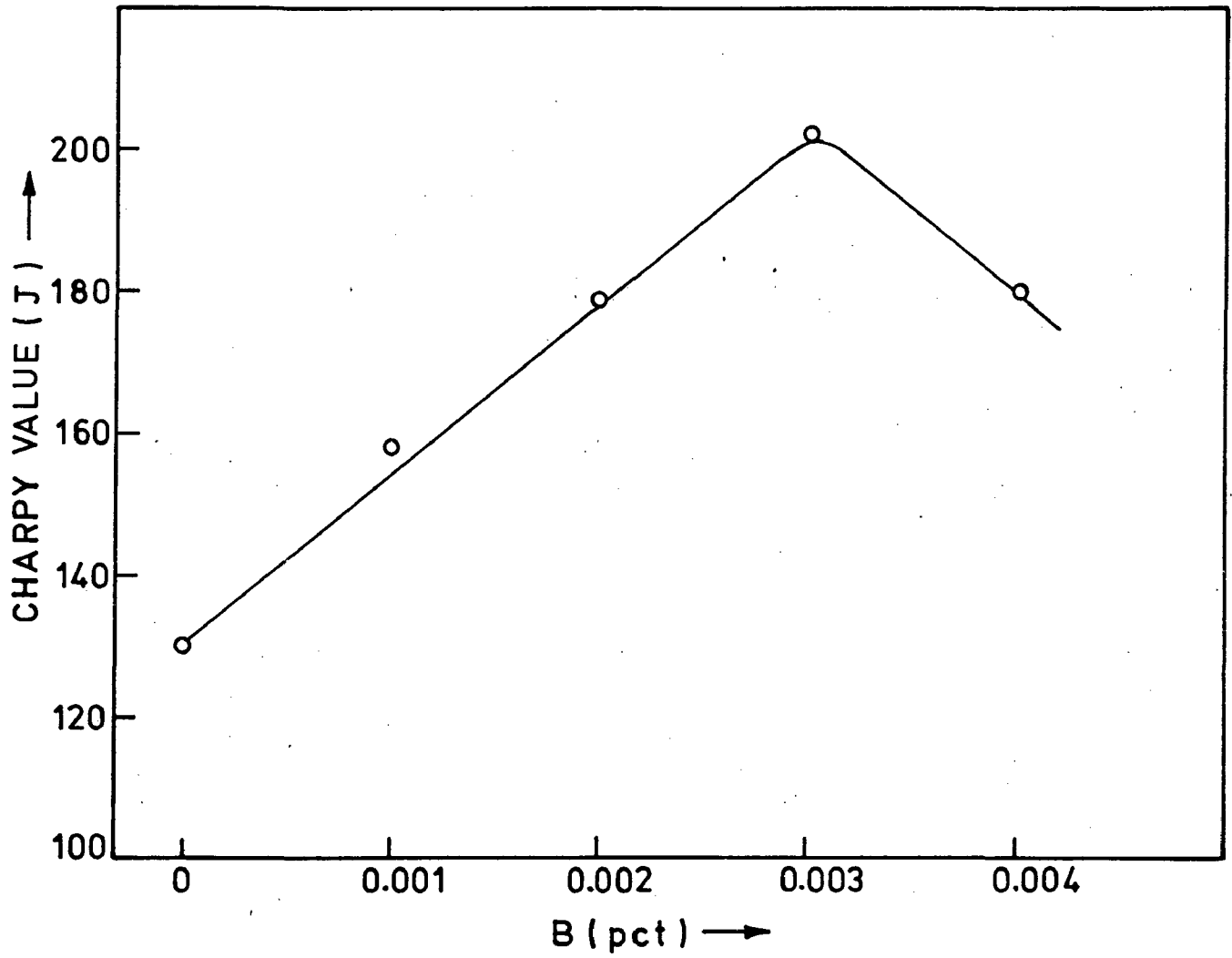


FIG.4.16 EFFECT OF BORON ADDITIONS ON IMPACT VALUE.

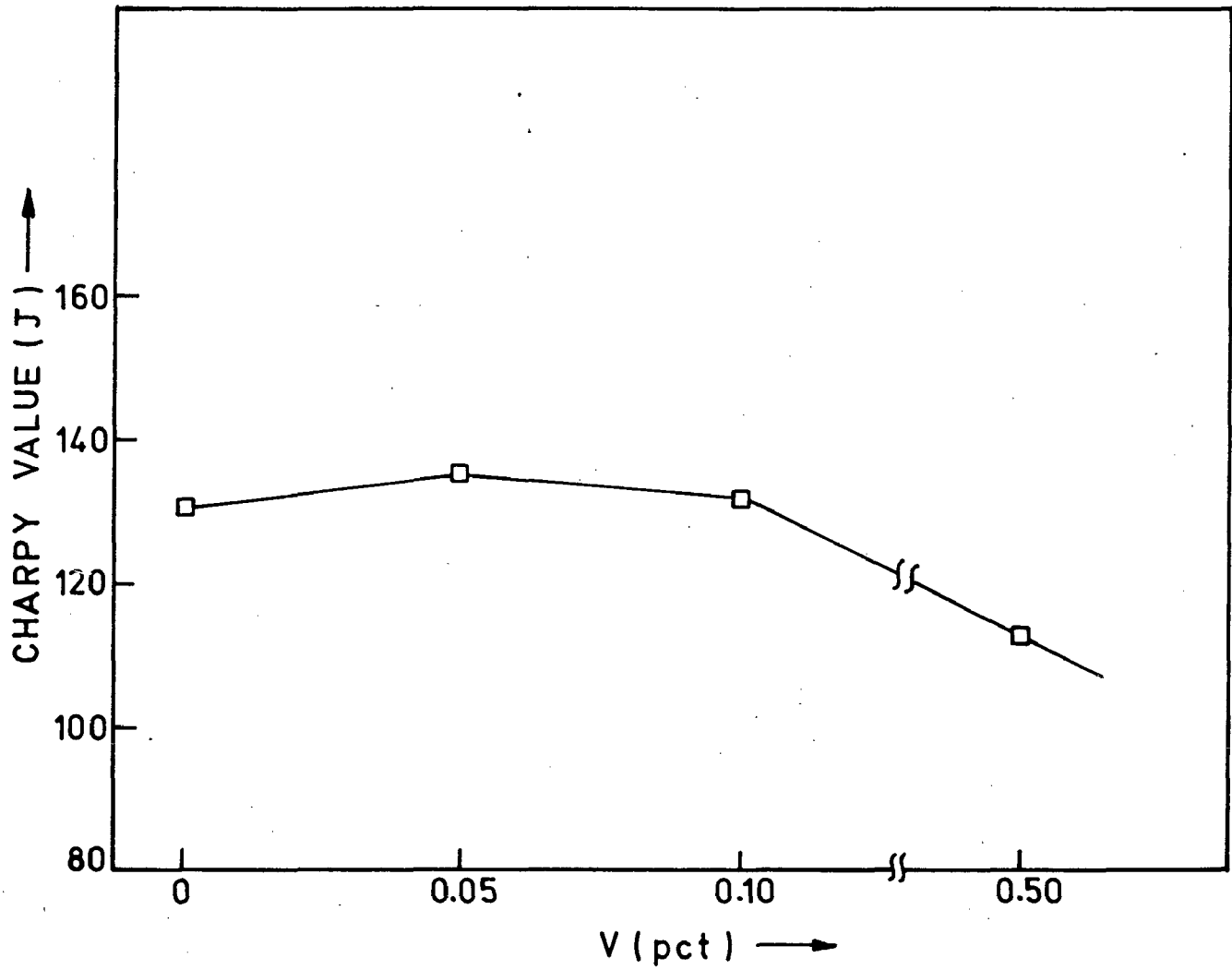


FIG. 4.17 EFFECT OF VANADIUM ADDITIONS ON IMPACT VALUE.

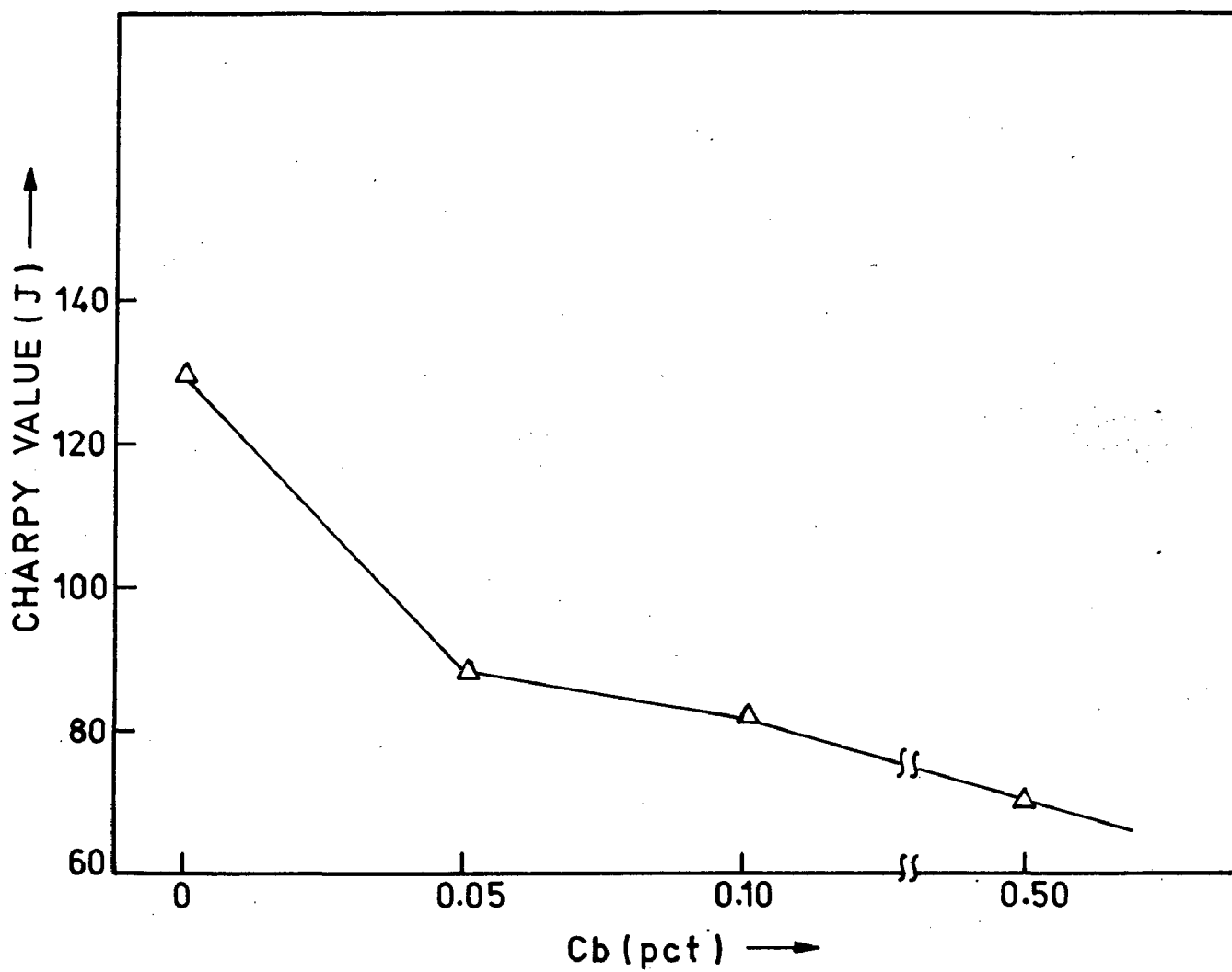


FIG. 4.18 EFFECT OF COLUMBIUM ADDITIONS ON IMPACT VALUE.

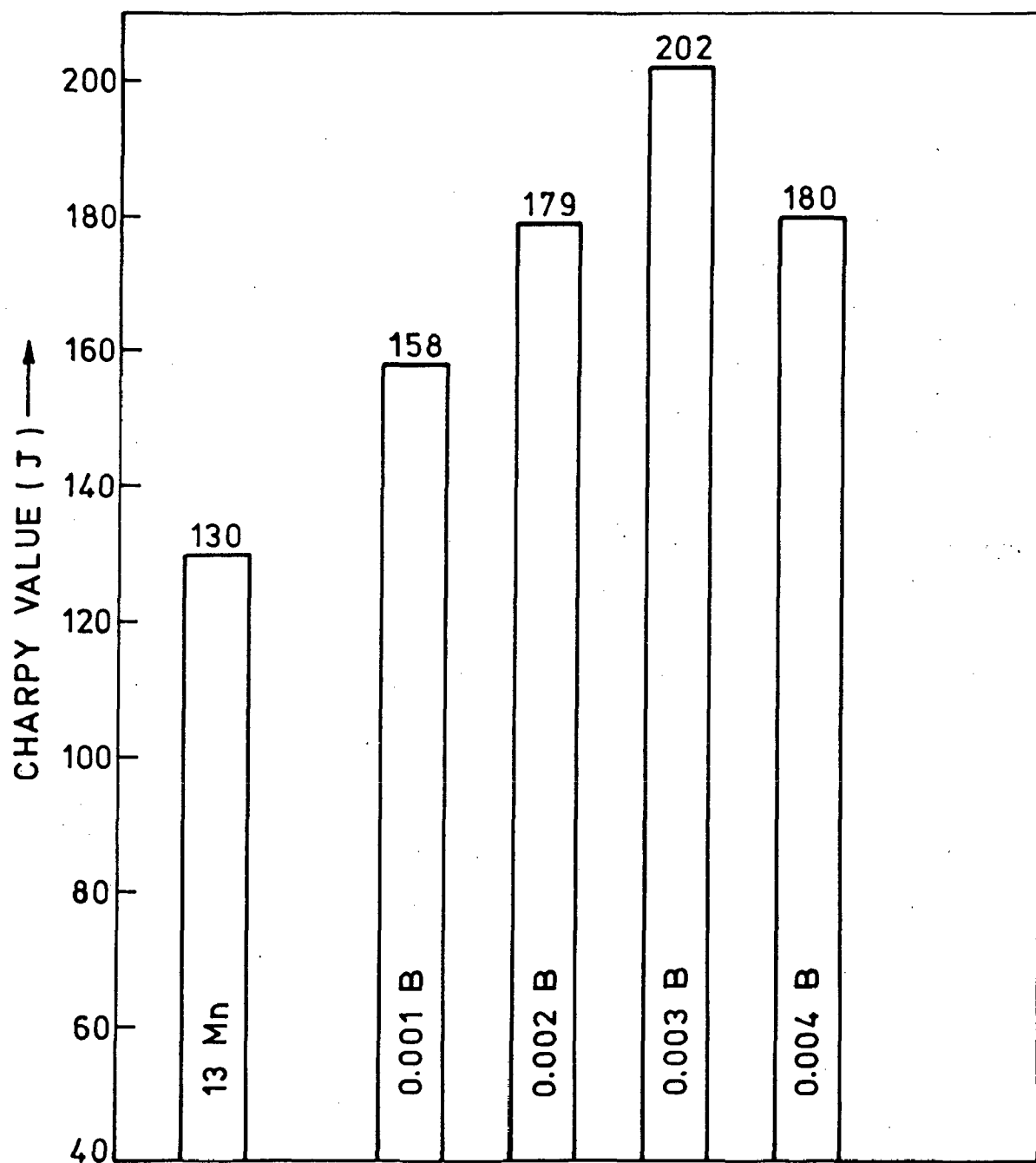


FIG. 4.19 EFFECT OF BORON ADDITIONS ON IMPACT VALUE.

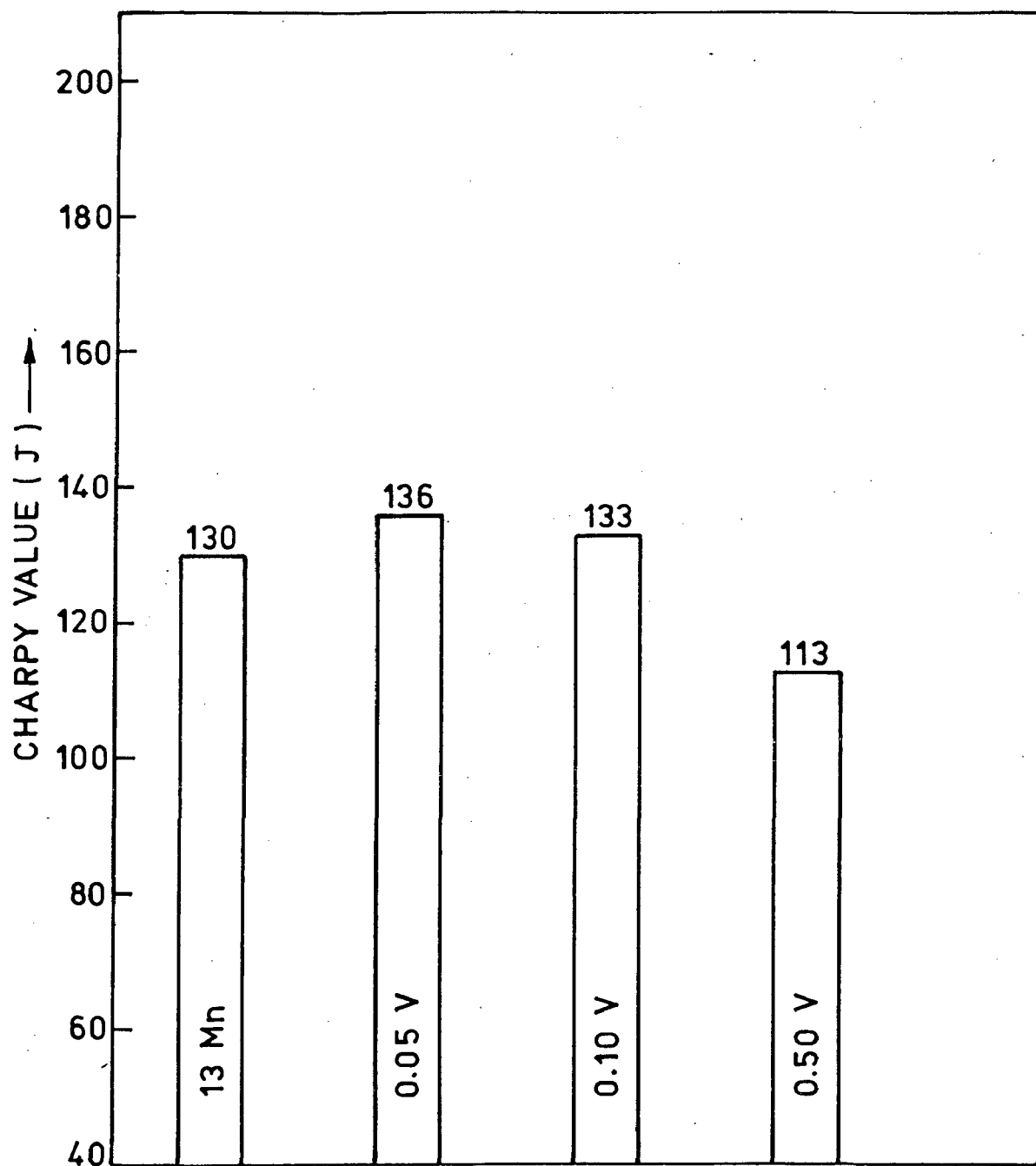


FIG. 4.20 EFFECT OF VANADIUM ADDITIONS ON IMPACT VALUE.



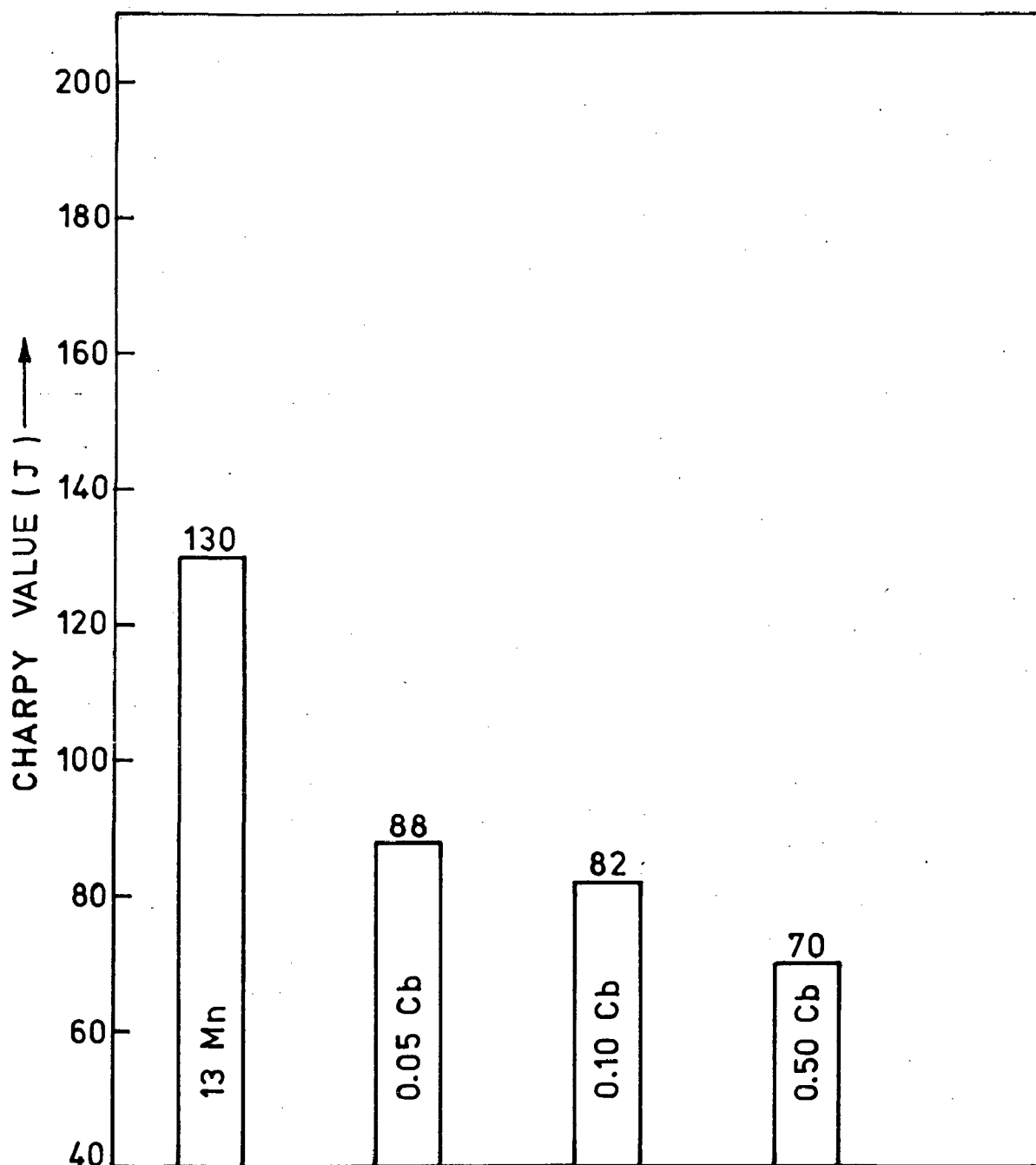


FIG. 4.21 EFFECT OF COLUMBIUM ADDITIONS ON IMPACT VALUE.

In 0.10 V alloy the impact strength is almost in the same level as of 13 Mn steel. However, higher concentration of V(0.50 V alloy) lowers the toughness to 113 J (Figs.4.17,4.20). Columbium additions drastically drop the impact strength of Hadfield steel (Figs.4.18, 4.21). It is seen that 0.05 pct. Cb to basic 13 Mn composition decreases the impact value from 130 J to 88 J. Further increase in Cb brings down the impact value further to 70 J as observed in 0.50 Cb alloy.

Figs.4.22 to 4.24 represent the extent of improvement/deterioration in mechanical properties of 13 Mn steel by micro alloying. It is seen (Fig.4.22) that 0.001 B enhances YS by 16.5 pct., UTS by 17.2 pct. and El by 15.0 pct. There is decrease in as quenched hardness by 1.7 pct. and toughness gets improved by 21.5 pct. Further increase in B concentration (0.002 B and 0.003 B alloy) causes marginal decrease in YS and UTS in comparison to 0.001 B alloy, but there is significant improvement in El and impact values, which in the 0.003 B alloy are improved by 78.5 pct. and 55.0 pct. respectively. The as quenched hardness is reduced by 4.5 pct. in this alloy. Further increase in B(0.004 B alloy) shows a downward trend specially in El and impact values, although there is slight improvement in YS, UTS and as quenched hardness. Thus it is observed that 0.003 B alloy appears to be having the most optimum combination of various mechanical properties.

The addition of V (Fig.4.23) enhances mechanical properties of 13 Mn alloy. In the 0.05 V alloy there is improvement

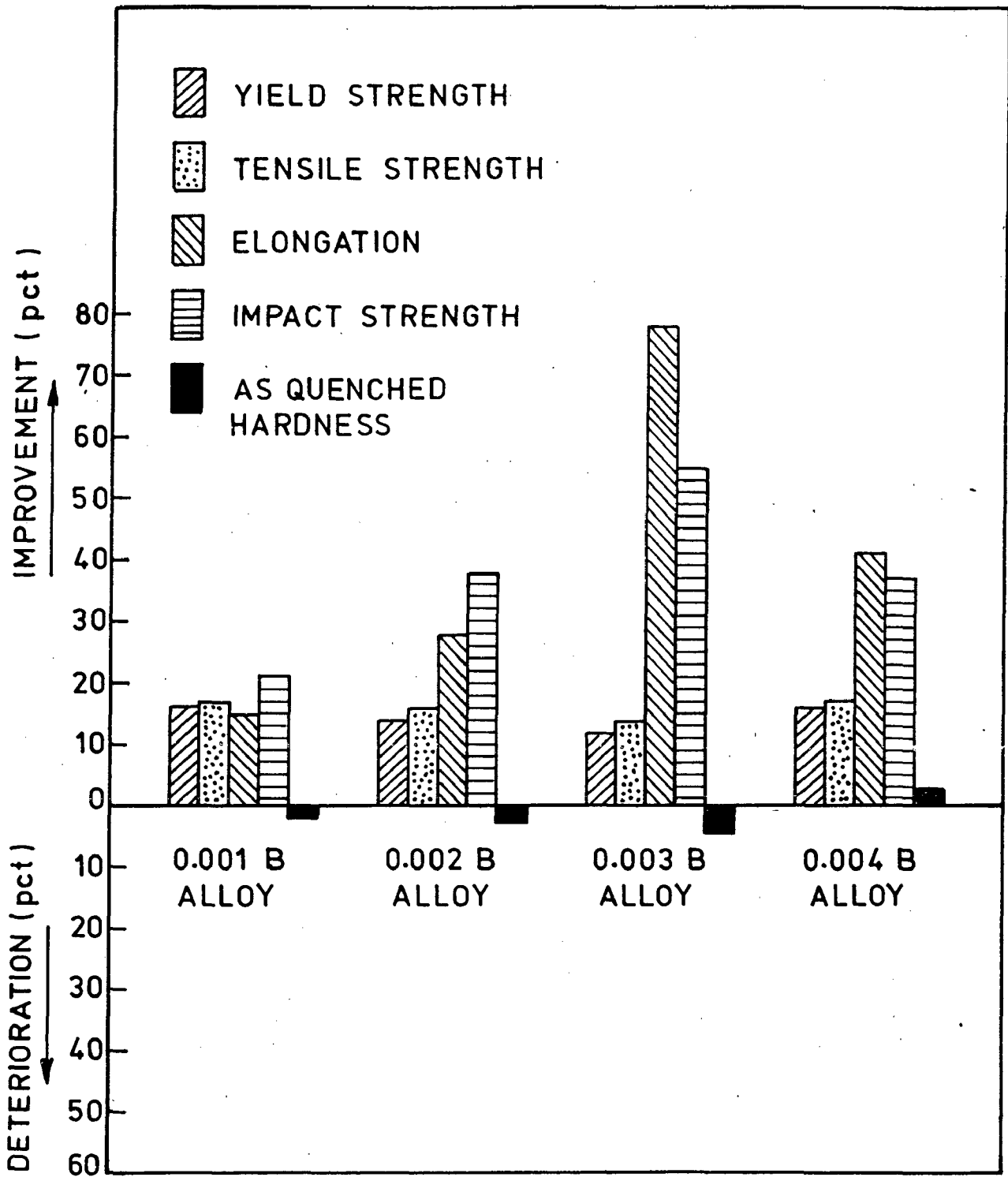


FIG. 4.22 EFFECT OF BORON ADDITIONS ON IMPROVEMENT/DETERIORATION IN MECHANICAL PROPERTIES OF 13 Mn ALLOY.

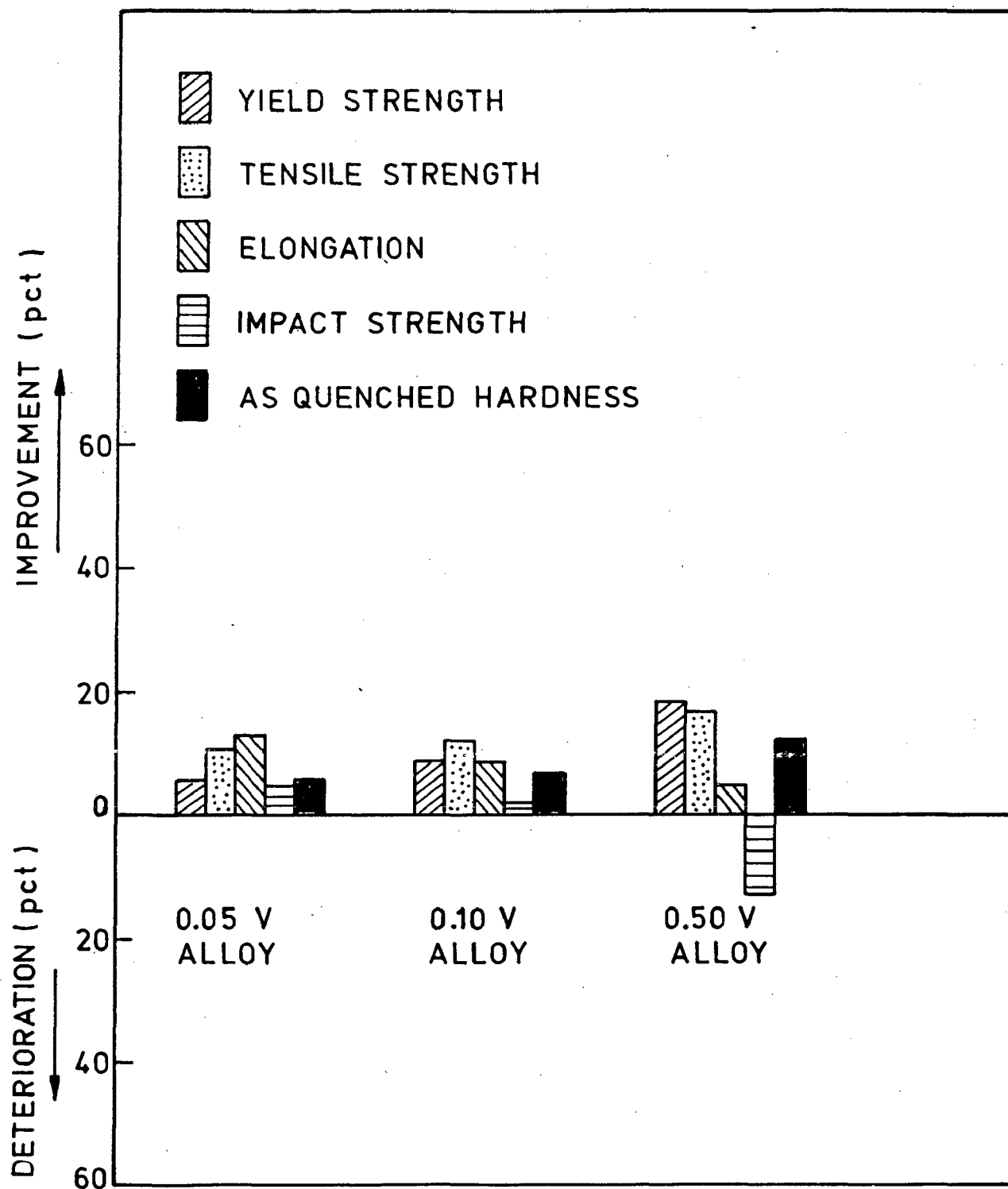


FIG. 4.23 EFFECT OF VANADIUM ADDITIONS ON IMPROVEMENT / DETERIORATION IN MECHANICAL PROPERTIES OF 13 Mn ALLOY.

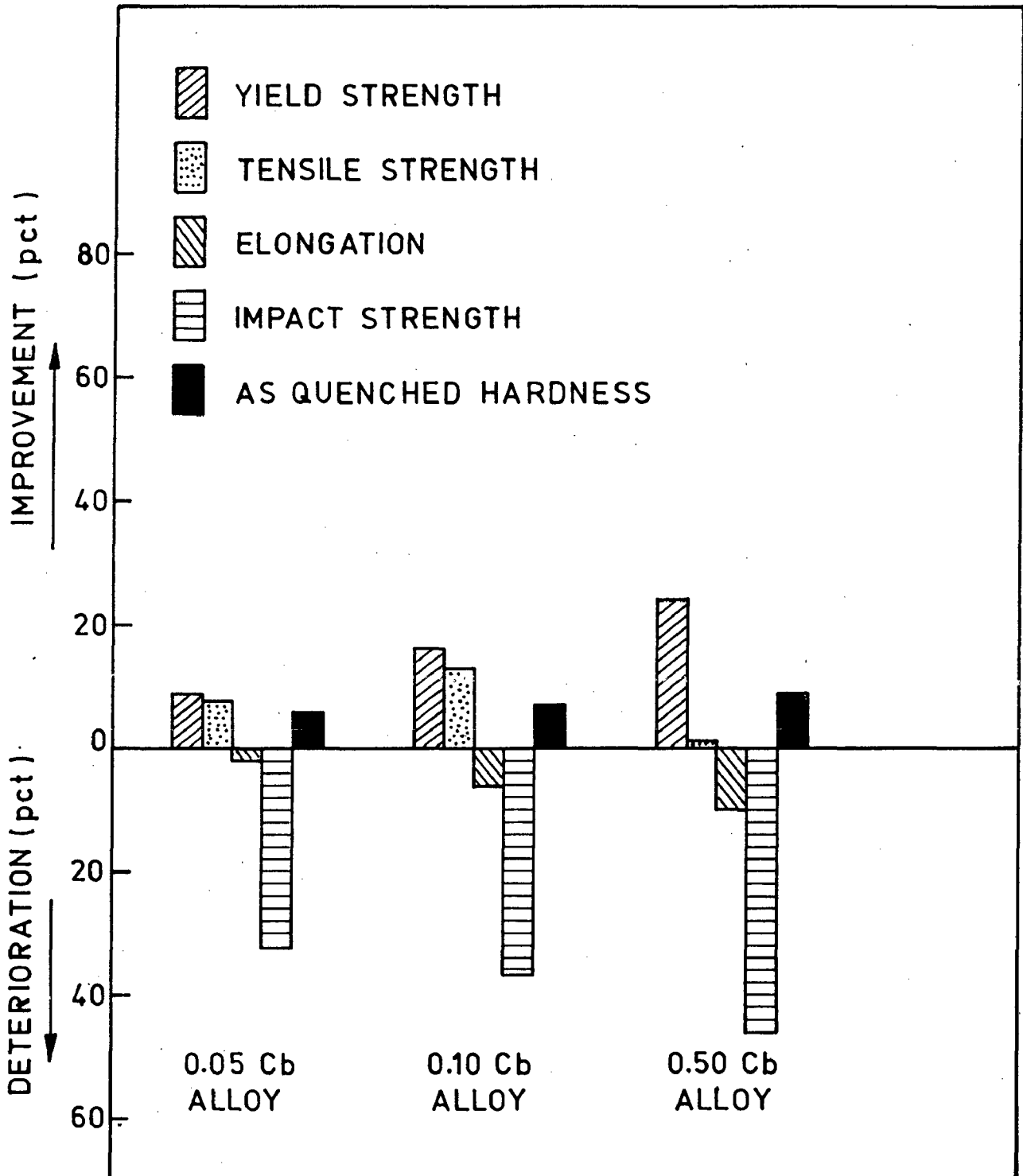


FIG. 4.24 EFFECT OF COLUMBIUM ADDITIONS ON IMPROVEMENT / DETERIORATION IN MECHANICAL PROPERTIES OF 13 Mn ALLOY.

in YS by 6.0 pct., UTS by 10.7 pct. and El by 13.0 pct. Toughness is also improved marginally by 4.6 pct. and as quenched hardness increases by 5.3 pct. 0.10 V addition further enhances the YS, UTS and as quenched hardness, but the improvement in El and impact value is slightly lower than that in 0.05V alloy. By addition of 0.50 V the YS, UTS, and as quenched hardness are although further increased, but the impact strength is drastically reduced. As seen in Fig.4.23 the impact strength of 0.50 V alloy is lower by 13 pct. in respect of the 13 Mn alloy and by 15.3 pct. in respect of 0.10 V alloy.

The extent of improvement/deterioration in mechanical properties of 13 Mn steel by additions of Cb is represented in Fig.4.24. It is seen that the impact strength is significantly reduced by Cb additions. For example, it is observed that by 0.50 Cb addition the impact strength of the base steel (13 Mn) is reduced by 46.1 pct. Additions of 0.50 Cb also reduces El by 10.0 pct. YS and as quenched hardness are continuously increased by micro alloying with Cb. It is seen that in 0.50 Cb steel the YS is higher by 24.2 pct. and as quenched hardness by 9.4 pct. UTS increases upto 0.1 Cb, beyond which the improvement in UTS with respect to the 13 Mn steel is only marginal.

It is seen from literature that wear resistance of any material is not only the function of hardness but it also largely

depends upon the mechanical properties of the material viz. YS, UTS, El and toughness [13,33,76,124,125,126]. Careful inspection of wear mechanisms has indicated [33,124] that, particularly in work hardening materials, wear occurs simultaneously by plastic deformation and brittle fracture. Hence a material with higher El and toughness will have better wear resistance. Ball [76] has correlated the wear rate with critical fracture strain and he suggested that materials, which are having large areas under their stress-strain curves and their work to fracture is high, will reach the critical fracture strain under abrasive stress conditions with much difficulty. Hence such materials will have high wear resistance. Therefore, it is higher UTS, El and toughness apart from hardness which appear to be very important parameters in controlling wear in Hadfield steel. It is observed from the results that 0.003 B alloy has highest El (35.7 pct.) and impact strength (202 J) alongwith higher UTS (740.4 MPa) among all the four concentrations of B studied in this investigation. Hence it is expected to result in significant improvement in wear characteristics. Therefore, 0.003 B alloy was selected for further studies of work hardening and wear. It is also seen from the results that 0.10 V alloy shows optimum mechanical properties out of three concentrations taken in this investigation. Higher concentration of V (0.50 V alloy) shows significant drop in toughness, which is one of the important parameters for improvement in wear characteristics. Since the YS, UTS and as quenched hardness in the

0.10 V alloy are higher than in 13Mn alloy and impact strength is also not deteriorated with respect to the base composition, this alloy was chosen for further investigations. As regard Cb additions, all the compositions micro alloyed with this element exhibited poor elongation and toughness values, but there is an increase in YS and as quenched hardness. Hence the general wear characteristics of this alloy were not expected to be good. The criterion of high YS was chosen for Cb bearing steels as according to some studies [13,76] this parameter also affects wear properties. Also YS is an important property, specially in Hadfield steel since the heat treated steel has low YS and as such it is not very suitable for applications requiring close dimensional tolerances. With this view the 0.50 Cb alloy was selected for further investigations.

#### 4.1.4 Strain Hardening Coefficient

The strain hardening coefficient,  $\eta$ , was determined from the slope of the log-log plot of true stress-true strain diagram in the plastic range (Fig.4.25). The values of  $\eta$  represent the rate of work hardening in the alloys investigated. Following values of strain hardening coefficients were obtained for different alloys :

13 Mn alloy	:	$\eta$	= 0.45
0.003 B alloy	:	$\eta$	= 0.58
0.10 V alloy	:	$\eta$	= 0.80
0.50 Cb alloy	:	$\eta$	= 0.70



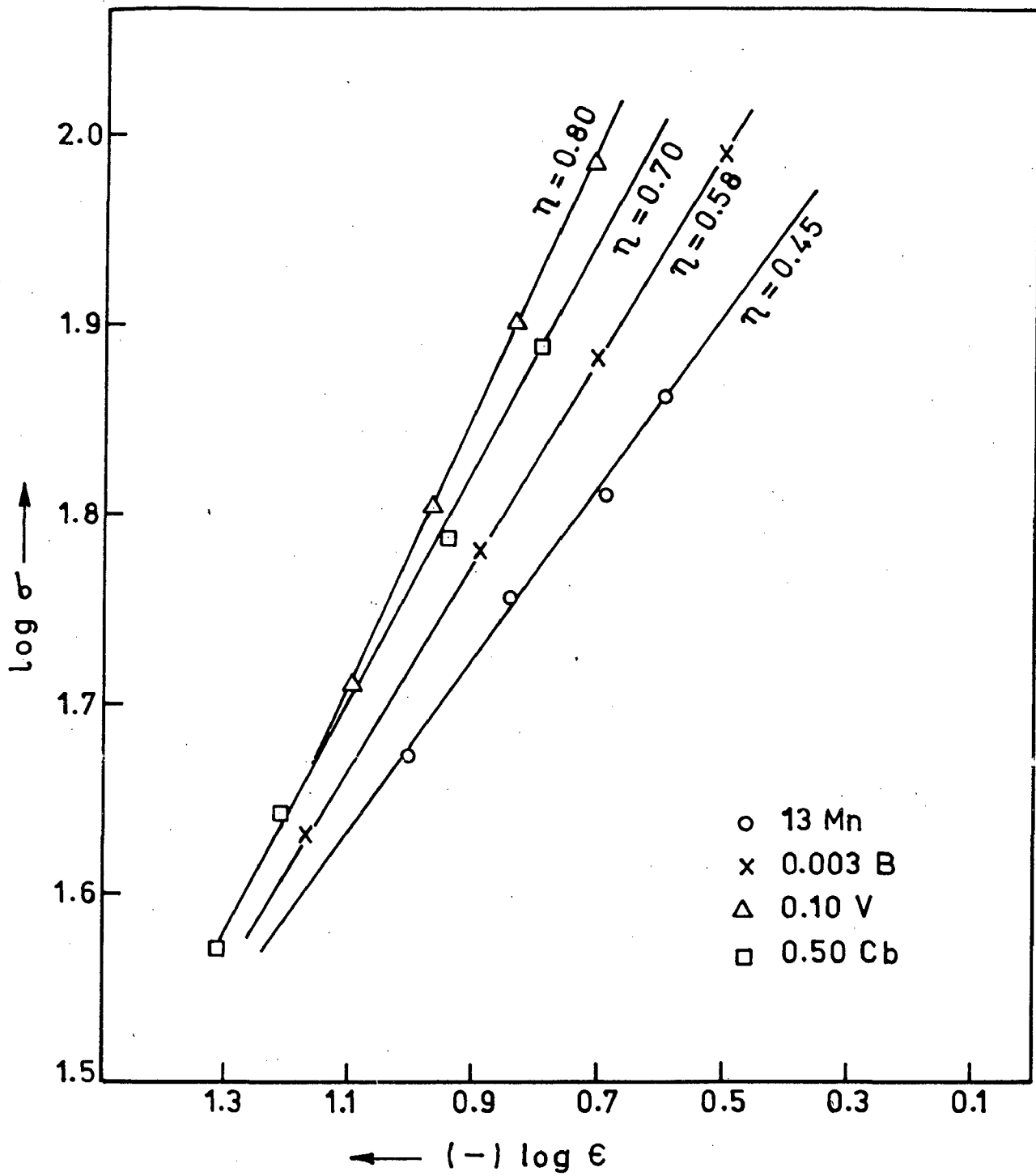


FIG. 4.25 EFFECT OF MICRO ALLOYING ON STRAIN HARDENING EXPONENT ( $\eta$ )

Thus it is observed that all the micro alloying additions increase the work hardening coefficients of the base steel; the effect of V addition being maximum.

Hadfield Mn steel with micro alloying additions, when strained in tension at strain rate of  $3 \times 10^{-4} \text{ sec}^{-1}$  on 'INSTRON' machine exhibited serrated flow (jerky stress-strain curves). Portions of load-elongation curves for all the alloys studied are presented in Fig.4.26. It is seen that magnitude and frequency of serrations vary largely in various samples. The 0.10 V alloy shows maximum increase in the frequency and amplitude of serrations. In the 0.50 Cb alloy the serrations comparatively are less predominant. In the 0.003 B alloy the magnitude and frequency of serrations are slightly higher than those in 13 Mn alloy but lower than those in 0.50 Cb or 0.10 V alloys. A comparison between Figs.4.25 and 4.26 shows that the serrations in load-elongation diagrams at slow strain rates become more and more pronounced as the value of work hardening coefficient ( $\eta$ ) calculated from normal load-elongation diagrams (plotted at usual strain rates in hydraulic tensile machine) increases. Thus we see that in the 0.10 V alloy, which gives highest value of  $\eta$  (0.80), the serrations in the curves obtained at slow strain rate ( $\dot{\epsilon} = 3 \times 10^{-4} \text{ sec}^{-1}$ ) are also most pronounced. These serrations are indication of dynamic strain aging which is responsible for work hardening in Hadfield steel [38]. But it has been observed that such serrations were not present in normal tensile testing on UTM-301 machine.

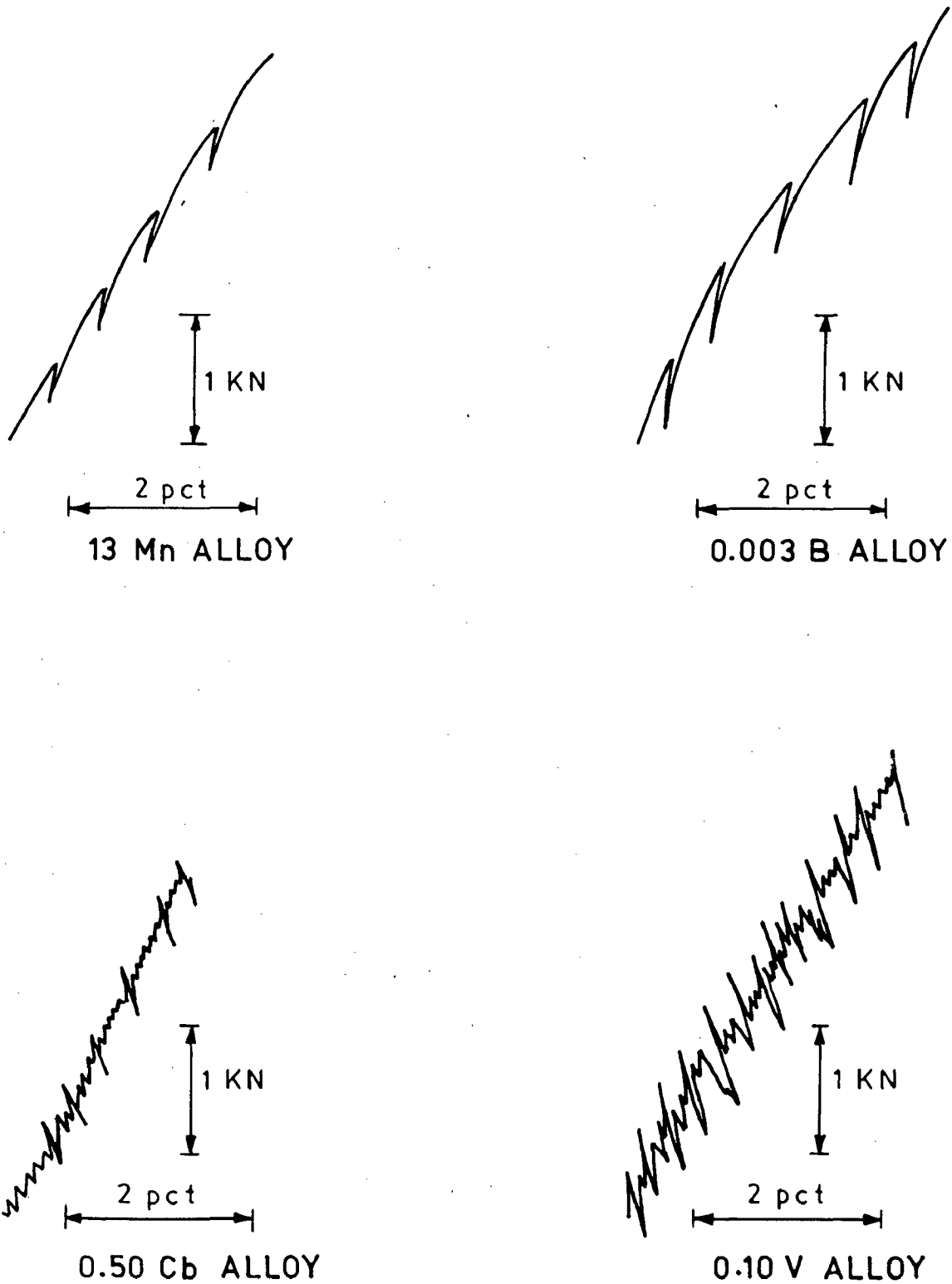


FIG. 4.26 PORTIONS OF LOAD-ELONGATION CURVES SHOWING THE EFFECT OF MICRO ALLOYING ON SERRATED FLOW (STRAIN RATE  $3 \times 10^{-4} \text{ s}^{-1}$ )

#### 4.2 EFFECT OF MICRO ALLOYING ON HARDENING UNDER IMPACT LOADING

Hadfield Mn steel is well known for its hardening under impact loading. The results showing effect of micro alloying on change in surface hardness of 13 Mn steel under impact loading are presented in Figs.4.27 - 4.30. Following observations are made from the results obtained.

The maximum improvement in hardness is observed in 0.003B steel. The 0.10 V alloy shows almost the same hardness level as observed in 13 Mn steel. However there is decrease in the hardness level with Cb addition as observed in the 0.50 Cb alloy (Figs.4.27,4.28). The 13 Mn alloy attains a maximum hardness level of 462 VHN from an initial hardness of 224 VHN after 100 number of blows of constant impact force. The increase in the hardness is rapid in first 75 blows and then slows down as it reaches the saturation hardness. There is no further increase in the surface hardness after 100 number of blows which gives saturation to the hardness value. The 0.003 B steel attains 474 VHN very rapidly in 50 number of blows. After 50 blows, the increase in hardness is very little. It rises from 474 to 480 and 486 VHN in subsequent intervals of 25 blows and then attains saturation. There is no further increase in the surface hardness after further impact. It is seen that the saturated hardness attained under impact loading of 0.003B steel is higher by 24 VHN than the 13 Mn steel. It is also observed that increase in hardness at each level of impact

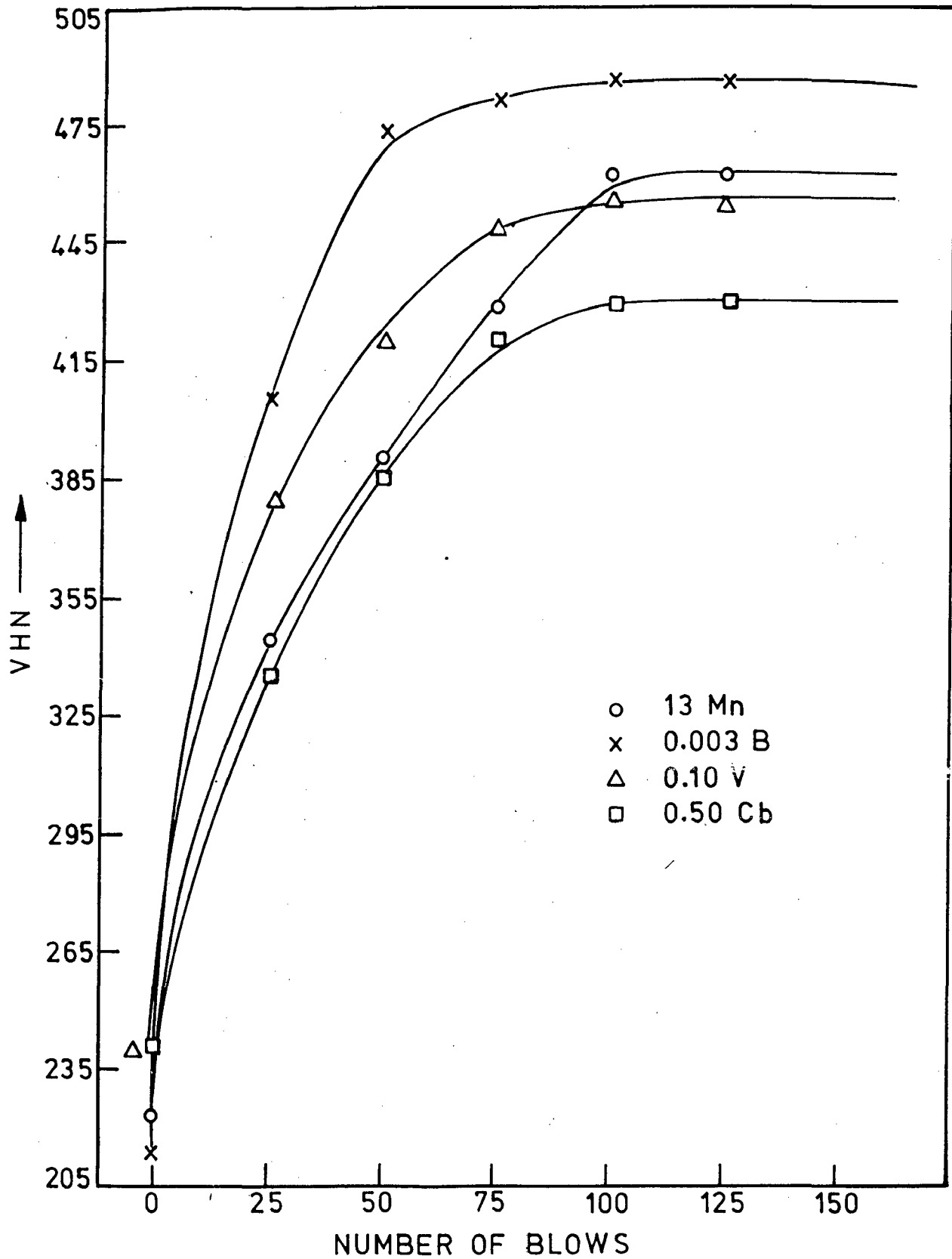


FIG. 4.27 EFFECT OF MICRO ALLOYING ON HARDENING UNDER IMPACT LOADING.

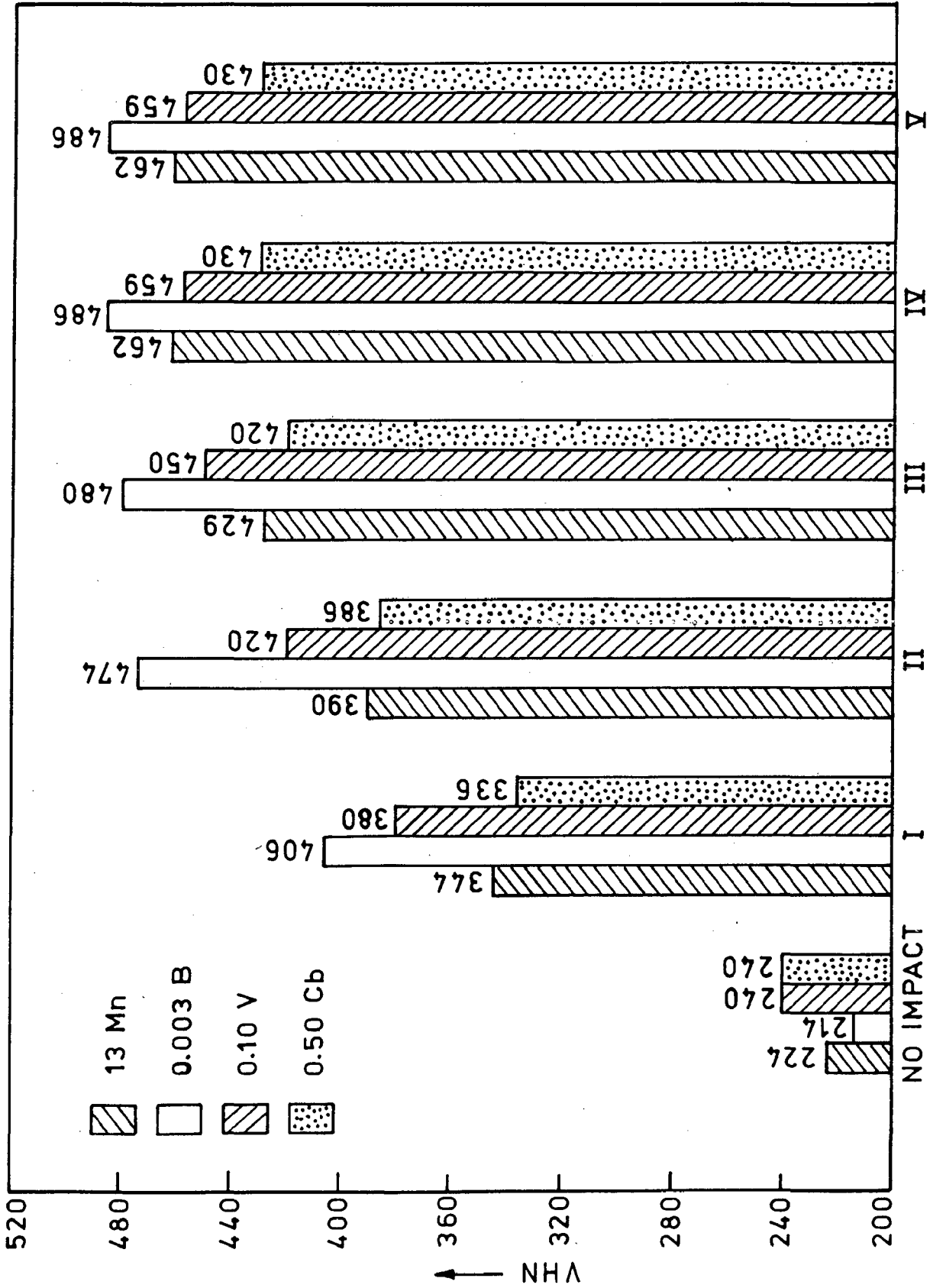


FIG. 4.28 HISTOGRAM SHOWING EFFECT OF MICRO-ALLOYING ON HARDENING UNDER IMPACT LOADING AT INTERVALS OF 25 BLOWS.

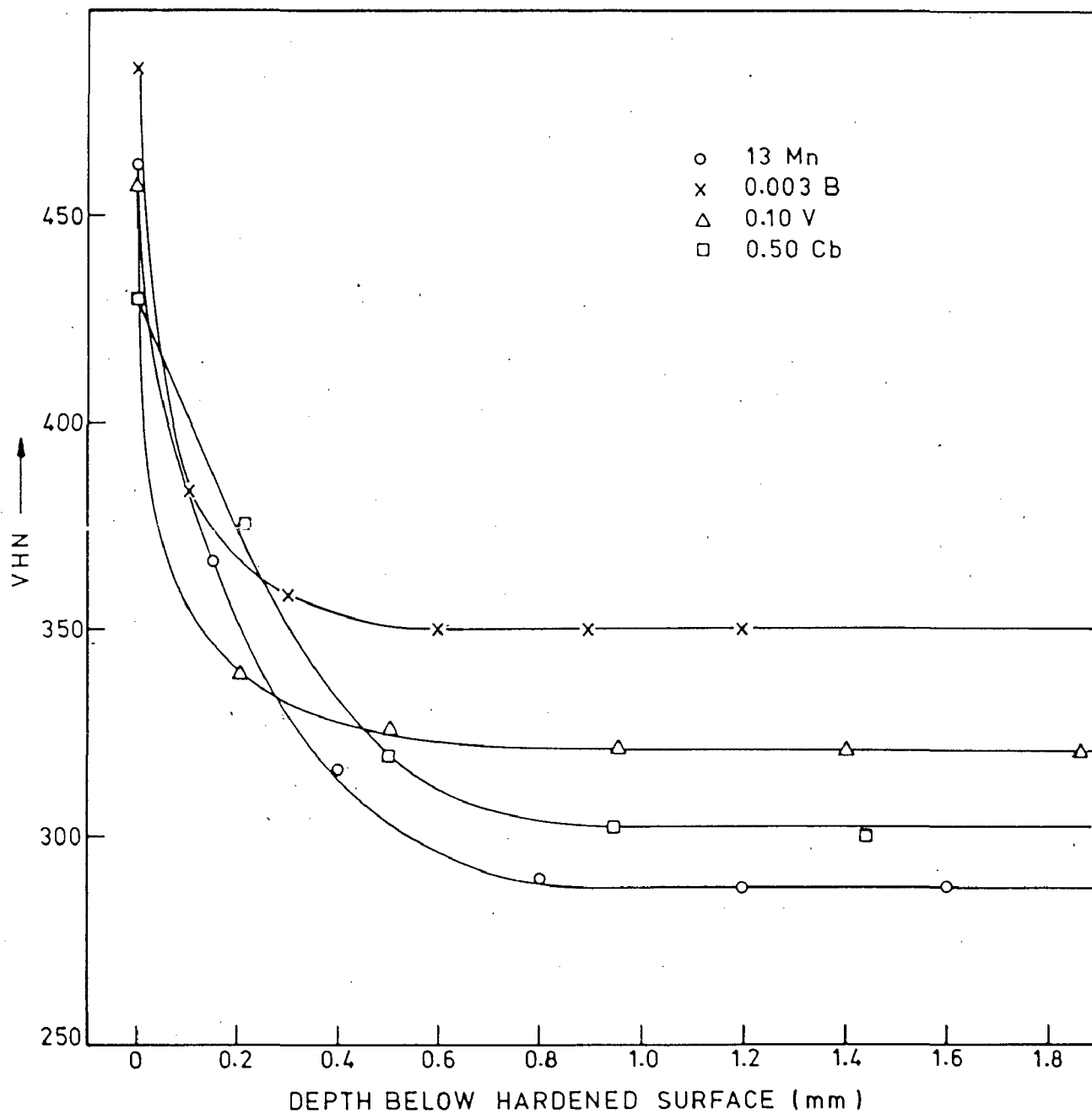


FIG. 4.29 DEPTH OF HARDENING IN IMPACT HARDENED ALLOYS.

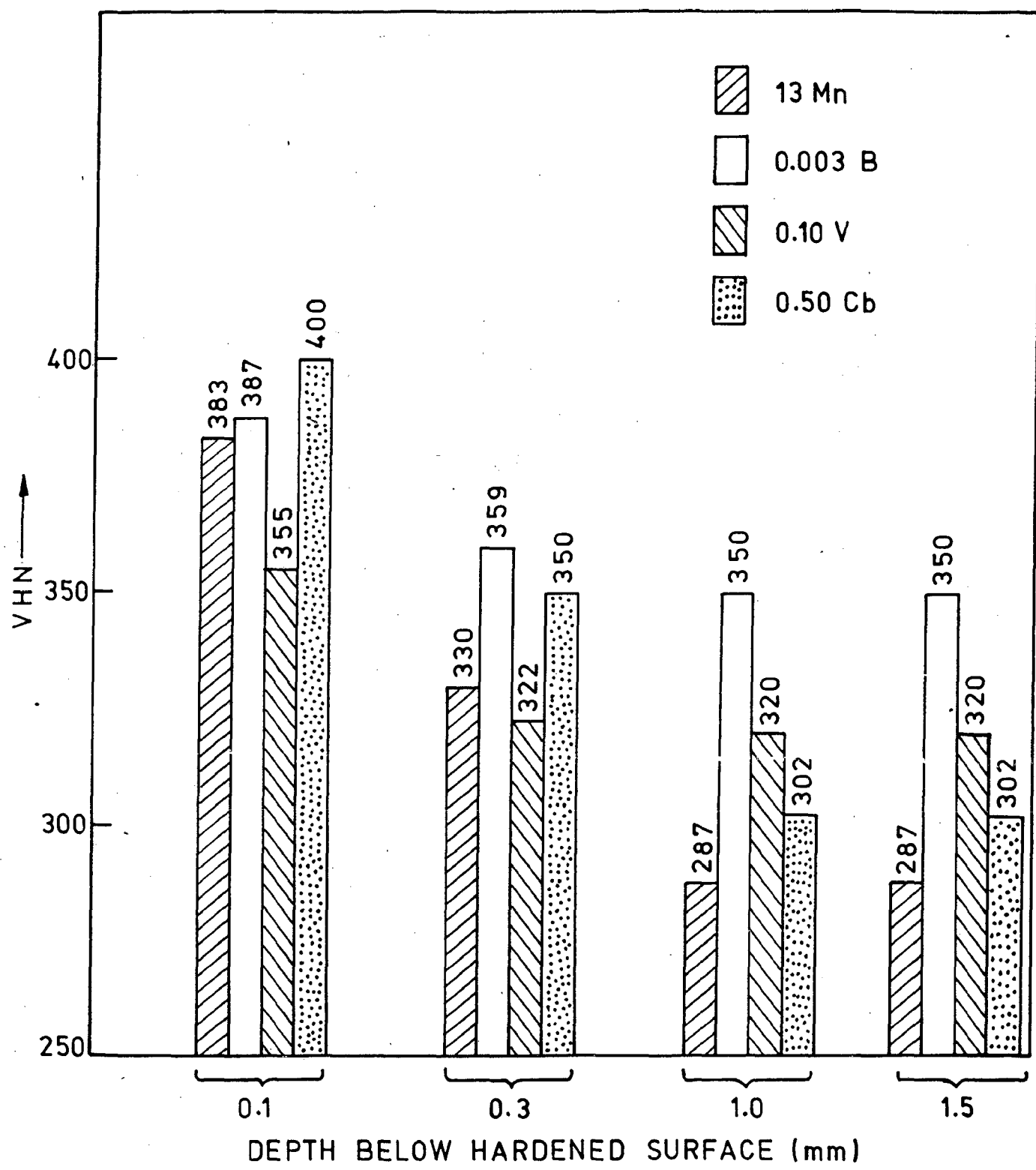


FIG. 4.30 HISTOGRAM SHOWING DEPTH OF HARDENING IN IMPACT HARDENED ALLOYS.



loading is much higher in 0.003 B alloy than in all the other alloys studied. The 0.10 V alloy attains saturation hardness after 100 number of blows. The level of hardness at saturation is 459 VHN which is nearly same as attained in 13 Mn steel. It is seen that in 0.10 V steel the increase in the hardness at successive intervals is always higher than in 13 Mn steel but it is lower than in 0.003 B steel. The addition of Cb (0.50 Cb alloy) gives lower hardness at saturation level and also at successive intervals of 25 number of blows in comparison to 13 Mn alloy. The maximum hardness attained at saturation is 430 VHN which is lower by 32 VHN from 13 Mn steel and 56 VHN from 0.003 B steel. The saturation in hardness is attained after 100 blows. In the 0.50 Cb alloy the increase in hardness at successive intervals of impact blows is always lower than in all other compositions studied.

It is seen that micro alloying with B, V and cb has a significant effect on the level of saturation hardness. The effect of B additions seems to be most significant in this respect. The impacted samples after saturation hardening were subjected to wear test on the wear testing machine. At successive stages of wear grinding the hardness at various depths was measured. Figs. 4.29 and 4.30 show the effect of micro alloying on the depth of hardening as a result of impact loading to saturation hardness. It is seen that there is sharp drop in the hardness below the impacted surface upto a depth of 0.3-0.8 mm beyond which the hardness attains a constant level which

is about 60 to 140 VHN higher than the as quenched hardness.

Most predominant effect on work hardening by impact loading is observed in the 0.003 B alloy. In this alloy the thickness of variable hardness below the impacted layer is only 0.30 mm beyond which the hardness remains more or less constant at 350 VHN. This hardness level is about 140 VHN higher than the as quenched hardness of this alloy. In the 0.10 V alloy the thickness of the variable hardness layer is approximately 0.50 mm whereas in the 13 Mn and 0.50 Cb alloy the variation in hardness goes upto about 0.80 mm. The hardness in the constant value zone after the variable hardness layer is 320 VHN in the 0.10 V alloy as against 287 VHN and 302 VHN in the 13 Mn and 0.50 Cb alloys respectively. As discussed later both the thickness of the variable hardness layer below the impacted surface and the constant hardness level below this layer appear to play a vital role in the general wear characteristics of the Hadfield steel compositions which undergo simultaneous impact loading and slide wear.

#### 4.3 EFFECT OF MICRO ALLOYING ON WEAR CHARACTERISTICS

The effect of micro alloying on wear characteristics of various Hadfield compositions has been studied under conditions of impact-slide and slide (by grinding on emery wheel). The Hadfield steel components in actual practice undergo various conditions of loading. To simulate the laboratory tests with practical conditions both these types of wear performance have

been studied. The results obtained are presented in Figs.4.31 to 4.35.

#### 4.3.1 Impact-slide wear

Fig.4.31 shows the effect of micro alloying on resistance to impact-slide wear measured in terms of 'abrasion loss' at successive stages of abrasion grinding at 30 second intervals. The samples after impact hardening to saturation limit were subjected to abrasive wear and the loss in weight of the samples was measured after every 30 seconds of abrasive grinding. It is seen that high wear resistance is developed in all the alloys after impact hardening as observed by very small amounts of abrasion loss after stage I of abrasive grinding. The loss of metal between two consecutive stages of grinding increases as the wear grinding is carried out further. This shows that the impact-slide wear resistance decreases continuously as the surface layer is removed and it attains a constant value after 120 seconds (stage IV) of abrasive grinding. From this it becomes apparent that in general the wear resistance increases with increase in the hardness of the work hardened layer after impact loading. From Fig.4.31 it is also seen that the impact-slide wear resistance  $(W)^{-1}$  in various alloys studied is in the order.

$$(W)_{0.003B}^{-1} > (W)_{13 Mn}^{-1} > (W)_{0.10V}^{-1} > (W)_{0.50 Cb}^{-1}$$

Thus, as far as the impact-slide wear resistance is concerned,

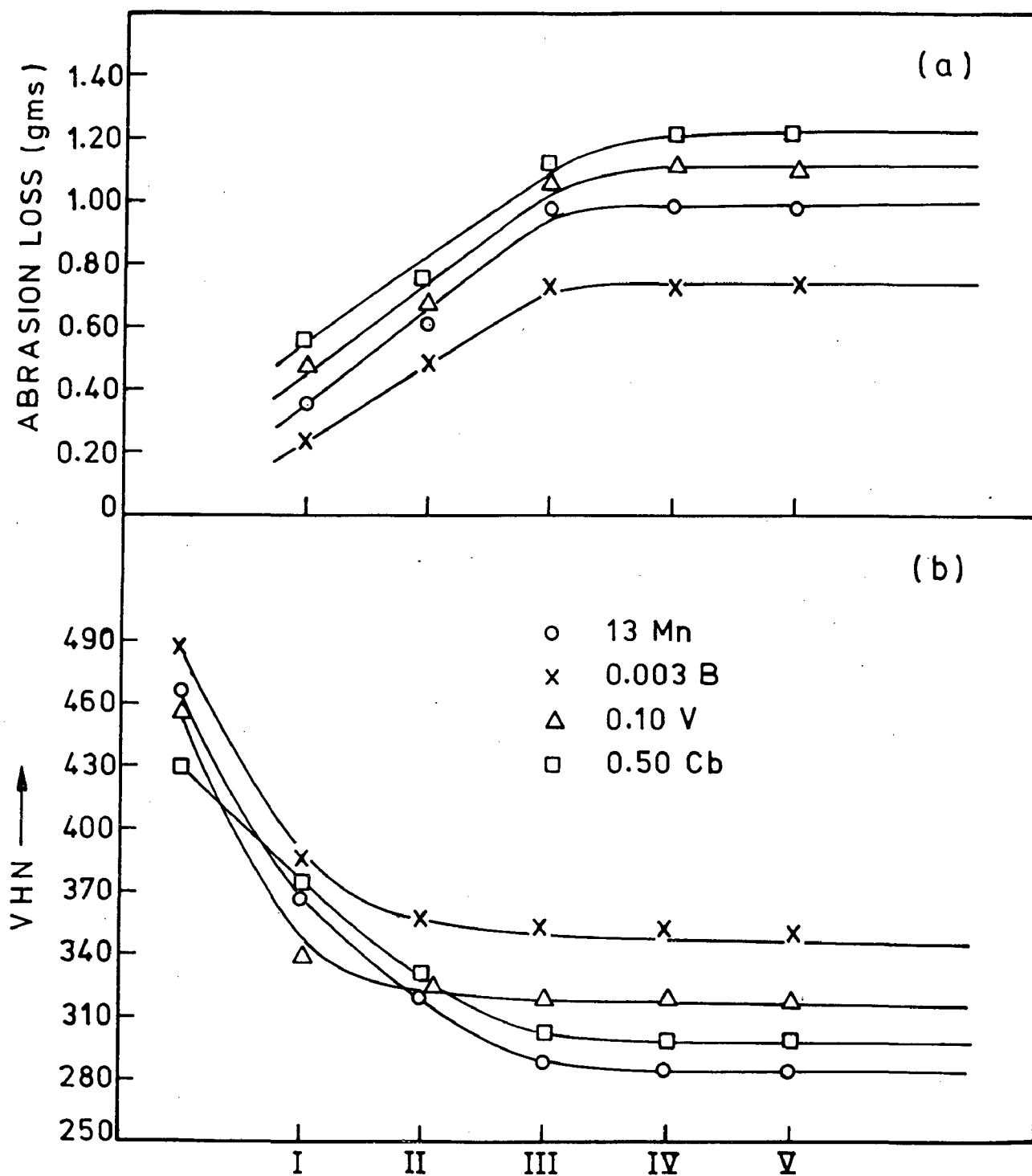


FIG. 4.31 HARDNESS AND ABRASION LOSS IN IMPACT-SLIDE WEAR AFTER SUCCESSIVE STAGES OF 30 SECOND INTERVALS.

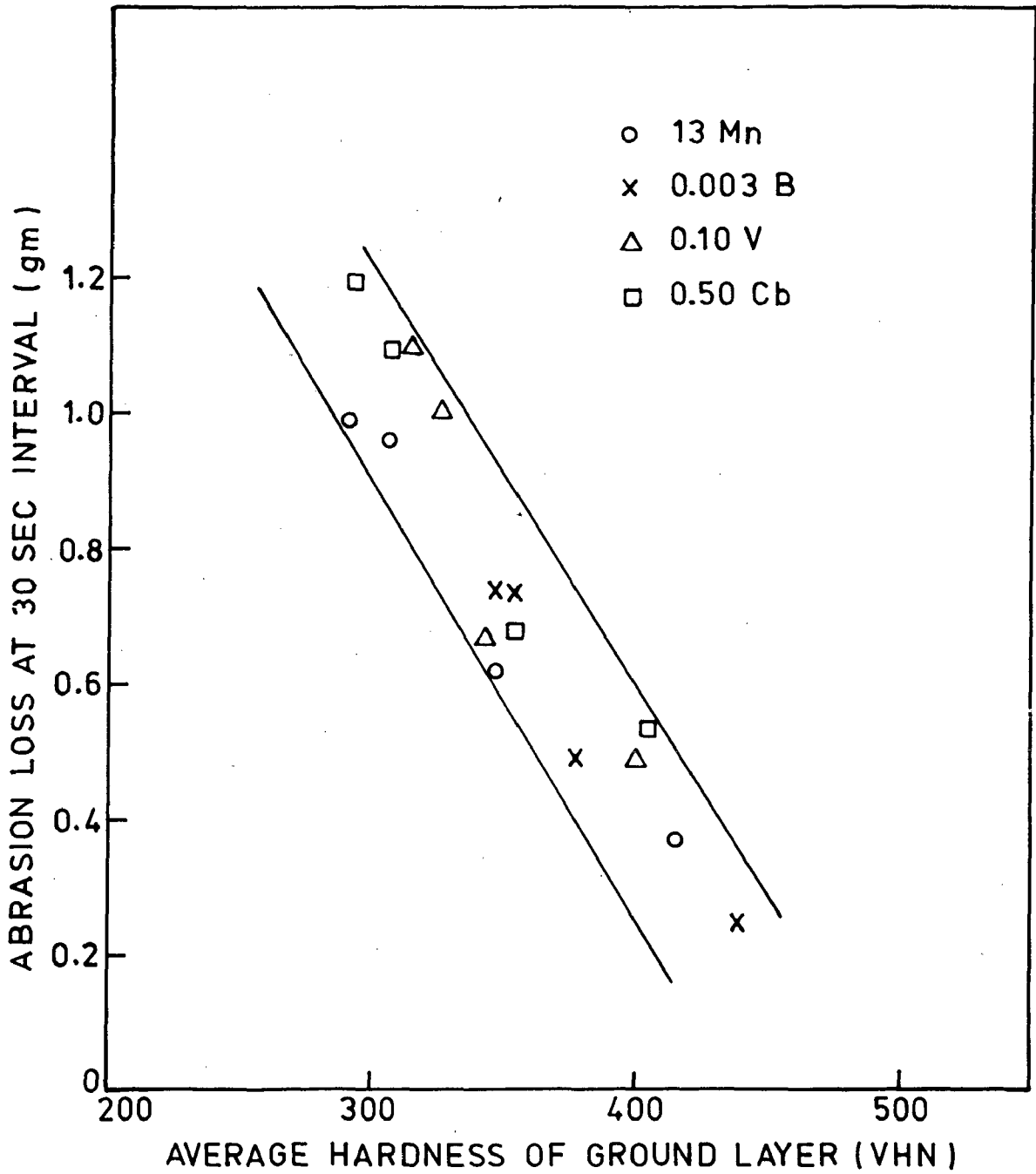


FIG. 4.32 GENERAL RELATIONSHIP BETWEEN ABRASION LOSS AND HARDNESS IN IMPACT-SLIDE WEAR.

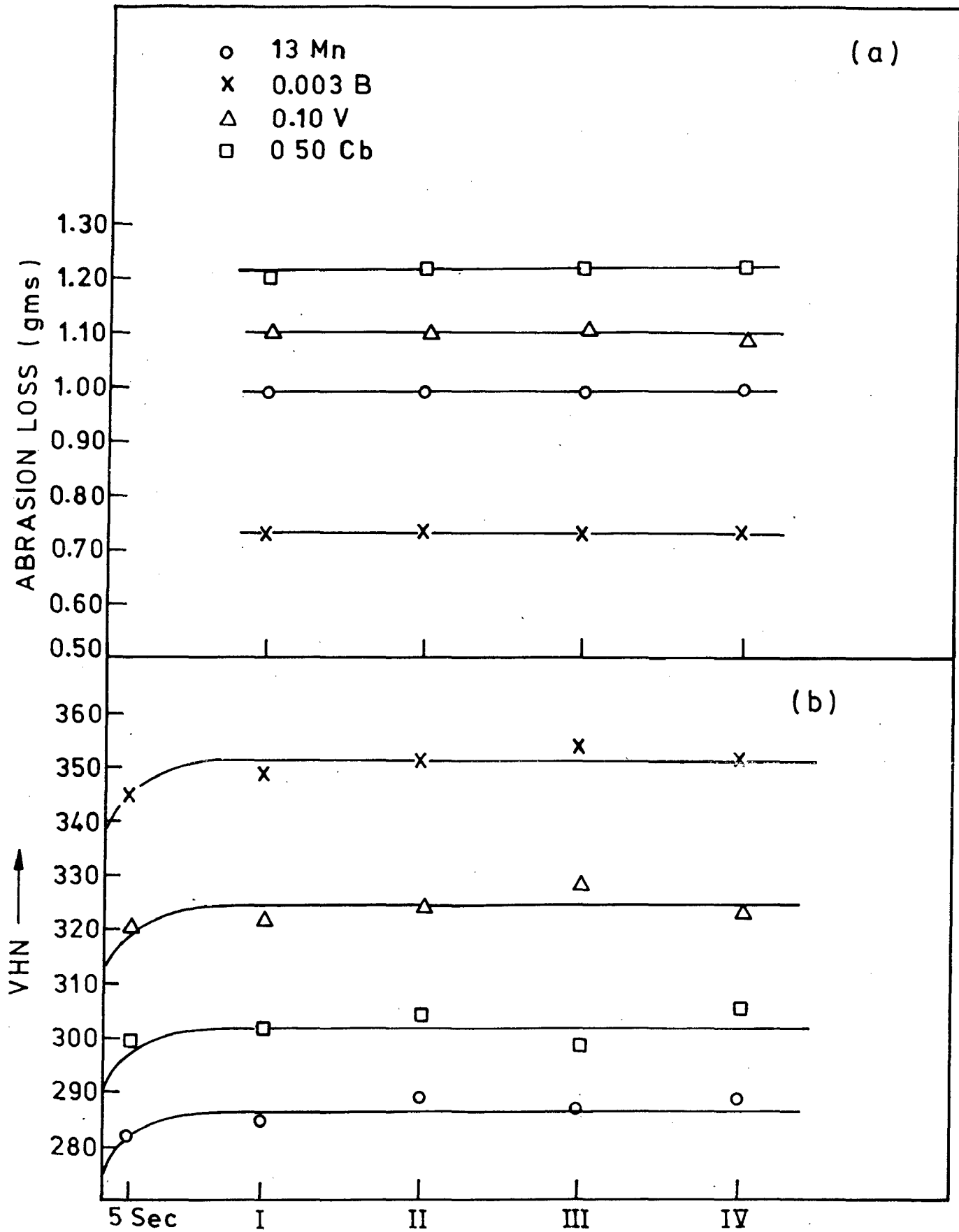


FIG. 4.33 HARDNESS AND ABRASION LOSS IN SLIDE-WEAR AFTER SUCCESSIVE STAGES OF 30 SECOND INTERVALS.

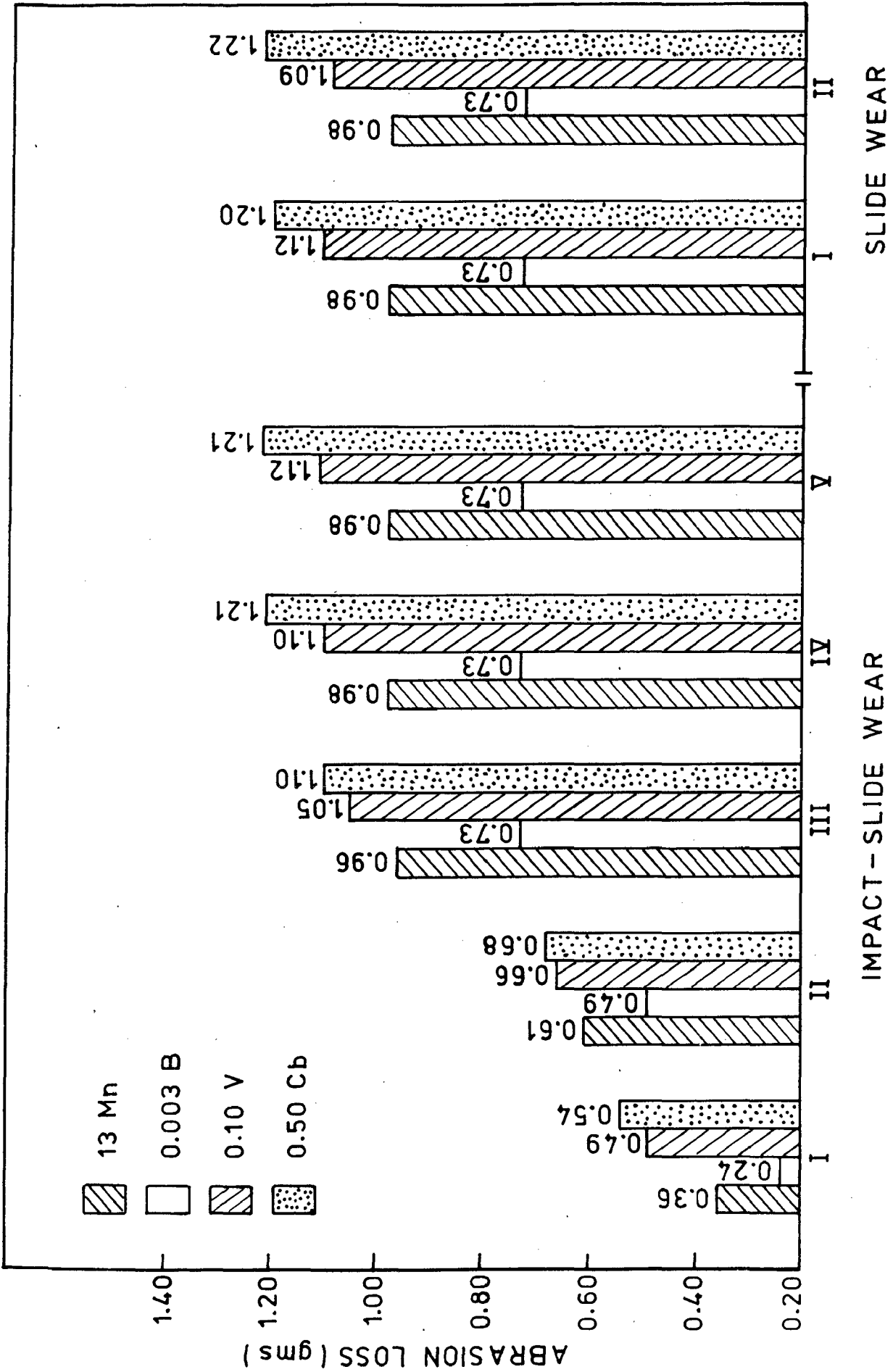


FIG. 4.34 HISTOGRAM SHOWING ABRASION LOSS IN IMPACT-SLIDE WEAR AND SLIDE WEAR AT SUCCESSIVE INTERVALS OF 30 SECONDS.

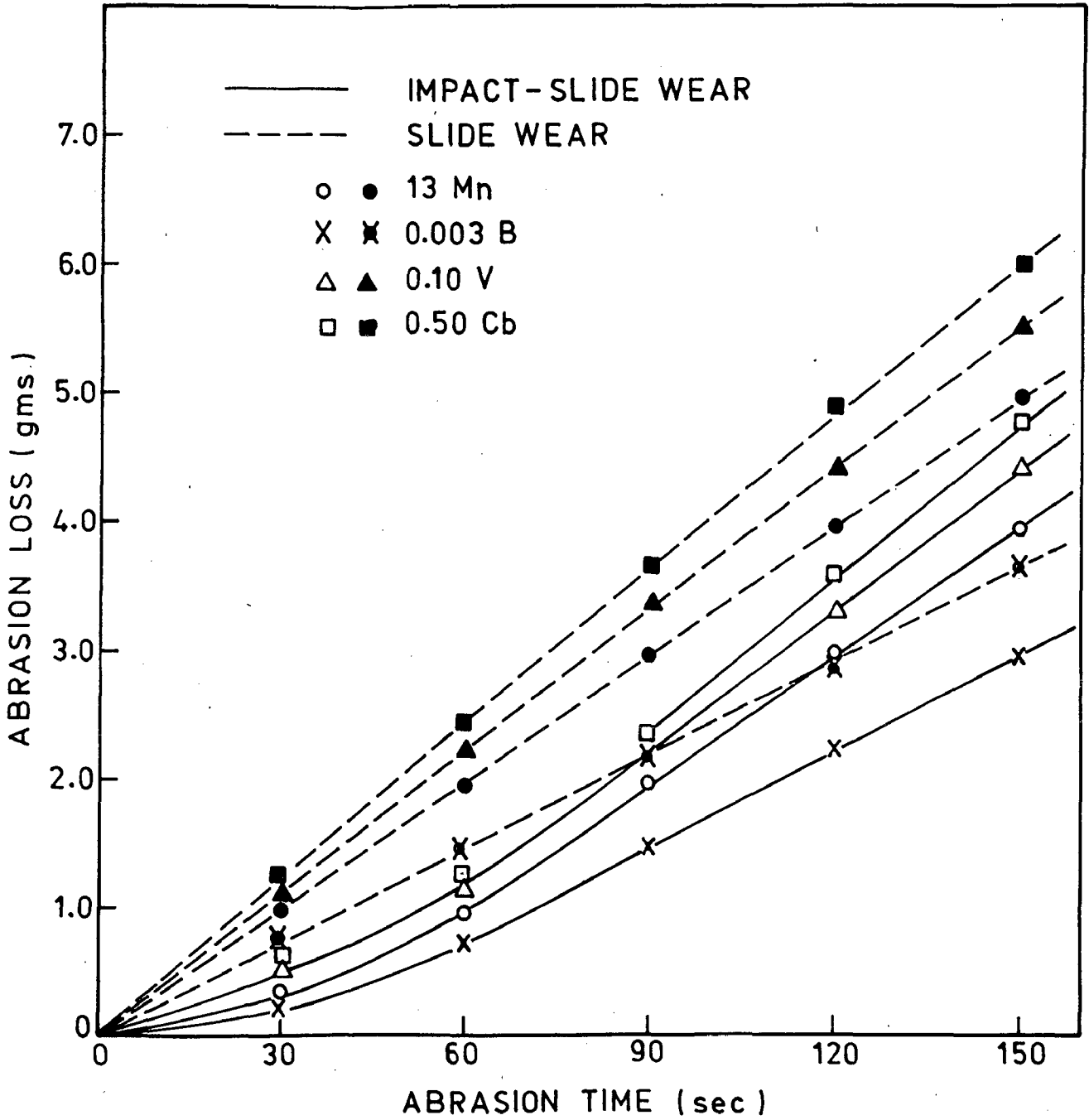


FIG. 4.35 CUMULATIVE ABRASION LOSS IN IMPACT-SLIDE WEAR AND SLIDE WEAR.



addition of B (0.003 B alloy) causes significant improvement (by about 33 pct .) and a deterioration by additions of V and Cb. In Fig.4.31(b) the surface hardness has been plotted after successive stages of wear grinding at 30 second intervals. It is clearly observed that there is a close correlation between the variations in impact-slide wear resistance and the hardness. A comparison of Fig.4.31(a) and 4.31(b) indicates that as the surface hardness falls the wear resistance also falls; and as the hardness attains a constant value the wear resistance also does not change and becomes more or less constant as observed by fixed amount of abrasion loss between two consecutive stages of abrasive grinding. It is however, interestingly observed that in the region of constant hardness and wear resistance, the order of relative hardness is different than that of wear resistance. For example, it is observed that in the region in which the abrasion loss and hardness values do not show any variations, the wear resistance  $(W)^{-1}$  of various alloys studied is in the order:

$$(W)_{0.003B}^{-1} > (W)_{13 Mn}^{-1} > (W)_{0.10V}^{-1} > (W)_{0.50 Cb}^{-1}$$

However, the hardness(H) is in this order:

$$(H)_{0.003B} > (H)_{0.10V} > (H)_{0.50 Cb} > (H)_{13 Mn}$$

Thus the present investigation indicates that the variation in impact-slide wear at various depths below the impact hardened layer is linked with variation in the hardness. It, however, does not directly depend on the absolute hardness value.

This observation may be more clearly illustrated with the help of Fig.4.32 in which the amount of abrasion loss at successive stages of impact-slide wear at 30 second intervals has been shown as a function of average hardness of ground layer for all the alloys studied in this investigation. It shows that a general trend may exist between the hardness and the wear resistance, but the same value of hardness in different alloys does not lead to same wear resistance. Thus it appears that, although hardness of the core material is an important property in controlling wear mechanism, the role of metallographic structure and other properties like toughness, UTS and El. etc.can not be ignored.

#### 4.3.2 Slide Wear

The present investigation reveals that the mechanism of normal slide wear (under constant load) is quite different than that of impact-slide wear. Fig.4.33(a) indicates the slide wear resistance (as measured by abrasion loss) at successive stages of abrasion grinding at 30 second intervals. In this case the samples were not subjected to any impact hardening and slide wear tests were conducted under constant load of 2.5 kg. on all alloy samples after the standard heat treatment. It is seen that abrasive wear loss is constant at all stages of abrasive grinding. It is observed that 0.003 B addition causes an improvement in slide wear resistance of 13 Mn alloy by about 30 pct. Additions of 0.10 V and 0.50 Cb deteriorate the slide wear resistance by about 10 and 21 pct. respectively.

The order of slide wear resistance  $(W)^{-1}$  is as follows:

$$(W)_{0.003B}^{-1} > (W)_{13 \text{ Mn}}^{-1} > (W)_{0.10V}^{-1} > (W)_{0.50 \text{ cb}}^{-1}$$

During slide wear test under load the surface gets work hardened within a few seconds of the test. Fig.4.32(b) indicates the variation in surface hardness after 5 seconds at various stages of abrasive grinding at 30 second intervals. It is clearly seen that the work hardening due to abrasive wear gets saturated in all alloys within a few seconds and the surface hardness remains constant throughout the wear test. Thus it is seen that both hardness and wear resistance remain constant more or less throughout the entire test. This also reaffirms the observation made in Fig.4.31 that variations in wear resistance are linked to variations in hardness, whereas the absolute value of wear resistance does not directly depend on the absolute value of hardness. From Fig.4.33(b) it is seen that the surface hardness developed during slide wear test has the order:

$$(H)_{0.003B} > (H)_{0.10V} > (H)_{0.50 \text{ cb}} > (H)_{13 \text{ Mn}}$$

which is entirely different than the order of wear resistance.

An interesting observation is made by a comparison of Figs.4.31(b) and 4.33(b). It is observed that in all alloys the core hardness values in the constant hardness region of impact-slide wear test curves are identical to the hardness values obtained in slide wear tests. It has already been indica-

ted earlier that as the surface layer is gradually removed in impact hardened samples the mechanism of wear also changes. From this investigation it appears that with the gradual removal of impact hardened layer the core hardness approaches that obtained in slide wear indicating a gradual change of the impact-slide wear mechanism to that of slide wear. This is also confirmed by a comparison of data of Figs.4.31(a) and 4.33(a), which is represented in the form of histograms in Figs.4.34. It is clearly seen from Fig.4.33 that in all alloys the impact slide abrasion losses in stages IV and V are identical to the corresponding abrasive losses in all stages of slide wear.

The present investigation clearly reveals that the wear resistance under impact-slide condition of loading is in general superior to that in slide condition. The wear data in terms of cumulative wear loss as a function of wear test duration has been reproduced in Fig.4.35 both for impact-slide and slide conditions. It is clearly observed that in all the alloys the cumulative wear loss is much less in conditions of impact-slide than in slide alone. Hence the micro alloyed Hadfield steels should in general perform better under working conditions involving simultaneous impact and slide.

#### 4.4 MICROSTRUCTURAL OBSERVATIONS

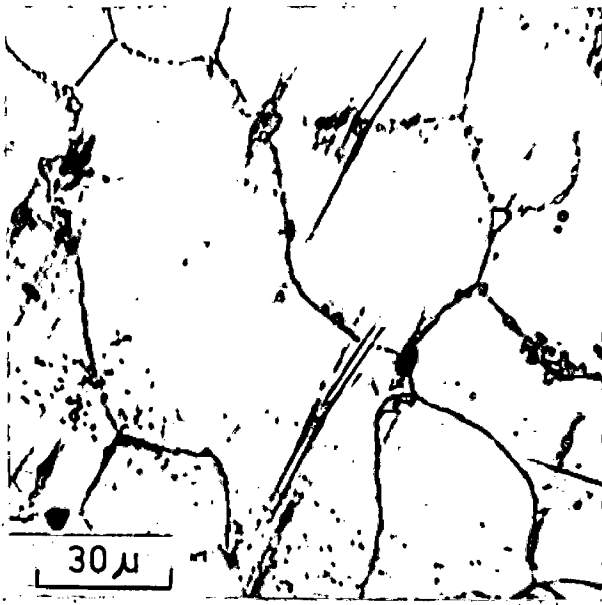
Optical microscopic studies on all alloys under investigation were conducted in the cast condition as well as after

the standard heat treatment, i.e. solution treatment and water quenching. All the heat treated alloys were also studied under optical microscope after impact hardening to saturation hardness by repeated impact blows at a constant stress level.

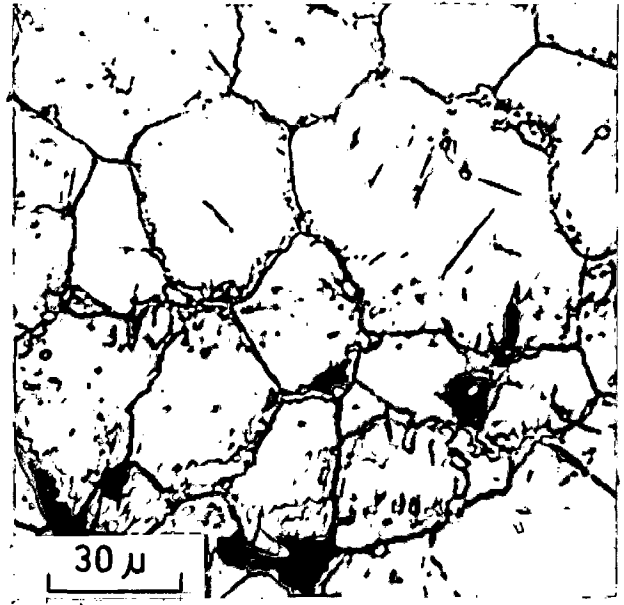
#### 4.4.1 As Cast Microstructures

The as cast microstructures of the various alloys are given in Fig.4.36. All the cast structures show the presence of carbide particles located mostly at the austenite grain boundaries. The maximum concentration of these particles is observed in 0.50 Cb alloy and the minimum concentration is observed in 0.003 B alloy.

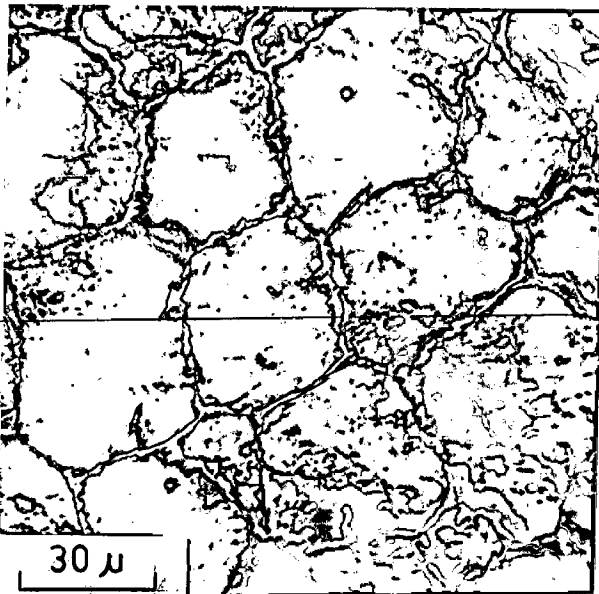
Electron microprobe analysis of the carbides was not conducted. However from literature it appears that the carbide particles in the 13 Mn steel correspond to the composition  $(\text{Fe Mn})_3\text{C}$  [13,14]. The  $(\text{Fe Mn})_3\text{C}$  particles are also formed in 0.003 B alloy together with the possibility of formation of some amount of borocarbide of  $(\text{FeMn})_3\text{B,C}$  [123]. In the 0.10 V and 0.50 Cb alloys  $\text{V}_4\text{C}_3$  and  $\text{Cb}_4\text{C}_3$  particles are expected to form together with the formation of  $(\text{Fe Mn})_3\text{C}$  carbides. In the 0.003 B samples formation of mechanical twins at a few locations was also observed indicating a low stacking fault energy of this alloy. It is also seen that additions of micro alloying elements refine the grain structure of the 13 Mn steel. The degree of grain refinement, however, is almost same in all



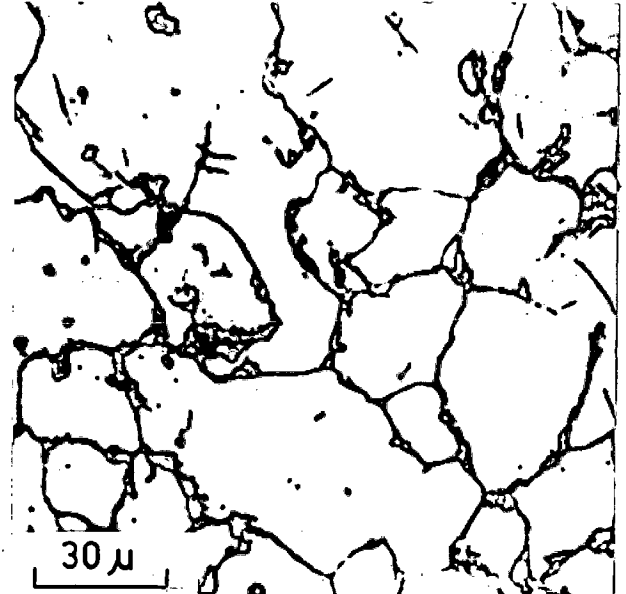
(a)



(b)



(c)



(d)

FIG. 4.36 AS CAST MICROSTRUCTURE

(a) 13 Mn

(b) 0.003 B

(c) 0.10 V

(d) 0.50 Cb

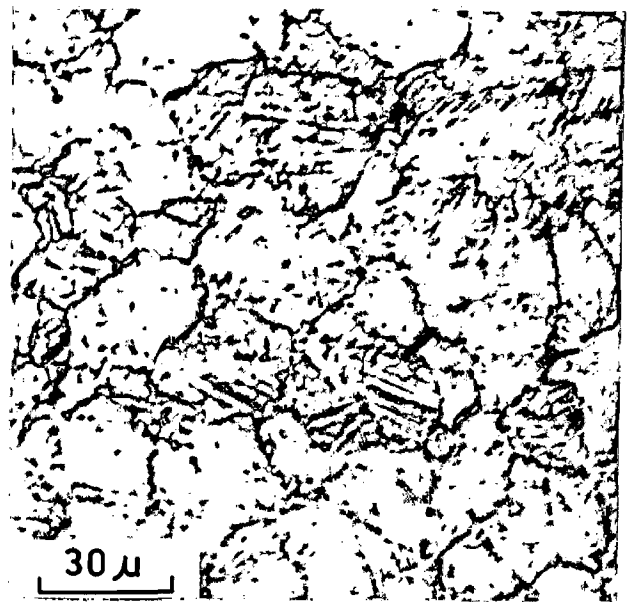
the cases. In the 13 Mn alloy the ASTM Grain Size Number is in the range 2-3. In the as cast micro alloyed steels the grain size corresponds to ASTM Number 4-5.

#### 4.4.2 As Heat Treated Microstructure

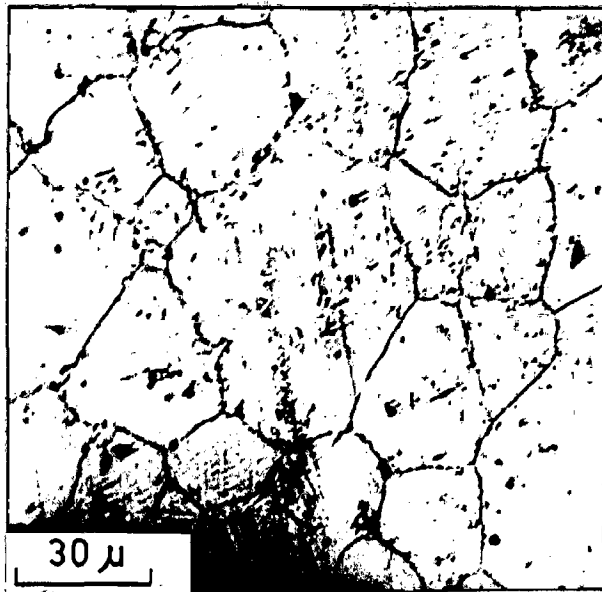
Fig.4.37 represents the microstructures of all the alloys after the austenitising followed by water quenching treatment. It is seen that the grain size is not altered after the heat treatment. The concentration of carbides is, however, drastically reduced. No precipitates are observed in the 0.003 B alloy due to their complete dissolution during the austenitising treatment. Small dark spots in the microstructure of this alloy are due to etching products which are formed by deep etching to reveal the grain boundaries. Thick particles of  $\text{Cb}_4\text{C}_3$  Carbide ( $\approx 2.5\mu$  size) are observed in the heat treated 0.50 Cb alloy. The  $\text{Cb}_4\text{C}_3$  particles are located mostly at grain boundaries and are left in the alloys due to their insolubility in austenite phase at the austenitising temperature [109-112]. The carbides in the 0.10 V alloy get dissolved to a great extent by austenitising treatment. However, very fine particles ( $\approx 1.0\mu$ ) are still left due to their limited solubility at the austenitising temperature [81]. These are more or less uniformly distributed in the matrix and there is no preferential formation of carbides at grain boundaries. In the 13 Mn alloy after heat treatment almost all the carbide particles are dissolved in the austenite. However at few locations some carbides are still observed in



(a)



(b)



(c)



(d)

FIG. 4.37 MICROSTRUCTURE OF HEAT TREATED ALLOYS

(a) 13 Mn

(b) 0.003 B

(c) 0.10 V

(d) 0.50 Cb

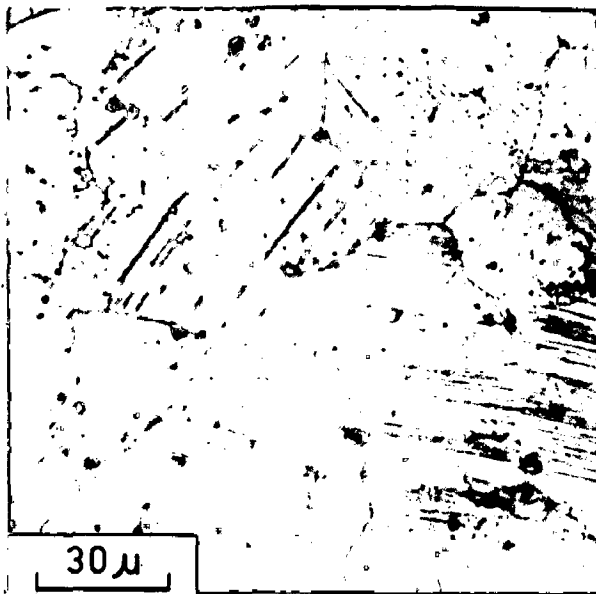


the samples taken from the core of the test pieces. This presumably results due to slower quenching rates in the core of test material. In all the microalloyed specimens micro twins are observed to form during polishing presumably due to their high sensitivity to stacking fault generation due to mechanical stresses involved during polishing for metallographic examination.

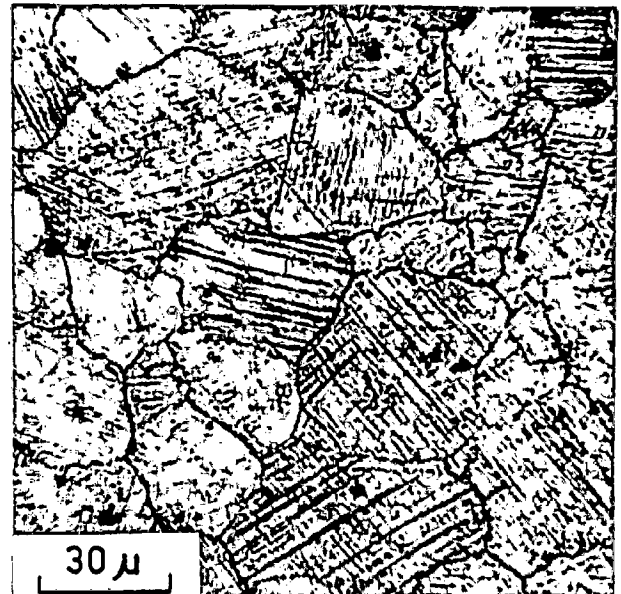
The carbides in the Hadfield steels, according to the observations made in this investigation, control the grain growth during austenitising treatment, as the grain size does not increase due to heating involved during austenitising. The carbide particles, according to this study, also play vital role in affecting the various mechanical properties and the work hardening characteristics of these steels.

#### 4.4.3 Microstructures of Impact Hardened Alloys

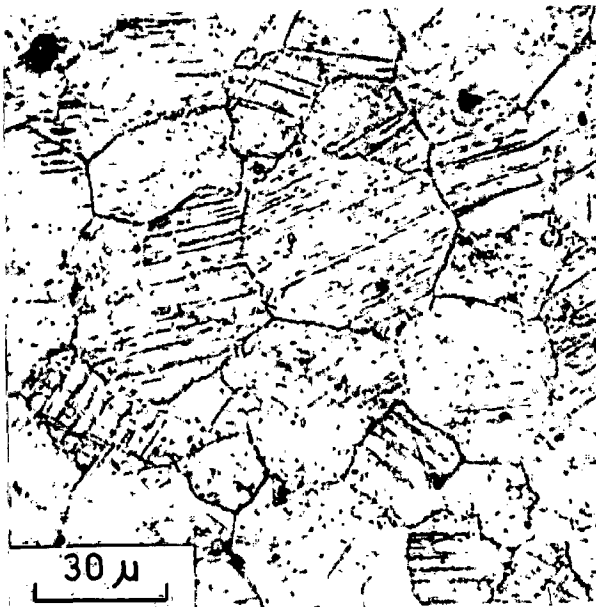
Formation of mechanical twins is observed predominantly in all the alloys after impact hardening as shown in Figs.4.38 and 4.39. According to some studies these twins have important bearing on the work hardening characteristics of Hadfield steel [46-48]. A close analysis of microscopic examination shows that the density of twins is different in different alloys. For example, maximum density of mechanical twins is observed to occur in the 0.003 B alloy. In fact the density of twins ( $\rho$ ) varies in the order  $\rho_{0.003 B} > \rho_{13 Mn} > \rho_{0.10 V} > \rho_{0.50 Cb}$ . It is of interest to note that the development of mechanical



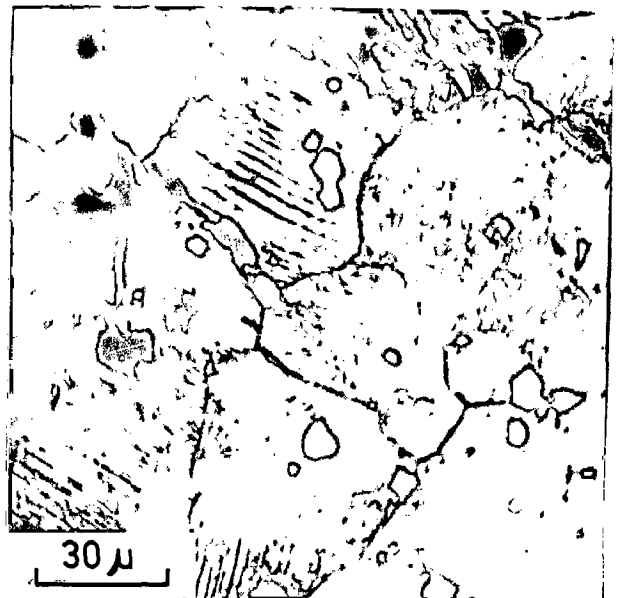
(a)



(b)



(c)



(d)

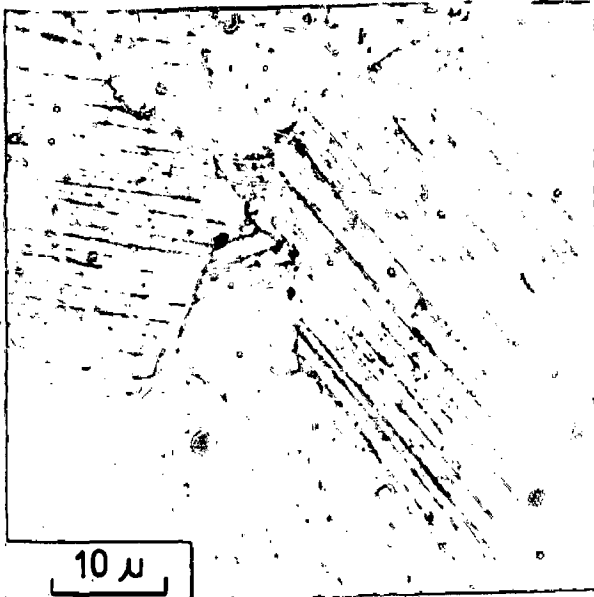
FIG. 4.38 TWINS IN IMPACT HARDENED ALLOYS ( LOW MAGNIFICATION )

(a) 13 Mn

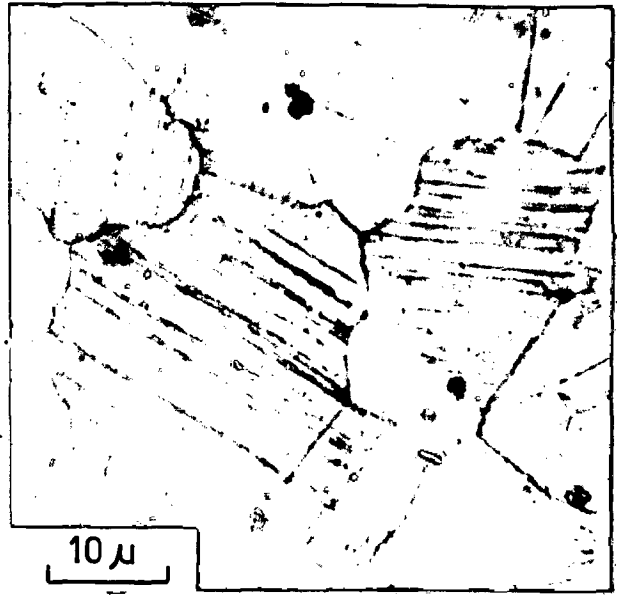
(b) 0.003 B

(c) 0.10 V

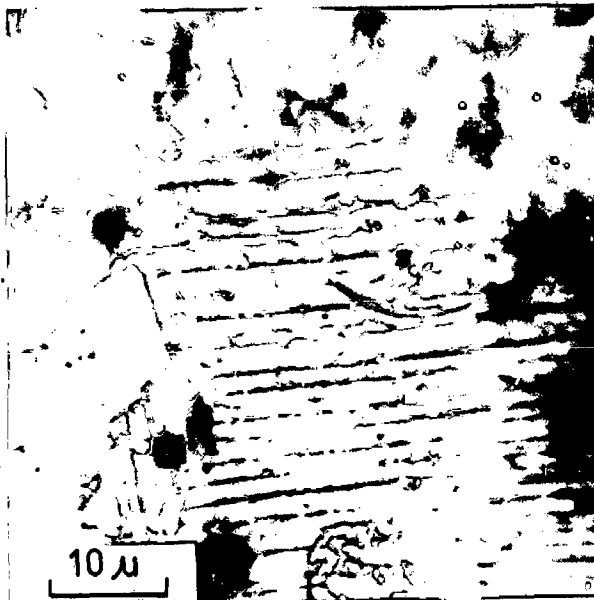
(d) 0.50 Cb



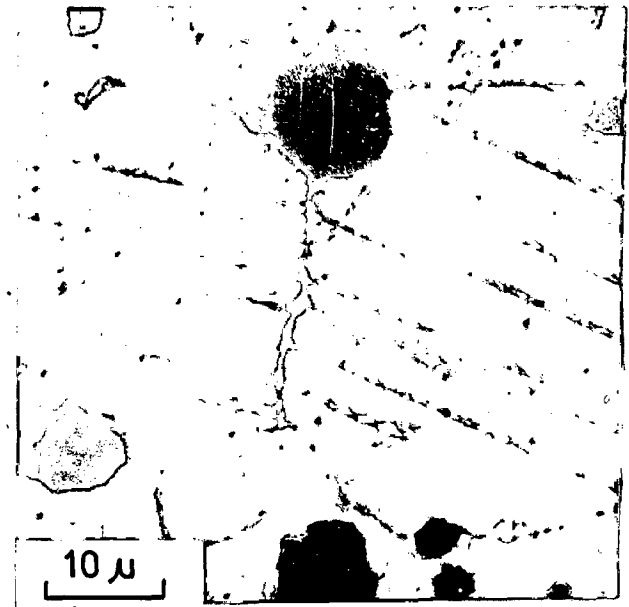
(a)



(b)



(c)



(d)

FIG. 4.39 TWINS IN IMPACT HARDENED ALLOYS ( HIGH MAGNIFICATION )

(a) 13 Mn

(b) 0.003 B

(c) 0.10 V

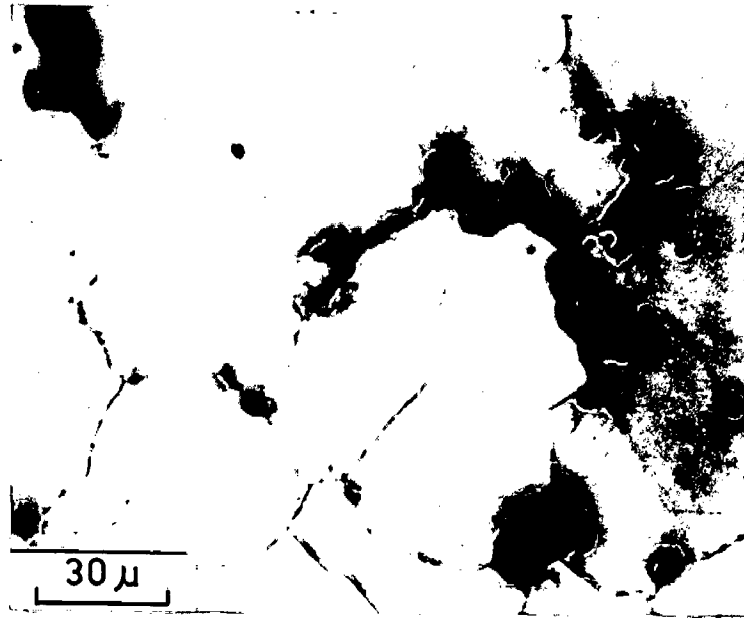
(d) 0.50 Cb

twins during impact hardening is closely related to saturation hardness on the sample surface. As reported in Section 4.2 the surface hardness (H) of impact hardened alloys varies in the order :

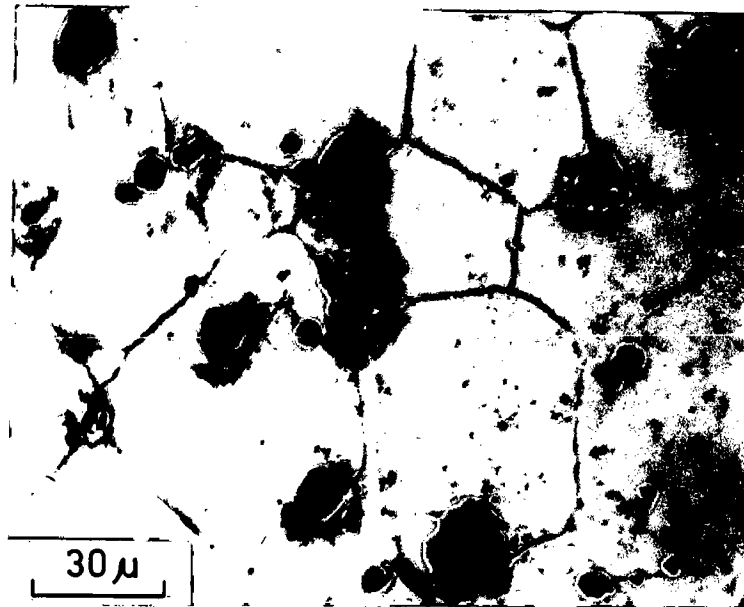
$$H_{0.003 \text{ B}} > H_{13 \text{ Mn}} > H_{0.10\text{V}} > H_{0.50 \text{ Cb}}$$

Thus it is observed that the density of twins formed varies in the same order as the saturation hardness. This relationship is of direct relevance in the development of wear resistance in these alloys by work hardening.

From this investigation it is revealed that carbide particles play an important role in influencing the various mechanical properties and especially the wear properties. Figs.4.40-4.42 indicate the effects produced on the particle-matrix interfaces by impact hardening. By repeated impact loading the matrix material adjoining these interfaces gets preferentially work hardened to the extent of developing brittleness. As a result, decohesion starts occurring at the particle-matrix interfaces. Since the carbide particles are of brittle nature, this decohesion causes the particles to come out of the grain boundaries and the matrix during loading under repeated impact. The voids so produced may function as sharp notches in the matrix and may be extremely dangerous from the view point of various mechanical properties and especially the wear characteristics. Figs.4.40(a) and 4.41(a) respectively show such void formation in 0.50 Cb and 0.10V alloys. Such voids are clearly revealed



(a) LIGHT ETCHED



(b) DEEP ETCHED

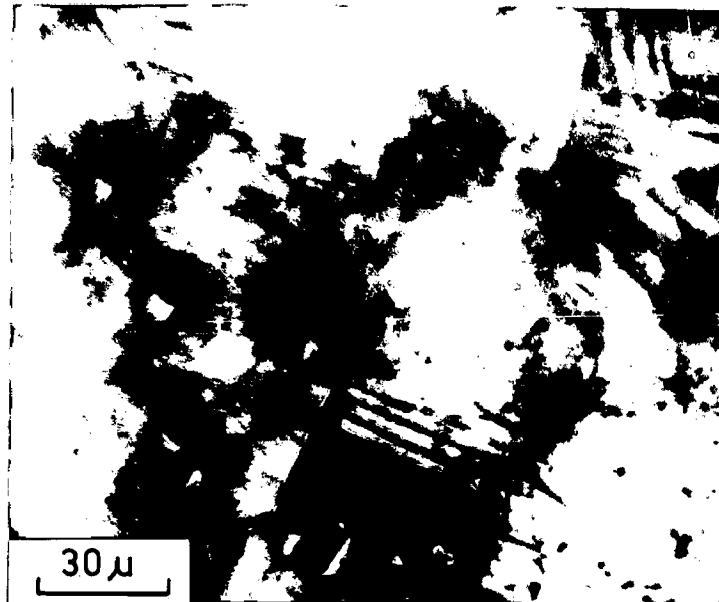
FIG. 4.40 DECOHESION AT CARBIDE-MATRIX INTERFACES  
IN 0.50 Cb ALLOY

(a) Formation of voids

(b) Formation of white etching layer



(a) LIGHT ETCHED

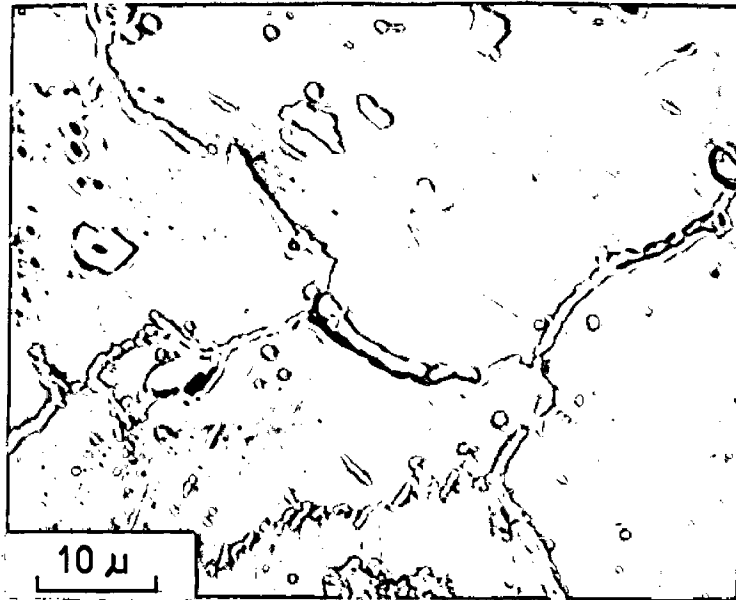


(b) DEEP ETCHED

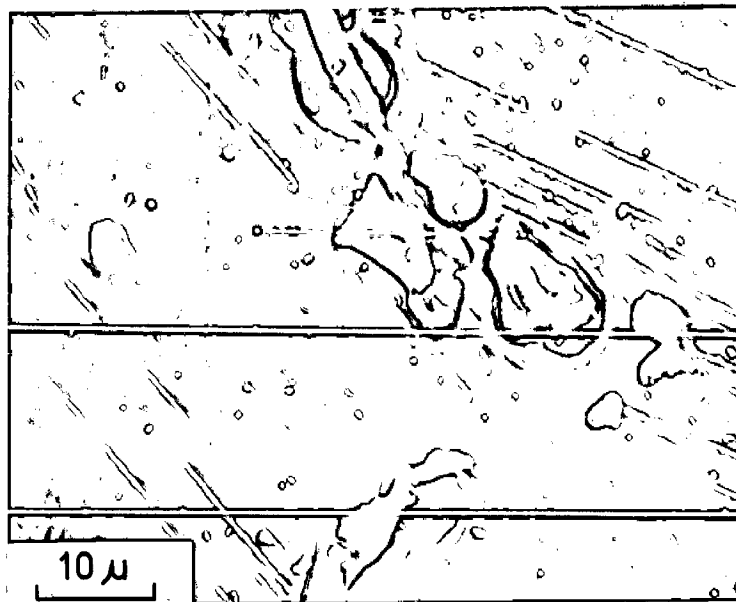
FIG. 4.41 DECOHESION AT CARBIDE - MATRIX INTERFACES  
IN 0.10 V ALLOY

(a) Formation of voids

(b) Formation of white etching layer



(a)



(b)

FIG. 4.42 SCANNING ELECTRON MICROGRAPHS SHOWING DECOHESION AROUND CARBIDE PARTICLES

(a) 0.10 V

(b) 0.50 Cb

in optical microscope on very light etching. Since the volume fraction and size of carbides in 0.50 Cb alloy are greater, the void formation on impacting is accordingly more predominant in this alloy than in the 0.10 V alloy. In the 13 Mn and 0.003B alloys this kind of observation is made in view of absence of carbide precipitates in these alloys. Deep etching of the 0.50 Cb and 0.10 V alloys indicates the formation of white etching layers around the carbide precipitates as shown in Figs.4.40(b) and 4.41(b) respectively. This white etching zone is more predominantly observed in 0.50 Cb alloy. Scanning electron micrographs showing these zones around carbide particles are given in Fig.4.42. The white etching layers are indicative of extremely brittle zones and are reported to be closely associated with material abrasion during wear applications [127]. The formation of this zone also seems to be responsible for poor work hardening of 0.50 Cb and 0.10 V alloys.

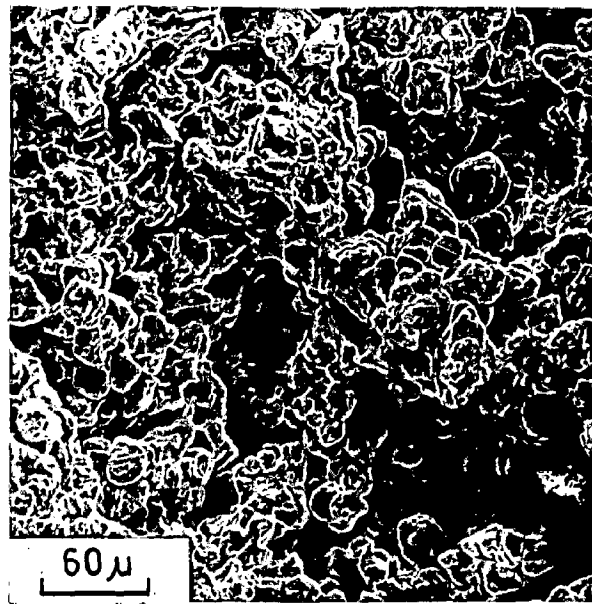
#### 4.5 FRACTOGRAPHIC STUDIES

A systematic study of the tensile and impact fracture surfaces was carried out by examination under the Philips SEM 501 scanning electron microscope. The results of the SEM study are shown in representative micrographs in Figs.4.43-4.49.

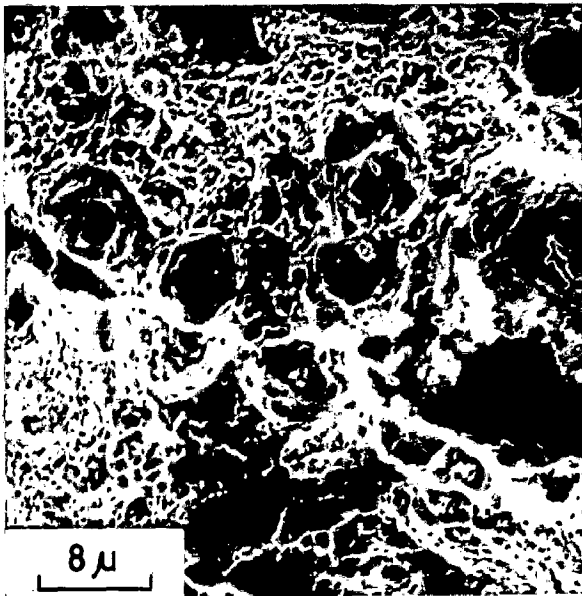
##### 4.5.1 Fracture Under Tensile Loading

The present study reveals that under tensile loading

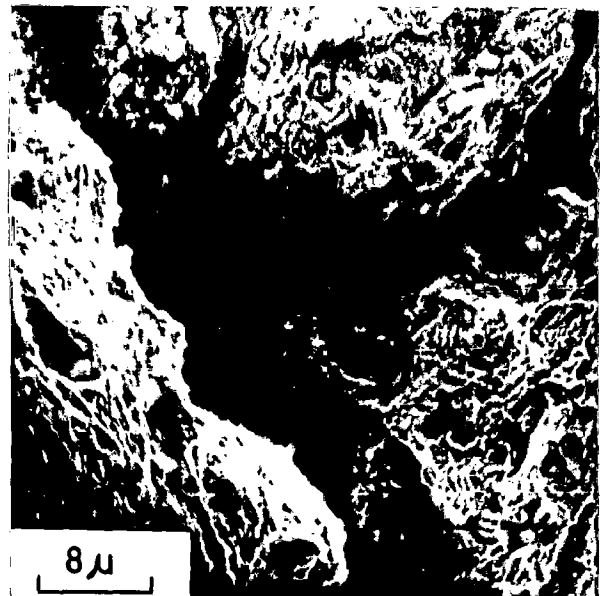




(a)

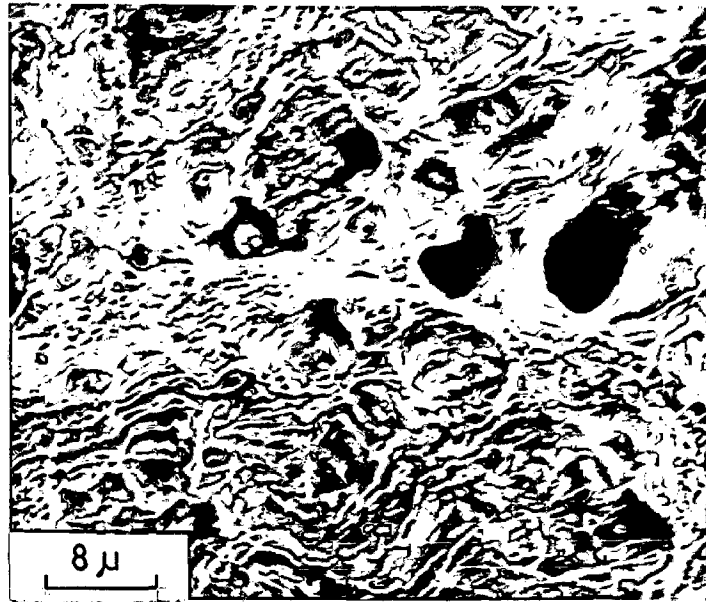


(b)



(c)

FIG.4.43 SEM MICROGRAPHS SHOWING CHARACTERISTICS OF TENSILE FRACTURE IN 13 Mn ALLOY.  
( a,b and c different locations )

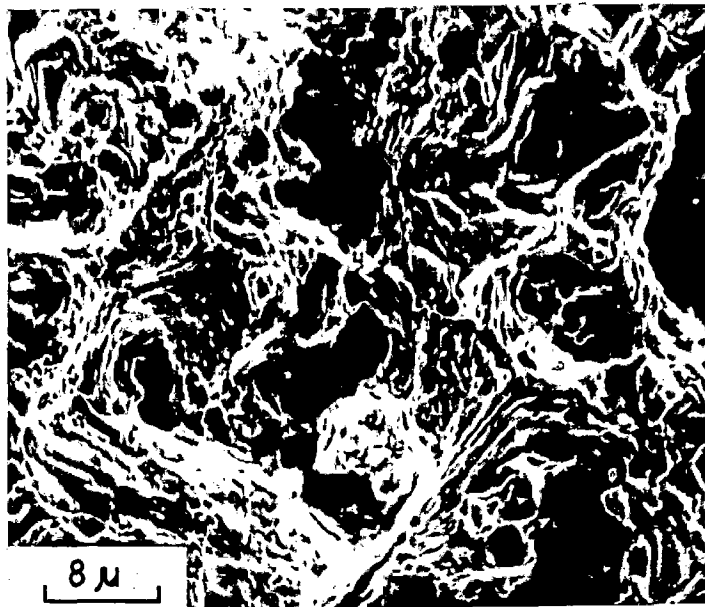


(a)

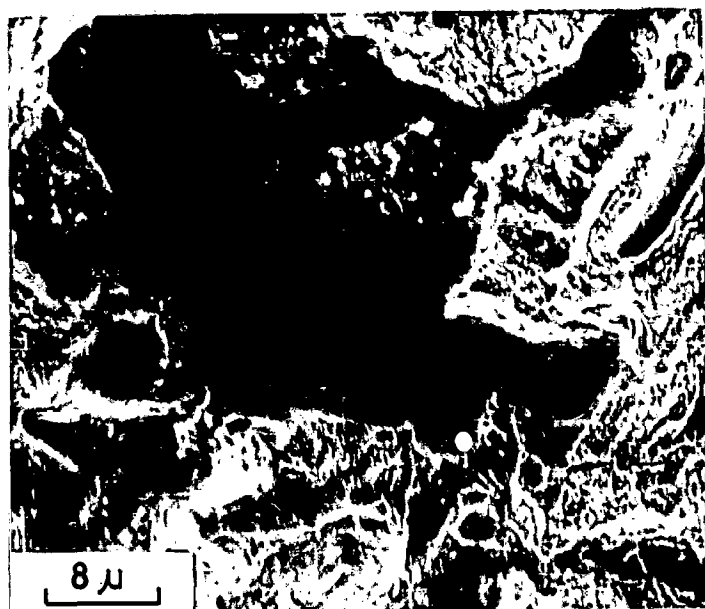


(b)

FIG. 4.44 SEM MICROGRAPHS SHOWING CHARACTERISTICS OF TENSILE FRACTURE IN 0.003 B ALLOY  
(a and b different locations )

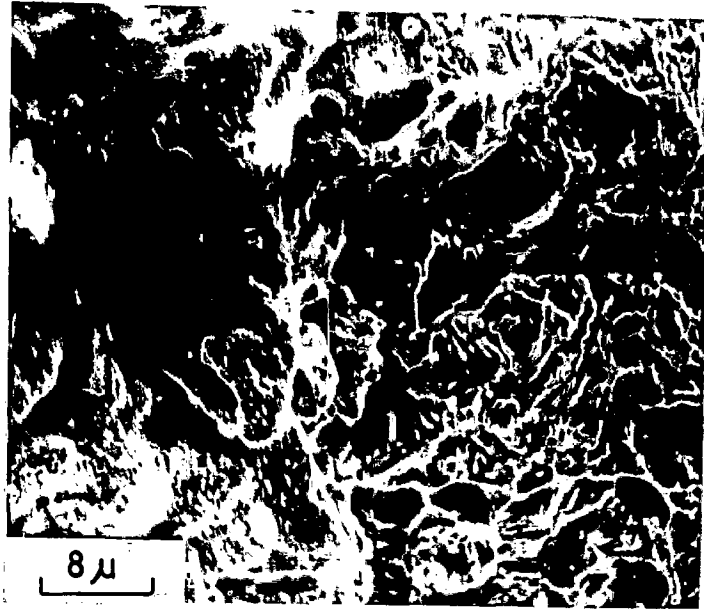


(a)



(b)

FIG. 4.45 SEM MICROGRAPHS SHOWING CHARACTERISTICS OF TENSILE FRACTURE IN 0.10 V ALLOY ( a and b different locations )

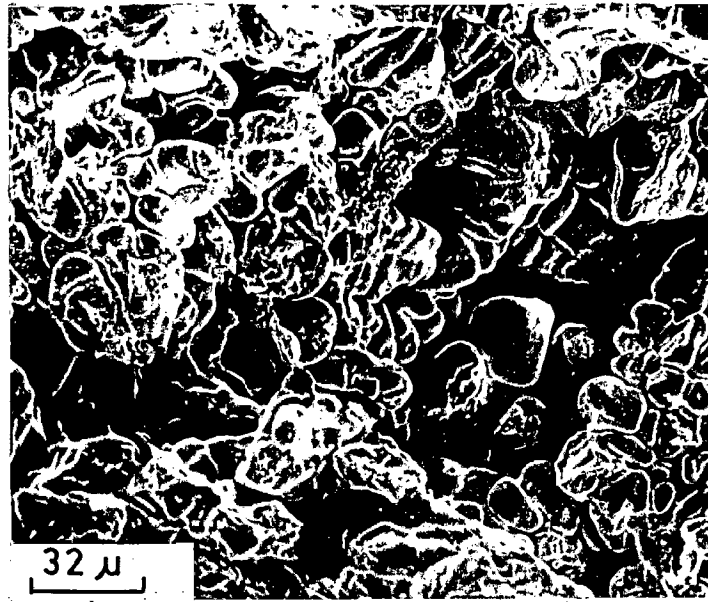


(a)

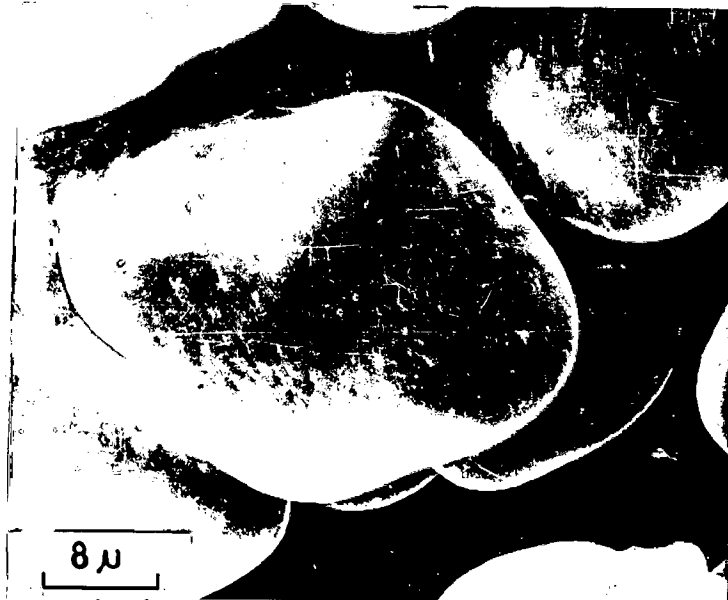


(b)

FIG. 4.46 SEM MICROGRAPHS SHOWING CHARACTERISTICS  
OF TENSILE FRACTURE IN 0.50 Cb ALLOY  
( a and b different locations )



(a)



(b)

FIG. 4.47 SEM MICROGRAPHS SHOWING CHARACTERISTICS OF IMPACT FRACTURE IN 13 Mn ALLOY (a and b different locations)



(a)



(b)

FIG. 4.48 SEM MICROGRAPHS SHOWING CHARACTERISTICS  
OF IMPACT FRACTURE IN 0.003 B ALLOY  
( a and b different locations )



(a)



(b)

FIG. 4.49 SEM MICROGRAPHS SHOWING CHARACTERISTICS OF IMPACT FRACTURE IN (a) 0.10 V ALLOY and (b) 0.50 Cb ALLOY

the failure occurs basically by (i) formation and interaction of striations (ii) particle-matrix decohesion and (iii) formation of intergranular voids. The characteristic appearance of striations is observed to vary widely in various micro alloyed compositions. The striations interact with each other leading to the formation of dimples and micro voids, which coalesce to form large voids. Formation of voids is preferentially observed at particle-matrix interfaces.

Among all the alloys studied, maximum density of striations is observed in 0.003B alloy (Fig.4.44). The close spacing of the striations is indicative of very high deformations occurring in this alloy prior to fracture. The SEM observations confirm the highest  $E1$  observed in this alloy in tensile tests. As seen in Fig.4.44(a) the closely spaced striations interact to form microdimples which further lead to the formation of larger voids. Fig.4.44(b) shows clearly the grain boundaries at the fracture surface, indicating that the formation of voids has preferentially occurred at intergranular spacings. Thus in the Hadfield steels the nature and structure of grain boundaries play a vital role in their tensile properties. Presence of brittle constituents at grain boundaries is extremely deleterious to the various mechanical properties. Since the carbide particles are absent in 0.003 B alloy, it shows highest UTS and  $E1$  among all the alloys studied.



The SEM studies indicate a close correlation between the density of striations and the degree of deformation as measured in tensile tests. The density ( $\rho$ ) of striations as revealed by SEM studies varies in the order  $\rho_{0.003B} > \rho_{0.10V} > \rho_{13Mn} > \rho_{0.50Cb}$  which is the same as that of deformations (El) observed in tensile tests. Fig.4.43 shows the fractographs of 13 Mn alloy. It is seen that striations are not so densely spaced as in the 0.003 B alloy. In this alloy a very small concentration of carbide particles exist even after heat treatment. Fig.4.43(b) shows the formation of voids around such particles. From Fig.4.43(c) it is observed that failure mostly occurs by intergranular voids. The role of carbide particles on the formation of voids at particle-matrix interfaces is clearly seen from Figs.4.45 and 4.46, which represent fractographs of 0.10V and 0.50Cb alloys respectively. In these alloys due to rapid failure at the particle-matrix interfaces the overall deformation as observed by the density of striations is much less than that in 0.003B or 13 Mn alloy. Since the particles have maximum size and concentration in the 0.50 Cb alloy, the failure is most rapid in this alloy without undergoing much deformation prior to fracture. This is also verified by low values of UTS and El observed in this alloy. Figs.4.45(b) and 4.46(b) also indicate that failure under tensile loading has occurred primarily by intergranular fracture.

#### 4.5.2 Fracture Under Impact Loading

The SEM studies carried out on the impact fracture sur-

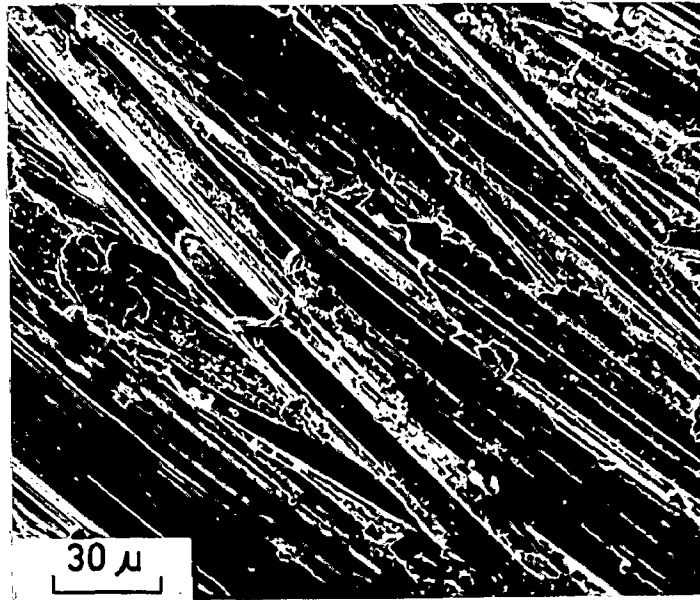
faces reveal that the fracture to be intergranular as shown in Figs.4.47-4.49. In all the alloys studied the fracture occurs along grain boundaries, which again emphasises the importance of nature and structure of grain boundaries in controlling the impact strength of Hadfield steels. In the 0.10V and 0.50Cb embrittlement is caused at the grain boundaries by the presence of carbide particles, which essentially lead to low-impact values in these alloys. Again maximum deterioration in toughness would occur in 0.50 Cb alloy as it has maximum concentration of carbides at grain boundaries.

Fig.4.48 shows the fractographs of 0.003 B alloy. It is clearly observed that, prior to fracture, extensive deformation (as observed by elongation of grains in the direction of impact force) has occurred in this alloy. This would mean a high toughness in this alloy, as is also revealed by the high value of impact strength observed by impact tests. The elongation of grains in the 13 Mn alloy is somewhat less in comparison to 0.003 B alloy as is revealed by a comparison of Figs.4.47 and 4.48. Thus the impact strength observed in the 13 Mn alloy is less than in 0.003 B alloy. The deformation of grains in 0.10V and 0.50 Cb alloys is comparatively much less as seen from Figs.4.49a and 4.49b respectively as the impact fracture in these alloy could occur easily due to the presence of brittle carbides.

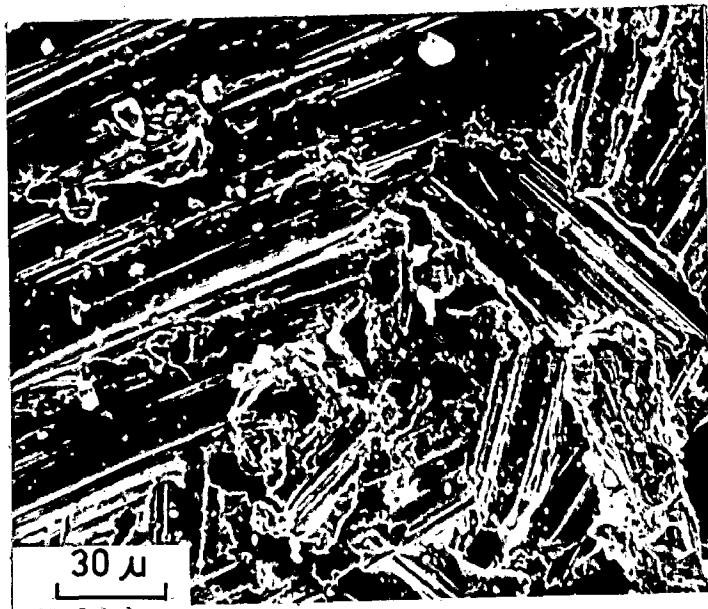
#### 4.6. SEM STUDIES OF WEAR SURFACES

SEM studies were conducted on the worn surfaces of all alloys. The samples, after heat treatment, were impact hardened by repeated loading at a constant stress level and were subsequently subjected to wear testing. Wear surfaces were studied under SEM after applying slide wear against a rotating emery wheel for durations of 5 sec., 15 sec., and 120 sec. Slide wear for these test durations caused gradual removal of the work hardened layers. This enabled SEM studies of the mechanisms of impact-slide wear at various depths from the saturation hardened surfaces. The observations are represented in Figs.4.50-4.58.

In all the samples wear starts occurring at the edges and continuously proceeds towards the centre. In the first stage microploughing is observed to occur. There is significant difference in the depths of ploughs in different alloys as shown in Figs.4.50-4.53. The depth of ploughs also increases with increase in the duration of wear. It is observed that the depth of ploughs is minimum in 0.003 B and maximum in 0.50Cb alloy. There appears to be a correlation between the depth of initial ploughs (observed after 5 sec. of wear test) and the saturation hardness after impact hardening. The depth 'd' of ploughs in various alloys after 5 seconds of wear appears to vary in the order:

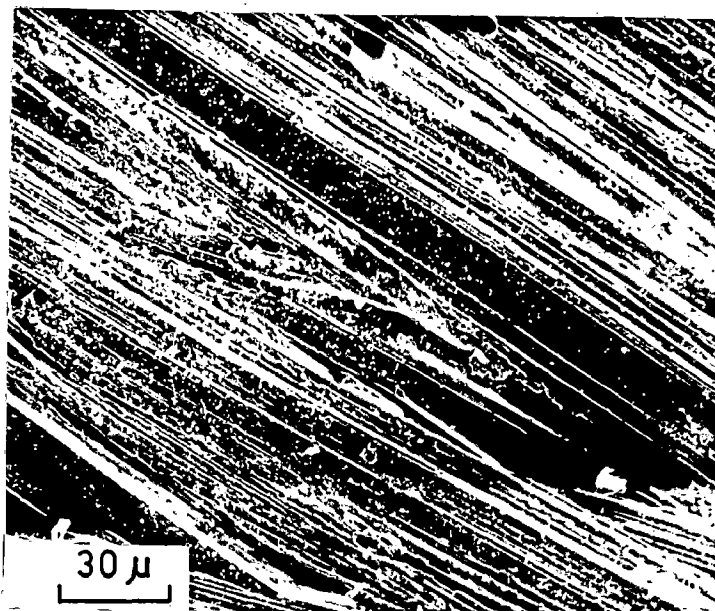


(a)

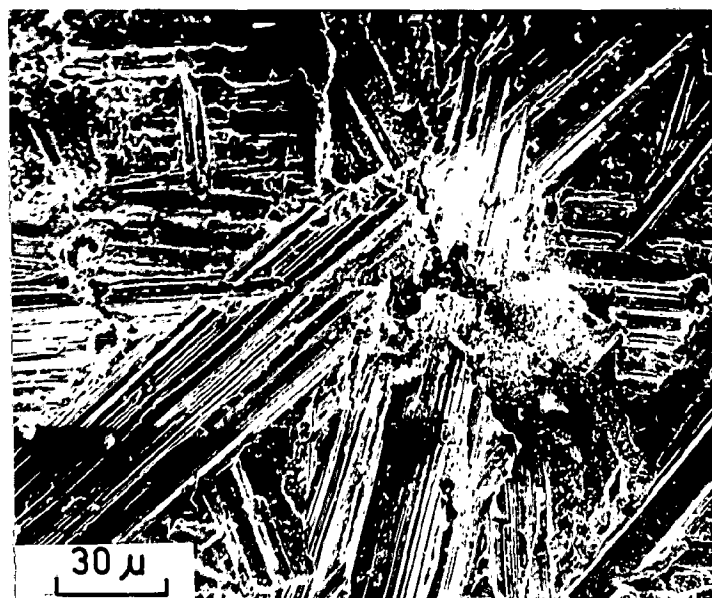


(b)

FIG. 4.50 MICROPLOUGHING IN 13 Mn ALLOY AT DIFFERENT INTERVALS OF IMPACT-SLIDE WEAR  
(a) 15 SECONDS      (b) 2 MINUTES



(a)

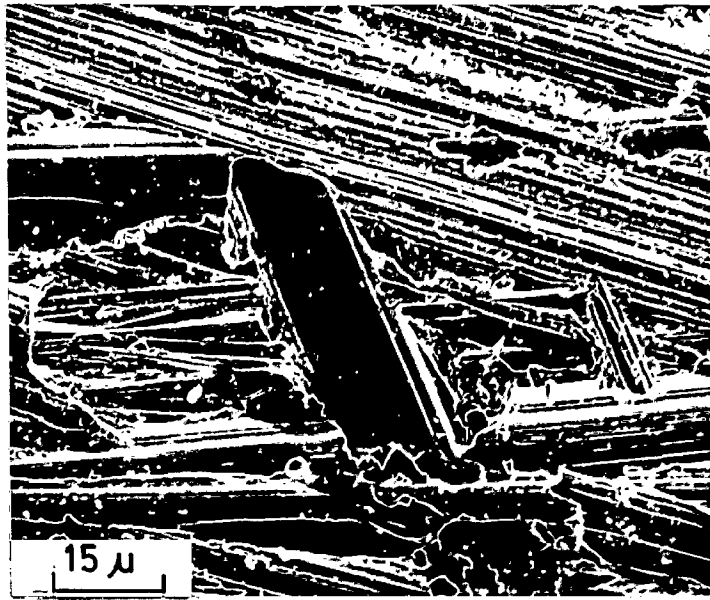


(b)

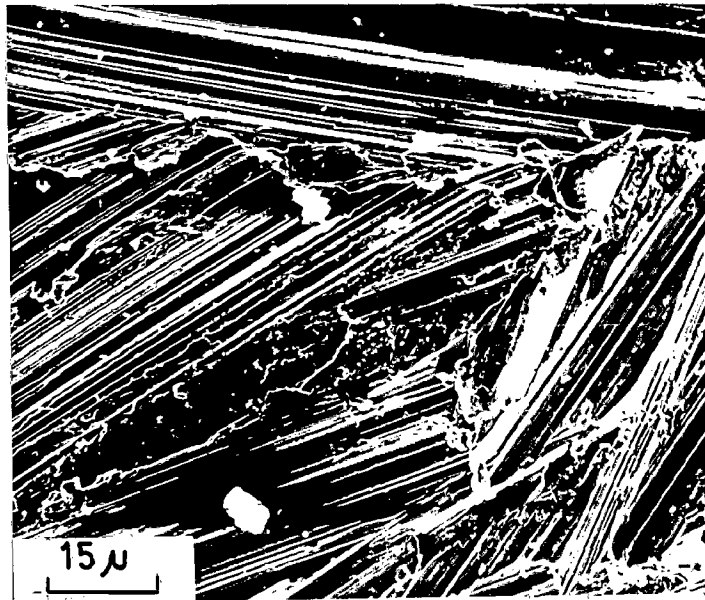
FIG. 4.51 MICROPLOUGHING IN 0.003 B ALLOY AT DIFFERENT INTERVALS OF IMPACT - SLIDE WEAR

(a) 15 SECONDS

(b) 2 MINUTES

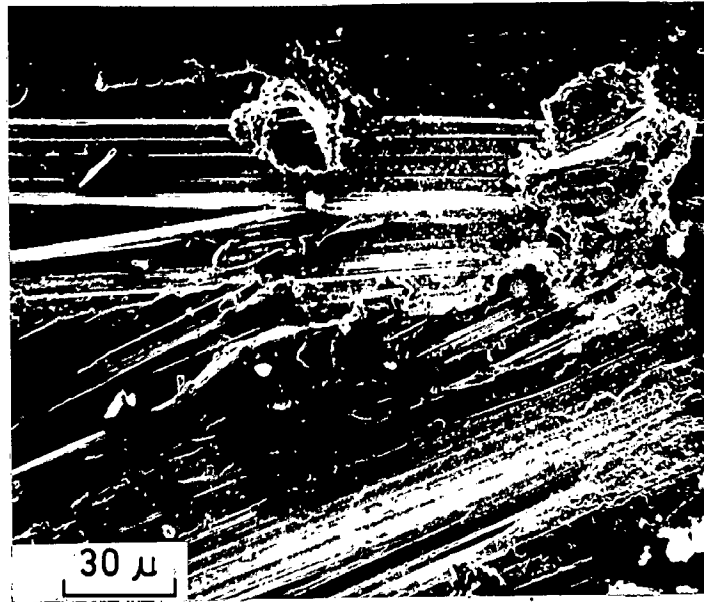


(a)

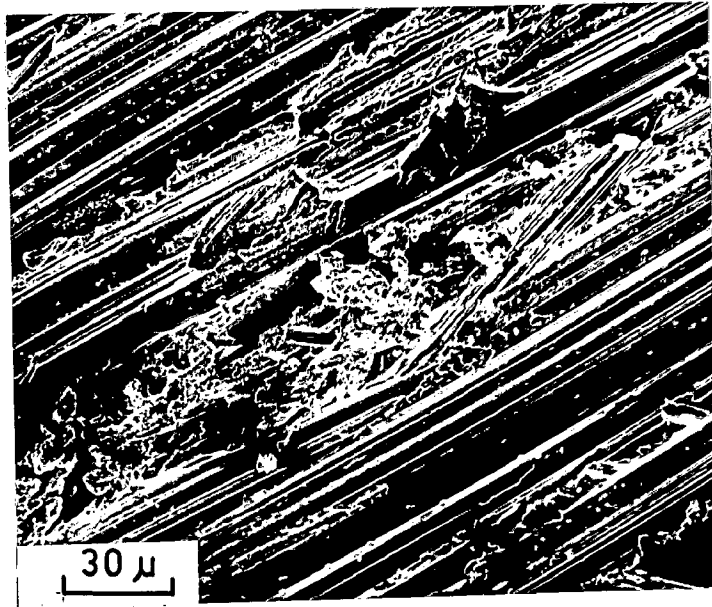


(b)

FIG. 4.52 MICROPLOUGHING IN 0.10 V ALLOY AT DIFFERENT INTERVALS OF IMPACT-SLIDE WEAR  
(a) 5 SECONDS                      (b) 2 MINUTES



(a)

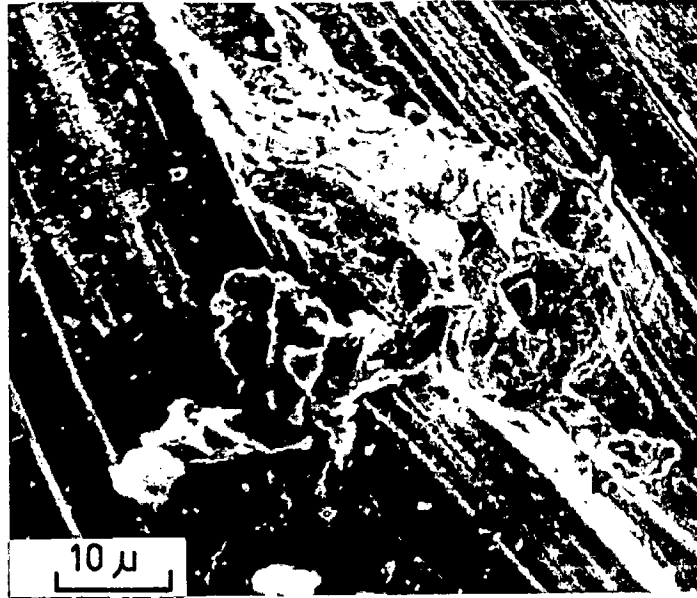


(b)

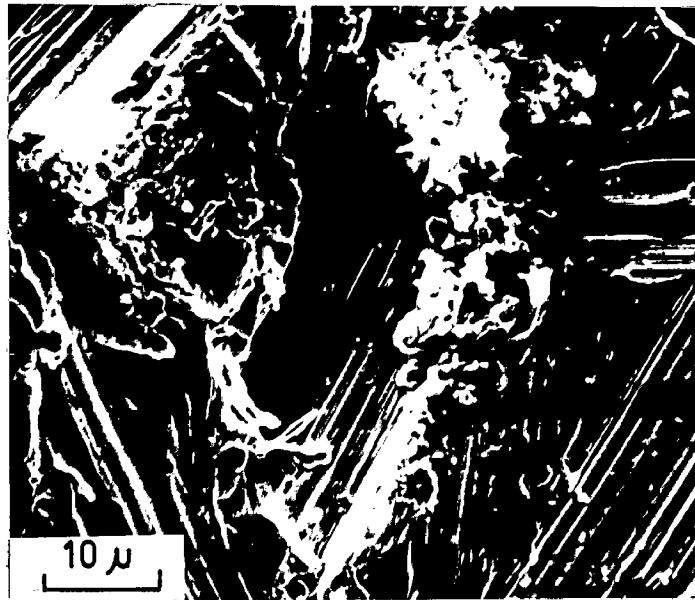
FIG. 4.53 MICROPLOUGHING IN 0.50 Cb ALLOY AT DIFFERENT INTERVALS OF IMPACT - SLIDE WEAR

(a) 5 SECONDS

(b) 2 MINUTES



(a)



(b)

FIG. 4.54 EXTENSIVE PLASTIC DEFORMATION DURING IMPACT-SLIDE WEAR IN 0.003 B ALLOY

(a) 5 SECONDS

(b) 2 MINUTES





(a)

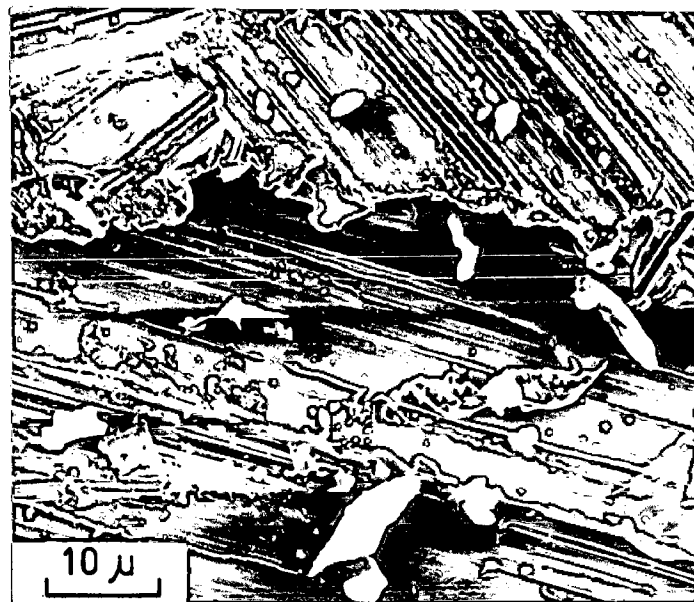


(b)

FIG. 4.55 FRAGMENTATION OF DEFORMED REGIONS DURING  
IMPACT-SLIDE WEAR IN 0.003 B ALLOY  
(a) 5 SECONDS                      (b) 2 MINUTES

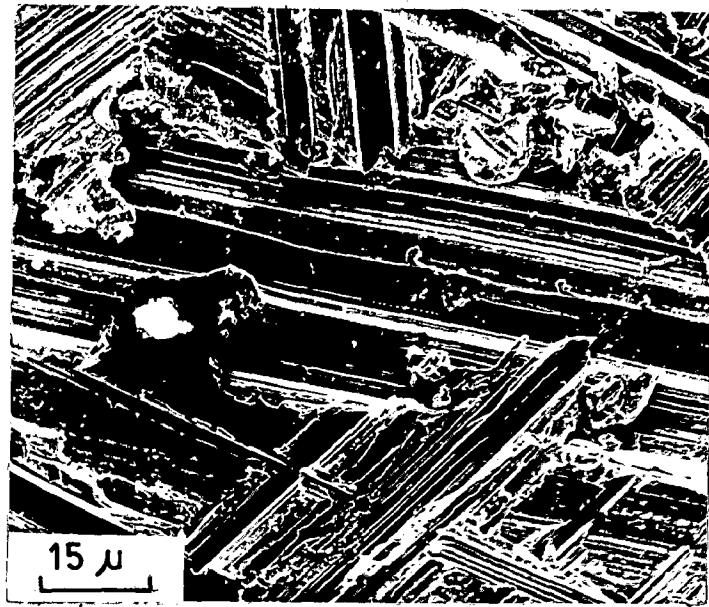


(a)



(b)

FIG. 4.56 (a) FORMATION OF DEFORMED LAYER AND  
(b) SUBSEQUENT FRAGMENTATION DURING  
IMPACT-SLIDE WEAR IN 13 Mn ALLOY.



(a)

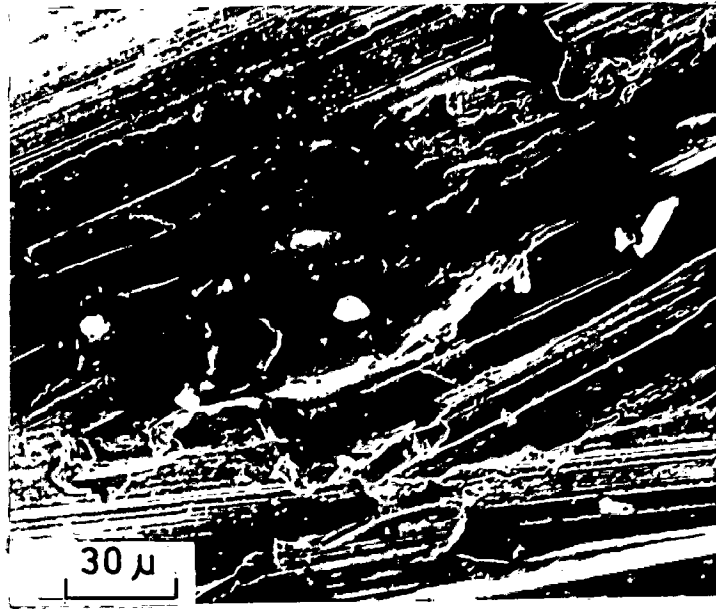


(b)

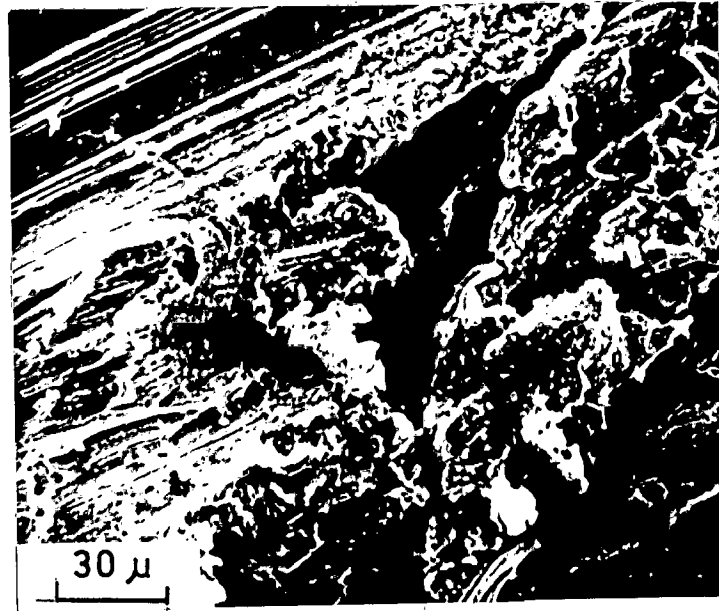
FIG. 4.57 PARTICLE - MATRIX DECOHESION AND VOID FORMATION DURING IMPACT - SLIDE WEAR IN 0.10 V ALLOY.

(a) 15 SECONDS

(b) 2 MINUTES



(a)



(b)

FIG. 4.58 PARTICLE - MATRIX DECOHESION AND VOID FORMATION DURING IMPACT-SLIDE WEAR IN 0.50 Cb ALLOY

(a) 5 SECONDS

(b) 2 MINUTES

$$d_{0.50 \text{ Cb}} > d_{0.10 \text{ V}} > d_{13 \text{ Mn}} > d_{0.003 \text{ B}}$$

As already reported the saturation hardness 'H' varies in the order:

$$H_{0.50 \text{ Cb}} < H_{0.10 \text{ V}} < H_{13 \text{ Mn}} < H_{0.003 \text{ B}}$$

Thus it is seen that the depth of microploughs is low in those alloys which develop high work hardening by repeated impact loading. From this study it is also observed that the depth of micro-ploughs increases in all the alloys with increase in the duration of wear test as is clearly seen from Figs.4.50-4.53.

It is observed that during wear the material starts getting removed in the form of fine flakes in all alloys. The size of these flakes is in the same order as that of depth of micro-ploughs. For example, it is seen that in 0.003 B alloy the flakes formed are of smallest size (Fig.4.51a). Largest size flakes are observed in 0.50 Cb alloy (Fig.4.53a). In the 13 Mn and 0.10 V alloys the flakes formed are of medium size (Figs.4.50a and 4.52a). An interesting observation made is that formation of flakes at the wear surfaces is associated with occurrence of plastic deformation preferentially at junctions of micro-ploughs. Thus in the initial stages impact-slide wear occurs by micro-ploughing, micro-cutting and localised plastic deformation which causes fine particles and flakes to form which are subsequently removed from the surface.

From the SEM studies of wear surfaces it is observed that plastic deformation, particularly at cross junctions of micro-ploughs, occurs during impact-slide wear before material in the form of particles or flakes is removed. This mechanism becomes more and more predominant as the work hardened layer is gradually removed. It is seen that extent of deformation is maximum in the 0.003 B alloy and it becomes more predominant as the hardened layer is removed after two minutes of abrasion (Fig.4.54). The deformed region finally becomes brittle and develops fine cracks and fragments in the form of small pieces and flakes are slowly detached from the material surface and thereby even large cavities are formed. The fragmented particles are of smallest size in the 0.003 B alloy as clearly seen in Fig.4.55. In the alloys containing carbide particles (especially 0.10V and 0.50 Cb) the SEM observations indicate that the carbide particles play a dominant role in wear. The extent of deformation is reduced in these alloys and wear appears to be occurring primarily by decohesion at the particle-matrix interfaces. As already reported, the carbides develop a brittle zone around them and even several particles are removed from the matrix during impact hardening. This leads to formation of voids at their interfaces which subsequently grow by additional removal of material during wear. In the case of 13 Mn alloy the extent of deformation is more relative to 0.10V and 0.50Cb alloys and decohesion at particle matrix interfaces is not very prominent. As seen in Fig.4.56, in the 13 Mn alloy material flakes are formed during abrasion by deformation; which on

\*\*\*\*\*

CHAPTER-5

DISCUSSION

\*\*\*\*\*

## Chapter-5

### DISCUSSION

The effects of various micro alloying elements on mechanical properties and wear characteristics has their origin in the structural characteristics of the alloy. Accordingly, optical and scanning electron microscopic (SEM) studies have been utilised to understand the influence of micro alloying on various properties of Hadfield steels. Micro alloying additions also effect de-oxidation during melting. The cast structure obtained consists of fine grains. All these factors are considered responsible for the observed effects of these additions in Hadfield steels.

#### 5.1 EFFECT OF MICRO ALLOYING ON STRUCTURAL CHARACTERISTICS AND MECHANICAL PROPERTIES

The alloy under investigation contains C, Mn and Si as principal alloying elements and P as impurity element. The presence of Mn in Fe-C system tends to suppress the transformation of austenite into ferrite and carbide phases. A fully austenitic structure, essentially free of carbides and reasonably homogeneous with respect to C and Mn, is obtained with high temperature treatment and water quenching.

Boron in small percentages (0.0005-0.003 pct.) has been very successfully used to increase the stability of austenite phase in steels and to significantly improve the mechanical properties. In the present investigation the addition of B in the range



of 0.001 to 0.004 pct. has resulted in significant improvement in tensile and impact properties of conventional Hadfield steel [Figs.4.1,4.4,4.7,4.10,4.16 and 4.19]. The optical and SEM studies on 0.003 B steel also show the absence of any carbide precipitation along the austenite grain boundaries, which leads to a tougher austenite in these steels as compared to 13 Mn alloy. It is seen from the fractograph of impact sample that there is substantial elongation in the grains before fracture which shows higher toughness of 0.003 B alloy [ Figs.4.47 and 4.48 ].

Boron, like C, forms an interstitial solid solution with gamma iron. The solubility of B in gamma iron is upto 0.003 pct. at equilibrium transformation temperature and the rate of diffusion of B in austenite is roughly same as that of C [88,89]. It does not get altered with presence of C in solid solution of austenite. Beyond the solubility limits, B leads to the formation of  $\text{Fe}_3(\text{Fe, Mn})$  (B,C) carbo-borides in a cell type structure [123] which deteriorates the mechanical properties. It has been observed from the results obtained [Figs.4.1,4.10 and 4.16] that there is improvement in the mechanical properties, specially elongation and toughness, upto 0.003 pct. B. Deterioration in these properties with higher B addition (0.004 B alloy) is due to embrittlement caused by the precipitation of carbo-borides.

The various mechanism given in literature support how the small addition of B in solubility limits improves the

strengthening of 13 Mn alloy. Embrittlement by carbide precipitation in austenite matrix has adverse effect on the mechanical properties in conventional Hadfield steel which is significantly reduced by B additions. The fractographs of tensile and impact tests of 13 Mn alloy [Figs.4.43 and 4.47] and 0.003B alloy [Figs.4.44 and 4.48] indicate intergranular failure. Hence embrittlement on grain boundaries adversely affected the mechanical properties.

Columbium and V are strong carbide and nitride forming elements and are effective even in relatively low concentrations. Looking at the position of these two elements in the periodic chart, they have equal tendencies to form carbides or nitrides required for precipitate strengthening and grain refinement. Columbium in C- and low alloy steels forms a carbide having the cubic NaCl type of structure, which has been assigned the formula  $CbC$  by most investigators [128,129]. Eggers and Peter [128] suggested the presence of  $Cb_4C_3$  type carbides. The possibility that both types of carbide exist has been discussed by Goldschmidt [129], who proposed that  $Cb_4C_3$  and  $CbC$  might be analogous to the V-carbides i.e.  $V_4C_3$  and  $VC$ , which can exist independently and which have limited solid solubility. Columbium as a strong carbide forming element stands above Cr, Mn and V in comparison to Ti and Ta in affinity for C and Cb-carbide is less soluble in austenite than Cr, Mn, V and Ti carbides. The undissolved particles of Cb-carbide are the principal causes of the inherent fine grain size characteristics of Cb-bearing steels. Recent work [81] suggests that the V-carbide

formed is not the stoichiometric VC or  $V_4C_3$ . It has the general composition  $VC_{1-X}$  (where X is a function dependent on the extent to which the interstitial C sites in the fcc are filled).

The general increase in YS and UTS by V and Cb additions [Figs. 4.2, 4.3, 4.5, 4.6, 4.8 and 4.9] may be attributed to the precipitation hardening and grain refinement [Figs. 4.36 and 4.37] caused by their presence. These elements inhibit grain growth during solidification as well as during heat treatment due to strong interaction of carbides with grain boundaries. This interaction results from the elimination of grain boundary area (energy) when the boundary intersects the carbide particle. Any movement of the grain boundary away from the particles would result in a local increase in energy and have a drag effect on the migrating boundary. The binding force between particles and boundary is greater than that available by thermal activation during heat treatment. Hence in 0.10V and 0.50 Cb steels no appreciable grain coarsening is observed during austenitising as seen from Fig. 4.37. The carbide forming tendency by the addition of V and Cb leads to a lower stability of austenite as compared to B bearing steels. Moreover the precipitation of carbides also depletes C concentration in the austenite matrix, which in turn lowers the general solid solution strengthening in 0.10 V and 0.50 Cb steels. All the mechanical properties of 0.003 B steel are, therefore, superior to those of 0.10 V and 0.50 Cb steels. The Cb-carbide formed during solidification is relatively insoluble in austenite.

stability of austenite phase. Boron atoms are adsorbed preferentially at austenite grain boundaries leading to lowering of grain boundary energy [96,104]. According to Fisher[103] this lowering of austenite grain boundary energy retards the nucleation of carbides. In his view the effect of B on austenite-carbide interfacial energy is much less as compared to that on the austenite grain boundary energy. Boron preferentially concentrates at imperfections in the austenite lattice, which are abundant at grain boundaries [105]. The presence of B at imperfections reduces the energy level hence reducing the nucleation sites for carbide precipitation. Therefore, presence of B increases the stability of the austenite phase by retarding carbide precipitation which is the normal occurrence in conventional Hadfield steel specially in thicker sections. This, in turn, helps in keeping the total C in solid solution of austenite causing improvement in tensile strength, elongation and toughness remarkably by solid solution strengthening. It is seen from thermodynamic data [38], that Mn decreases moderately the activity of C in austenite, indicating an attractive force between Mn and C. This combination is unique in that their interaction energy is appreciable but not so high that carbides are quickly precipitated. The presence of B further retards the possibility of carbide precipitation. Hence it allows the large concentration of Mn and C both held in supersaturated solution of austenite giving increased solid solution strengthening. Hence improvement in YS, UTS, El and toughness are associated with improvement in solid solution

No significant dissolution of Cb-carbide occurs at austenitising temperature of 1050°C in Hadfield Mn steels. It is observed that in 0.50 Cb alloy Cb-carbide is present on the austenite grain boundaries even after quenching heat treatment [Fig.4.37]. In the as cast structure a high concentration of carbides is seen which are mix of Fe-Mn-Carbides and carbides of micro alloying additions[Fig.4.36]. However, after austenitising treatment only Cb-carbide particles are observed.No solubility is observed during austenitising treatment in case of Cb-carbide particles. Vanadium carbide particles, on the other hand, have a tendency of partial dissolution into austenite at 1050°C. Whereas the presence of Cb-carbide and V-carbide particles produce a fine grain structure which results into better casting characteristics and improvement in YS and UTS, high concentrations of these elements are deleterious to all mechanical properties, especially El and Charpy impact energy. This is primarily due to the embrittling effect of these carbides in the matrix. Since V-carbide has a tendency to distribute itself more or less evenly and finely along grain boundaries as well as within the grains [Figs.4.37c], its adverse effect is also evenly distributed. As a result, VHN, YS and UTS of V containing Hadfield steel increase for all V additions [Figs.4.2,4.5,4.8 and 4.14]. Elongation and impact energy values in V bearing steels, on the other hand, are improved only by small additions of V, and at high concentrations there is a deterioration in these properties due to the embrittling effect of V-carbides [Figs.4.11,4.17 and 4.20]. The particles of Cb-

carbides are mainly formed at the austenite grain boundaries; as a result they assume coarser size as compared to V-carbide particles. As already reported, addition of Cb causes deterioration in elongation as well as in impact energy at all concentrations studied [Figs.4.12,4.18 and 4.21]. The fact that Cb-carbide does not even partially dissolve during austenitising also adds to the adverse effect of this element. The observation that by additions of V and Cb El and impact property are more drastically affected than the tensile strength is easily understood by the decohesion occurring at the particle-matrix interfaces during deformation [Figs.4.40-4.42]. During tensile tests these interfaces open up slowly, whereas in dynamic impact testing these interfaces are opened up more or less immediately during loading. The SEM studies of the tensile and impact fracture characteristics in 0.10 V and 0.50 Cb alloys [Figs.4.45, 4.46 and 4.49] indicate that under tensile and impact loading the fracture that occurs is of intergranular nature. It is therefore obvious that failure will be accelerated by the presence of brittle carbides on grain boundaries. These carbides preferentially open up the cleavage at their interfaces which act as notches to cause rapid failure without undergoing extensive deformation. Thus the resultant El and toughness in 0.50 v and 0.50 cb steels are much lower than those in 13 Mn or 0.003 B alloys. Since massive carbide particles are formed by Cb additions as compared to V addition, deterioration in impact properties is observed to a much greater extent in Cb

containing steels. In V bearing steels the impact shows an upward trend at low V concentrations and it is lowered only when V concentration becomes high. At low V concentrations (upto 0.10 pct.) the carbides are of fine size and are not very much effective in causing decohesion. Moreover the partially dissolved V causes solid solution strengthening which results in improved impact strength.

The improvement in the mechanical properties by micro alloying additions can be partially attributed to the de-oxidising tendency of these elements during melting and solidification. These elements form stable oxides due to their tendency to readily combine with oxygen. Gurry [130] and Derge [131] concluded that de-oxidising power of B is comparable to that of Si but not as effective as that of Al. In Ellingham diagram B finds place below Si but above Al. Similarly V and Cb are also close to Si and below Mn. Normally steel is thoroughly killed before additions of these micro alloying elements. But it is seen from the recovery of the various micro alloying additions that these elements partly combine with dissolved gases in the melt resulting in lower concentration of dissolved gases. steels with lower dissolved gas contents show superior mechanical properties, especially toughness. This is related to the reduction in the residual stresses by removal of oxygen atoms from the matrix. Hence, the improvement in the mechanical properties, mainly by addition of B, which is the most powerful deoxidising agent among the three additions made, could be

subsequent wear operation become brittle and are removed from the surface as fragments. In the 0.10V and 0.50Cb wear occurs by decohesion which leads to separation of comparatively large particles from the wear surface as shown in Figs.4.57 and 4.58. The particle-matrix decohesion is maximum in the 0.50 Cb alloy, which also shows the poorest impact-slide wear resistance among all the alloys studied. The SEM study indicates that the mechanism of slide wear is the same as in the constant hardness zone of impact hardened samples after the variable hardness layers are removed. This again matches with the observation made in section 4.3 that the hardening produced in slide wear is the same as that observed in the constant hardness zone after the variable hardness layer is removed from the impact hardened surface in case of all the alloys studied.



containing steels. In V bearing steels the impact shows an upward trend at low V concentrations and it is lowered only when V concentration becomes high. At low V concentrations (upto 0.10 pct.) the carbides are of fine size and are not very much effective in causing decohesion. Moreover the partially dissolved V causes solid solution strengthening which results in improved impact strength.

The improvement in the mechanical properties by micro alloying additions can be partially attributed to the de-oxidising tendency of these elements during melting and solidification. These elements form stable oxides due to their tendency to readily combine with oxygen. Gurry [130] and Derge [131] concluded that de-oxidising power of B is comparable to that of Si but not as effective as that of Al. In Ellingham diagram B finds place below Si but above Al. Similarly V and Cb are also close to Si and below Mn. Normally steel is thoroughly killed before additions of these micro alloying elements. But it is seen from the recovery of the various micro alloying additions that these elements partly combine with dissolved gases in the melt resulting in lower concentration of dissolved gases. Steels with lower dissolved gas contents show superior mechanical properties, especially toughness. This is related to the reduction in the residual stresses by removal of oxygen atoms from the matrix. Hence, the improvement in the mechanical properties, mainly by addition of B, which is the most powerful deoxidising agent among the three additions made, could be

partially attributed to this effect. The presence of de-oxidation products i.e. oxides or nitrides of these elements in the melt also provide preferential nucleation sites for the new grains to form. Since B forms very fine oxide particles, which have poor coalescing tendency, these particles do not easily float to the surface. Therefore, the presence of these particles in the melt provides sites for nucleation of new grains resulting into a fine grain structure and also their presence inhibits the grain growth during solidification. Oxides and nitrides provide lower contact angles and thereby preferable sites for easy nucleation. This results in grain refinement in Hadfield steels by all the three additions [Fig.4.36] which not only give improvement in casting characteristics but also in the mechanical properties. The fact that in all the alloys investigated intergranular fracture occurs during tensile and impact tests could be to a great extent attributed to the presence of fine oxides and nitrides at the grain boundaries.

## 5.2 EFFECT OF MICRO ALLOYING ON MECHANISM OF WORK HARDENING

There have been numerous studies [38-72] in the past to understand the mechanisms of rapid work hardening in Hadfield steel. Until recently the view was widely held that the work hardening resulted from the decomposition of the austenite to martensite. For example, Hall [132] found x-ray evidence for martensite transformation, while Krivobok[133] considered that martensite plates formed on the slip bands in the austenite.

Chavenard[134] came to a similar conclusion from thermodynamic studies. In more recent years, doubt has been thrown on the martensite theory. several workers [40-44] have reported that the austenite is stable during plastic strain even below  $-196^{\circ}$  C. Photomicrographs [Figs.4.38 and 4.39] of the work hardened samples do not show any trace of martensite in this investigation, which is in agreement with the observations made by these workers. In various studies conducted in recent years rapid work hardening in Hadfield steels has been attributed to different mechanisms by different workers [38-72]. These mechanisms include fragmentation of austenite grains, formation of stacking faults, mechanical twinning, dynamic strain ageing and precipitation of carbides.

The present investigation indicate that different work hardening mechanisms operate for different micro alloying additions and for different conditions of loading. The results of tensile tests show that all micro alloying additions increase the strain hardening exponent ( $\eta$ ). Maximum increase in the value of  $\eta$  is observed in 0.10 V steel. As seen in Fig.4.25  $\eta$  for 0.10 V steel is 0.80 as against 0.45 for the 13 Mn steel. For 0.003 B and 0.50 cb steels the values of  $\eta$  are 0.58 and 0.70 respectively. The work hardening behaviour of the steels studied under impact loading is quite different from that observed in normal tensile loading using a hydraulic universal machine. For example, work hardening by impact loading (as measured by increase in hardness) is observed to be maximum by B

addition [Fig.4.27], whereas addition of Cb deteriorates the work hardening tendency. Vanadium additions are observed to have negligible influence on the work hardening behaviour under impact loading.

Metallographic studies show that at room temperature work hardening tendency is greatly influenced by the formation of deformation twins [Figs.4.38 and 4.39]. Rapid work hardening in Hadfield steels has also been attributed to the formation of mechanical twins by several authors [41,46,47]. Detailed transmission electron microscopy investigation conducted by Raghavan et al [47] have revealed numerous individual intrinsic faults at small plastic deformation. With increased plastic deformation, the stacking faults thicken into twin lamellae which in turn subdivide the original austenite matrix into smaller domains. The twin boundaries act as strong barriers to subsequent dislocation motion and is in a sense equivalent to grain refinement. It is this 'grain refinement' which is believed to be an important cause of the very high work hardening rates in Hadfield steels. In the present study it is seen that a high concentration of twins is formed in the impact loaded samples giving rise to extremely high work hardening by all alloying additions.

In the case of twin, there is no chemical driving force for its formation and it is generally necessary to provide the required driving force by an applied stress, i.e. strain

energy. In the case of the hcp structure the transformation from the fcc modification can occur spontaneously (martensitically) since a decrease in chemical energy does in fact occur, however, an applied stress will provide an even greater driving force towards complete transformation. Since the twins can act as potential barriers to further plastic deformation [47, 135], marked strengthening effects can be anticipated. It is also clear that these effects should be greatest in steels of the austenitic type, i.e. the fcc type, which have high shear modulus. In order to pass a dislocation through a twinned crystal, interface dislocations must in general be generated. This generation costs energy which in turn raises the applied stress for dislocation motion. The finer the distribution of twins the greater will be the density of interface dislocations and thus greater will be the applied stress for dislocation motion.

The present investigation shows that while stacking faults can act as impediments to further deformation and cause hardening mainly by raising the stress necessary to force cross slip to occur, it does not seem to provide the whole answer to the problem. The different attitudes of work hardening during normal tensile loading and during impact loading are not clear from the concept of mechanical twinning alone. Also it does not become clear as to why different microalloying additions show different work hardening rates under both types of loading. For example, it is interesting to note that Cb addition causes hardening

of base Hadfield steel during normal tensile tests, whereas during impact the work hardening is reduced by its addition [Figs.4.25 and 4.27]. It has been suggested that high concentration of carbon atoms must play a part in locking the dislocations [71,72]. Dastur and Leslie [38] and Colette et al [71] observed serrated stress/strain curves (the Portevin - Le Chatlier effect) in tension at temperature near and above room temperature, which supports their contention of C locking. In this investigation serrations have been detected in stress-strain curves recorded at very low strain rate of  $3 \times 10^{-4} \text{ sec}^{-1}$  at room temperature [Fig.4.26]. It is seen that by microalloying the amplitude and frequency of serrations are increased, the maximum effect being by addition of V. The formation of these serrations have been attributed to dynamic strain ageing, which is associated with rapid work hardening [38]. Dynamic strain ageing has been observed to be associated with rapid work hardening in other materials, e.g. low C steel [54], austenitic stainless steel [55] and maraging steels [56]. Serrated flow curves during dynamic strain ageing have been explained in terms of the initiation, propagation and pinning of Lüder bands [60-62]. Numerous studies [63-70] have shown that the increased work hardening accompanying serrations can be attributed to an increased rate of dislocation multiplication, which increases the dislocation density for a given strain. It is reported [38] that pinning of Lüders band is a diffusion controlled process with an activation energy much below that for bulk diffusion of C atoms in this steel. For

example, the activation energy for onset of serrations is reported approximately  $104 \pm 15$  KJ/Mol in comparison to  $140 \pm 10$  KJ/Mole for bulk diffusion of C atoms in austenitic Mn steel [21,30]. Hence dynamic strain ageing is associated with short range diffusion of C in the core of dislocations. Thermodynamic data for the Fe-Mn-C [136] alloys show that Mn decreases moderately the activity of C in austenite, indicating an attractive force between Mn and C, which is necessary to produce point defect pairs which pin dislocations. The pinning of dislocations may also be associated with stress induced ordering of C atoms arising from the distortion of octahedral sites by neighbouring Mn atoms as reported by Ke and Wang [137] and Kandarpa and Spretnak [138]. The C-Mn combination has high interaction energy, but not so high that carbides are quickly precipitated. Thus, large concentrations of both C and Mn can be held in supersaturated solid solution in austenite which aids work hardening. Micro alloying of 13 Mn steel with B, V and Cb is reported to lower the activity of C in austenite, the effect of V and Cb being more than of B. Hence V and Cb readily form carbides in the matrix. The large serrations observed in 0.10 V and 0.50 cb steels could be both due to the pinning effect of dislocation cores by their additions, as well as by the formation of their carbides. As already stated, serrations in stress-strain curves become visible only when tested at extremely low strain rate. It is therefore very difficult to attribute to high values of strains hardening exponent ( $\eta$ ) obtained from load-elongation diagrams recorded in normal tensile

tests (conducted at relatively fast speeds) with the amplitude and frequency of serrations observed in constant strain rate tests conducted at an extremely low constant strain rate ( $3 \times 10^{-4} \text{ sec}^{-1}$ ). Although, as is seen from Figs. 4.25 and 4.26 that higher the value of  $\eta$ , more pronounced are the serrations in all compositions studied. The situation becomes more complex by the formation of carbides in V and Cb bearing steels, which should also play an important role in the overall mechanism of work hardening. Since in impact loading deformation rates are very high, dynamic strain ageing can not be the governing mechanism of work hardening. In impact the work hardening can only be attributed to solid solution strengthening, microtwinning and the presence of carbides.

The mechanism of work hardening in the Hadfield steels containing V and Cb becomes a complex phenomenon due to the presence of carbide particles. Columbium carbide particles ( $\text{Cb}_4\text{C}_3$ ) are observed to precipitate at grain boundaries, whereas in 0.10 V steel the  $\text{V}_4\text{C}_3$  carbides are precipitated in the matrix also. The carbides of Cb are coarser in size as compared to  $\text{V}_4\text{C}_3$  particles [Fig. 4.37]. The general strengthening of austenite will depend upon the size, shape, number and distribution of these particles. The presence of these carbides act as obstacles to the movement of dislocations. During movement, the dislocations leave small loops around the carbide particles. These dislocation loops exert a back stress which must be overcome by dislocations moving on the slip planes. This requires



higher stress to continue deformation. Thus, the presence of dispersed particles leads to increased work hardening. It is also well established that finely distributed particles in austenite will lead to high increment in strain hardening exponent. This explains the maximum increase in strain hardening exponent in 0.10 V steel, since the carbide distribution in this steel is finest. Strain hardening in 0.50 Cb steel is somewhat lower than 0.10 V steel in view of the fact that the  $Cb_4C_3$  carbide is distributed only at grain boundaries and not within the grains. Addition of B causes only solid solution strengthening and no carbides are observed to precipitate, thus as noted by the  $\eta$  value, the work hardening in B bearing steel is although greater than in 13 Mn steel, but it is less than that in 0.10 V or 0.50 Cb steel. The carbide particles provide source of dislocation generation at their interfaces which also causes work hardening during subsequent straining. The existence of carbides appear to be dominating factor in the mechanism of work hardening of all the steels studied under impact loading. It is seen that whereas V and Cb increase work hardening tendency during normal tensile loading, their presence in the austenite deteriorates the work hardening rate during impact loading. Fig.4.27 shows that under impact loading (by a constant impact force) saturation hardness in 0.10V and 0.50 Cb steels is reached after 100 blows as against 50 blows in 0.003 B steel. In the 13 Mn steel saturation in hardness is attained after 100 blows. It is also seen that saturation hardness in 0.003 B steel is maximum, followed by 13 Mn and

0.10 V steels, which show almost same value of saturation hardening. In the case of 0.50 Cb steel the work hardening under impact loading is even less than in 13 Mn steel. As already stated, the impact strength is adversely affected by the presence of carbides. The carbide particles are brittle with respect to the matrix and their interfaces with the matrix are locations of great decohesion (Figs. 4.40-4.42). Therefore, a considerable proportion of the impact energy is absorbed in fragmentation of carbides and in causing cracking along the carbide-matrix interfaces, as supported by SEM observations [Fig. 4.42]. Only a small fraction of impact energy is utilised in increasing matrix hardening which is also greatly reduced due to low concentrations of C around these particles. Decohesion along second phase-matrix interfaces has been attributed to lower impact strength even in Al-alloys [139-143]. Since the carbide particles in 0.50 Cb steel are very coarse and are precipitated at grain boundaries, the decohesion at carbide boundaries is very rapid. Fig. 4.40 is an optical micrograph showing opening of matrix of the carbide-matrix interfaces in 0.50 Cb steel. In addition, white etching layers around carbide particles are formed which indicate the region around the carbides in a state of high stresses which may even lead to its brittle failure. The 0.50 Cb steel shows even less work hardening than 0.10 V steel [Fig. 4.27] which possess a finer and uniform distribution of carbides throughout the matrix. Work hardening is most rapid as well as the saturation hardness is maximum in 0.003 B steel because of high solid solution strengthening

effects generated by B additions and absence of carbides. The impact strength is like-wise maximum in this steel.

The hardness variation in the core of impact hardened samples after grinding off successive layers also shows maximum work hardening in the core of 0.003 B steel [Fig.4.29]. Due to the presence of carbides the hardening in the core of 0.10 V and 0.50 Cb steels is lower than that in 0.003 B steel. The hardness in the core of 13 Mn steel is lowest due to the fact that this steel also shows minimum core hardness in the as quenched condition. The core hardness values measured after removal of successive hardness layers correspond to the values induced by work hardening due to the grinding operations in the unimpacted samples [Fig.4.33].

From the present investigation it is observed that the mechanism of work hardening in Hadfield steel differs widely depending upon the mode of deformation. Hardening due to formation of deformation twins seems to be an essential mechanism under all conditions of working. At extremely low strain rates hardening due to dynamic strain ageing also seems to be a contributory factor. Dynamic strain ageing appears to be less effective at strain rates normally encountered in practice and its contribution under impact loading seems to be almost negligible. The presence of carbide particles plays an important role especially under conditions of impact loading.

### 5.3 . EFFECT OF MICRO ALLOYING ON WEAR MECHANISM

Careful inspection of the results obtain indicates that wear in Hadfield steels occurs simultaneously by plastic deformations (micro-ploughing and micro-cutting) and brittle fracture (micro-cracking and fragmentation). The presence of thin flakes or tongues of material on the wear surface [Figs.4.54-4.56] suggests that metal loss may occur by a delamination mechanism [113]. According to the theory, subsurface deformation in wear leads to the nucleation of cracks, which propagate below the wear surface but parallel to it. Ultimately the cracks shear to the surface at points of weakness, causing thin sheets or fragments of material to form and delaminate. It appears from the present investigation that such a mechanism occurs both in impact-slide wear and slide wear. The mechanism also suggests that wear rate should be faster in materials which are prone to cracking due to presence of second phase brittle particles. The materials undergoing extensive deformation prior to cracking or fragmentation should result in improved wear resistance. The extensive decohesion at carbide-matrix interfaces and formation of white etching brittle zones [Figs.4.40-4.42] around carbide particles also cause rapid material loss during wear.

#### 5.3.1 Impact-Slide Wear

The wear resistance shows significant improvement in impact hardened samples. Figs. 4.31-4.35 show that material loss in impact-side wear is much less than that in slide wear.

Obviously work hardening generated during impact loading has played an important role in the mechanism of wear. The presence of carbides, especially in 0.10 V and 0.50 Cb alloys, have attributed significantly towards wear loss.

From the results obtained it is observed that a close correlation exists between the variations in impact-slide wear resistance and the hardness of the work hardened layer. Thus 0.003 B steel, which develops maximum work hardening on impact loading, shows minimum wear loss. Both V and Cb additions reduce the work hardening tendency of base 13 Mn steel which results in deterioration of wear life of 0.10 V and 0.50 Cb steels. High work hardening of the austenite matrix resists the formation of deep microploughs, as a result of which the wear life is increased. The SEM studies have shown that formation of deep microploughs are most resisted in 0.003 B alloy [Figs.4.50-4.53] among all the alloys studied. Further, during wear occurrence of plastic deformation is resisted by high solid solution strengthening and due to a high density of microtwins generated during impact loading [Figs.4.38 and 4.39]. The segregation of solute atoms occurs on these twins as this further reduces the energy of the twins. Although thermodynamic data is not available, it is reported that, among all the elements added B segregates maximum on the stacking faults in Hadfield steel [149]. The high wear resistance of 0.003 B steel is therefore primarily due to the obstacles caused in the movement of glide dislocations by high density of mechanical twins. From Figs.4.31,4.32,4.34 and 4.35 it is observed that in all alloys as the work hardened layer is gradually removed by grind-

ing on the emery wheel the wear loss is also continuously increased due to reduced concentration of deformation twins. The present investigation indicates that the twin density is reduced by additions of V and Cb which causes deterioration in the wear resistance of 0.10 V and 0.50 cb alloys. Jost and schmidt [33] and Bauschke et al [35] have observed a direct relation between the hardness of the surface layer and the wear life in case of low Mn-steels. According to them wear resistance is related quite linearly with the surface hardness resulting from the work hardening. They propose that the wear mechanism as related to the surface hardness are same both in work hardened and martensite hardened samples.

As already stated, addition of V and Cb cause the formation of carbides in the austenite. Existing particles may be coarsened and fresh particles may be produced during impact-slide wear. It has been suggested [144] that under impact loading the temperature rise may cause additional precipitation of carbides. These particles reduce the wear resistance in several ways. During grinding the particles crack due to their brittle character which causes micro cracking. The micro cracks are associated with high concentration of triaxial stresses and thus propagate at high speeds and come out on the surface on weak locations thus causing extensive material removal. The decohesion occurring at the particle-matrix interfaces is another important parameter which accelerates wear [Figs.4.57

and 4.58]. Due to decohesion micro cracks are produced during impact loading at the particle-matrix interfaces as also revealed by metallographic examinations [Figs.4.40-4.42]. As a result, the whole or part of the carbide particles come out of the matrix leaving sharp edged voids which propagate rapidly leading to extensive wear loss. Formation of white etching layer around carbide particles, especially in 0.10 V and 0.50Cb alloys, indicates the development of a brittle zone around the particles due to intense work hardening. This brittle zone also causes fragmentation of the matrix leading to high wear loss. Since relatively coarse carbides are formed in 0.50 Cb alloy the wear loss is also maximum in this alloy. In this steel largest size flakes are formed during wear [Fig.4.53]. Smaller flakes are formed in 0.10 V and 13 Mn alloys [Figs. 4.50 and 4.52]. Since in the 0.003 B alloy no carbides are formed the wear occurs only by microcracking in the matrix due to brittleness caused by extensive deformation. As a result very fine flakes or fragments are produced which are indicative of high wear life of the material. SEM studies confirm extensive plastic deformation [Fig.4.54] and formation of fine size fragments [Fig.4.55] during wear of 0.003 B steel.

A possible mechanism of decohesion occurring at carbide-matrix interfaces lies in the recognition of the role played by stress waves effect[127]. In impact-slide wear the impact conditions produce compressive stress waves at the material surface,

which propagate into the near-surface regions at acoustic velocities. When such a stress wave strikes a carbide-matrix interface, its behaviour depends on the characteristic impedance of the two phases, where the characteristic impedance of a material is product of its density ( $\rho$ ) and the velocity( $C$ ) at which waves propagate through it [145]. If, for example, the  $\rho C$  value of matrix is higher than that of carbide particle, a tensile partial wave will be reflected from the interface back into the austenite matrix and a compressive partial wave (with reduced intensity) will be transmitted into the carbide phase. This will cause preferential decohesion and separation at the interface resulting in microcracking. Once a fracture has occurred, subsequent impacts will cause further reflections to take place from the fracture surface (since the effective  $\rho C$  of the gap will be zero). This will cause rapid spalling of the fractured material.

A significant microstructural feature indicative of an alternate decohesion mechanism is the presence of a white etching layer around the carbide particles. Figs.4.40-4.42 show this effect in 0.10V and 0.50 Cb alloys. White etching surface layer formation has received a considerable amount of attention over a number of years [150]. It has been inferred that the white etching layer forms as a consequence of intense plastic deformation around the carbide particles. This layer has been stated to possess a very high hardness, greater than that which can be produced by conventional hardening process [151]. For



example, the white etching layer on a 0.24 pct. C steel was found to have a hardness of 1100 VHN, whilst the hardness of martensite produced in the same steel produced by austenitising and quenching was only 500 VHN [151]. Thus the layer would be expected to be very brittle and would result in easy decohesion at the particle-matrix interface during impact-slide wear.

The influence of decohesion at the second phase-matrix interface on the wear mechanism has been given by Archard [146] in terms of the relation

$$W = k \frac{A}{A_0}$$

where  $W$  = wear loss,  $k$  = coefficient of wear, which also expresses the probability of decohesion of the matter in the asperity area  $A$ , and  $A_0$  = nominal surface area of the sliding material. Since the wear occurs simultaneously by plastic deformation and brittle fracture, the coefficient of wear  $k$  is divided into two components characterising the deformation ( $k_d$ ) and the brittle fracture ( $k_f$ ) [147, 148]. Thus

$$\begin{aligned} W &= (k_d + k_f) \frac{A}{A_0} \\ &= (k_d + k_f) \frac{\sigma}{H_0 + \Delta H} \end{aligned}$$

where  $\sigma$  = compressive stress in the surface,  $H_0$  = hardness of virgin austenite and  $\Delta H$  = increase in hardness in the surface.

It seems from the present investigation that in Hadfield steels containing carbide particles the brittle fracture component  $k_f$  controls the wear mechanism. Obviously in 0.10 V and 0.50 Cb alloys the increase in hardness due to work hardening is over-compensated by a decrease in the fracture energy of the hardened layer or increase in the value of  $k_f$ . As a result, wear occurs preferentially by growth of existing cracks at the particle-matrix interfaces rather than by plastic deformation. Since in 0.003 B alloy wear occurs predominantly by deformation which requires high energy, the overall wear loss is minimum.

### 5.3.2 Slide Wear

It is observed that wear loss during slide wear is much more than that during impact-slide wear indicating that the wear mechanisms in the two cases may be different. Due to very low work hardening, depth of the micro-ploughs is also much higher than that observed in impact hardened samples. The plastic deformation due to low density of mechanical twins also occurs with ease. All this causes the wear characteristics under slide wear conditions much inferior to those observed under impact-slide wear. The order of slide wear resistance  $(W)^{-1}$  is observed is :  $(W)_{0.003 B}^{-1} > (W)_{13 Mn}^{-1} > (W)_{0.10 V}^{-1} > (W)_{0.50 Cb}^{-1}$ , which is the same as observed during impact-slide wear. However the order of hardness (H) developed by slide wear is :  $(H)_{0.003 B} > (H)_{0.10 V} > (H)_{0.50 Cb} > (H)_{13 Mn}$ . Thus

contrary to impact wear, the wear resistance is not directly related to the hardness developed as a result of work hardening during slide wear. The role of carbides seems to be more dominating than that of work hardening. as discussed in Section 5.3.1 presence of carbides causes decohesion resulting in poor wear properties. Thus 0.003 B alloy, which is completely free of carbides, shows maximum wear resistance. Maximum wear loss is observed in 0.50 Cb alloy due to presence of coarse carbides. Slide wear in 13 Mn is superior than that in carbide bearing 0.10 V and 0.50 Cb alloys. The present investigation shows that in impact hardened samples as the work hardened layer is gradually removed by grinding, the mechanism changes to that of slide wear. This is also confirmed by hardness measurements. As the impact hardened layer is gradually removed the core hardness approaches that obtained in slide wear as shown in Fig. 4.34.

#### 5.4 CORRELATION OF MECHANICAL PROPERTIES WITH WEAR

An attempt has been made in Fig. 5.1 to correlate the observed wear in slide and impact-slide conditions with mechanical properties of various alloys studied in this investigation. The wear resistance as measured by loss in the weight of the material after five minutes of slide or impact-slide operations is observed to be directly and closely related to the impact values. The  $E_1$  as determined from normal tensile

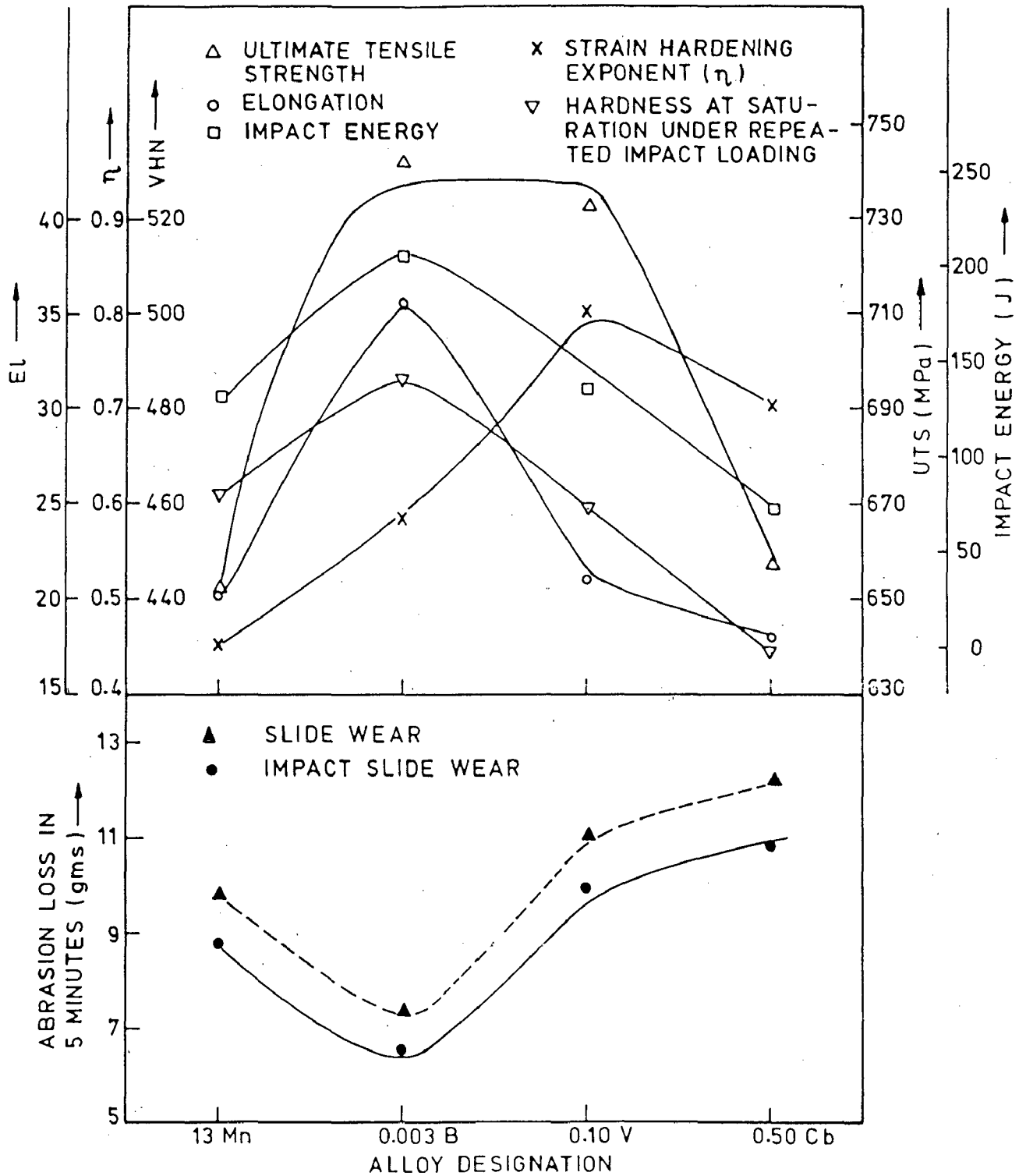


FIG. 5.1 RELATIONSHIP BETWEEN WEAR RESISTANCE AND VARIOUS MECHANICAL PROPERTIES OF MICRO-ALLOYED HADFIELD STEELS.

- iii) The additions of Cb improve the YS and UTS at low concentrations, but the El and toughness are dropped. Higher concentrations of Cb even deteriorate the UTS apart from ductility and toughness. The deterioration in mechanical properties is attributed to the presence of coarse carbides at austenite grain boundaries.
- iv) Fractographic studies show that in all the alloys studied fracture under tensile loading as well as under impact loading is of intergranular character. Thus the formation of embrittling constituents at austenite grain boundaries should be avoided as far as possible.
- v) All the micro alloying additions refine the cast grain structure of Hadfield steel. The extent of grain refinement is almost same by all the micro alloying additions. The cast grain structure is not altered by subsequent heat treatment, i.e. austenitising and quenching.
- vi) Work hardening by impact loading is much higher than by tensile loading. The magnitude of work hardening by repeated impact blows is maximum in B bearing steel. Additions of 0.10 pct. V and 0.50 Cb reduce the work hardening under impact loading. The work hardening is attributed to the formation of mechanical twins, which have

\*\*\*\*\*

CHAPTER-6

CONCLUSIONS AND SUGGESTIONS  
FOR FUTURE WORK

\*\*\*\*\*

## Chapter-6

### CONCLUSIONS AND SUGGESTIONS FOR FUTURE WORK

---

#### 6.1 CONCLUSIONS

The present investigation has been carried out to study the effect of micro alloying additions of B, V and Cb on mechanical properties and wear characteristics of Hadfield Mn steel. The main conclusions of this study are as follows:

- i) The additions of B significantly improve the mechanical properties, viz. YS, UTS, El and toughness. Maximum improvement in mechanical properties is observed with 0.003 pct. B addition (0.003 B alloy). Improvement in properties by B addition is attributed to (a) solid solution strengthening, (b) reduction in the activity of C in solid solution and (c) increase in the stability of austenite.
- ii) The additions of V in low concentrations (upto 0.10 pct.) improve the mechanical properties, whereas at higher concentrations deterioration is observed in ductility and toughness due to embrittlement caused by the presence of undissolved carbides in the matrix and on the grain boundaries of austenite.

maximum density in 0.003 B steel. Lowering of work hardening in 0.10 V and 0.50 Cb steels is attributed to the decohesion and embrittling effects of carbides in these steels.

vii) In all the micro alloyed steels resistance to impact-slide wear is much higher than the resistance to slide wear. This occurs due to rapid work hardening in conditions of impact-slide wear. It is observed that as the impact hardened layer is gradually removed the wear resistance also decreases. When the impact hardened layer is completely removed the hardness observed corresponds to that developed in slide wear and the wear mechanism also changes to that of the slide wear.

viii) Among all the elements added, B significantly enhances the resistance to wear both under impact-slide and slide conditions. Additions of V and Cb reduce the wear resistance of Hadfield steel; the 0.50 Cb alloy shows poorest wear resistance.

ix) Metallographic studies indicate that wear occurs by simultaneously plastic deformation (micro-ploughing and micro-cutting) and brittle fracture (micro-cracking). In 0.003 B alloy maximum impact-slide wear resistance



is observed due to hinderance of glide dislocations by high density of twins. In the 0.10 V and 0.50 Cb steels the wear resistance is deteriorated by the presence of carbide particles. These particles enhance wear rate by decohesion at the carbide-matrix interfaces which lead to easy micro-cracking.

- x) In general the wear resistance of Mn steels is controlled by mechanical properties as well as the metallographic structure. High toughness and El alongwith high UTS lead to high wear resistance as observed in B containing steel. Presence of embrittling particles in the metallographic structure, especially at grain boundaries, causes deterioration in the wear resistance.

## 6.2 SUGGESTIONS FOR FUTURE WORK

On the basis of the present study, further work is proposed on the following lines:

- i) The present study has shown that resistance to wear depends upon the type of loading. For example, superior wear resistance is observed in impact hardened condition as compared to slide wear on unimpacted samples. Wear studies need to be undertaken under conditions of simultaneous impact and slide operations in order to simulate the test results with those in actual operating conditions.

- ii) It has been observed that second phase particles in austenite play a major role in affecting work hardening and wear characteristics of Hadfield Mn steel. Systematic investigations are required to study the effect of shape, size, distribution and composition of these particles on wear characteristics.
  
- iii) The decohesion at the particle-matrix interfaces is observed to be responsible for low impact strength and poor wear resistance. A white etching layer around carbides has been observed which is stated to be very brittle. Such layers at the void edges have also been reported by previous workers. Since this white etching layer appears to be playing an important role in the particle-matrix decohesion, efforts must be made to study the nature, character and structure of this layer.
  
- iv) Experimental studies need to be undertaken on the effect of micro alloying elements on the distribution of C and Mn in the austenite matrix, at the grain boundaries and around the carbide particles. Since clustering of solutes at stacking faults affects work hardening and wear properties, such investigations will give more insight into the mechanism of wear as affected by micro alloying additions.

- v) The micro alloying additions of B, V and Cb effect de-oxidation of Hadfield steel melts resulting in better mechanical properties. However, detailed investigations are needed to study the deoxidation mechanism and the resultant changes in the microstructure.
- vi) The present study shows that micro addition of B is extremely beneficial in improving the various mechanical properties and wear resistance of Hadfield steel. Investigations are needed to standardise the shop floor practice for addition of B to the steel melt. The effect of holding time in the liquid bath on the effectiveness of micro alloying with B needs to be specially studied.

\*\*\*\*\*

REFERENCES

\*\*\*\*\*

REFERENCES

1. R.A. Hadfield  
'Discovery of Mn steel and its importance to modern engineering'.  
British Science Guide (1923) 1
2. R.A. Hadfield  
'Metallurgy and its influence on modern progress;'.  
Oxford University, Jr. Scientific Club, Chapman  
and Hall Ltd., London (1925).
3. R.A. Hadfield  
'Mn steel'  
Inst. Civil Engrs. (1888).
4. R.A. Hadfield  
'Mn steel'  
JISI (1888)
5. R.A. Hadfield  
'Iron alloys with special references to Mn Steels'  
Trans. AIME, International Engineering Congress, Aug.  
(1893).
6. R.A. Hadfield  
'Some newly discovered properties of Fe and Mn'  
Inst. Civil Engrs. (1888).
7. ASTM A 128-75 a  
Annual Book of ASTM Standards, Part 2(1979) 95
8. E.R. Hall  
ASM.Technical Report, (1966) 15

9. R.W. Powell and M.J.Hickman  
'The physical properties of a series of steels'  
Alloy Research Committee, JISI (1946)
10. W.F. Barrett  
'The physical properties of Mn steels'  
Royal Dublin Society (1886)
11. J.H. Awbery and A.R.Chahanev  
'The physical properties of a series of steel;  
Alloy Steels Research Committee ISI (1946)
12. R.A. Hadfield and B. Hopkinson  
'The Magnetic and Mechanical properties of Mn steel'  
JISI 89 (1914)
13. Austenitic Mn steel  
Metal Handbook 9th edition 3, 568
14. E.W. Colbeck  
'Manganese steel'  
Printed at Mccorquodale(Scotland) Ltd. Glasgow(1977)
15. E.C. Bain  
'Alloying elements in steel'  
ASM (1939) 312
16. T. Ishiwara  
'Equilibrium diagrams of Al-Mn, Cu-Mn and Fe-Mn systems'  
Sci. Rep. Tohoku Imp. Univ. 19 (1930)
17. V.N. Krivobok  
'A study of the constitution of high Mn steels'  
Trans. ASST 15 (1929) 893

18. M. Isobe  
'Equilibrium diagram of ternary alloys system of Fe-Mn-C;  
Science Report of Research Institute, Tohoku University  
Sci. Rep. Ritu. 3 (1951)
  
19. Tofante and Linden  
Archiv für das Eisenhüttenwesen 11(1937) 515
  
20. V.N. Krivobok and C. Wells  
'Alloys of Fe, Mn and C,  
Part V, Microscopic studies of binary Fe-Mn alloys'  
Trans.ASST 21 (1933)
  
21. H. Scott  
'Transformational characteristics of Fe-Mn-alloys'  
Trans AIME, Iron and Steel Division, 95(1931)
  
22. F.M. Walters and C.Well  
'Alloys of Iron, Mn and carbon, thermal analysis of  
the binary alloys'  
Trans. ASST 19 (1932)
  
23. F.M. Walters and M.Gensamer  
'Alloys of iron, Mn and C, Part IV, a dilatometric study  
of iron-Mn binary alloys'  
Trans. ASST 19 (1932)
  
24. F.M. Walters  
'Alloys of Iron, Mn and C. Part VI, factors affecting  
transformation in the binary Fe-Mn alloys'  
Trans. ASST 21 (1933)

25. C. Wells and F.M. Walters  
'Alloys of Iron and Mn, part XIII, The constitution of the binary alloys of Fe and Mn'  
Trans. ASM 23 (1935)
26. E.C. Bain, E.C. Davenport and W.S.N. Waring  
'The equilibrium diagram of Fe-Mn-C alloys of commercial purity'  
Trans. AIME 100 (1932) 228
27. C.H. Shih, B.L. Averbach and M.Cohen.  
'Work hardening and martensite formation in Mn-alloys'  
MIT Research Report (1953)
28. G. Range and J.M. Kiefer  
'Transformation of austenite on continuous cooling and its relation to transformation at constant temperature'  
Trans. ASM 29 (1941) 85
29. J.V. Russell and F.T. Megujre  
'A metallographic study of decomposition of austenite in Mn steels'  
Trans. ASM 33 (1944) 101
30. R.A. Hadfield  
'Heating and cooling curves of Mn steel'  
JISI (1913)
31. R.A. Hadfield  
'The result of heat treatment on Mn steel and then of C steel'  
JISI (1894)



32. Metal Hand book  
ASM, 8th edition, 1
33. N. Jost and I. Schmidt  
'Friction induced martensite transformation in austenitic  
Mn steel'Wear 111 (1986) 377
34. E. Hornbogen  
Z. Metallkd. 75 (1984) 739
35. H.M. Bauschke, E. Hornbogen and K .H. Zumghar  
Z. Metallkd. 72 (1981) 1
36. H. Berns and W. Trojahn  
Z. Werkstofftech 14 (1983) 382
37. R.A. Hadfield  
'Mn steel rails'  
Trans. AME (1914)
38. Y.N. Dastur and W.C. Leslie  
'Mechanism of work hardening in Hadfield Mn steel'.  
Met. Trans. 12A (1981) 749
39. R.W. Cahn  
The Encyclopedia of Ignorance, Pergamen Press(1977)
40. H.M. Otte.  
Acta Met. 5 (1957) 614.
41. W.N. Roberts  
Trans. TMS. AIME 230 (1964) 373

42. S.A. Sastri  
Proc. 3rd ICSMA, Cambridge, England 1(1973) 596.
43. H.C. Doepken  
Trans. AIME 194 (1952) 166
44. R.W.K. Honeycomb and C.H. White  
JISI 200 (1962) 457
45. D.E. Diesburg and F. Borik  
'Symposium on materials for mining industry'  
Elemax molybdenum Company, Greenwich CN (1974) 15
46. H. Nakagowa, Z. Nishiyama and M. Oka  
Mem. Inst. science Ind. Research, Osaka University  
21 (1964) 57
47. K.S. Raghavan, A.S. Sastri and M.J. Marcinkowski  
Trans. TMS-AIME 245 (1969) 1569
48. O.O. Lambakakhar and Yu.J.Parkal  
Izv Vyssh Vehebn. Zeved Fiz. 16 (1973) 26
49. Dj. Drobnjak and J.G. Parr.  
Met. Trans. 40 (1975) 554.
50. P.Yu Volusevieh, V.N. Grindnev and Yu.N. Petrov.  
Fiz. met. metalloved 40 (1975) 554.
51. T.J. Brofman and G.S. Ansell  
Met. Trans. 9A (1978) 879.

52. D.J.H. Cockayne, M.L. Jenkins and I.L.F. Ray  
Philos. Mag. 24 (1971) 1383
53. M.L. Jenkins  
Philos. Mag. 26 (1972) 747.
54. A.S. Keh, Y. Nakada and W.C. Leslie  
Dislocation dynamics, McGraw Hill Book Co. NY (1968)  
381.
55. J.T. Barnby  
JISI 203 (1965) 392
56. A. Santhanam and R.E. Reedhill  
Scr. Metall 4 (1970) 529
57. T. Shimomura, T. Kainuma and R. Watanabe  
J. Less Common Met. 57 (1978) 147
58. R.A. Mulford and U.F. Kocks  
Acta Met. 15 (1967) 885
59. I.S. Kim and M.C. Chaturvedi  
J. Met. Sci. 13 (1979) 691
60. A.H. Windle and G.C. Smith  
J. Met. Sci. 4 (1970) 136
61. L.J. Cuddy and W.C. Leslie  
Acta. Met. 20 (1972) 1157
62. P.R. Cetlin, A.S. Gulec, and R.E. Reed-Hill  
Met. Trans. 4 (1973) 513.

63. D.J. Dingley and D. Mclean  
Acta Met. 15 (1967) 885
64. J.W. Edington and R.E. Smallman  
Acta Met. 12 (1964) 1313.
65. B.A. Wilcox and G.C. Smith  
Acta met. 12 (1964) 371.
66. J.S. Blakemore  
Met. Trans. 1 (1970) 151
67. B.J. Brindley and J.T. Barnby  
Acta. Met. 14 (1966) 1765
68. J.D. Baird and C.R. Mac kenzie  
JISI 202 (1964) 247.
69. T. Takeyama and H. Takahashi  
Trans. ISI Jap. 13 (1973) 293
70. W.C. Leslie and A.S. Keh  
Mechanical Working of Steel,  
Garden And Breach Sc. Publishers, NY 2(1965) 337.
- 71., G. Collette, C. Crussard, A.Kohn, J. Plateau, G. Pormeys,  
and M. weisz.  
Rev. De Metal 54 (1957) 433.
72. W.C. Leslie  
Metallurgical Effects at high strain rates  
Plenum Press, NY. (1973) 571.

73. H.S. Avery  
'Austenitic Mn Steel'  
American Brake Shoe Co. (1949).
74. H. Berns, Klarner and Schmidtman  
Arch. Eisenüettenwes 38 (1967) 447
75. F. Borik and W.G. Scholz  
'Gouging abrasion test for materials used in ore and  
rock crushing'.  
J. Materials 6 Sept. (1971) 590.
76. A. Ball  
'On the importance of work hardening in the design of  
wear resistant materials'  
Wear 91 (1983) 201
77. A.W.J. De Gee  
Wear 81 (1981) 373
78. C. Allen, A. Ball and B.E. Protheroe  
Wear 74 (1981-1982) 287
79. G. Thomas and W.J. Salesky  
Wear 75 (1982) 21
80. C.J. Heathcock, B.E. Protheroe and A. Ball  
Proc. 5th Int. Conf. On the Strength of Metals and Allays,  
Oxford (1979) 219.
81. C.E. Dremann  
'C-Fe-V ternary alloys'  
ASM, Metal Handbook, 8th edition, 8,415

82. V.I. Grigorkin, I.V. Frantsenyuk, I.P. Galkin, A.A. Osltrov, A.I. Chemris and Cherenilov  
Metolovedenie Termikays Kaya Obrabotka Metallov. 4  
(1974) 68.
83. P.J. Marion  
'Modifield Hadfield Mn steel'  
B.Sc. Thesis, Deptt. of Metallurgical Engineerings.  
Queen's University, Kingston, Ontario, Canada (1970)2
84. D.C. Richardson, W.B.F. Mackay and R.W. Smith.  
'An improved Hadfield steels for use in railway castings'  
Deptt. of Met. Engineerings, Queen's University, Kingston,  
Ontario (1980).
85. N.G. Motenson  
'The effect of vanadium additions on Hadfield Mn steel'  
Report for degree in Bergsigenjor at Terniska Hogskalon  
Stockholm, Sweden (1980).
86. H.S. Avery and M.J. Day  
ASM Handbook, 1948 edition, 526
87. M.E. Nicholzen  
'Constitution of Fe-B alloys in the low B range'  
Trans. AIMME 200 (1954) 185
88. C.C. McBride, J.W. Spretnak and R. Speiser  
Trans. ASM 46 (1954) 499
89. P.E. Busby, M.E. Warga and C. Wells  
'Diffusion and solubility of B in iron and steel'  
Trans. AIMME 197 (1953) 1463

90. J.C. Shyne and E.R. Margan  
'Deboronization of Steels'  
Metal Progress 65 (1954) 88
91. K.G. Carrol, L.S. Darken, E.W. Fiter and L.J. Zwell  
'A new iron Boro-carbide'  
Nature 174 (1954) 978
92. M.A. Grossmann  
Trans. AIMME 150 (1942) 227
93. R.B. Schenck  
'Special addition agent steels'  
Trans. SAE 51 (1943) 385
94. R.B. Corbett and A.J. Williams,  
'Effect of B in steels'  
Bureau of mines, R.I., No.3816 (1945) 21
95. D.P. Buswell, L.A. Danse and H.T. Mcgrath  
'Report on investigation of B-treated Steels'  
~~SAE Technical Board, SP-10 (1946) 72~~
96. R.A. Grange and T.M. Garvey  
'Factors influencing the hardenability of B treated steels'  
Trans. ASM 37 (1946) 136
97. T.G. Digges and F.M. Reinhart  
'Influence of B on some properties of experimental and commercial steels'  
Bureau of Standards J. Research 39 (1947) 67

98. R. Potaszkin and M. Jaspert  
Second report of the committee on Boron steels  
Rev. Metall., Mem. 48 (1951) 379.
99. Atlas of Isothermal Transformation Diagrams  
Pittsburg, Pa., 2nd ed., (1951) 143.
- 100 T.G. Digges  
'How B enhances the hardenability of steel'  
SAE Journal 61 (1953) 24
- 101 H.T. Chandler and M.A. Bredig  
Trans. ASM 37 (1946) 179.
- 102 J.W. Spretnak and R. Speiser  
'Grain boundry films in B steels'  
Trans. AIMME 197 (1953) 445
- 103 J.C. Fisher  
'Influence of B on hardenability of steel'  
Trans. AIMME 200 (1954) 1146
- 
- 104 A.M. Adair, J.W. Spretnak and R. Speiser  
'Effect of B on the relative interfacial tension of  
gamma iron'  
Trans AIMME 203 (1955) 353
- 105 C.R. Simcoe A.R. Elasea and G.K. Manning  
'Study of the effect of B on the decomposition of  
austenite.  
Trans. AIMME 203 (1955) 193.



- 106 R. Genders and R. Harrison  
'Niobium - iron alloys'  
JISI 140 (1939) 29
- 107 F. Wever and W. Peter  
Arch. Eisenhüttenw, 15 (1942) 357
- 108 C.L. Shapiro and J. Strauss  
'The influence of various elements upon the position  
of the eutectoid in Fe-C system'.  
Trans. AIMME 158 (1944) 335
- 109 W. Peter and M. Neu  
'Influence of cooling rate upon the transformations  
of Cb steels'  
Kaiser-Wilhelm-Institut für Eisenforschung,  
Report No.64 (1945) 15
- 110 F.M. Becket and R. Franks  
'Effects of Cb in Cr-Ni steels'  
Trans. AIMME, 113 (1934) 143
- 
- 111 R. Franks  
'Effects of Cb and other addition agents on low Cr steels'  
Trans. ASM 27 (1939) 505
- 112 R. Franks, W.O. Binder, and C.R. Bishop  
'The effect of Mo and Cb on the structure, physical  
properties, and corrosion resistance of austenitic stain-  
less steels'  
Trans. ASM 29 (1941) 35

- 113 N.P. Suh  
Wear 44 (1977) 1
- 114 B. Kos, J. Czikel, E. Krainer, and H. Pacyna  
'Modification of the Mn steel structure-effects of susceptibility to hot tearing and resistance to wear'  
54th International Foundry Congress, New Delhi(1987).
- 115 G.F. Comstock  
Trans. AIMME 150 (1942) 408
- 116 G.T. Harris  
JISI 176 (1954) 209
- 117 A.I. Krynitsky and H. Stern  
'Effect of B on the structure and some physical properties of plain cast irons'  
Bureau of Standards, J. Research 42 (1949) 465
- 118 N.F. Tisdale  
'Boron in malleable iron'  
Foundry 73 (1945) 107
- 119 W.G. Wilson and N.F. Tisdale  
Trans. AFS 60 (1952) 470
- 120 W.R. Breeler  
'Development in Mo high-speed cutting steels'  
Trans. ASM 27 (1939) 289

- 121 R. Wasmuht  
Arch. Eisenhüttenw 5 (1931) 261
- 122 R. Wasmuht  
'Iron-Boron alloys and 18-8 steel plus B'  
Metals and alloys, 3 (1932) 105
- 123 A. Göcke, I. Schmidt and M. Wilhelm  
'Gouging and sliding abrasion of austenitic Mn steels  
reinforced by hard phases'  
Wear 119 (1987) 313.
- 124 M. Naim and S. Bahadur  
'Effect of microstructure and mechanical properties  
on the erosion of 18 Ni (250) maraging steel'  
Wear 112 (1986) 217
- 125 H. Czichos and K. Heinzhabig  
'Wear of medium carbon steel; a systematic study of  
the influences of materials and operating parameters'  
Wear 110 (1986) 389.
- 
- 126 P.J. Bolton and P. Clayton  
'Rolling sliding wear damage in rail and tyre steel'  
Wear 93 (1984) 145.
127. I.R. Sare  
'Repeated impact abrasion of ore crushing hammers'.  
Wear 87 (1983) 207.
128. H.Eggers and W. Peter  
Mitt. Kaiser-Wilhelm-Inst. Eisenforsch, 20  
(1938) 199.

129. H.J. Goldschmidt  
JISI 160 (1948) 345.
130. R.W. Gurry  
Trans.AIMME 158 (1944) 98.
131. G. Derge  
Trans.AIMME 167 (1946) 93
132. J.H. Hall  
Trans. AIME 84 (1929) 382.
133. V.N. Krivobok  
Trans. ASST 15 (1929) 893.
134. P. Chevenard  
Met.Corr. Ind. 10 (1935) 194
135. J. Friedel  
Dislocations, adelison-Wesley Publishing Company, Inc.  
(1964).
- 
136. J. Chipman and E.Brush  
Trans. TMS-AIME 242 (1968) 35
137. T.S. Ke and C.M. Wang  
Sci. Sin., 4 (1955) 501
138. V. Kandarpa and J.W. Spretnak  
Trans. TMS-AIME 245 (1969) 1439

139. S. Singh  
'Thermo mechanical ageing of 2014 Al alloy'  
Ph.D. thesis, University of Roorkee, India (1985).
140. J.H. Mulherin and H. Rosenthal  
Met. Trans. 2A (1971) 427.
141. C.J. Peel and P.J.E. Forsyth  
Metal Sci. J. 7 (1973) 121
142. B.J. Dunwoody, D.M. Moore and A.T. Thomas  
J. Inst. Metals 101 (1973) 172
143. G.T. Hahn and A.R. Rosenfield  
Met. Trans. 64 (1975) 653.
144. C. Zener and J.H. Hollomon  
'Effect of strain rate upon plastic flow in steel'.  
J. Appl. Phys. 15 (1944) 22.
145. H.Kolsky  
'Stress waves in solids'  
Oxford University Press, London (1953).
146. J.F. Archard  
J. Appl. Phys. 24 (1953) 981.
147. E. Hornbogen  
Z. Metallkd. 66 (1975) 507.
148. K.H. Zum Ghar  
Z. Metallkd. 69 (1978) 643

149. R.W.K. Honeycomb  
'Plastic deformation of metal'  
Edward Arnold (Pub.) Ltd, (1968)
150. A.J. Bedford, A.L. Wingrove and K.R.L. Thompson  
'The phenomenon of adiabatic shear deformation'  
J. Aust. Inst. Met. 19 (1974) 61
151. T.S. Eyre and A. Baxter  
'The formation of white layers at rubbing surfaces'  
Tribology 5 (1972) 256.

\*\*\*\*\*

APPENDIX

Tables of Experimental Data

\*\*\*\*\*

TABLE-1

## MECHANICAL PROPERTIES OF 13 Mn STEEL

---

YS(MPa)	392.4
UTS(MPa)	650.4
El(pct)	20.0
VHN	224
Impact strength	130

---



TABLE - 2

EFFECT OF B ADDITIONS ON MECHANICAL PROPERTIES

Property	Alloy designation		
	0.001B	0.002B	0.003B 0.004B
YS(MPa)	457.0	448.0	439.0 455.0
UTS(MPa)	762.7	750.5	740.4 756.8
EI(pct)	23.0	25.6	35.7 28.3
VHN	220	217	214 230
Impact strength (J)	158	179	202 180

TABLE - 3

## EFFECT OF V ADDITIONS ON MECHANICAL PROPERTIES

Property	Alloy designation		
	0.05V	0.10V	0.50V
YS(MPa)	416.0	428.0	466.0
UTS(MPa)	720.0	731.8	762.2
EI(pct)	22.6	21.8	19.6
VHN	236	240	252
Impact strength (J)	136	133	113

TABLE - 4

EFFECT OF Cb ADDITIONS ON MECHANICAL PROPERTIES

Property	Alloy designation	
	0.05Cb	0.50Cb
YS(MPa)	430.0	487.0
UTS(MPa)	703.0	657.0
El (pct.)	19.6	18.0
VHN	238	245
Impact strength (J)	88	70

TABLE -5

EFFECT OF MICRO ALLOYING ON STRAIN HARDENING EXPONENT( $\eta$ )

Alloy designation	Value of $\eta$
13 Mn	0.45
0.003 B	0.58
0.10 V	0.80
0.50 Cb	0.70

TABLE -6

EFFECT OF IMPACT LOADING ON SURFACE HARDENING

Alloy designation	As quenched VHN	Surface hardness(VHN) after intervals of 25 impact blows				
		I 25 blows	II 50 blows	III 75 blows	IV 100 blows	V 125 blows
13 Mn	224	344	390	429	462	462
0.003 B	214	406	474	480	486	486
0.10 V	240	380	420	450	459	459
0.50 Cb	240	336	386	420	430	430

TABLE - 7

WORK HARDENING AND SLIDE-WEAR CHARACTERISTICS OF 13 Mn STEEL

As quenched hardness VHN	Successive stage of grinding (30 sec interval)	Reduction in height of specimen mm	Cumulative reduction in height mm	Loss in weight gm	Cumulative loss in weight gm	Surface hardness VHN
224	I	0.402	0.402	0.98	0.98	285
	II	0.401	0.803	0.98	1.96	287
	III	0.398	1.201	0.97	2.93	285
	IV	0.399	1.600	0.98	3.91	287

TABLE - 8

WORK HARDENING AND SLIDE-WEAR CHARACTERISTICS OF 0.003B STEEL

As quenched hardness VHN	Successive stage of grinding (30 sec interval)	Reduction in height of specimen mm	Cumulative reduction in height mm	Loss in weight gm	Cumulative loss in weight gm	Surface hardness VHN
214	I	0.301	0.301	0.73	0.73	348
	II	0.299	0.600	0.73	1.46	352
	III	0.300	0.900	0.73	2.19	354
	IV	0.298	1.198	0.73	2.82	352

TABLE - 9

WORK HARDENING AND SLIDE-WEAR CHARACTERISTICS OF 0.10 V STEEL

As quenched hardness VHN	Successive stage of grinding (30 sec interval)	Reduction in height of specimen mm	Cumulative reduction in height mm	Loss in weight gm	Cumulative loss in weight gm	Surface hardness VHN
240	I	0.452	0.452	1.12	1.12	320
	II	0.450	0.902	1.09	2.21	322
	III	0.451	1.353	1.11	3.32	324
	IV	0.499	1.852	1.08	4.40	322



TABLE - 10

WORK HARDENING AND SLIDE-WEAR CHARACTERISTICS OF 0.50 Cb STEEL

As quenched hardness VHN	Successive stage of grinding (30 sec interval)	Reduction in height of specimen mm	Cumulative reduction in height mm	Loss in weight gm	Cumulative loss in weight gm	Surface hardness VHN
240	I	0.493	0.493	1.20	1.20	302
	II	0.495	0.988	1.22	2.42	304
	III	0.495	1.483	1.22	3.64	298
	IV	0.496	1.979	1.23	4.87	304

TABLE - 11

WORK HARDENING AND IMPACT SLIDE WEAR CHARACTERISTICS OF 13 Mn STEEL

Surface hardness of impact-ed sample	Successive stage of grinding	Reduction in height of specimen	Cumulative reduction in height	Loss in weight	Cumulative loss in weight	Surface hardness after grinding	Average hardness of ground layer
VHN	( 30 sec interval)	mm	mm	gm	gm	VHN	VHN
462	I	0.150	0.150	0.36	0.36	366	414
	II	0.249	0.399	0.61	0.97	322	344
	III	0.398	0.797	0.96	1.93	290	306
	IV	0.400	1.197	0.98	2.91	287	288
	V	0.400	1.597	0.98	3.89	287	287

TABLE - 12

WORK HARDENING AND IMPACT SLIDE WEAR CHARACTERISTICS OF 0.003 B STEEL

Surface hardness of impact-ground sample	Successive stage of grinding	Reduction in height of specimen	Cumulative reduction in height	Loss in weight	Cumulative loss in weight	Surface hardness after grinding	Average hardness of ground layer
VHN	( 30 sec interval)	mm	mm	gm	gm	VHN	VHN
486	I	0.099	0.099	0.24	0.24	383	434
	II	0.199	0.298	0.49	0.73	357	378
	III	0.301	0.599	0.73	1.46	352	354
	IV	0.300	0.899	0.73	2.19	350	351
	V	0.300	1.199	0.73	2.92	350	350

TABLE - 13

WORK HARDENING AND IMPACT SLIDE WEAR CHARACTERISTICS OF O.10V STEEL

Surface hardness of impacted sample	Successive stage of grinding	Reduction in height of specimen	Cumulative reduction in height	Loss in weight	Cumulative loss in weight	Surface hardness after grinding	Average hardness of ground layer
VHN	( 30 sec interval)	mm	mm	gm	gm	VHN	VHU
459	I	0.199	0.199	0.49	0.49	340	400
	II	0.270	0.469	0.66	1.15	329	334
	III	0.430	0.899	1.05	2.20	322	325
	IV	0.450	1.349	1.10	3.30	320	321
	V	0.451	1.800	1.12	4.42	320	320

TABLE - 14

WORK HARDENING AND IMPACT SLIDE WEAR CHARACTERISTICS OF 0.50 Cb STEEL

Surface hardness of impact-ground sample	Successive stage of grinding	Reduction in height of specimen	Cumulative reduction in height	Loss in weight	Cumulative loss in weight	Surface hardness after grinding	Average hardness of ground layer
VHN	(30 sec interval)	mm	mm	gm	gm	VHN	VHN
430	I	0.220	0.220	0.54	0.54	375	402
	II	0.280	0.500	0.68	1.22	330	352
	III	0.450	0.950	1.10	2.32	302	316
	IV	0.495	1.445	1.21	3.53	300	301
	V	0.496	1.941	1.21	4.74	300	300